AUTOPHAGY IN MAMMALIAN DEVELOPMENT AND DIFFERENTIATION

EDITED BY: Federica Di Sano, Sabrina Di Bartolomeo, Konstantinos Zarbalis and Lucia Latella
PUBLISHED IN: Frontiers in Cell and Developmental Biology

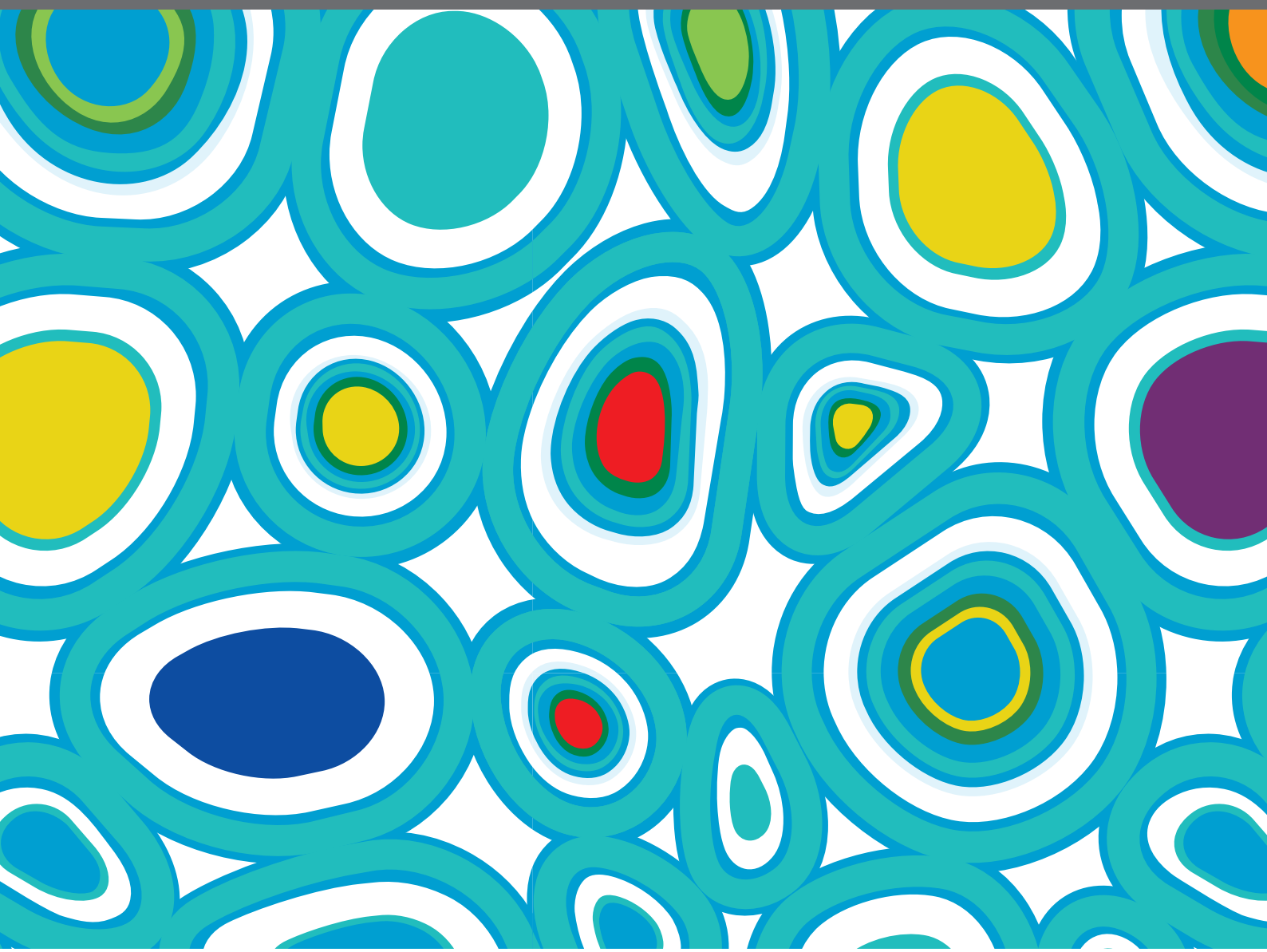

frontiers Research Topics

frontiers

ISSN 1664-8714
ISBN 978-2-88971-339-4
DOI 10.3389/978-2-88971-339-4

About Frontiers

Frontiers is more than just an open-access publisher of scholarly articles: it is a pioneering approach to the world of academia, radically improving the way scholarly research is managed. The grand vision of Frontiers is a world where all people have an equal opportunity to seek, share and generate knowledge. Frontiers provides immediate and permanent online open access to all its publications, but this alone is not enough to realize our grand goals.

Frontiers Journal Series

The Frontiers Journal Series is a multi-tier and interdisciplinary set of open-access, online journals, promising a paradigm shift from the current review, selection and dissemination processes in academic publishing. All Frontiers journals are driven by researchers for researchers; therefore, they constitute a service to the scholarly community. At the same time, the Frontiers Journal Series operates on a revolutionary invention, the tiered publishing system, initially addressing specific communities of scholars, and gradually climbing up to broader public understanding, thus serving the interests of the lay society, too.

Dedication to Quality

Each Frontiers article is a landmark of the highest quality, thanks to genuinely collaborative interactions between authors and review editors, who include some of the world's best academicians. Research must be certified by peers before entering a stream of knowledge that may eventually reach the public - and shape society; therefore, Frontiers only applies the most rigorous and unbiased reviews.
Frontiers revolutionizes research publishing by freely delivering the most outstanding research, evaluated with no bias from both the academic and social point of view. By applying the most advanced information technologies, Frontiers is catapulting scholarly publishing into a new generation.

What are Frontiers Research Topics?

Frontiers Research Topics are very popular trademarks of the Frontiers Journals Series: they are collections of at least ten articles, all centered on a particular subject. With their unique mix of varied contributions from Original Research to Review Articles, Frontiers Research Topics unify the most influential researchers, the latest key findings and historical advances in a hot research area! Find out more on how to host your own Frontiers Research Topic or contribute to one as an author by contacting the Frontiers Editorial Office: frontiersin.org/about/contact

AUTOPHAGY IN MAMMALIAN DEVELOPMENT AND DIFFERENTIATION

Topic Editors:
Federica Di Sano, University of Rome Tor Vergata, Italy
Sabrina Di Bartolomeo, University of Molise, Italy
Konstantinos Zarbalis, University of California, Davis, United States
Lucia Latella, Italian National Research Council, Italy

Citation: Di Sano, F., Di Bartolomeo, S., Zarbalis, K., Latella, L., eds. (2021). Autophagy in Mammalian Development and Differentiation. Lausanne: Frontiers Media SA. doi: 10.3389/978-2-88971-339-4

Table of Contents

frontiers in Cell and Developmental Biology

EDITORIAL
published: 27 July 2021
doi: 10.3389/fcell.2021.722821

Editorial: Autophagy in Mammalian Development and Differentiation

Sabrina Di Bartolomeo[1], *Lucia Latella*[2,3], *Konstantinos Zarbalis*[4,5,6] *and Federica Di Sano*[7]*

[1] Department of Biosciences and Territory, University of Molise, Pesche, Italy, [2] Institute of Translational Pharmacology, National Research Council of Italy, Rome, Italy, [3] Epigenetics and Regenerative Medicine, IRCCS Fondazione Santa Lucia, Rome, Italy, [4] Department of Pathology and Laboratory Medicine, University of California, Davis, Davis, CA, United States, [5] Institute for Pediatric Regenerative Medicine, Shriners Hospitals for Children, Sacramento, CA, United States, [6] MIND Institute, University of California, Davis, Davis, CA, United States, [7] Department of Biology, University of Rome "Tor Vergata," Rome, Italy

Keywords: autophagy, differentiation, stem cells, reprogramming, lysosomes

Editorial on the Research Topic

Autophagy in Mammalian Development and Differentiation

Autophagy is a cellular degradation and recycling process by which cytoplasmic components, including macromolecules and organelles, are sequestered into specialized autophagosomal vesicles to be delivered and degraded in lysosomes (Klionsky and Emr, 2000; Levine and Klionsky, 2004; He and Klionsky, 2009). Autophagy is highly active during the earliest stages of development regulating stem cell pluripotency and differentiation (Jang et al., 2016; Xu et al., 2020), but also fundamental to later morphogenetic processes that together with apoptosis are decisive in tissue remodeling and shaping the embryo's organization (Qu et al., 2007). Moreover, autophagic process likely protects cells during metabolic stress and nutrient deprivation that occur during tissue remodeling. It is therefore evident that the close interplay between autophagy and the processes of cell death, proliferation, and differentiation determine eukaryotic development.

This Research Topic aimed at providing further context to the role of autophagy in orchestrating cellular development, differentiation, and aging in both physiological and pathological conditions.

In this context Perrotta et al. reviewed recent findings that further illuminate autophagy's impact on differentiation and maintenance of endothelium, muscle, immune system, and brain. Their detailed description provides a comprehensive framework of emerging results and highlights the pivotal role of autophagic response in a multitude of tissue functions that critically depend on stem cell maintenance and differentiation.

Campanario et al. describe two strategies for assessing autophagic activity in satellite cells. Adult skeletal muscle has the capability to regenerate by virtue of its resident stem cells (satellite cells). With aging, satellite cell regenerative capacity declines, correlating with loss of autophagy. Enhancing autophagy in aged satellite cells restores their regenerative functions, underscoring this proteostatic activity's relevance for tissue regeneration. Thus, the methods presented in this study allow a rapid assessment of autophagic flux in muscle stem cells by flow cytometry and immunofluorescence enabling researchers in investigating the role of autophagy in muscle homeostasis, regeneration and diseases (Campanario et al.).

Reactivating autophagy in COL6 null mice ameliorates the myopathic phenotype. The findings by Metti et al. point at the effects of pterostilbene (Pt), a non-toxic polyphenol belonging to the stilbenoid family, on skeletal muscle homeostasis. The authors show that Pt is an effective autophagy-inducing nutraceutical for skeletal muscle with great potential in counteracting

OPEN ACCESS

Edited and reviewed by:
You-Wen He,
Duke University, United States

***Correspondence:**
Federica Di Sano
federica.di.sano@uniroma2.it

Specialty section:
This article was submitted to Cell Death and Survival, a section of the journal Frontiers in Cell and Developmental Biology

Received: *09 June 2021*
Accepted: *30 June 2021*
Published: *27 July 2021*

Citation:
Di Bartolomeo S, Latella L, Zarbalis K and Di Sano F (2021) Editorial: Autophagy in Mammalian Development and Differentiation. Front. Cell Dev. Biol. 9:722821. doi: 10.3389/fcell.2021.722821

the major pathogenic hallmarks of COL6-related myopathies, a valuable feature that may be also beneficial in other muscle pathologies characterized by a defective regulation of the autophagic machinery.

These data point at Pt as an effective non-toxic, caloric restriction mimetic that can be exploited for the treatment of autophagy-deficient pathologies (Metti et al.).

Cui et al. found that miR-204 is highly expressed in chicken atrophic ovaries promoting granulosa cell apoptosis *via* repressing FOXK2 through PI3K/AKT/mTOR pathway and inhibited autophagy by impeding the TRPM3/AMPK/ULK pathway. In fact, it is known that ovarian tumor is accompanied by an increase in follicular atresia, cell apoptosis, and autophagy (Ma et al., 2019). Functions of miR-204 have been linked to many biological processes, including maintenance of joint homeostasis and protection against osteoarthritis, tumor growth, migration and anoikis of cancer cells, and autophagy. This study could be useful in identifying the regulators of miR-204 target genes and their roles in signaling pathways associated with both the development and function of the ovary.

Histone deacetylases (HDACs) are a group of enzymes that remove acetyl groups from both histone and non-histone proteins Zhan et al. found that HDAC6 regulates the fusion of autophagosome and lysosome during odontogenesis. Interestingly, this study provides a new viewpoint into the role of autophagy in odontoblast differentiation.

In the past few years, our understanding of the interplay between autophagy and genomic stability has greatly increased and several papers suggested a molecular connection between the DNA damage response (DDR) and autophagy.

Ataxia-telangiectasia mutated kinase (ATM) is the product of a gene whose mutation leads to the development of a rare genetic neurodegenerative disorder, Ataxia-telangiectasia (A-T). Importantly, ATM kinase plays a central role in the DDR and it can finely tune the balance between senescence and apoptosis: activated ATM promotes autophagy and sustains the lysosomal–mitochondrial axis. In the review by Stagni et al., recent advances in understanding the molecular mechanisms linking DNA damage, oxidative stress and autophagy to senescence are summarized, pointing out the role of ATM kinase in these cellular responses. The significance of this regulation in the pathogenesis of A-T is also discussed.

Still regarding the role of autophagy in detoxifying the cellular environment and ensuring cellular survival, we report the work from Vanasco et al.. The authors identify a novel DRP1-Parkin1-VMP1 selective autophagy pathway, which mediates the selective degradation of damaged mitochondria by mitophagy in acute pancreatitis therefore restoring mitochondrial functions (Vanasco et al.).

The role of Oleic Acid (OA) in hepatocellular carcinoma (HCC) through autophagy has been investigated by Giulitti et al.. OA is one of the most abundant monounsaturated fatty acid representing the main component of olive oil (70–80%) that has beneficial effects in counteracting liver steatosis and cardiovascular diseases (Perez-Martinez et al., 2011; Perdomo et al., 2015).

The authors report a OA- specific effect on lipid accumulation, viability, proliferation, migration, and invasion which is partially due to a reduced autophagy leading to an OA anti-tumor effect in HCC.

Lastly, it has been observed that autophagy inhibition through poly (ADP-ribose) polymerase-1 (PARP1) inactivation protects cardiomyocytes from Myocardial ischemia–reperfusion injury (MIRI), characterized by post-ischemic cardiomyocytes death and reperfusion myocardial damage (Xu et al.)

We hereby thank all the authors that participated in this Research Topic. Their articles significantly contribute to a more comprehensive understanding of the roles that autophagy plays in regulating different aspects of mammalian development and differentiation and add new concerns to uncovering mechanisms underlying human disease.

AUTHOR CONTRIBUTIONS

FD and SD conceived and wrote the Editorial. LL and KZ reviewed and edited the manuscript. All authors contributed to the article and approved the submitted version.

FUNDING

FD and SD were supported by grants from Italian Ministry of University and Research. KZ was supported by NIH grants HL151611 and MH115347. LL was supported by H2020-MSCA-ITN-2019 grant # 860034 and Ministry of Health PE-2016-02363049.

REFERENCES

He, C., and Klionsky, D. J. (2009). Regulation mechanisms and signaling pathways of autophagy. *Annu. Rev. Genet.* 43, 67–93. doi: 10.1146/annurev-genet-102808-114910

Jang, J., Wang, Y., Lalli, M. A., Guzman, E., Godshalk, S. E., Zhou, H., et al. (2016). Primary cilium-autophagy-Nrf2 (PAN) axis activation commits human embryonic stem cells to a neuroectoderm fate. *Cell* 165, 410–420. doi: 10.1016/j.cell.2016.02.014

Klionsky, D. J., and Emr, S. D. (2000). Autophagy as a regulated pathway of cellular degradation. *Science* 290, 1717–1721. doi: 10.1126/science.290.5497.1717

Levine, B., and Klionsky, D. J. (2004). Development by self-digestion: molecular mechanisms and biological functions of autophagy. *Dev. Cell* 6, 463–477. doi: 10.1016/S1534-5807(04)00099-1

Ma, L., Zheng, Y., Tang, X., Gao, H., Liu, N., Gao, Y., et al. (2019). miR-21–3p inhibits autophagy of bovine granulosa cells by targeting VEGFA *via* PI3K/AKT signaling. *Reproduction* 158, 441–452. doi: 10.1530/REP-19-0285

Perdomo, L., Beneit, N., Otero, Y. F., Escribano, O., Diaz-Castroverde, S., Gomez-Hernandez, A., et al. (2015). Protective role of oleic acid against cardiovascular insulin resistance and in the early and late cellular atherosclerotic process. *Cardiovasc. Diabetol.* 14:75. doi: 10.1186/s12933-015-0237-9

Perez-Martinez, P., Garcia-Rios, A., Delgado-Lista, J., Perez-Jimenez, F., and Lopez-Miranda, J. (2011). Mediterranean diet rich in olive oil and obesity, metabolic syndrome and diabetes mellitus. *Curr. Pharm. Des.* 17, 769–777. doi: 10.2174/138161211795428948

Qu, X., Zou, Z., Sun, Q., Luby-Phelps, K., Cheng, P., Hogan, R. N., et al. (2007). Autophagy gene-dependent clearance of apoptotic cells during embryonic development. *Cell* 128, 931–946. doi: 10.1016/j.cell.2006.12.044

Xu, Y., Zhang, Y., Garcia-Canaveras, J. C., Guo, L., Kan, M., Yu, S., et al. (2020). Chaperone-mediated autophagy regulates the pluripotency of embryonic stem cells. *Science* 369, 397–403. doi: 10.1126/science.abb4467

Conflict of Interest: The authors declare that the research was conducted in the absence of any commercial or financial relationships that could be construed as a potential conflict of interest.

Publisher's Note: All claims expressed in this article are solely those of the authors and do not necessarily represent those of their affiliated organizations, or those of the publisher, the editors and the reviewers. Any product that may be evaluated in this article, or claim that may be made by its manufacturer, is not guaranteed or endorsed by the publisher.

frontiers in Cell and Developmental Biology

BRIEF RESEARCH REPORT
published: 29 September 2020
doi: 10.3389/fcell.2020.580933

The Polyphenol Pterostilbene Ameliorates the Myopathic Phenotype of Collagen VI Deficient Mice via Autophagy Induction

Samuele Metti[1†], Lisa Gambarotto[1†], Martina Chrisam[1], Martina La Spina[2], Martina Baraldo[2], Paola Braghetta[1], Bert Blaauw[2,3] and Paolo Bonaldo[1,4]*

[1] Department of Molecular Medicine, University of Padova, Padua, Italy, [2] Department of Biomedical Sciences, University of Padova, Padua, Italy, [3] Venetian Institute of Molecular Medicine, Padua, Italy, [4] CRIBI Biotechnology Center, University of Padova, Padua, Italy

OPEN ACCESS

Edited by:
Sabrina Di Bartolomeo, University of Molise, Italy

Reviewed by:
Claudia Fuoco, University of Rome Tor Vergata, Italy
Said Hashemolhosseini, University of Erlangen Nuremberg, Germany

***Correspondence:**
Paolo Bonaldo
bonaldo@bio.unipd.it

[†] These authors have contributed equally to this work

Specialty section:
This article was submitted to Cell Death and Survival, a section of the journal Frontiers in Cell and Developmental Biology

Received: 07 July 2020
Accepted: 03 September 2020
Published: 29 September 2020

Citation:
Metti S, Gambarotto L, Chrisam M, La Spina M, Baraldo M, Braghetta P, Blaauw B and Bonaldo P (2020) The Polyphenol Pterostilbene Ameliorates the Myopathic Phenotype of Collagen VI Deficient Mice via Autophagy Induction. Front. Cell Dev. Biol. 8:580933. doi: 10.3389/fcell.2020.580933

The induction of autophagy, the catabolic pathway by which damaged or unnecessary cellular components are subjected to lysosome-mediated degradation and recycling, is impaired in Collagen VI (COL6) null mice and COL6-related myopathies. This autophagic impairment causes an accumulation of dysfunctional mitochondria, which in turn leads to myofiber degeneration. Our previous work showed that reactivation of autophagy in COL6-related myopathies is beneficial for muscle structure and function both in the animal model and in patients. Here we show that pterostilbene (Pt)—a non-toxic polyphenol, chemically similar to resveratrol but with a higher bioavailability and metabolic stability—strongly promotes *in vivo* autophagic flux in the skeletal muscle of both wild-type and COL6 null mice. Reactivation of autophagy in COL6-deficient muscles was also paralleled by several beneficial effects, including significantly decreased incidence of spontaneous apoptosis, recovery of ultrastructural defects and muscle remodeling. These findings point at Pt as an effective autophagy-inducing nutraceutical for skeletal muscle with great potential in counteracting the major pathogenic hallmarks of COL6-related myopathies, a valuable feature that may be also beneficial in other muscle pathologies characterized by defective regulation of the autophagic machinery.

Keywords: skeletal muscle, autophagy, muscle remodeling, congenital muscular dystrophies, nutraceutical agent, Collagen VI

INTRODUCTION

Macroautophagy (hereafter autophagy) is an evolutionarily conserved and multistep self-eating mechanism, by which damaged or unnecessary intracellular components are engulfed into specific double-membrane vesicles, called autophagosomes, and subjected to lysosome-mediated degradation and recycling (Mizushima, 2007). Autophagy is a very dynamic process that needs to be finely tuned in the different tissues and cell types. Indeed, any perturbation in autophagy regulation may seriously endanger cell viability and function, especially in post-mitotic cells (Levine and Kroemer, 2008).

Skeletal muscle is a highly plastic tissue, able to adapt its metabolism, mass and strength to several physiological conditions, via balancing protein synthesis and degradation (Schiaffino et al., 2013). In particular, the autophagic pathway plays a crucial role during muscle development and maintains cellular homeostasis and energy balance in mature fibers (Bonaldo and Sandri, 2013). Autophagy dysregulation is involved in the etiopathogenesis of various muscle disorders, such as muscular dystrophies, congenital myopathies, cachexia and sarcopenia (Grumati and Bonaldo, 2012; Castets et al., 2016). A well-characterized model of impaired autophagy induction in skeletal muscle is the COL6 null (*Col6a1*$^{-/-}$) mouse (Bonaldo et al., 1998; Cescon et al., 2015), in which accumulation of dysfunctional mitochondria and abnormal organelles in myofibers leads to muscle wasting and weakness (Irwin et al., 2003; Grumati et al., 2010). Similar alterations are present in patients affected by Bethlem myopathy (BM) and Ullrich congenital muscular dystrophy (UCMD), two rare inherited muscle disorders caused by mutations of COL6 genes and for which no cure is yet available (Grumati et al., 2010; Bönnemann, 2011). Of note, defective regulation of autophagy was also reported in the dystrophin-deficient *mdx* mouse (De Palma et al., 2012; Spitali et al., 2013) and in the MTM1 null mouse (Fetalvero et al., 2013), animal models for Duchenne muscular dystrophy and X-linked myotubular myopathy, respectively.

In the last decade, targeted approaches aimed at promoting the autophagic flux gained increasing interest as a novel option for prospective therapeutic strategies in a range of disorders and pathological conditions (Rubinsztein et al., 2012). The easiest and most characterized way to boost autophagy is represented by caloric or nutritional restriction, which can be elicited by different means, such as fasting or decreased protein intake (Rubinsztein et al., 2012; Bagherniya et al., 2018). Regarding COL6-related myopathies, these approaches were shown to be beneficial both in preclinical studies in *Col6a1*$^{-/-}$ mice (Grumati et al., 2010; Chrisam et al., 2015) and in a pilot clinical trial in UCMD and BM patients, in which autophagy was successfully promoted through a 1-year-long low protein diet (Castagnaro et al., 2016). However, such dietary regimen unavoidably requires a deep and rigorous lifestyle change that may challenge patients' compliance and the bench-to-bedside process. An increasingly attractive option for autophagy stimulation is represented by a broad range of nutraceutical compounds that act as caloric restriction mimetics (Madeo et al., 2019; Maiuri and Kroemer, 2019), such as the polyamine spermidine (Madeo et al., 2018).

Pterostilbene (trans-3,5-dimethoxy-4′-hydroxystilbene, Pt) is a non-toxic polyphenol belonging to the stilbenoid family, naturally found in grapes and berries. Compared to the better-known stilbenoid resveratrol (3,4′,5-trihydroxystilbene), Pt has a dimethoxy group that allows it to be more bioavailable, metabolically stable and, therefore, highly suitable for *in vivo* administration (Kapetanovic et al., 2011; Azzolini et al., 2014). Stilbenes exert several pharmacological activities, including antiproliferative, anti-inflammatory, antiaging, antidiabetic, neuroprotective, and cardioprotective properties (Roupe et al., 2006; Kosuru et al., 2016). The beneficial effects of these compounds lie in their antioxidant properties and in their ability to directly or indirectly modulate signaling pathways also involved in autophagy regulation (Akinwumi et al., 2018).

So far, the proautophagic activity of Pt was mostly investigated in cancer cell lines and tumorigenic conditions (Lee et al., 2019; Ma et al., 2019), whereas much less is known about it in other physiological and pathological conditions. For skeletal muscle, the studied effects of Pt administration have mainly regarded insulin sensitivity (Gómez-Zorita et al., 2015; Tastekin et al., 2018) and muscle adaptation to exercise (Zheng et al., 2020), but autophagy was not investigated in those studies. In light of this, we investigated the autophagy-modulating action of Pt in fibroblast cultures and in skeletal muscle of wild-type and COL6 null mice, and found that Pt treatment potently induces the autophagic flux and is able to ameliorate the muscle pathology of COL6 null animals. These data point at Pt as an effective non-toxic, caloric restriction mimetic that can be exploited for the treatment of autophagy-deficient pathologies.

METHOD

Animals

Six-month-old wild-type and *Col6a1*$^{-/-}$ mice in the C57BL/6N background (Irwin et al., 2003) were used. All mice were housed in controlled temperature (23°C) and light (12 h light/12 h dark cycle) conditions, with *ad libitum* access to water and food. Animal procedures were performed according to the Italian laws and approved by the Animal Ethics Committee of the University of Padova (OPBA) and by the Italian Ministry of Health (license protocol n. 480/2019-PR).

Mouse Treatments

Pt (gently provided by Dr. Mario Zoratti) was dissolved at 500 mM in dimethyl sulfoxide (DMSO, Sigma-Aldrich). Pt stock solution was diluted in distilled water to 90.2 mg/kg body weight in a final volume of 100 μL. Pt was administered by oral gavage for 1 or 5 consecutive days. Control mice received a vehicle solution of DMSO in distilled water. Autophagic flux was investigated by co-treatment with colchicine (Sigma-Aldrich) (Klionsky et al., 2016). Colchicine was dissolved in physiological solution and i.p. injected at 0.4 mg/kg body weight, once a day for 2 consecutive days (Ju et al., 2010). The day after the last injection, mice were sacrificed by cervical dislocation. Once dissected, muscles were quickly frozen in liquid nitrogen-precooled isopentane and stored at −80°C for subsequent histological and biochemical analyses.

Cell Cultures and Treatments

Primary dermal fibroblasts were isolated from C57BL/6N wild-type mice as described (Takashima, 2001). Briefly, mice were shaved and back skin was removed, washed in phosphate-buffered saline (PBS) supplemented with 3% penicillin-streptomycin (P/S, Life Technologies), and digested for 30 min in 0.25% trypsin-EDTA solution (Thermo Fisher Scientific) at 37°C. Subsequently, the tissue explant was cut into small pieces and placed in a petri dish. The specimens were incubated in Dulbecco's Modified Eagle's Medium (DMEM,

Thermo Fisher Scientific) supplemented with 20% fetal bovine serum (Thermo Fisher Scientific) and 1% P/S, and maintained at 37°C in 5% CO_2 until fibroblasts reached confluence. Only P4 to P5 passages from initial fibroblast isolation were used for the experiments. Fibroblasts were treated in the Petri dish for 2.5 h with 15 μM Pt or 0.1% DMSO, added to the culture medium. In order to study the autophagic flux (Klionsky et al., 2016), fibroblasts were co-treated with 50 μM chloroquine (Sigma-Aldrich) during the last 2 h of Pt treatment.

Western Blotting

Frozen tibialis anterior (TA) muscle was pulverized by grinding in liquid nitrogen and lysed in SDS extraction buffer (50 mM Tris-HCl, pH 7.5; 150 mM NaCl; 10 mM $MgCl_2$; 1 mM EDTA; 10% glycerol; 0.5 mM DTT; 2% SDS; 1% Triton X-100) supplemented with protease (Roche) and phosphatase (Sigma-Aldrich) inhibitors. Primary dermal fibroblasts (0.7×10^6 cells) were cultured in 6-well plates. Cells were washed twice with PBS and scraped in NP-40 lysis buffer (50 mM Tris-HCl, pH 7.5; 20 mM EDTA; 150 mM NaCl; 0.5% NP-40) supplemented with protease and phosphatase inhibitors. SDS-PAGE of protein lysates (10–30μg) was carried out in 12% or 4–12% gradient polyacrylamide Novex NuPAGE Bis-Tris gels (Invitrogen), according to protein molecular weight, and electrotransferred onto PVDF membrane (Millipore). Membranes were saturated for 1 h in 5% non-fat milk in Tris-buffered saline containing 0.1% Tween 20 (TBS-T) and incubated overnight at 4°C with the following primary antibodies diluted in 2.5% milk in TBS-T: rabbit anti-LC3B (1:1,000; Thermo Fisher Scientific, PA1-16930); rat anti-LAMP1 (1:300; DSHB, clone 1D4B); guinea pig anti-p62/SQSTM1 (1:300; Santa Cruz Biotechnology, sc-25575); mouse anti-BNIP3 (1:500; Sigma-Aldrich, B7931); mouse anti-GAPDH (1:125,000; Millipore, MAB374); mouse anti-vinculin (1:1,000; Sigma-Aldrich, clone VIN-11-5); mouse anti-β-actin (1:1,500; Sigma-Aldrich, A5316). Horseradish peroxidase-conjugated secondary antibodies (1:2,000; Bethyl Laboratories) were used in 2.5% milk in TBS-T. Signal was detected by chemioluminescence using SuperSignal West Pico (Thermo Fisher Scientific). Densitometric quantification was carried out by ImageJ software (Schneider et al., 2012). When needed, membranes were stripped with an acidic stripping solution (25 mM glycine, 1% SDS, pH 2), saturated and reprobed.

RNA Extraction and Gene Expression Analyses

Whole frozen tibialis anterior muscles were grinded in liquid nitrogen using pestle and mortar. Total RNA was isolated using TRIzol reagent (Invitrogen), according to manufacturer's instructions, quantified using Nanodrop ND2000 (Thermo Fisher Scientific) and finally retrotranscribed with the SuperScript III Reverse Transcriptase kit (Thermo Fisher Scientific) using random hexamers. Quantitative PCR was performed on a Rotor-Gene Q Thermal cycler instrument (Qiagen) using SYBR green-containing mastermix (Qiagen). Primer sequences are detailed in **Supplementary Table S1**. *Actb* was used as a housekeeping gene.

Muscle Histology

Cryosections of TA muscle (10-μm-thick) were stained with hematoxylin-eosin (Sigma-Aldrich, 51275 and HT110116) following standard protocols. For picrosirius red staining, TA cross-sections were fixed for 15 min in 4% PFA, washed in water and stained for 90 min with Picrosirius Red Stain Kit (Polysciences). Bright-field images were captured using a Leica DM-R microscope equipped with a digital camera. Wheat germ agglutinin (WGA) conjugated with Alexa Fluor 488 (Invitrogen) was used to stain sarcolemma and the extracellular space. TA cross-sections (10-μm-thick) were incubated with WGA (1 μg/mL) and Hoechst 33258 (2.5 μg/mL, Sigma-Aldrich) in PBS for 20 min at room temperature. Slides were washed twice in PBS and mounted in 80% glycerol. Partially overlapping images of the entire muscle section were captured using a Leica DM5000B microscope equipped with a digital camera and stitched with ImageJ software. MATLAB application SMASH (Smith and Barton, 2014) was used to segment the fluorescent stitched images and to measure the cross-sectional area of each myofiber. SMASH parameters were chosen to optimize the segmentation procedure and maintained constant for all the analyses. Wrong selections were manually corrected. Centrally nucleated myofibers, embryonic myosin heavy chain (eMHC)-positive myofibers and the total amount of myofibers per TA section were counted manually.

Immunofluorescence

Dermal fibroblasts (0.1×10^6 cells) were plated on glass coverslips pre-coated with 0.1% gelatin (Sigma-Aldrich) in PBS. At the end of the treatments described above, cells were washed twice with PBS and incubated in cold 1:1 methanol-acetone solution for 10 min at −20°C. The same fixation/permeabilization procedure was performed on 10-μm-thick cross cryosections of TA muscles. Slides were saturated with 10% goat serum in PBS for 30 min at room temperature and incubated overnight with the following antibodies: rat anti-LAMP1 (1:100; DSHB, clone 1D4B); rabbit anti-LC3B (1:150; Thermo Fisher Scientific, PA1-16930); guinea pig anti-p62/SQSTM1 (1:100; Progen, GP62-C); mouse anti-eMHC (1:25; DSHB, clone F1.652); rabbit anti-Laminin (1:800; Sigma-Aldrich, clone L9393). Slides were washed in PBS and incubated for 1 h at room temperature with the appropriate secondary antibodies (Jackson ImmunoResearch). Slides were mounted in 80% glycerol-PBS and images were taken by using a Zeiss LSM700 laser-scanning confocal microscope.

In situ TUNEL Assay

Quantitative determination of apoptotic cells was performed by terminal deoxynucleotidyl transferase dUTP-mediated nick-end labeling (TUNEL) assay. TA cross-sections (10-μm-thick) were air-dried and apoptotic nuclei were detected by the *In situ* Cell Death Detection Kit TMR red (Roche), according to the manufacture's guidelines. All nuclei were subsequently counterstained with Hoechst 33258 (Sigma).

Random fields were selected using a Leica DM5000B microscope equipped with a digital camera and TUNEL-positive nuclei were manually counted.

Transmission Electron Microscopy

TA muscles were longitudinally stretched and fixed overnight at 4°C with 2.5% glutaraldehyde (Sigma-Aldrich) and 2% formaldehyde (Sigma-Aldrich) in 0.1 M sodium cacodylate buffer pH 7.4, and postfixed for 2 h at 4°C with 1% osmium tetroxide in 0.1 M sodium cacodylate buffer. After three water washes, samples were dehydrated in a graded ethanol series and embedded in an epoxy resin (Sigma-Aldrich). Ultrathin sections (60–70 nm) were obtained with an Ultrotome V (LKB) ultramicrotome, counterstained with uranyl acetate and lead citrate. Images were acquired with a FEI Tecnai 12 transmission electron microscope (FEI Company) operating at 100 kV and equipped with a Veleta CCD digital camera (Olympus Soft Imaging System).

Statistics

Comparisons were made by using a two-tailed unpaired Student's *t*-test and $P < 0.05$ was considered as statistically significant. Data are represented as mean ± s.e.m. The number of biological replicates (always greater than 3) is indicated in each figure caption.

RESULTS

Pterostilbene Treatment Elicits Autophagy in Primary Dermal Fibroblasts and Muscles

The proautophagic properties of Pt had been extensively investigated in immortalized cell lines, but little is known about primary cell cultures. For this reason, we first evaluated the capability of Pt to positively modulate autophagy in primary dermal fibroblasts prepared from wild-type mice. To monitor the autophagic flux, we incubated cells with chloroquine, an inhibitor of lysosome acidification and function (Klionsky et al., 2016). Western blotting showed a significantly higher chloroquine-dependent accumulation of LC3B-II, the best-characterized autophagosome marker, in cultures treated for 2.5 h with Pt when compared to vehicle-treated cultures (**Figures 1A,B**), indicating that Pt promotes autophagosome formation in primary fibroblasts.

Autophagosome-lysosome fusion represents the final step of the autophagic flux and is equally important for the entire process. Indeed, lysosomes play an essential role in cargo degradation, both in basal condition and during autophagy induction (Huynh et al., 2007; Zhou et al., 2013). In agreement with the Pt-dependent induction of the autophagic flux, primary fibroblasts displayed significantly increased levels of lysosome-associated membrane protein 1 (LAMP1), a *bona fide* marker of the endo-lysosomal compartment, upon Pt treatment (**Figures 1A,C**). This result was confirmed by immunostaining analysis, showing increased LAMP1-positive signal in fibroblasts upon Pt treatment, when compared to vehicle-treated cells (**Figure 1D**). When autophagy is activated, the co-localization of autophagosomes with lysosomes reflects the trafficking and degradation of autophagic cargoes. As expected, Pt-treated fibroblasts showed a distinctive increase in the number of LC3B-positive puncta, with extensive co-localization with LAMP1, especially in the perinuclear regions (**Figure 1D**). Taken together, these data show that Pt is able to induce autophagic flux in primary fibroblast cultures.

In order to evaluate the ability of Pt to induce autophagy *in vivo*, we treated wild-type mice with a single administration of Pt or vehicle via oral gavage and collected skeletal muscles 8 h later. Autophagic flux was assessed by i.p. injection of colchicine, a commonly used alkaloid able to prevent microtubule polymerization (Klionsky et al., 2016). Western blot analysis of protein extracts from TA muscle revealed a significantly higher LC3B lipidation in Pt-treated mice already in basal conditions, without colchicine injection. In addition, enhanced colchicine-dependent LC3B-II accumulation was detectable in Pt-treated mice when compared with vehicle-treated animals (**Figures 1E,F**). Altogether these results indicate that Pt promotes the autophagic flux in skeletal muscle.

Pterostilbene Reactivates the Autophagic Flux of Col6a1$^{-/-}$ Myopathic Mice

Considering that defective regulation of autophagy plays a key role in the muscle pathology of both *Col6a1*$^{-/-}$ mice and patients affected by COL6-related myopathies (Grumati et al., 2010; Castagnaro et al., 2016), and that its reactivation leads to beneficial effects (Chrisam et al., 2015; Castagnaro et al., 2016), we investigated the effects elicited by Pt administration to *Col6a1*$^{-/-}$ mice. Western blot analysis for LC3B lipidation showed that a single Pt treatment by oral gavage was able to elicit a robust increase in LC3B-II protein content in TA muscle of COL6-deficient mice (**Supplementary Figure S1**). Based on these data, we lengthened the treatment time, in order to allow for muscle remodeling and unravel any phenotypic amelioration.

Autophagic flux analysis on skeletal muscle of *Col6a1*$^{-/-}$ mice treated with Pt by oral gavage for 5 days revealed strong upregulation of autophagy. Indeed, western blotting on protein extracts from TA muscles showed a significantly higher colchicine-dependent accumulation of LC3B-II in *Col6a1*$^{-/-}$ mice treated with Pt when compared to vehicle-treated *Col6a1*$^{-/-}$ animals (**Figure 2A**). As expected, vehicle-treated *Col6a1*$^{-/-}$ mice did not display colchicine-dependent LC3B-II accumulation (**Figure 2A**), in agreement with the previously described autophagy impairment (Grumati et al., 2010). Together with increased LC3B lipidation, Pt-treated *Col6a1*$^{-/-}$ mice showed a significant decrease in p62/SQSTM1 protein levels when compared to vehicle-treated animals (**Figure 2B**), coherently with the higher degradation rate of this autophagic receptor. Conversely, following autophagy flux blockade with colchicine, a significant accumulation of p62/SQSTM1 protein was detectable only in samples from mice treated

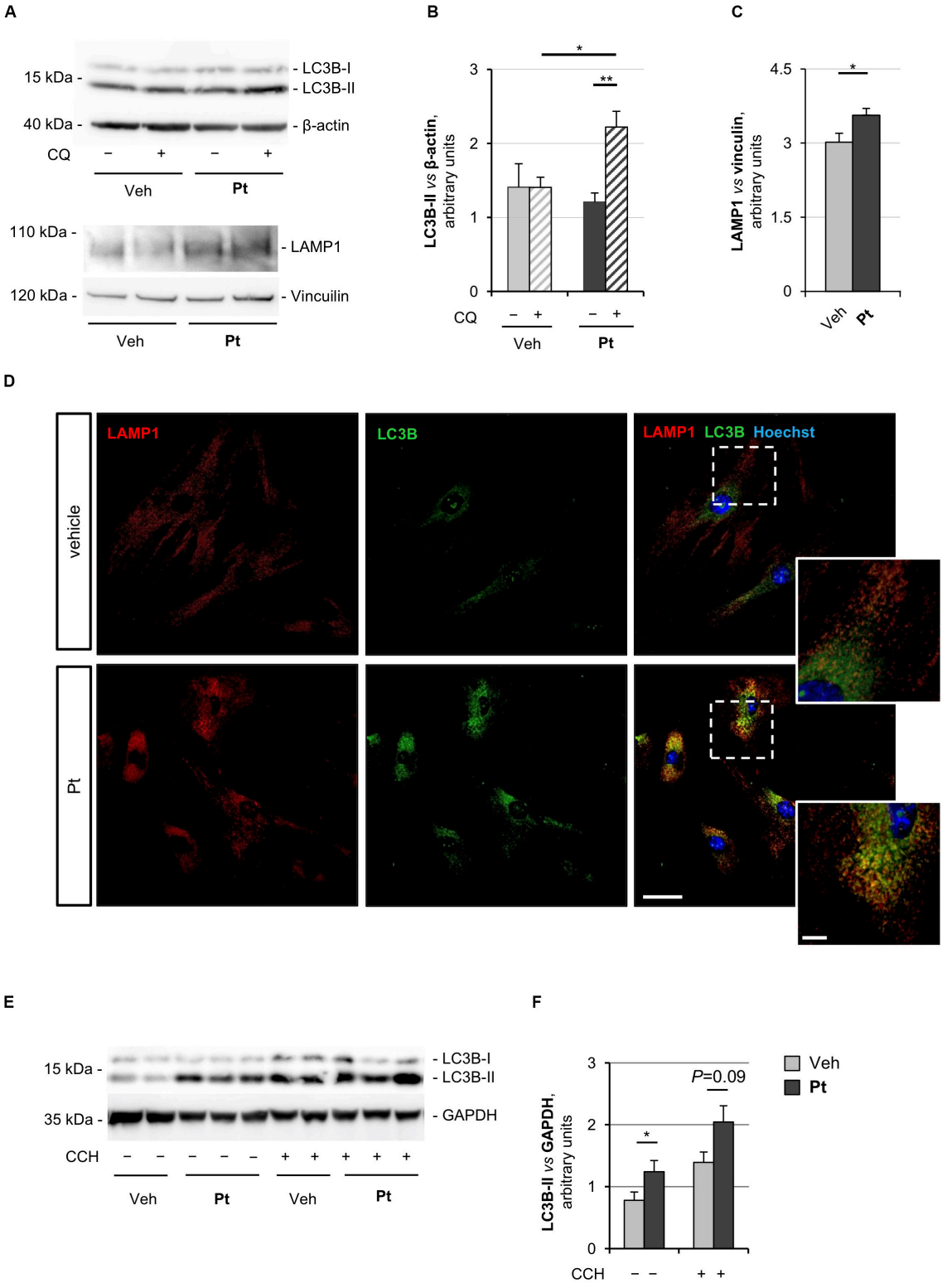

FIGURE 1 | Pterostilbene treatment elicits autophagy in primary dermal fibroblasts and in skeletal muscle of wild-type mice. **(A)** Western blot analysis for LC3B and LAMP1 in protein extracts of primary dermal fibroblasts from wild-type mice, treated with vehicle or with 15 μM Pt and incubated (+) or not (–) with chloroquine (CQ). β-actin and vinculin were used as loading controls. **(B,C)** Densitometric quantifications of LC3B-II vs. β-actin **(B)** and LAMP1 vs. vinculin **(C)**, as determined by at least three independent western blot experiments as in **(A)**. Data are shown as mean ± s.e.m. ($n = 4–6$, each condition; $^*P < 0.05$; $^{**}P < 0.01$). **(D)**

(Continued)

FIGURE 1 | Continued
Immunofluorescence confocal images for LAMP1 (red) and LC3B (green) on primary dermal fibroblast cultures from wild-type mice, treated for 2.5 h with 15 μM Pt or with vehicle. Nuclei were counterstained with Hoechst (blue). The dotted area is shown at higher magnifications on the right. Scale bar, 100 or 10 μm (magnifications). **(E)** Western blot analysis for LC3B in protein extracts of TA muscles from wild-type mice treated with a single oral gavage of vehicle or Pt (90.2 mg/kg body weight) and sacrificed 8 h after the treatment. Autophagic flux was assessed by i.p. injection of colchicine (CCH, +) or physiological solution (–). GAPDH was used as a loading control. **(F)** Densitometric quantification of LC3B-II vs. GAPDH, as determined by at least three independent western blot experiments as in **(E)**. Data are shown as mean ± s.e.m. (n = 3–4, each condition; $^*P < 0.05$). Veh, vehicle.

with Pt (**Figure 2B**), consistently with the upregulation of autophagosome formation revealed by LC3B-II lipidation.

Previous studies demonstrated that *Col6a1*$^{-/-}$ muscles display a down-regulation of the mitophagy mediator BNIP3 (Grumati et al., 2010). Western blot analysis of TA muscle showed a significant increase in BNIP3 protein level in Pt-treated mice compared to the vehicle-treated controls (**Figure 2C**), suggesting that Pt may be able to promote also mitophagy in *Col6a1*$^{-/-}$ muscles. It has been recently demonstrated that the lysosomal compartment is strongly affected in cells lacking COL6 (Castagnaro et al., 2018). TA muscles from Pt-treated *Col6a1*$^{-/-}$ mice showed a significant increase in LAMP1 protein levels when compared to vehicle-treated animals (**Figure 2D**). These findings are in agreement with autophagy upregulation, as an increase in lysosomal content leads to a rapid and efficient autophagosome degradation (Zhou et al., 2013).

The above findings were also confirmed by immunofluorescence microscopy on TA cross-sections, showing a reduction of p62/SQSTM1 puncta and an increase of LAMP1-positive signal in TA sections from Pt-treated *Col6a1*$^{-/-}$ mice when compared to vehicle-treated controls (**Figure 2E**). Altogether, these data indicate that *in vivo* Pt administration leads to an increased rate of autophagosome formation and degradation in the skeletal muscle of autophagy-deficient *Col6a1*$^{-/-}$ mice.

Pterostilbene Remodels COL6-Deficient Skeletal Muscle

To assess whether the autophagy induction promoted by Pt administration is accompanied by skeletal muscle remodeling, we carried out histological and morphometric analyses on muscles from Pt- and vehicle-treated *Col6a1*$^{-/-}$ mice. Five days of Pt treatment led to a significant decrease in the average cross-sectional area and minimum Feret diameter of *Col6a1*$^{-/-}$ myofibers (**Figures 3A–C**). Accordingly, by plotting the distribution of cross-sectional area and minimum Feret diameter among the analyzed myofibers, a shift toward smaller fiber classes was evident in Pt-treated mice (**Figures 3B,C**). These findings support the concept of catabolic effects elicited by Pt in *Col6a1*$^{-/-}$ muscles, in line with robust autophagy induction. On the other side, Pt does not activate an atrophy process mediated by atrogenes, as highlighted by transcript analysis for Murf-1/*Trim63* and Atrogin-1/*Fbxo32* (**Supplementary Figure S2A**). Hematoxylin-eosin staining on TA cross-sections did not reveal any detrimental changes in muscle architecture of Pt-treated mice (**Figure 3D**), and Sirius red staining confirmed that there was no noticeable sign of fibrosis in Pt-treated mice (**Supplementary Figure S2B**). Furthermore, the percentage of centrally nucleated fibers was similar between Pt- and vehicle-treated animals (**Figure 3E**), and was consistent with previously published data for COL6-deficient muscles (Bonaldo et al., 1998). Interestingly, upon 5 days of Pt treatment *Col6a1*$^{-/-}$ muscles displayed a significantly higher number of myofibers per area unit (**Figure 3F**) and this was accompanied by a significant increase of newly formed, eMHC-positive myofibers (**Figure 3G**).

Altogether these results support the concept that Pt treatment promotes myofiber remodeling due to both increased autophagy and enhanced regeneration.

Pterostilbene Treatment Ameliorates the Myopathic Phenotype of Col6a1$^{-/-}$ Mice

Since the above data showed that Pt promotes autophagy *in vivo* and rescues the autophagy impairment of COL6-deficient skeletal muscle, we evaluated whether Pt treatment is able to ameliorate the myopathic phenotype of *Col6a1*$^{-/-}$ mice. Spontaneous myofiber apoptosis is a typical feature of COL6-related myopathies and its amelioration is beneficial both in *Col6a1*$^{-/-}$ murine model and in BM and UCMD patients (Chrisam et al., 2015; Castagnaro et al., 2016). TUNEL assay revealed a significant decrease in the incidence of apoptotic myonuclei in TA of *Col6a1*$^{-/-}$ mice treated for 5 days with Pt (**Figures 4A,B**), thus showing that Pt is able to counteract myofiber apoptosis in COL6-deficient muscle.

Abnormal mitochondria with altered cristae and dilated sarcoplasmic reticulum are distinctive ultrastructural defects of COL6-deficient muscles (Irwin et al., 2003; Grumati et al., 2010). Transmission electron microscopy of TA cross-sections showed that 5 days of Pt treatment led to a strong amelioration of muscle ultrastructure, with a dramatic decrease of mitochondrial swelling and dilated sarcoplasmic reticulum in Pt-treated *Col6a1*$^{-/-}$ mice when compared to vehicle-treated animals (**Figures 4C–H**). Moreover, the muscles of Pt-treated animals displayed autophagic vacuoles and multivesicular bodies (**Figures 4G,H**), supporting autophagy induction and recycling of damaged organelles triggered by Pt administration (Fader and Colombo, 2009). Five-day Pt treatment did not lead to any overt alteration in sarcomeric and sarcolemmal ultrastructure (**Figure 4G** and data not shown).

Altogether these data confirm the beneficial effect of Pt in counteracting the pathogenic hallmarks of *Col6a1*$^{-/-}$ muscles.

DISCUSSION

Autophagy deregulation is linked to the pathogenesis of several disorders, including muscle congenital diseases. In

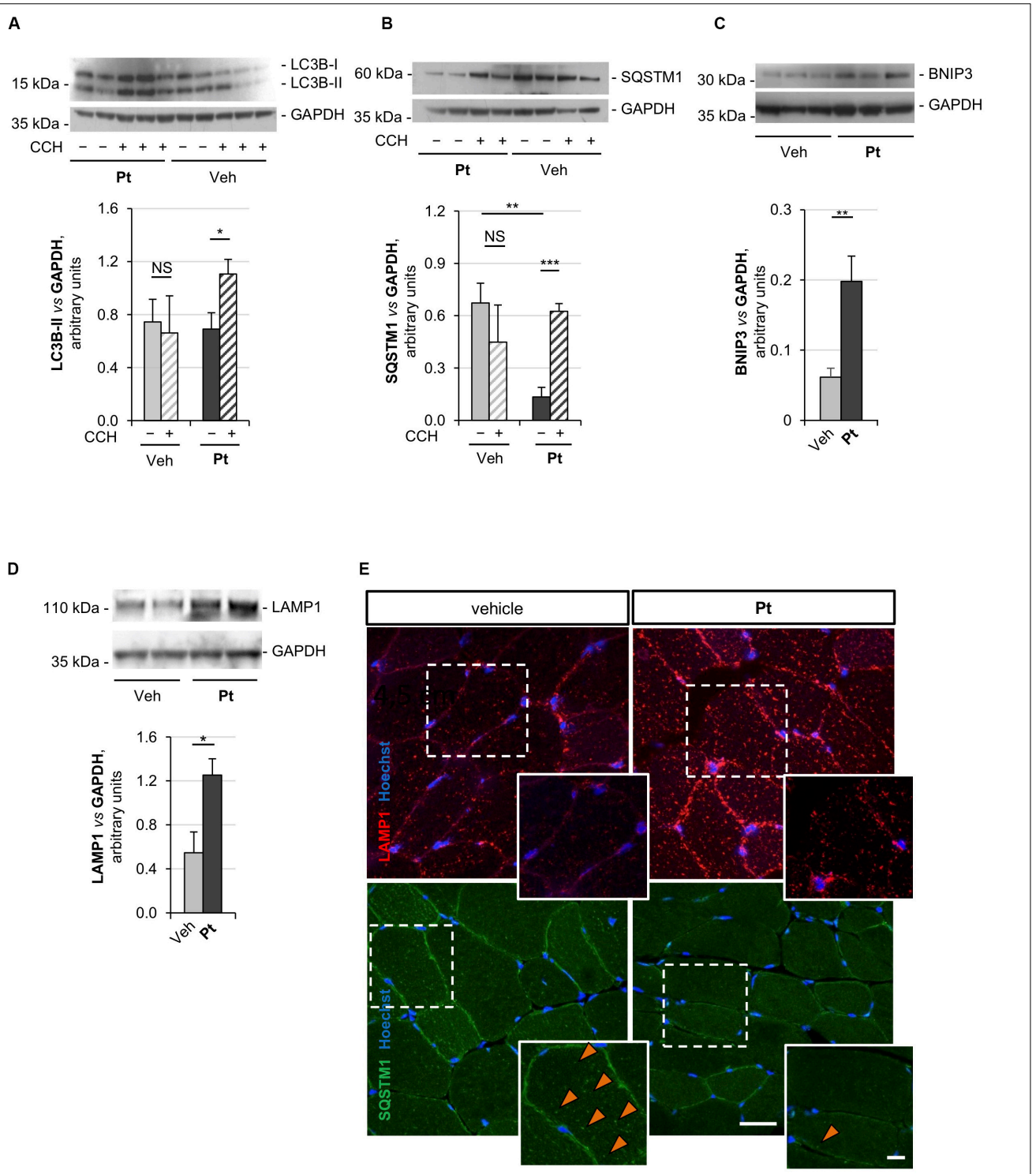

FIGURE 2 | Pterostilbene reactivates the autophagic flux in the skeletal muscle of *Col6a1*$^{-/-}$ mice. **(A–D)** Western blot analysis for LC3B **(A)**, p62/SQSTM1 **(B)**, BNIP3 **(C)**, and LAMP1 **(D)** in protein extracts of TA muscles from *Col6a1*$^{-/-}$ mice treated by oral gavage for 5 days with vehicle or with Pt (90.2 mg/kg body weight). Autophagic flux was determined by i.p. injection of colchicine (CCH, +) or physiological solution (–). GAPDH was used as a loading control. Densitometric quantifications, as determined by at least three independent western blot experiments, are shown in the respective bottom panels. Data are shown as mean ± s.e.m. (n = 4–5, each condition; NS = not significant; *$P < 0.05$; **$P < 0.01$; ***$P < 0.001$). **(E)** Immunofluorescence confocal images for LAMP1 (red) and p62/SQSTM1 (green) in TA cross sections from *Col6a1*$^{-/-}$ mice treated by oral gavage for 5 days with vehicle or with Pt (90.2 mg/kg body weight). Nuclei were counterstained with Hoechst (blue). The dotted area is shown at higher magnifications in the smaller panels. Orange arrowheads indicate p62/SQSTM1-positive puncta. Scale bar, 30 or 10 µm (magnifications). Veh, vehicle.

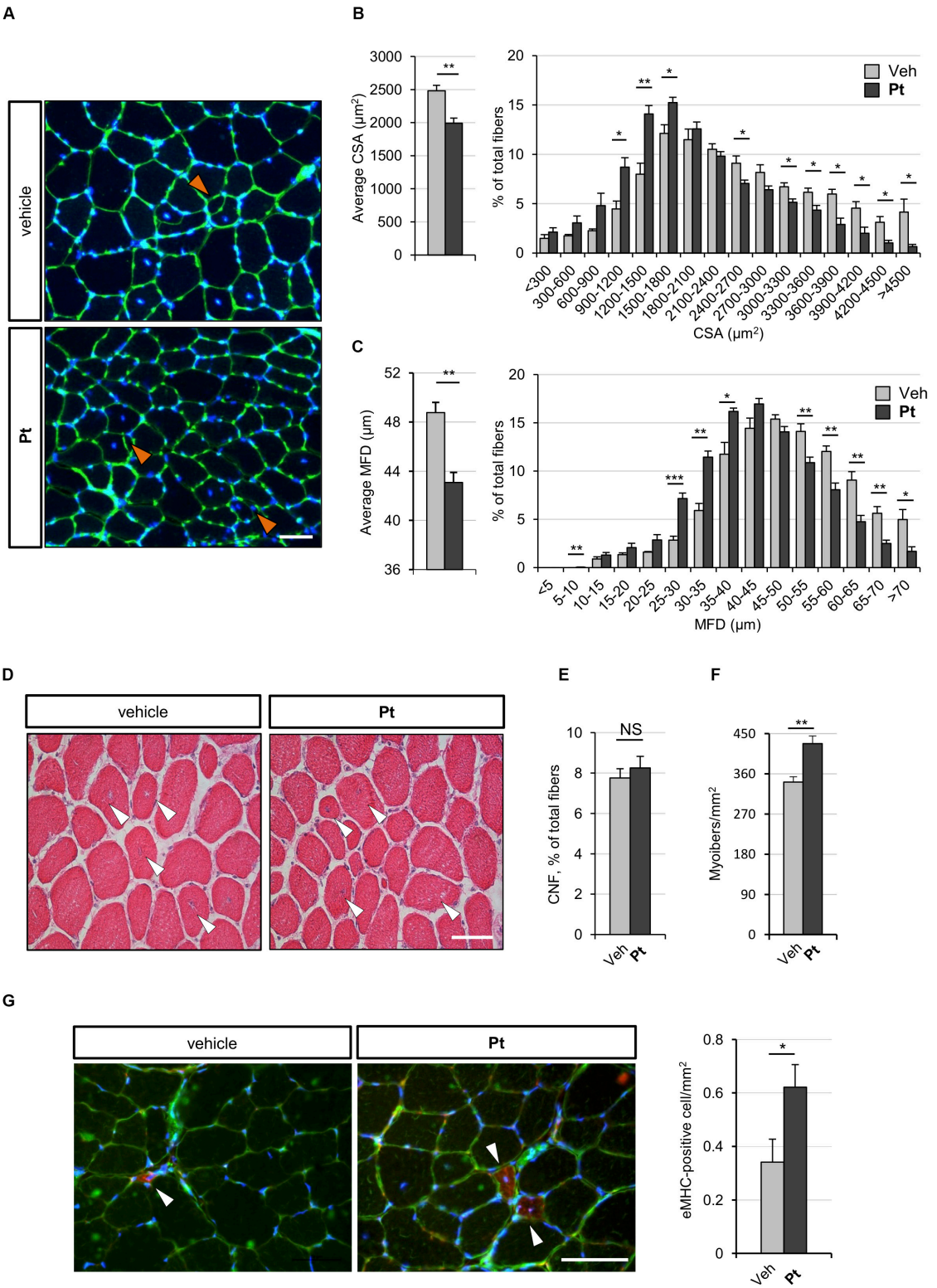

FIGURE 3 | Pterostilbene remodels COL6-deficient skeletal muscle. **(A)** Representative fluorescence microscopy images of TA cross sections of *Col6a1*$^{-/-}$ mice treated by oral gavage for 5 days with vehicle or with Pt (90.2 mg/kg body weight) and stained with fluorophore-conjugated wheat germ agglutinin (WGA, green) and Hoechst (blue). Orange arrowheads indicate tiny fibers. Scale bar, 50 μm. **(B)** Morphometric analysis for average cross-sectional area (left panel) and cross-sectional area distribution among myofibers (right panel), as determined from reconstructed images taken from entire TA muscle cross sections as in **(A)**. Data are shown as

(Continued)

FIGURE 3 | Continued
mean ± s.e.m. (n = 4 mice, each condition; *P < 0.05; **P < 0.01). **(C)** Morphometric analysis for average minimum Feret diameter (left panel) and minimum Feret diameter distribution among myofibers (right panel), as determined from reconstructed images taken from entire TA muscle cross sections as in **(A)**. Data are shown as mean ± s.e.m. (n = 4 mice, each condition; *P < 0.05; **P < 0.01; ***P < 0.001). **(D)** Hematoxylin-eosin staining of TA cross sections from *Col6a1*$^{-/-}$ mice treated by oral gavage for 5 days with vehicle or with Pt (90.2 mg/kg body weight). White arrowheads point at centrally located myonuclei. Scale bar, 50 μm. **(E,F)** Average percentage of centrally nucleated myofibers per muscle section **(E)** and average number of myofibers per unit area **(F)**, as determined on reconstructed images taken from whole TA cross sections as in (**D**). Data are shown as mean ± s.e.m. (n = 4; NS = not significant;**P < 0.01). **(G)** Representative fluorescence microscopy images of TA cross sections of *Col6a1*$^{-/-}$ mice treated by oral gavage for 5 days with vehicle or with Pt (90.2 mg/kg body weight) and stained with antibodies for eMHC (red) and laminin (green). Nuclei were counterstained with Hoechst (blue). White arrowheads indicate eMHC-positive fibers. On the right, quantification of eMHC-positive cells per area unit (in mm^2). Data are shown as mean ± s.e.m. (n = 6; *, P < 0.05). Scale bar, 50 μm. CSA, cross-sectional area; MFD, minimum ferret diameter; Veh, vehicle.

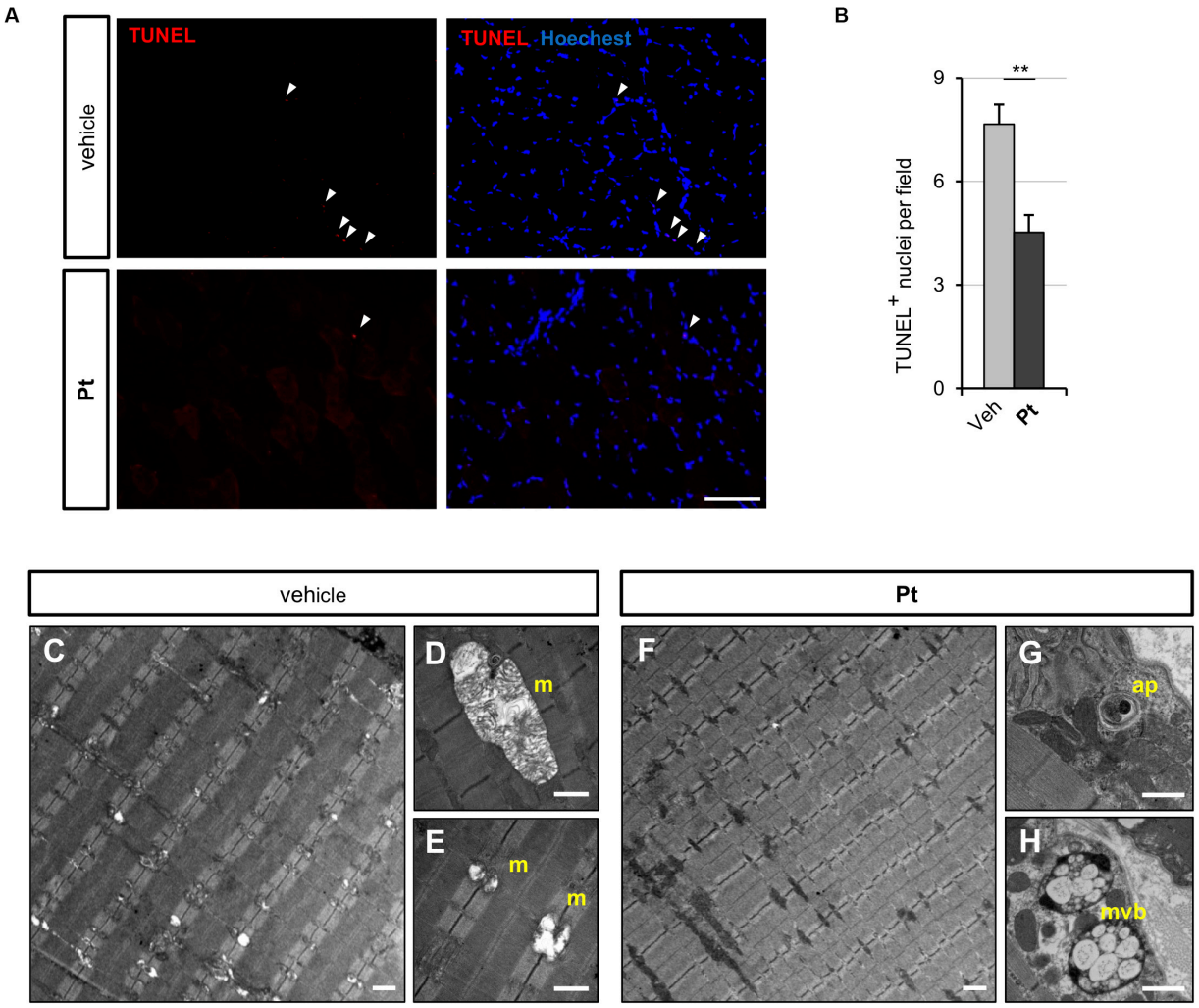

FIGURE 4 | Pterostilbene treatment ameliorates the myopathic phenotype of Col6a1$^{-/-}$ mice. **(A)** Representative fluorescence microscopy images of TA cross sections of Col6a1$^{-/-}$ mice treated for 5 days with vehicle or with Pt (90.2 mg/kg body weight) and stained for apoptotic nuclei (TUNEL assay, red) and Hoechst (blue). White arrowheads indicate TUNEL-positive nuclei. Scale bar, 100 μm. **(B)** Quantification of TUNEL-positive myonuclei in TA cross sections from Col6a1$^{-/-}$ mice treated with by oral gavage for 5 days with vehicle or with Pt (90.2 mg/kg body weight). Data are shown as mean ± s.e.m. (n = 4; **P < 0.01). **(C–H)** Transmission electron microscopy images of TA longitudinal sections from Col6a1$^{-/-}$ mice treated by oral gavage for 5 days with vehicle **(C–E)** or with Pt (90.2 mg/kg body weight) **(F–H)**. Scale bar, 1 μm. ap, autophagosome; m, mitochondrion; mvb, multivesicular body; Veh, vehicle.

Col6a1$^{-/-}$ mice, the best-characterized animal model of COL6-related myopathies, defective regulation of the autophagic process leads to the accumulation of dysfunctional and harmful organelles, which dramatically affects myofiber viability (Grumati et al., 2010). This is exacerbated by impaired muscle regeneration, as COL6 is a key component of the muscle stem cell niche and its absence compromises the self-renewal capability of satellite cells upon muscle injury (Urciuolo et al., 2013).

Two pharmacological approaches have so far been assessed in the preclinical setting, based on rapamycin and cyclosporin A treatments (Grumati et al., 2010; Urciuolo et al., 2013; Gattazzo et al., 2014). The proautophagic and promyogenic properties of these two drugs are well known, but their strong immunosuppressive activity makes them unsuitable for the long-term chronic treatment of patients affected by muscular dystrophies (Merlini et al., 2011). To overcome this unwanted side effect, a drug-free approach, based on a low protein diet, has been tested both in the preclinical setting and in a pilot clinical trial, confirming its beneficial effect in terms of muscle structure and function (Grumati et al., 2010; Castagnaro et al., 2016). However, this dietary regimen requires quite a profound change in food habits and it is not recommended for infants or most severely affected patients.

A promising way to rescue the myopathic phenotype of COL6 deficient mice consists in the administration of nutraceutical autophagy-inducing compounds. Nutraceuticals represent non-toxic molecules, generally found in food, able to provide health benefits and exploitable as a dietary supplement. The polyamine spermidine and the polyphenol resveratrol are among the most characterized ones. Their ability to boost autophagy is well known, as they act as caloric restriction mimetics through different but converging molecular pathways (Morselli et al., 2011). Spermidine was already demonstrated to display beneficial effects in the myopathic *Col6a1*$^{-/-}$ mouse model (Chrisam et al., 2015), however nothing is known about the therapeutic potential of resveratrol in this myopathic condition.

The major aim of the present study was to investigate the ability of Pt, a resveratrol analog characterized by higher bioavailability and chemical stability (Kapetanovic et al., 2011), to promote autophagy in skeletal muscle. Indeed, this stilbenoid was previously shown to have antioxidant and pro-autophagic properties in various pathophysiological conditions (Akinwumi et al., 2018), however no study has ever exploited its effects on autophagy in skeletal muscle. Our data in wild-type mice indicate that Pt exerts a strong promoting effect on the autophagic flux of skeletal muscle already after 8 h from oral administration, suggesting that it has a rapid onset of action, according to the post-translational nature of phagophore nucleation. Based on these data, we moved forward performing a 5-day-long Pt treatment in COL6 null mice, in which autophagy activation in skeletal muscle is resistant even to 24-h fasting (Grumati et al., 2010). Pt strongly reactivates the processes of autophagosome formation and degradation in *Col6a1*$^{-/-}$ mice under fed condition, together with an increase in lysosomal content, thus highlighting the high pro-autophagic efficacy of this stilbenoid molecule. These effects, together with the Pt-induced myofiber regeneration, result in the observed skeletal muscle remodeling in COL6 null mice, manifesting as a decreased myofiber size and an increased number of newly forming myofibers. This suggests a prospective translational relevance for COL6 pathologies, as stimulating myogenesis in COL6-deficient muscles is beneficial both in the *Col6a1*$^{-/-}$ animal model and in UCMD patients (Merlini et al., 2011; Gattazzo et al., 2014).

The high incidence of apoptotic myofibers is a well-characterized feature of COL6-related myopathies (Irwin et al., 2003; Angelin et al., 2007; Merlini and Bernardi, 2008; Grumati et al., 2010). Pt has a remarkable effect in decreasing the incidence of TUNEL-positive nuclei in *Col6a1*$^{-/-}$ muscle, pointing at increased myofiber viability in COL6-deficient muscles following Pt administration. This anti-apoptotic effect of Pt is likely due to the autophagy-mediated clearance of swollen mitochondria and dilated sarcoplasmic reticulum, since a marked recovery of organelle ultrastructure is clearly visible after 5-day Pt treatment. Indeed, it is well known that a compromised mitochondrial network is prone to release several proapoptotic factors, detrimental for cell survival.

Of note, despite the remarkable proautophagic effects of 5-day Pt treatment in COL6 null mice, muscle ultrastructure was positively affected, suggesting that the Pt-promoted induction of the autophagic flux is not excessive, but instead well-tolerated and with a beneficial outcome in COL6 deficient muscles. Future work will allow ascertaining the lowest, but still effective, Pt dosages able to elicit functional outcomes, as muscle strength recovery, in *Col6a1*$^{-/-}$ mice under long-term administration regimens. Furthermore, it will be interesting to exploit the possible synergistic effects of Pt with other drugs or natural compounds, such as non-immunosuppressive cyclosporin A derivatives (Zulian et al., 2014) or spermidine (Chrisam et al., 2015).

Altogether, our findings point at Pt as a promising autophagy-inducing nutraceutical for skeletal muscle, able to counteract the myopathic phenotype of *Col6a1*$^{-/-}$ mice. Indeed, our data indicate that Pt is an excellent nutraceutical with a valuable prospective medical relevance for COL6-related myopathies, as well as for other pathological conditions characterized by an autophagy deficiency, such as Duchenne muscular dystrophy and age-related sarcopenia.

DATA AVAILABILITY STATEMENT

The raw data supporting the conclusions of this article will be made available by the authors, without undue reservation, to any qualified researcher.

ETHICS STATEMENT

The animal study was reviewed and approved by the Animal Ethics Committee of the University of Padova (OPBA); Italian Ministry of Health (license protocol n. 480/2019-PR).

AUTHOR CONTRIBUTIONS

SM and LG conceptualized and performed the experiments, analyzed and interpreted the data, and wrote the manuscript. MC performed muscle autophagy analysis. PBr contributed to mouse treatments. MB and BB contributed to muscle experiments. PBo coordinated the study and contributed to manuscript writing

and revision. ML contributed to mouse treatments. All authors contributed to the article and approved the submitted version.

FUNDING

This work was supported by the Italian Ministry of University and Research (Grants 2015FBNB5Y and 201742SBXA), the Telethon Foundation (Grants GGP14202 and GGP19229), the Cariparo Foundation, and the University of Padova.

ACKNOWLEDGMENTS

We thank Martina La Spina for her involvement in the initial study, Mario Zoratti for providing the Pt powder, and Dario Bizzotto for the maintenance of knockout mouse colonies. We thank all the members of Bonaldo lab for helpful discussions and suggestions.

SUPPLEMENTARY MATERIAL

The Supplementary Material for this article can be found online at: https://www.frontiersin.org/articles/10.3389/fcell.2020.580933/full#supplementary-material

FIGURE S1 | A single bout of pterostilbene induces LC3B lipidation in *Col6a1*$^{-/-}$ mice. Western blot analysis for LC3B (left panel) and relative densitometric quantification (right panel) in protein extracts of TA muscle from *Col6a1*$^{-/-}$ mice treated with a single oral gavage of vehicle or Pt (90.2 mg/kg body weight) and sacrificed 8 h after the treatment. GAPDH was used as a loading control. Data are shown as mean ± s.e.m. (n = 3–4; $^*P < 0.05$). Veh, vehicle.

FIGURE S2 | Pterostilbene remodels COL6-deficient skeletal muscle. **(A)** Quantitative RT-qPCR analysis of mRNA levels for Atrogin1 (*Fbxo32*), MURF-1 (*Trim63*), and Cathepsin L (*Ctsl*) in RNA extracts of TA muscle from *Col6a1*$^{-/-}$ mice treated by oral gavage for 5 days with vehicle or with Pt (90.2 mg/kg body weight). Data are shown as mean ± s.e.m. (n = 5; $^*P < 0.05$). **(B)** Picrosirius-red staining of TA cross sections from *Col6a1*$^{-/-}$ mice treated by oral gavage for 5 days with vehicle or with Pt (90.2 mg/kg body weight). Scale bar, 50 μm. Veh, vehicle.

REFERENCES

Akinwumi, B. C., Kimberly, A. M., and Hope, D. A. (2018). Biological activities of stilbenoids. *Int. J. Mol. Sci.* 19:792. doi: 10.3390/ijms19030792

Angelin, A., Tiepolo, T., Sabatelli, P., Grumati, P., Bergamin, N., Golfieri, C., et al. (2007). Mitochondrial dysfunction in the pathogenesis of Ullrich congenital muscular dystrophy and prospective therapy with cyclosporins. *Proc. Natl. Acad. Sci. U.S.A.* 104, 991–996. doi: 10.1073/pnas.0610270104

Azzolini, M., La Spina, M., Mattarei, A., Paradisi, C., Zoratti, M., and Biasutto, L. (2014). Pharmacokinetics and tissue distribution of pterostilbene in the rat. *Mol. Nutr. Food Res.* 58, 2122–2132. doi: 10.1002/mnfr.201400244

Bagherniya, M., Butler, A. E., Barreto, G. E., and Sahebkar, A. (2018). The effect of fasting or calorie restriction on autophagy induction: a review of the literature. *Ageing Res. Rev.* 47, 183–197. doi: 10.1016/j.arr.2018.08.004

Bonaldo, P., Braghetta, P., Zanetti, M., Piccolo, S., Volpin, D., and Bressan, G. M. (1998). Collagen VI deficiency induces early onset myopathy in the mouse: an animal model for Bethlem myopathy. *Hum. Mol. Genet.* 7, 2135–2140. doi: 10.1093/hmg/7.13.2135

Bonaldo, P., and Sandri, M. (2013). Cellular and molecular mechanism of muscle atrophy. *Dis. Model Mech.* 6, 25–39. doi: 10.1242/dmm.010389

Bönnemann, C. G. (2011). The collagen VI-related myopathies: muscle meets its matrix. *Nat. Rev. Neurol* 7, 379–390. doi: 10.1038/nrneurol.2011.81

Castagnaro, S., Chrisam, M., Cescon, M., Braghetta, P., Grumati, P., and Bonaldo, P. (2018). Extracellular collagen VI has prosurvival and autophagy instructive properties in mouse fibroblasts. *Front. Physiol.* 9:1129. doi: 10.3389/fphys.2018.01129

Castagnaro, S., Pellegrini, C., Pellegrini, M., Chrisam, M., Sabatelli, P., Toni, S., et al. (2016). Autophagy activation in COL6 myopathic patients by a low-protein-diet pilot trial. *Autophagy* 12, 2484–2495. doi: 10.1080/15548627.2016.1231279

Castets, P., Frank, S., Sinnreich, M., and Rüegg, M. A. (2016). "Get the balance right": pathological significance of autophagy perturbation in neuromuscular disorders. *J. Neuromuscul. Dis.* 3, 127–155. doi: 10.3233/JND-160153

Cescon, M., Gattazzo, F., Chen, P., and Bonaldo, P. (2015). Collagen VI at a glance. *J. Cell Sci.* 128, 3525–3531. doi: 10.1242/jcs.169748

Chrisam, M., Pirozzi, M., Castagnaro, S., Blaauw, B., Polishchuck, R., Cecconi, F., et al. (2015). Reactivation of autophagy by spermidine ameliorates the myopathic defects of collagen VI-null mice. *Autophagy.* 11, 2142–2152. doi: 10.1080/15548627.2015.1108508

De Palma, C., Morisi, F., Chel, S., Pambianco, S., Cappello, V., Vezzoli, M., et al. (2012). Autophagy as a new therapeutic target in Duchenne muscular dystrophy. *Cell Death Dis.* 3:e418. doi: 10.1038/cddis.2012.159

Fader, C. M., and Colombo, M. I. (2009). Autophagy and multivesicular bodies: two closely related partners. *Cell Death. Differ.* 16, 70–78. doi: 10.1038/cdd.2008.168

Fetalvero, K. M., Yu, Y., Goetschkes, M., Liang, G., Valdez, R. A., Gould, T., et al. (2013). Defective autophagy and mTORC1 signaling in myotubularin null mice. *Mol. Cell. Biol.* 33, 98–110. doi: 10.1128/MCB.01075-12

Gattazzo, F., Molon, S., Morbidoni, V., Braghetta, P., Blaauw, B., Urciuolo, A., et al. (2014). Cyclosporin A promotes in vivo myogenic response in collagen VI-deficient myopathic mice. *Front Aging Neurosci.* 6:244. doi: 10.3389/fnagi.2014.00244

Gómez-Zorita, S., Fernandez-Quintela, A., Aguirre, L., Macarulla, M. T., Rimando, A. M., Portillo, M. P., et al. (2015). Pterostilbene improves glycaemic control in rats fed an obesogenic diet: involvement of skeletal muscle and liver. *Food Funct.* 6, 1968–1976. doi: 10.1039/c5fo00151j

Grumati, P., and Bonaldo, P. (2012). Autophagy in skeletal muscle homeostasis and in muscular dystrophies. *Cells* 1, 325–345. doi: 10.3390/cells1030325

Grumati, P., Coletto, L., Sabatelli, P., Cescon, M., Angelin, A., Bertaggia, E., et al. (2010). Autophagy is defective in Collagen VI muscular dystrophies and its reactivation rescues myofiber degeneration. *Nat. Med.* 16, 1313–1320. doi: 10.1038/nm.2247

Huynh, K. K., Eskelinen, E. L., Scott, C. C., Malevanets, A., Saftig, P., and Grinstein, S. (2007). LAMP proteins are required for fusion of lysosomes with phagosomes. *EMBO J.* 26, 313–324. doi: 10.1038/sj.emboj.7601511

Irwin, A., Bergamin, N., Sabatelli, P., Reggiani, C., Meginghian, A., Merlini, L., et al. (2003). Mitochondrial dysfunction and apoptosis in myopathic mice with collagen VI dseficiency. *Nat. Genet.* 35, 367–371. doi: 10.1038/ng1270

Ju, J. S., Varadhachary, A. S., Miller, S. E., and Weihl, C. C. (2010). Quantitation of "autophagic flux" in mature skeletal muscle. *Autophagy* 6, 929–935. doi: 10.4161/auto.6.7.12785

Kapetanovic, I. M., Muzzio, M., Huang, Z., Thompson, T. N., and McCormick, D. L. (2011). Pharmacokinetics, oral bioavailability, and metabolic profile of resveratrol and its dimethylether analog, pterostilbene, in rats. *Cancer Chemother. Pharmacol.* 68, 593–601. doi: 10.1007/s00280-010-1525-4

Klionsky, D. J., Abdelmohsen, K., Abe, A., Abedin, M. D., Abeliovich, H., Acevedo Arozena, A., et al. (2016). Guidelines for the use and interpretation of assays for monitoring autophagy (3rd Edition). *Autophagy* 12, 1–222. doi: 10.1080/15548627.2015.1100356

Kosuru, R., Rai, U., Prakash, S., Singh, A., and Singh, S. (2016). Promising therapeutic potential of pterostilbene and its mechanistic insight based on preclinical evidence. *Eur. J. Pharmacol.* 789, 229–243. doi: 10.1016/j.ejphar.2016.07.046

Lee, Y. H., Chen, Y. Y., Yeh, Y. L., Wang, Y. J., and Chen, R. J. (2019). Stilbene compounds inhibit tumor growth by the induction of cellular senescence and

the inhibition of telomerase activity. *Int. J. Mol. Sci.* 20, 2716. doi: 10.3390/ijms20112716

Levine, B., and Kroemer, G. (2008). Autophagy in the pathogenesis of disease. *Cell* 132, 27–42. doi: 10.1016/j.cell.2007.12.018

Ma, Z., Zhang, X., Xu, L., Liu, D., Di, S., Li, W., et al. (2019). Pterostilbene: mechanisms of its action as oncostatic agent in cell models and in vivo studies. *Pharmacol. Res.* 145:104265. doi: 10.1016/j.phrs.2019.104265

Madeo, F., Carmona-Gutierrez, D., Hofer, S. J., and Kroemer, G. (2019). Caloric restriction mimetics against age-associated disease: targets, mechanisms, and therapeutic potential. *Cell Metab.* 29, 592–610. doi: 10.1016/j.cmet.2019.01.018

Madeo, F., Eisenberg, T., Pietrocola, F., and Kroemer, G. (2018). Spermidine in health and disease. *Science* 359:eaan2788. doi: 10.1126/science.aan2788

Maiuri, M. C., and Kroemer, G. (2019). Therapeutic modulation of autophagy: which disease comes first? *Cell Death Differ.* 26, 680–689. doi: 10.1038/s41418-019-0290-0

Merlini, L., and Bernardi, P. (2008). Therapy of collagen VI-related myopathies (Bethlem and Ulrich). *Neurotherapeutics* 5, 613–618. doi: 10.1016/j.nurt.2008.08.004

Merlini, L., Sabatelli, P., Armaroli, A., Gnudi, S., Angelin, A., Grumati, P., et al. (2011). Cyclosporine A in Ullrich congenital muscular dystrophy: long-term results. *Oxid. Med. Cell Longev.* 2011:139194. doi: 10.1155/2011/139194

Mizushima, N. (2007). Autophagy: process and function. *Genes Dev.* 21, 2861–2873. doi: 10.1101/gad.1599207

Morselli, E., Marino, G., Bennetzen, M. V., Eisenberg, T., Megalou, E., Schroeder, S., et al. (2011). Spermidine and resveratrol induce autophagy by distinct pathways converging on the acetylproteome. *J. Cell Biol.* 192, 615–629. doi: 10.1083/jcb.201008167

Roupe, K., Connie, R., Jaime, Y., and Davies, N. (2006). Pharmacometrics of stilbenes: seguing towards the clinic. *Curr. Clin. Pharmacol.* 1, 81–101. doi: 10.2174/157488406775268246

Rubinsztein, D. C., Codogno, P., and Levine, B. (2012). Autophagy modulation as a potential therapeutic target for diverse diseases. *Nat. Rev. Drug Discov.* 11, 709–730. doi: 10.1038/nrd3802

Schiaffino, S., Dyar, K. A., Ciciliot, S., Blaauw, B., and Sandri, M. (2013). Mechanisms regulating skeletal muscle growth and atrophy. *FEBS J.* 280, 4294–4314. doi: 10.1111/febs.12253

Schneider, C. A., Rasband, W. S., and Eliceiri, K. W. (2012). NIH Image to ImageJ: 25 year of image analysis. *Nat. Methods* 9, 671–675. doi: 10.1038/nmeth.2089

Smith, L. R., and Barton, E. R. (2014). SMASH - Semi-automatic muscle analysis using segmentation of histology: a MATLAB application. *Skelet Muscle.* 4:21. doi: 10.1186/2044-5040-4-21

Spitali, P., Grumati, P., Hiller, M., Chrisam, M., Aartsma-Rus, A., and Bonaldo, P. (2013). Autophagy is impaired in the tibialis anterior of dystrophin null mice. *PLoS Curr* 5, doi: 10.1371/currents.md.e1226cefa851a2f079bbc406c0a21e80

Takashima, A. (2001). Establishment of fibroblast cultures. *Curr. Prot. Cell Biol.* 1:2. doi: 10.1002/0471143030.cb0201s00

Tastekin, B., Pelit, A., Polat, S., Tuli, A., Sencar, L., Alparslan, M. M., et al. (2018). Therapeutic potential of pterostilbene and resveratrol on biomechanic, biochemical, and histological parameters in streptozotocin-induced diabetic rats. *Evid. Based Comp. Alternat. Med.* 9012352, 1–10. doi: 10.1155/2018/9012352

Urciuolo, A., Quarta, M., Morbidoni, V., Gattazzo, F., Molon, S., Grumati, P., et al. (2013). Collagen VI regulates satellite cell self-renewal and muscle regeneration. *Nat. Commun.* 4:1964. doi: 10.1038/ncomms2964

Zheng, J., Liu, W., Zhu, X., Ran, L., Lang, H., Yi, L., et al. (2020). Pterostilbene enhances endurance capacity via promoting skeletal muscle adaptations to exercise training in rats. *Molecules* 25:186. doi: 10.3390/molecules25010186

Zhou, J., Tan, S. H., Nicolas, V., Bauvy, C., Yang, N. D., Zhang, J., et al. (2013). Activation of lysosomal function in the course of autophagy via mTORC1 suppression and autophagosome-lysosome fusion. *Cell Res.* 23, 508–523. doi: 10.1038/cr.2013.11

Zulian, A., Rizzo, E., Schiavone, M., Palma, E., Tagliavini, F., Blaauw, B., et al. (2014). NIM811, a cyclophilin inhibitor without immunosuppressive activity, is beneficial in collagen VI congenital muscular dystrophy models. *Hum. Mol. Genet.* 23, 5353–5363. doi: 10.1093/hmg/ddu254

Conflict of Interest: The authors declare that the research was conducted in the absence of any commercial or financial relationships that could be construed as a potential conflict of interest.

frontiers in Cell and Developmental Biology

CORRECTION
published: 07 January 2021
doi: 10.3389/fcell.2020.615542

Corrigendum: The Polyphenol Pterostilbene Ameliorates the Myopathic Phenotype of Collagen VI Deficient Mice via Autophagy Induction

Samuele Metti[1†], *Lisa Gambarotto*[1†], *Martina Chrisam*[1], *Martina La Spina*[2], *Martina Baraldo*[2], *Paola Braghetta*[1], *Bert Blaauw*[2,3] *and Paolo Bonaldo*[1,4*]

[1] Department of Molecular Medicine, University of Padova, Padua, Italy, [2] Department of Biomedical Sciences, University of Padova, Padua, Italy, [3] Venetian Institute of Molecular Medicine, Padua, Italy, [4] CRIBI Biotechnology Center, University of Padova, Padua, Italy

Keywords: skeletal muscle, autophagy, muscle remodeling, congenital muscular dystrophies, nutraceutical agent, Collagen VI

OPEN ACCESS

Approved by:
Frontiers Editorial Office, Frontiers Media SA, Switzerland

***Correspondence:**
Paolo Bonaldo
bonaldo@bio.unipd.it

[†] *These authors have contributed equally to this work*

Specialty section:
This article was submitted to Cell Death and Survival, a section of the journal Frontiers in Cell and Developmental Biology

Received: *09 October 2020*
Accepted: *10 December 2020*
Published: *07 January 2021*

Citation:
Metti S, Gambarotto L, Chrisam M, La Spina M, Baraldo M, Braghetta P, Blaauw B and Bonaldo P (2021) Corrigendum: The Polyphenol Pterostilbene Ameliorates the Myopathic Phenotype of Collagen VI Deficient Mice via Autophagy Induction. Front. Cell Dev. Biol. 8:615542. doi: 10.3389/fcell.2020.615542

A Corrigendum on

The Polyphenol Pterostilbene Ameliorates the Myopathic Phenotype of Collagen VI Deficient Mice via Autophagy Induction

by Metti, S., Gambarotto, L., Chrisam, M., La Spina, M., Baraldo, M., Braghetta, P., et al. (2020). Front. Cell Dev. Biol. 8:580933. doi: 10.3389/fcell.2020.580933

"Martina La Spina" was not included as an author in the published article. The corrected Author Contributions Statement appears below.

"SM and LG conceptualized and performed the experiments, analyzed and interpreted the data, and wrote the manuscript. MC performed muscle autophagy analysis. PBr contributed to mouse treatments. MB and BB contributed to muscle experiments. PBo coordinated the study and contributed to manuscript writing and revision. ML contributed to mouse treatments. All authors contributed to the article and approved the submitted version."

The authors apologize for this error and state that this does not change the scientific conclusions of the article in any way. The original article has been updated.

frontiers in Cell and Developmental Biology

ORIGINAL RESEARCH
published: 05 November 2020
doi: 10.3389/fcell.2020.580072

High Expression of miR-204 in Chicken Atrophic Ovaries Promotes Granulosa Cell Apoptosis and Inhibits Autophagy

*Zhifu Cui[1], Lingbin Liu[2], Felix Kwame Amevor[1], Qing Zhu[1], Yan Wang[1], Diyan Li[1], Gang Shu[3], Yaofu Tian[1] and Xiaoling Zhao[1]**

[1] Farm Animal Genetic Resources Exploration and Innovation Key Laboratory of Sichuan Province, Sichuan Agricultural University, Chengdu, China, [2] College of Animal Science and Technology, Southwest University, Chongqing, China, [3] Department of Pharmacy, College of Veterinary Medicine, Sichuan Agricultural University, Chengdu, China

Chicken atrophic ovaries have decreased volume and are indicative of ovarian failure, presence of a tumor, or interrupted ovarian blood supply. Ovarian tumor is accompanied by an increase in follicular atresia, granulosa cell (GC) apoptosis, and autophagy. In a previous study, we found using high throughput sequencing that miR-204 is highly expressed in chicken atrophic ovaries. Thus, in the present study, we further investigated its function in GC apoptosis and autophagy. We found that overexpression of miR-204 reduced mRNA and protein levels of proliferation-related genes and increased apoptosis-related genes. Cell counting kit-8 (CCK-8), 5-ethynyl-2-deoxyuridine (EdU), and flow cytometry assays revealed that miR-204 inhibited GC proliferation and promoted apoptosis. Furthermore, we confirmed with reporter gene assays that *Forkhead box K2* (*FOXK2*) was directly targeted by miR-204. FOXK2, as a downstream regulator of phosphoinositide 3-kinase (PI3K)/AKT/mammalian target of rapamycin (mTOR) signal pathways, promoted GC proliferation and inhibited apoptosis. Subsequently, we observed that miR-204 was involved in GC autophagy by targeting *Transient Receptor Potential Melastatin 3* (*TRPM3*). The luciferase activities of the two binding sites of TRPM3 were decreased in response to treatment with a miR-204 mimic, and the autophagic flux was increased after miR-204 inhibition. However, overexpression of miR-204 had opposite results in autophagosomes and autolysosomes. miR-204 inhibits GC autophagy by suppressing the protein expression of TRPM3/AMP-activated protein kinase (AMPK)/ULK signaling pathway components. Inhibition of miR-204 enhanced autophagy by accumulating and degrading the protein levels of LC3-II (Microtubule Associated Protein Light Chain 3B) and p62 (Protein of 62 kDa), respectively, whereas miR-204 overexpression was associated with contrary results. Immunofluorescence staining showed that there was a significant reduction in the fluorescent intensity of LC3B, whereas p62 protein was increased after TRPM3 silencing. Collectively, our results indicate that miR-204 is highly expressed in chicken atrophic ovaries, which promotes GC apoptosis *via* repressing FOXK2 through the PI3K/AKT/mTOR pathway and inhibits autophagy by impeding the TRPM3/AMPK/ULK pathway.

Keywords: chicken, atrophic ovary, miR-204, apoptosis, autophagy, signaling pathway

OPEN ACCESS

Edited by:
Konstantinos Zarbalis, University of California, United States

Reviewed by:
Shaochun Yuan, Sun Yat-sen University, China
Yan Wu, Sun Yat-sen University, China

****Correspondence:***
Xiaoling Zhao
zhaoxiaoling@sicau.edu.cn

Specialty section:
This article was submitted to Cell Death and Survival, a section of the journal Frontiers in Cell and Developmental Biology

Received: *04 July 2020*
Accepted: *12 October 2020*
Published: *05 November 2020*

Citation:
Cui Z, Liu L, Kwame Amevor F, Zhu Q, Wang Y, Li D, Shu G, Tian Y and Zhao X (2020) High Expression of miR-204 in Chicken Atrophic Ovaries Promotes Granulosa Cell Apoptosis and Inhibits Autophagy. Front. Cell Dev. Biol. 8:580072. doi: 10.3389/fcell.2020.580072

INTRODUCTION

The ovary plays vital roles in female reproductive performance (Castagna et al., 2004; Gethoffer et al., 2018; Zhao et al., 2018) by promoting ovulation (exocrine function) and hormone secretion (endocrine function) (Sirotkin et al., 2018; Zangirolamo et al., 2018; Russell, 2019). The ovary is an ideal model for the study of ovarian biology and follicular development (Bahr, 1991), and the follicular granulosa cells (GCs) are often regarded as an important marker of follicular development because of their unique structural characteristics and important role in follicular development (Johnson and Woods, 2009). The development and fate of follicles, maturation or atresia, depend on the state of GCs in the follicles. Proliferation of GCs promotes maturation of follicles, while apoptosis led to GC atresia (Matsudaminehata et al., 2006). Abnormal growth and differentiation of GCs cause ovarian diseases, such as premature ovarian failure (Shelling, 2010), polycystic ovarian syndrome (Jiang et al., 2015), and GC tumors (Pilsworth et al., 2018). Atrophic signifies a structure that is shrunken or diminished in size and function. An atrophic ovary has decreased ovarian tissue volume and is indicative of ovarian failure and interrupted ovarian blood supply, which may therefore affect reproduction in animals. In general, an atrophic ovary will not generate or produce healthy eggs and may therefore affect reproduction (Pilsworth et al., 2018).

MicroRNAs (miRNAs) are endogenous 22∼24-nucleotide-long, small non-coding, single-stranded RNAs (Kim, 2005), many of which regulate translation by binding to the 3′-untranslated regions (3′-UTRs) of their target mRNAs to inhibit protein translation (Lee et al., 1993; Bernstein et al., 2001; Bartel, 2004; Chekulaeva and Filipowicz, 2009). Several studies reported that miRNAs are involved in a variety of important cellular biological processes, including cell proliferation, differentiation, and apoptosis (Ambros, 2004; Valadi et al., 2007; Kosaka et al., 2010). In the ovary of different animals, many miRNAs participate in the entire process of ovarian follicle development, including follicle growth, atresia, ovulation, and regulating GC proliferation and apoptosis (Baley and Li, 2012; Kim et al., 2013; Imbar and Eisenberg, 2014). For instance, miR-224 regulated mouse GC proliferation (Yao et al., 2010), while miR-23a was differentially expressed in premature ovarian failure patients and was involved in GC apoptosis (Yang et al., 2012). Meanwhile, let-7 family members were preferentially expressed in the ovary, and let-7g promoted follicular GC apoptosis by targeting transforming growth factor-β1 (TGF-β1) (Zhou et al., 2015). miR-183-96-182 cluster regulates bovine GC proliferation by targeting FOXO1 (Gebremedhn et al., 2016); however, miR-10 family members repressed proliferation and induced apoptosis in ovarian GCs (Jiajie et al., 2017). Some miRNAs, such as miR-21 (Carletti et al., 2010), miR-15a (Sirotkin et al., 2014), miR-383 (Yin et al., 2014), miR-92a (Liu et al., 2014), miR-145 (Yan et al., 2012), and miR-34a (Tu et al., 2014), were reported to regulate GC growth. These findings demonstrate that miRNAs are expressed in the ovary and are actively involved in regulating animal reproduction.

Functions of miR-204 have been linked to many biological processes, including maintenance of joint homeostasis and protection against osteoarthritis (Huang et al., 2019), tumor growth (Mikhaylova et al., 2012), migration and anoikis of cancer cells (Sacconi et al., 2012; Zhang et al., 2013), and autophagy (Xiao et al., 2011; Hall et al., 2014). Recently, we performed a whole-transcriptome analysis of atrophic ovaries in broody chickens and found that miR-204 was differentially expressed between atrophic and normal ovaries (Liu et al., 2018), suggesting that miR-204 regulates ovarian function. Therefore, it is imperative to identify the regulators of miR-204 target genes and their roles in signaling pathways associated with both the development and function of the ovary. This should generate information that can be used for improving reproductive performance by controlling the key factors in the regulatory networks.

MATERIALS AND METHODS

Animals and Sample Collection

Three hundred eighty-day-old chickens were raised at the Animal Breeding Farm, Sichuan Agricultural University (SAU) (Ya'an, China). Each of five egg-laying and broody birds was selected, and tissues were collected including hypothalamus, pituitary, heart, liver, spleen, lung, kidney, gizzard, glandular stomach, ovary, breast muscle, leg muscle, and small intestine. Atrophic ovaries were collected from broody birds and wrapped in foil, snap-frozen in liquid nitrogen, and transferred to a -80°C freezer for further analyses.

The animal experiments were approved by the Institutional Animal Care and Use Committee of Sichuan Agricultural University (Certification No. YCS-B2018102013). All experiments were conducted in accordance with the SAU Laboratory Animal Welfare and Ethics guidelines.

Cell Culture and Transfection

All pre-ovulatory follicles were dissected from the ovary and placed in sterile Hank's balanced salt solution. The GCs of follicles were isolated following the method of Gilbert (Gilbert et al., 1977), and the granular layers were digested using β-II collagenase (BaiTai Biotechnology, Chengdu, China). Cells were filtered with 200 mesh cell sieves and then resuspended in Dulbecco's modified Eagle medium (DMEM) + 10% fetal bovine serum (Gibco, Grand Island, NY, United States) + 0.1% mixture of penicillin–streptomycin (Invitrogen, Carlsbad, CA, United States). GCs were isolated and cultured in the cell culture incubator at 37°C, 5% CO_2, and 95% air saturated humidity for 3 h to ensure cell attachment. Thereafter, the medium was changed to remove non-adherent cells. All cells including GCs were further cultured in the cell culture incubator at 37°C, 5% CO_2, and 95% air saturated humidity, which was followed by medium being changed every 24 h. Afterward, the transfection procedure was performed with *Forkhead box K2* (*FOXK2*) small interfering RNA (Si-FOXK2), *Transient Receptor Potential Melastatin 3* (*TRPM3*) small interfering RNA (Si-TRPM3), and a miR-204 mimic or inhibitor using lipofectamine 3000 reagent (Invitrogen, United States), according

to the manufacturer's directions. Oligonucleotide sequences are provided in **Supplementary Table 1**.

Quantitative Real-Time PCR

Total RNA was extracted from the tissues and cells using TRIzol reagent (Takara, Tokyo, Japan) following the manufacturer's instructions. Quantitative real-time PCR (qRT-PCR) analysis was conducted in reaction volumes of 15 μl containing 1.5 μl of cDNA, 0.3 μl of forward and reverse primers, 6.25 μl of TB Green™ Premix (Takara), and 6.65 μl of DNase/RNase-Free Deionized Water (Tiangen, Beijing, China). Reaction conditions were based on the manufacturer's instructions, and the $2^{-\Delta\Delta Ct}$ method was used to calculate fold changes in gene expression (Livak and Schmittgen, 2001). The β-actin and U6 genes were used as internal controls, and primer sequences are listed in **Supplementary Table 2**.

Protein Extraction and Western Blot Analysis

Protein was extracted from the GCs using commercial protein extraction kits (BestBio Biotech Co., Ltd., Shanghai, China), and bicinchoninic acid kits (BestBio) were used to determine protein concentrations. The protein was denatured at 95°C for 5 min, and the total volume in each well included 16 μl of protein sample and 4 μl of reducing loading buffer (4:1). The protein was successively separated using 5% and 12% sodium dodecyl sulfate (SDS) polyacrylamide gel electrophoresis (Beyotime, Shanghai, China) and transferred to polyvinylidene difluoride membranes activated with methanol. Blocking buffer (Beyotime) was used to block the membranes at room temperature for 1 h, and the following primary antibodies were used to probe the target proteins: anti-FOXK2 [Cell Signaling Technology (CST), United States], cyclin-dependent kinase 2 (CDK2; ABclonal Technology, Wuhan, China), proliferating cell nuclear antigen (PCNA; ABclonal), Bcl-2 (Biorbyt, United Kingdom), caspase-3 (Abcam, Cambridge, United Kingdom), caspase-9 (Bioss, Beijing, China), phosphoinositide 3-kinase (PI3K; Bioss), Akt (CST), mammalian target of rapamycin (mTOR; Zen-Bio, Chengdu, China), TRPM3 (CST), AMP-activated protein kinase (AMPK; Bioss), ULK1 (Sigma Chemical Co., St. Louis, MO, United States), LC3 (CST), p62 (CST), and β-actin (Sigma), all overnight at 4°C. The membranes were rinsed with Wash Buffer (Beyotime), the corresponding secondary antibodies were added, and membranes were incubated for 1.5 h. The antibodies were diluted according to the manufacturer's instructions.

Cell Proliferation Assay

Primary GCs were cultured in 96-well plates. After transfection, cell proliferation was assessed with cell counting kit-8 (CCK-8; MeilunBio, Dalian, China) and a Cell-Light™ 5-ethynyl-2-deoxyuridine (EdU) Kit (RiboBio, Guangzhou, China) according to the manufacturer's protocols. Then, 10 μl of CCK-8 reagent was added to each well and incubated in the cell culture incubator for 2 h after which it was transfected at 12, 24, 36, and 48 h. The optical density (OD) value for each sample was detected with a microplate reader (Thermo Fisher, Varioskan LUX, United States) at 450 nm.

The state of proliferation of the GCs was determined using EdU kits adhering to the guidelines of the manufacturer. After addition of 100 μl of 50 μM EdU to each well, cells were incubated in the cell culture incubator for an additional 3 h. Cells were then washed with phosphate buffered saline (PBS) and then fixed with 4% paraformaldehyde for 30 min. Also, 50 μl of 2 mg/ml glycine was used to neutralize excess aldehyde groups, and 100 μl of 0.5% Triton X-100 PBS was added to increase the cell membrane permeability. Furthermore, 100 μl of Apollo was added, and the cells were subsequently incubated in a dark room at room temperature for 30 min. Afterward, the cells were washed with PBS, and the nucleus was stained with 100 ml of Hoechst 33342 reaction solutions, and then dark room temperature incubation continued for another 30 min. After the final incubation, a fluorescence microscope (DP80; Olympus, Japan) was used to visualize and quantify the numbers of EdU-stained cells. Three fields were randomly selected for statistical analysis.

Cell Apoptosis Analysis

Cells were washed with PBS, and the concentration was adjusted to 10^6 cells/ml. Also, 100 ml of single-cell suspension was centrifuged at 250 *g* for 5 min, and the supernatant solution was discarded, then 20 μl of binding buffer was added for cell resuspension. Subsequently, the cells were stained using 5 μl of Annexin V-FITC (Invitrogen, Australia) for 10 min, and then 10 μl of propidium iodide (PI; Invitrogen) was added for further staining in the dark at room temperature for 5 min. GC apoptosis was analyzed using flow cytometry (CytoFLEX, Backman, United States), and Kaluza 2.1 software was used to analyze the data.

Dual-Luciferase Reporter Assay

DF-1 cell lines of chicken embryo fibroblast cells (DF-1 cells) were cultured with DMEM + 10% fetal bovine serum and seeded in 48-well plates. The cells were co-transfected with plasmid (*FOXK2* 3′UTR wild type or mutant type, *TRPM3* 3′UTR wild type or mutant type) and mimic negative control (NC) or miRNA mimic when cell density coverage reached 70∼80%. After 48 h, we detected luciferase activity using a luciferase reporter assay kit (Promega, Madison, WI, United States), according to the manufacturer's instruction. The tests were conducted in triplicate.

PI3K/AKT/mTOR Pathway Analysis

LY294002 (PI3K inhibitor) and 740Y-P (PI3K activator) were used to test the relationship between PI3K and FOXK2. LY294002 and 740Y-P were purchased from Selleck Chemicals (Houston, Texas, United States) and were preincubated with cells for 2 h (Tu et al., 2018). CCK-8 assay was used to determine the optimum concentration of LY294002 and 740Y-P treatments.

Confocal Microscopy

The extent of an autophagic flux was evaluated with an adenovirus harboring tandem fluorescent mRFP-GFP-LC3

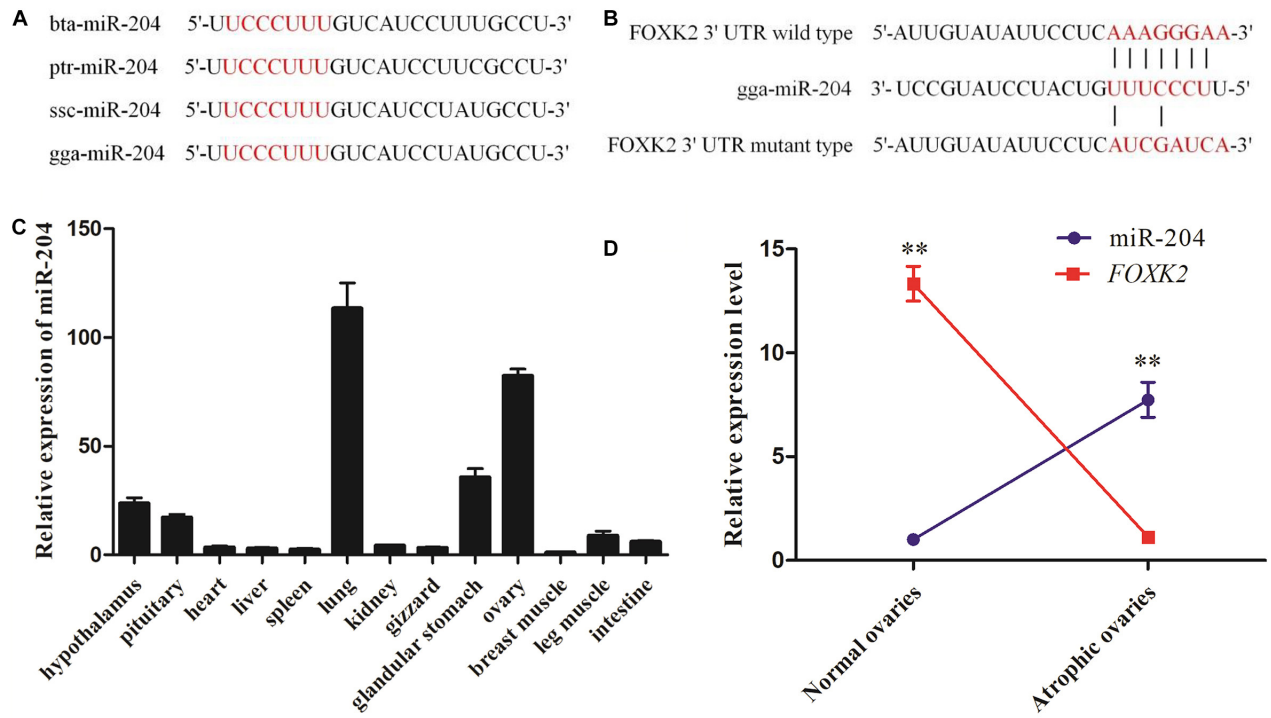

FIGURE 1 | Sequencing characteristics, expression patterns, and target gene prediction of miR-204 in chicken. **(A)** The mature sequence (red characters) of miR-204 among different animal species: gga, chicken; bta, cattle; ptr, chimpanzee; ssc, pig. **(B)** The target position of the miR-204 seed sequence on the gene Forkhead box K2 (FOXK2)-3′-untranslated region (UTR) sequence (red characters) was predicted by TargetScan software. **(C)** The expression patterns of miR-204 in chicken tissues including hypothalamus, pituitary, heart, liver, spleen, lung, kidney, gizzard, glandular stomach, ovary, breast muscle, leg muscle, and intestine. **(D)** The expression levels of miR-204 and *FOXK2* in chicken atrophic ovaries and normal ovaries. Data are presented as mean ± standard error (SE); $n = 5$. miR, microRNA.

(Hanbio, Shanghai, China). Prior to the autophagic flux evaluation, the GCs were cultured on cell slides in six-well plates and transfected with miR-204 mimic and mimic NC or miR-204 inhibitor and inhibitor NC. The adenovirus was later added into the cells for 6–8 h following the manufacturer's instructions. The culture medium was changed, and the GCs were further cultured for 48 h. Thereafter, the GCs were washed with cold PBS and later fixed with 4% paraformaldehyde for 30 min. The GCs were washed again for three consecutive times with PBS, after which they were observed under a confocal microscope (Olympus, Melville, NY, United States).

GCs were transfected with an interference vector (Si-*TRPM3*) and Si-NC. Later, the cells were washed with PBS for 5 min and were further fixed in 4% paraformaldehyde for 10 min. The cells were then washed with PBS, then 0.2% Triton X-100 was added to the cell, and incubation occurred for 10 min in order to ensure permeability of the cell membrane. The cells were washed and incubated with primary antibody rabbit anti-LC3B (CST) and mouse anti-p62 (CST) overnight at 4°C. Thereafter, the cells were washed three times and incubated with fluorescence-labeled secondary antibody in the dark at room temperature for 1 h. The cells were then washed three times in Tris-Buffered Saline Tween-20 (TBST), and then confocal microscopy was used to observe and analyze fluorescence intensity.

Statistical Analysis

Data collected were subjected to statistical analyses using SPSS 20 Statistical software, and the mean of three replicates was evaluated and is displayed as mean ± standard error (SE). Significance was determined using Duncan's multiple range tests and presented as $P < 0.05$ (*) and $P < 0.01$ (**).

RESULTS

Bioinformatics Analysis and Target Gene Prediction of miR-204

Whole-transcriptome sequencing analysis of atrophic ovaries in broody chickens revealed that miR-204 was expressed differentially between atrophic and normal ovaries. The Kyoto Encyclopedia of Genes and Genomes (KEGG) results of target genes revealed that the enriched pathways involved PI3K–Akt signaling, cell cycle, AMPK signaling, and apoptosis. We then found that FOXK2 and TRPM3 are two predicted target genes of miR-204 and are differentially expressed between atrophic and normal ovaries (Liu et al., 2018). After performing a sequence alignment, we found that the seed sequence of chicken miR-204 was conserved with mammals (**Figure 1A**). The seed region of miR-204 was complementary to the 3′UTR of the *FOXK2*

gene, as determined using Targetscan software[1] (**Figure 1B**). Additionally, miR-204 was relatively highly expressed in the chicken ovary (**Figure 1C**). The expression of miR-204 in atrophic ovaries was greater than in normal ovaries, whereas *FOXK2* had an opposite pattern of expression (**Figure 1D**).

miR-204 Inhibits Chicken Granulosa Cell Proliferation

To investigate the function of miR-204 in chicken GC proliferation, a miR-204 overexpression plasmid was transfected into the GCs and its expression level increased (**Figure 2A**), which led to a decrease in the mRNA levels of proliferation-related genes (*CDK2*, *cyclinD1*, and *PCNA*) (**Figure 2E**) and protein abundance of CDK2 and PCNA (**Figures 2G,H**). CCK-8 reagent was used to measure the proliferative state of GCs, and the OD value was significantly decreased after transfection of a miR-204 mimic (**Figure 2C**). In addition, we determined the change in cell numbers by EdU staining. The results indicated that the quantities of EdU-positive cells were reduced in the miR-204 mimic group (**Figures 2I,K**). After transfection of a miR-204 inhibitor, there was a significant decrease in the levels of miR-204 expression (**Figure 2B**), while the mRNA expression of *CDK2*, *cyclinD1*, and *PCNA* increased significantly (**Figure 2F**). However, the protein expressions of PCNA and CDK2 were similar (**Figure 2G**). The CCK-8 assay results showed that there was greater proliferation in response to transfection with the miR-204 inhibitor than the NC inhibitor (**Figure 2D**).

The EdU assay revealed an increase in the number of proliferating cells in response to transfection with a miR-204 inhibitor (**Figures 2I,J**). Overall, these results demonstrate that miR-204 inhibits chicken GC proliferation.

miR-204 Promotes Chicken Granulosa Cell Apoptosis

We investigated the effect of miR-204 on chicken GC apoptosis. We found that apoptosis was promoted by transfecting a miR-204 mimic, which was associated with an increase in the mRNA and cleavage levels of caspase-9 and caspase-3 but decreased expression of Bcl-2 (**Figures 3A,C,D**). The miR-204 inhibitor-treated group showed a different expression trend, where there was a reduction in the expression of caspase-9 and caspase-3 but increase in Bcl-2 expression (**Figures 3B–D**). Flow cytometry revealed an increase in the numbers of apoptotic cells in the miR-204 mimic group compared to the mimic NC (**Figures 3E,F**), whereas the increased apoptotic cell numbers in the miR-204 inhibitor group eventually decreased slightly after miR-204 inhibitor transfection (**Figures 3G,H**). Thus, these results collectively indicate that miR-204 promotes apoptosis in chicken GCs.

miR-204 Targets the FOXK2 Gene

Dual-luciferase reporter gene assays were performed to ascertain the direct target relationship between miR-204 and *FOXK2*. We found that the luciferase activity value of the *FOXK2* wild-type plasmid in the miR-204 group was decreased compared with the mutant-type plasmid (**Figure 4A**). We further analyzed the mRNA and protein expression of FOXK2 in the GCs of chickens after transfection of a miR-204 mimic or miR-204 inhibitor. The results show that there was decreased mRNA (**Figure 4B**) and protein (**Figures 4D,E**) expression of FOXK2 in the miR-204 mimic group. However, the group transfected with miR-204 inhibitor showed a significant increase in the mRNA and protein expression levels of FOXK2 (**Figures 4C–E**). These data demonstrate that FOXK2 is another target gene of miR-204 in chickens.

FOXK2 Promotes Granulosa Cell Proliferation *via* Another PI3K/AKT/mTOR Regulation Pathway

A recent study linked FOXK2 to regulation of liver cellular proliferation and apoptosis *via* the PI3K–Akt pathway (Sakaguchi et al., 2019). In this study, we examined the role of FOXK2 knockdown on chicken GC proliferation and apoptosis. Initially, the mRNA and protein expression of FOXK2 was significantly inhibited after treatment with FOXK2-specific siRNA (**Figures 5A,B**). Then, cells in a proliferation state were identified by CCK-8 and EdU staining, and the numbers of apoptotic cells were determined using flow cytometry. The results showed that Si-*FOXK2* influenced the decline in the OD value and EdU-positive cell numbers in the GCs (**Figures 5C–E**), while the numbers of early apoptotic cells were higher than in Si-NC group (**Figures 5I,J**). Finally, we detected changes in the expression of proliferation-related genes and proapoptotic factors. The results showed that the levels of mRNA and protein expression of caspase-3 and caspase-9 increased significantly, whereas the expression of Bcl-2, PCNA, and CDK2 decreased (**Figures 5F–H**). Thus, FOXK2 promotes the proliferation and inhibits apoptosis of chicken GCs.

Previous research reported that FoxKs translocation to the nucleus is dependent on the PI3K–Akt–mTOR pathway (Sakaguchi et al., 2019). To further explore the role of FOXK2 in the PI3K signaling pathway, a PI3K inhibitor (LY294002) and activator (740Y-P) were used. The optimal concentrations of 740Y-P and LY294002 were tested and found to be 30 μg/ml and 20 μM, respectively (**Figures 6A,B**). The results showed that 740Y-P significantly increased the protein expression of PI3K. Simultaneously, the protein expressions of Akt and mTOR were higher than those in the 740Y-P NC group, which resulted in an increased expression of FOXK2. On the contrary, LY294002 inhibited PI3K and also decreased the protein expression of Akt and mTOR, which led to a reduction in the protein expression of FOXK2 (**Figures 6C,D**). Meanwhile, the protein expression of ULK1 in the 740Y-P group was inhibited, while it was promoted in the LY294002 group. These results revealed that both FOXK2 and ULK1 are downstream regulators of PI3K/Akt/mTOR signal pathways and might be related to cell proliferation and autophagy.

[1] http://www.targetscan.org/vert_72/

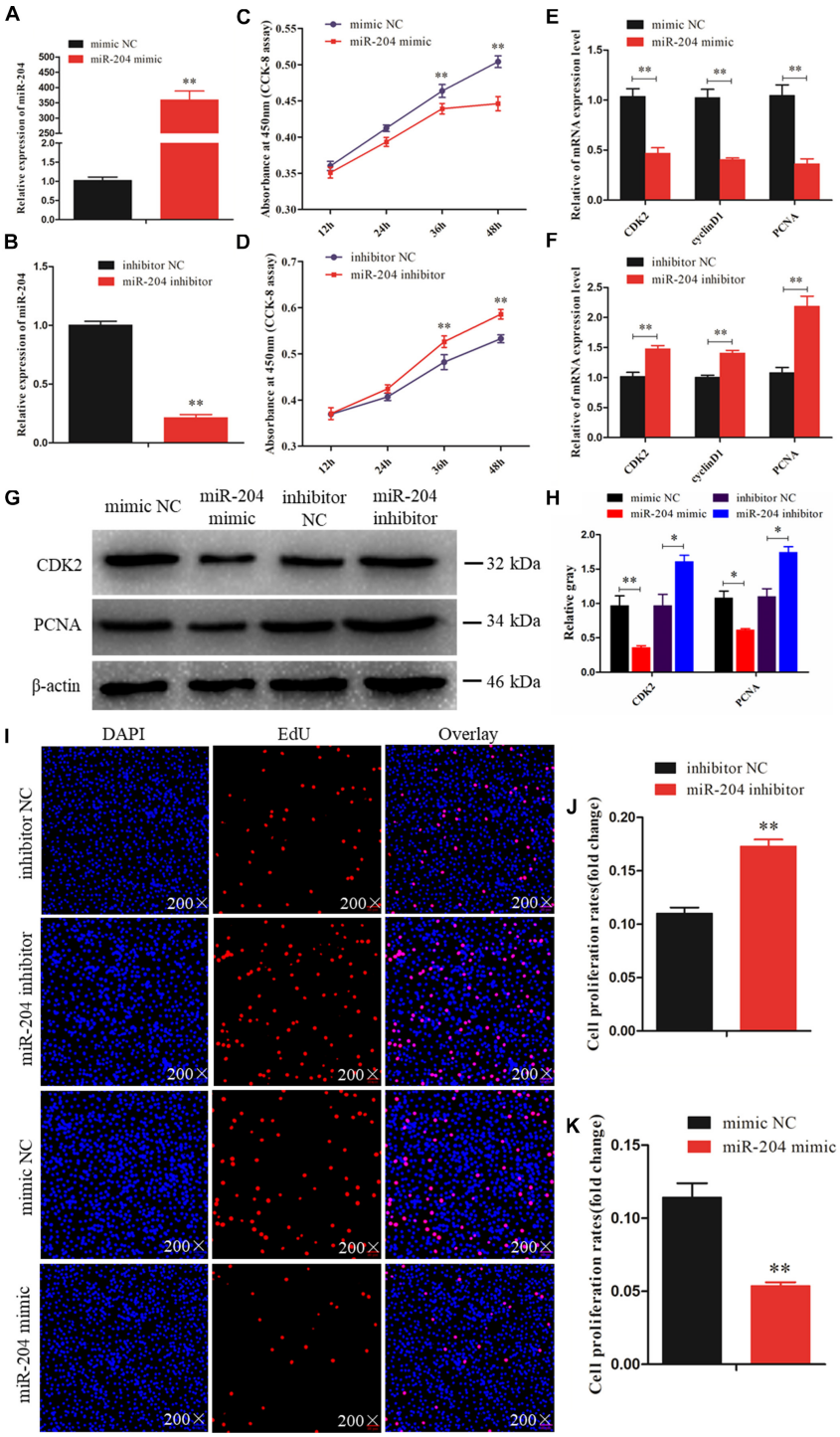

FIGURE 2 | miR-204 regulates the proliferation of chicken granulosa cells (GCs). **(A)** Quantitative real-time PCR (qRT-PCR) was used to determine the miR-204 expression level after transfection of miR-204 overexpression plasmid. **(B)** The miR-204 expression level after transfection of miR-204 inhibition plasmid. **(C)** Cell proliferation curves of chicken GCs were measured with cell counting kit-8 (CCK-8) reagent after overexpression of miR-204. **(D)** Cell proliferation curves of chicken GCs were measured with CCK-8 reagent after inhibition of miR-204. **(E)** Expression abundances of cell proliferation-related genes (*PCNA*, *CDK2*, and *cyclinD1*) were detected by qRT-PCR after overexpression of miR-204. **(F)** Expression levels of cell proliferation-related genes inhibited by miR-204. **(G, H)** The protein expression levels of cell proliferation-related genes [cyclin-dependent kinase 2 (CDK2) and proliferating cell nuclear antigen (PCNA)] were detected by Western blot analysis after a gain or loss of miR-204. β-actin was used as a reference gene. **(I)** 5-Ethynyl-2-deoxyuridine (EdU) staining-positive GCs were detected by EdU kit after overexpression and inhibition of miR-204. **(J, K)** The fold change of GC proliferation rates after overexpression and inhibition of miR-204, respectively. EdU (red), 4′,6-diamidino-2-phenylindole (DAPI) (blue); Replications = 3. Data are presented as mean ± SE; $^{*}P < 0.05$ and $^{**}P < 0.01$. miR, microRNA; NC, negative control.

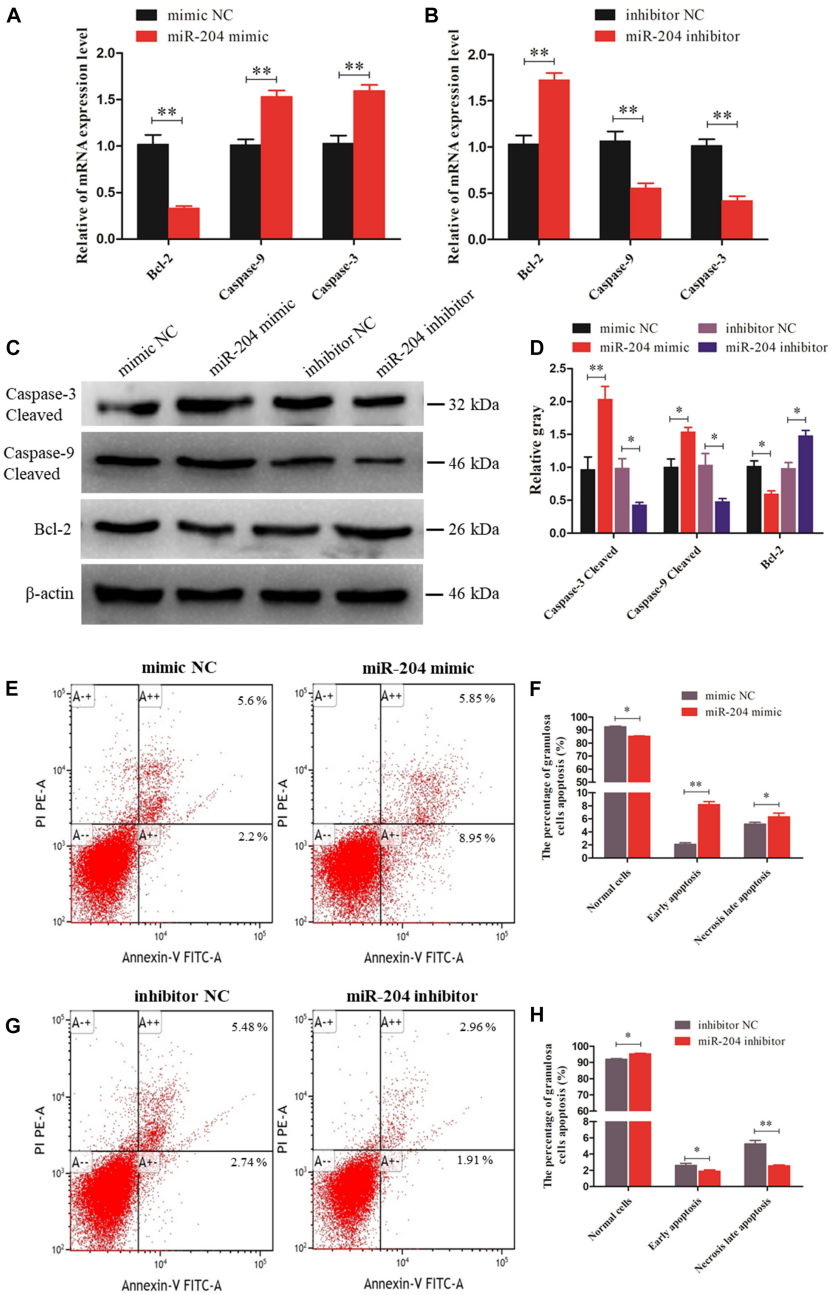

FIGURE 3 | miR-204 regulates the apoptosis of chicken granulosa cells (GCs). **(A, B)** Expression abundances of cell apoptosis-related genes (*Bcl-2*, *Caspase-9*, and *Caspase-3*) were detected by quantitative real-time PCR (qRT-PCR) after overexpression and inhibition of miR-204, respectively. **(C, D)** The Western blot analysis revealed caspase-3 and caspase-9 cleavage and protein expression of Bcl-2 after a gain or loss of miR-204. β-actin was used as a reference gene. **(E)** Apoptotic GCs were detected by annexin V-fluorescein isothiocyanate (FITC)/propidium iodide (PI) staining flow cytometry after overexpression of miR-204. **(F)** The percentages of GC apoptosis were measured after overexpression of miR-204. **(G)** Apoptotic GCs were detected by annexin V-FITC/PI staining flow cytometry being inhibited by miR-204. **(H)** The percentages of GC apoptosis were determined after inhibition of miR-204. Replications = 3. Data are presented as mean ± SE; $^{*}P < 0.05$ and $^{**}P < 0.01$. NC, negative control.

miR-204 Regulates Granulosa Cell Autophagy by Targeting TRPM3

Two predicted miR-204 binding sites in the TRPM3 3′UTR were identified by TargetScan (**Figure 7A**). Dual-luciferase reporter gene assays were used to validate whether miR-204 can directly interact with these two binding sites of TRPM3. The results showed that the luciferase activities of the two binding sites were decreased in response to miR-204 mimic (**Figures 7B,C**). Furthermore, both mRNA and protein expression levels of TRPM3 were increased by miR-204 inhibition (**Figures 7D,F,G**),

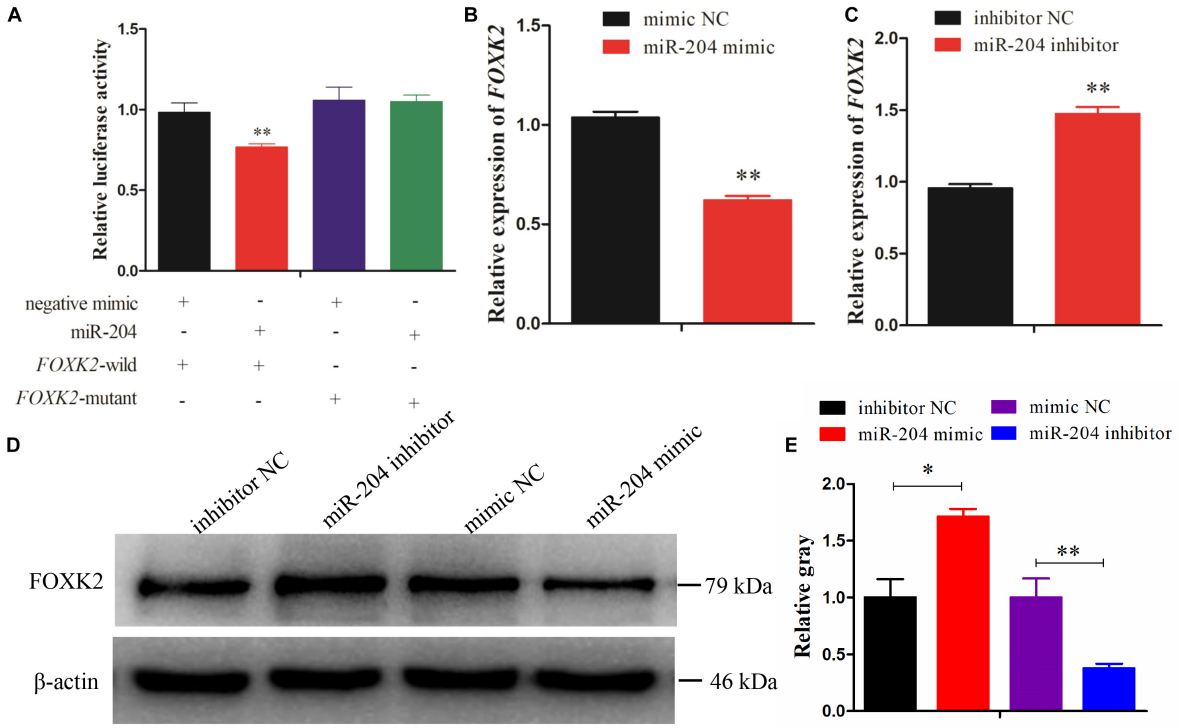

FIGURE 4 | Forkhead box K2 (FOXK2) is a target gene of miR-204. **(A)** Chicken DF-1 cells were co-transfected with FOXK2-3′-untranslated region (UTR) wild or mutant dual-luciferase vector and the miR-204 mimic or miR-negative control (NC). The relative luciferase activity was assayed 48 h later. **(B, C)** The mRNA expression of FOXK2 in chicken granulosa cells (GCs) was detected by quantitative real-time PCR (qRT-PCR) after overexpression and inhibition of miR-204. **(D, E)** The protein expression of FOXK2 in chicken GCs was detected by Western blot analysis after a gain or loss of miR-204. Replications = 3. Data are presented as mean ± SE; $^{*}P < 0.05$ and $^{**}P < 0.01$. miR, microRNA.

while overexpression of miR-204 inhibited mRNA and protein expression of TRPM3 (**Figures 7E–G**). The results thus demonstrate that TRPM3 is another target gene of miR-204.

Subsequent experiments were performed to evaluate the extent of autophagic flux using an adenovirus harboring tandem fluorescent mRFP-GFP-LC3, which differentiates between autophagosomes and autolysosomes (Kimura et al., 2007). The autophagosomes were dotted with both green [green fluorescent protein (GFP)] and red [monomeric red fluorescent protein (mRFP)] colors, and overlaid images revealed a yellow color where there was co-localization. Autolysosomes were dotted with mRFP but not GFP, and overlaid images showed a red color (Hariharan et al., 2011). After transfecting a miR-204 mimic, the dot numbers of GFP and mRFP were decreased (**Figures 8A,B**). In the overlaid images, fewer red dots were observed, indicating decreased autolysosome synthesis (**Figures 8A,B**). Compared with the NC inhibitor, the increased red dots reflected an increased level of autophagic flux after transfection of the miR-204 inhibitor (**Figures 8A,D,E**). These data suggest that miR-204 inhibits GC autophagy by suppressing TRPM3.

miR-204 Impedes the TRPM3/AMPK/ULK1 Pathway

miR-204 and TRPM3 regulate autophagy through the AMPK/ULK1 pathway (Hall et al., 2014). After transfection of a miR-204 mimic, the protein expressions of TRPM3, AMPK, and ULK were decreased, while mTOR protein expression was increased. Notably, after the overexpression of miR-204, the expression of LC3-II was significantly reduced, whereas p62, a polyubiquitin-binding protein known to be degraded during autophagy (Bjorkoy et al., 2005; Pankiv et al., 2007), was significantly increased. In contrast, TRPM3, AMPK, and ULK protein levels were increased, and mTOR protein expression was reduced after the knockdown of miR-204. miR-204 inhibition promotes the accumulation and degradation of LC3-II and p62, respectively (**Figures 8F,G**), which enhanced autophagy. These results confirmed that miR-204 inhibits autophagy by impeding the TRPM3/AMPK/ULK pathway.

TRPM3 Promotes Granulosa Cell Autophagy

Recent studies have demonstrated that TRPM3 is involved in the regulation of autophagy (Hall et al., 2014; Cost and Czyzykkrzeska, 2015). Therefore, we investigated the effect of TRPM3 knockdown on GC autophagy using siRNA. The results showed that the expression of TRPM3 was significantly inhibited (**Figures 9A,B**), and the protein expressions of AMPK and ULK1 were reduced, while the expressions of mTOR and p62 increased significantly. TRPM3 knockdown impeded the accumulation of LC3-II as compared with the Si-NC group (**Figures 9C,D**).

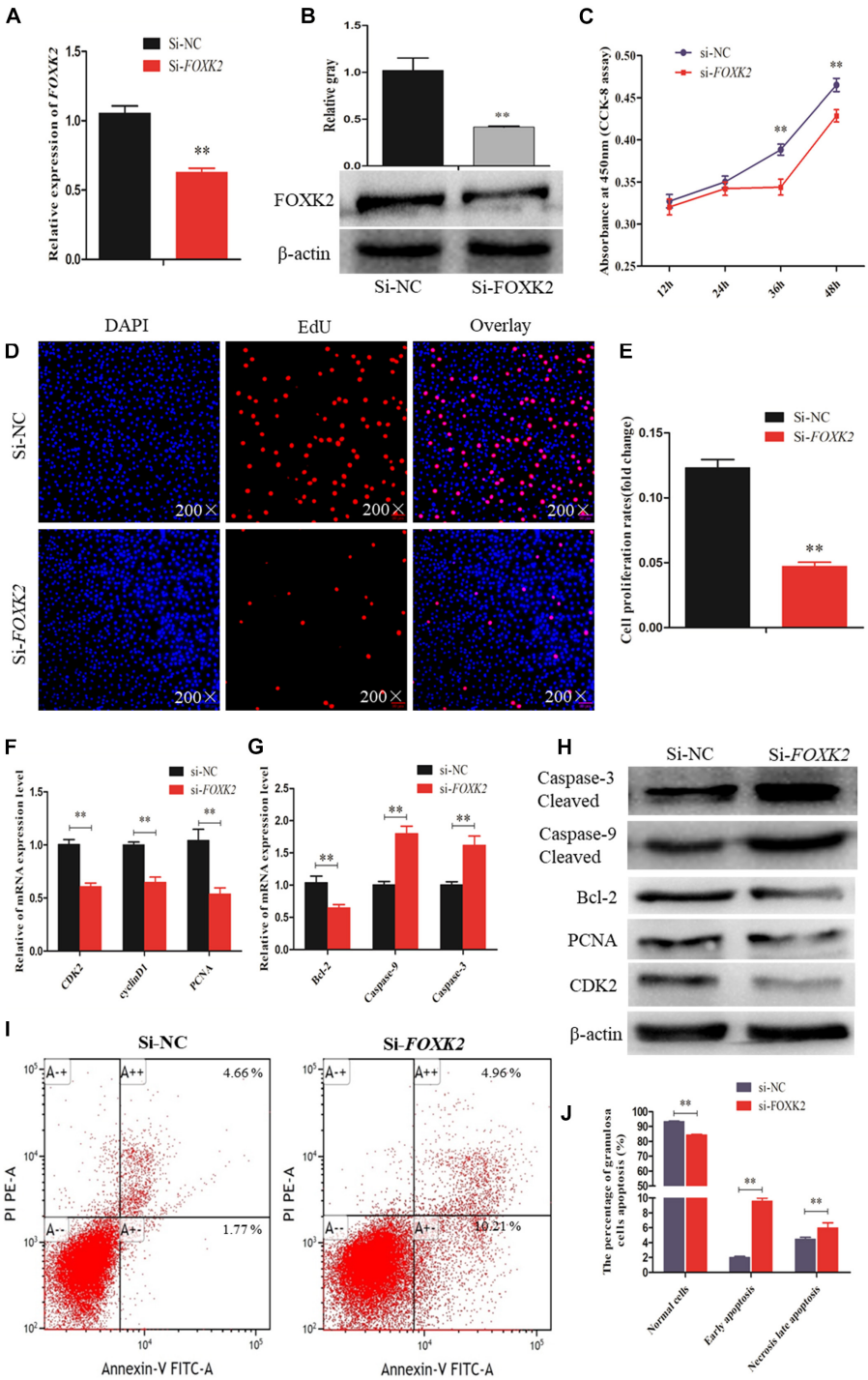

FIGURE 5 | Forkhead box K2 (FOXK2) regulates chicken granulosa cell (GC) proliferation and apoptosis. **(A, B)** The mRNA and protein expressions of FOXK2 were detected after transfection of Si-FOXK2, respectively. **(C)** Cell proliferation status was detected at 450 nm with cell counting kit-8 (CCK-8) reagent after silencing FOXK2. **(D, E)** 5-Ethynyl-2-deoxyuridine (EdU) staining-positive GCs were detected by EdU kit after downregulation of FOXK2. **(F)** The mRNA expression levels of cell proliferation-related genes (*PCNA*, *CDK2*, and *cyclinD1*) were detected by quantitative real-time PCR (qRT-PCR) after FOXK2 knockdown. **(G)** The mRNA expressions of cell apoptosis-related genes (*Bcl-2*, *Caspase-9*, and *Caspase-3*) were detected by qRT-PCR after downregulation of FOXK2. **(H)** The protein expression levels of cell proliferation-related genes (CDK2 and PCNA) and cell apoptosis-related gene (Bcl-2, Caspase-9, and Caspase-3) were detected by Western blot analysis after FOXK2 knockdown. **(I, J)** Apoptotic GCs were detected by annexin V-fluorescein isothiocyanate (FITC)/propidium iodide (PI) staining flow cytometry following FOXK2 silencing. Replications = 3. Data are presented as mean ± SE; Si, small RNA interference. $^{*}P < 0.05$ and $^{**}P < 0.01$.

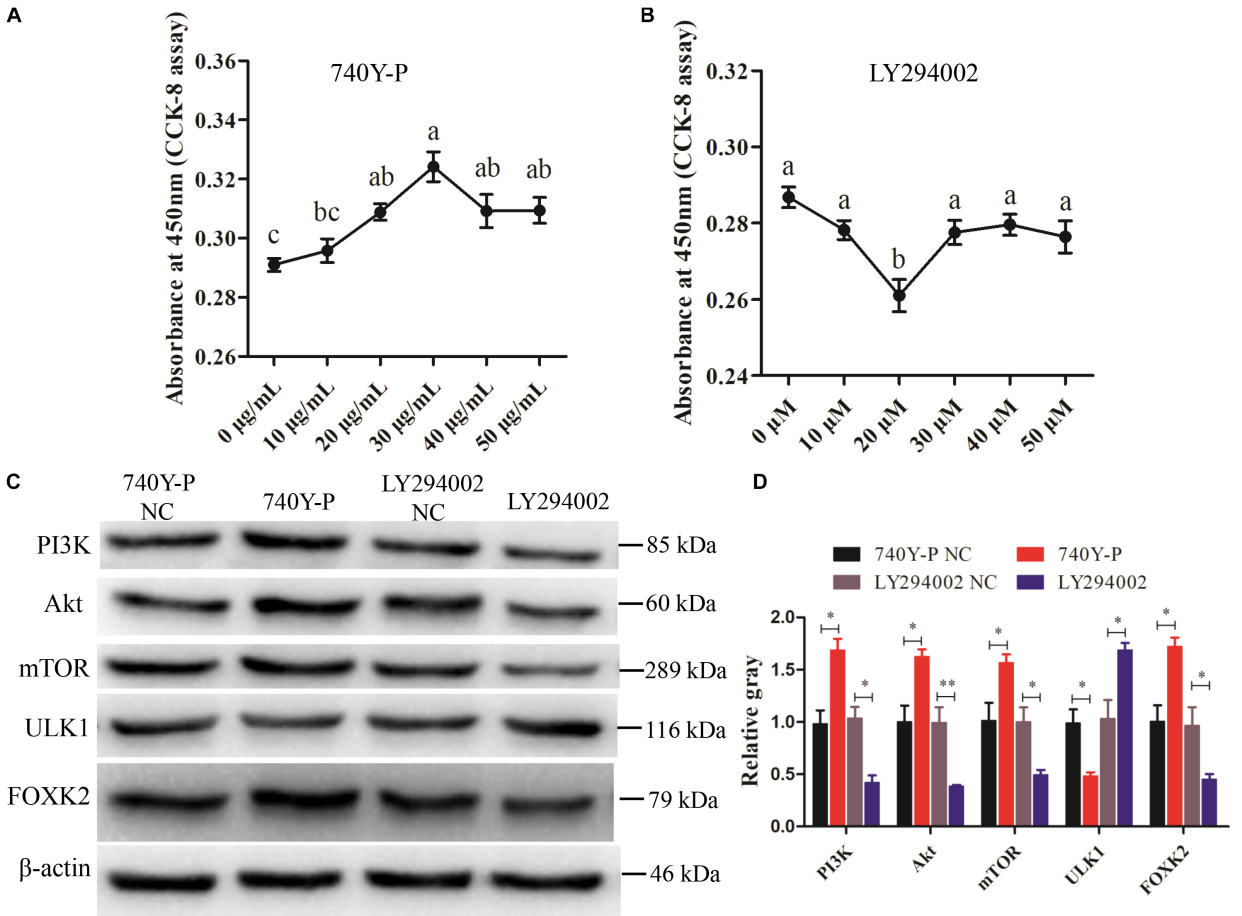

FIGURE 6 | Phosphoinositide 3-kinase (PI3K)/AKT/mammalian target of rapamycin (mTOR) pathway analysis. **(A, B)** Cell counting kit-8 (CCK-8) assay method was employed to determine the optimum concentration of PI3K activator (740Y-P) and PI3K inhibitor (LY294002) treatments. **(C, D)** The protein expressions of PI3K/AKT/mTOR pathway (PI3K, AKT, and mTOR) and downstream regulators [Forkhead box K2 (FOXK2) and ULK1] were detected by Western blot after the treatments of 740Y-P and LY294002. β-actin was used as a reference gene. Replications = 3. Data are presented as mean ± SE; $^{*}P < 0.05$ and $^{**}P < 0.01$.

Immunofluorescence showed that the fluorescent intensity of LC3B reduced significantly (**Figures 9E,F**), whereas p62 protein presented an opposite pattern after TRPM3 silencing (**Figures 9G,H**). Based on these results, we suggest that TRPM3 promotes autophagy in GCs. Thus, miR-204 is associated with chicken GC apoptosis and autophagy *in vivo*.

DISCUSSION

Ovarian tumors are associated with a high risk of morbidity and mortality (Wootipoom et al., 2006; Yamagami et al., 2017). Atrophic ovary is a common type of ovarian tumor accompanied by an increase in follicular atresia and GC apoptosis and autophagy (Fredrickson, 1987; Manabe et al., 2002; Yang et al., 2017). Our previous research showed that miR-204 was differentially expressed between chicken atrophic ovaries and normal ovaries (Liu et al., 2018). Aberrant expression of miR-204 has been frequently reported in cancer studies and correlates with cell proliferation and autophagy (Jian et al., 2011; Liu et al., 2013; Zhou et al., 2014; Wu et al., 2015). In this study, we speculated that miR-204 plays an important role in chicken GC proliferation, apoptosis, and autophagy. Therefore, series of experiments were conducted, and the results showed that miR-204 impeded chicken GC proliferation and promoted apoptosis by targeting *FOXK2*.

FOXK2 is a member of the Foxk family of forkhead transcription factors, which is specifically involved in regulating the balance between proliferation, differentiation, and cell survival (Der Heide et al., 2015). Previous studies demonstrated that FOXK2 suppressed the growth of lung cancer cells by targeting cyclin D1 and CDK4 (Chen et al., 2017) and also influenced CDKs, which linked it to the regulation of the cell cycle (Marais et al., 2010). Additionally, FOXK2 was reported to be involved in cellular processes and important signaling pathways, such as the p53 pathway (Shan et al., 2016), Wnt/β-catenin pathway (Wang et al., 2015), and the PI3K–Akt pathway (Lin et al., 2017). Overexpression of FOXK2 enhanced hepatocellular growth, whereas FOXK2 suppression is associated with decreased cell survival (Lin et al., 2017). Our current study showed that overexpression of miR-204 promoted

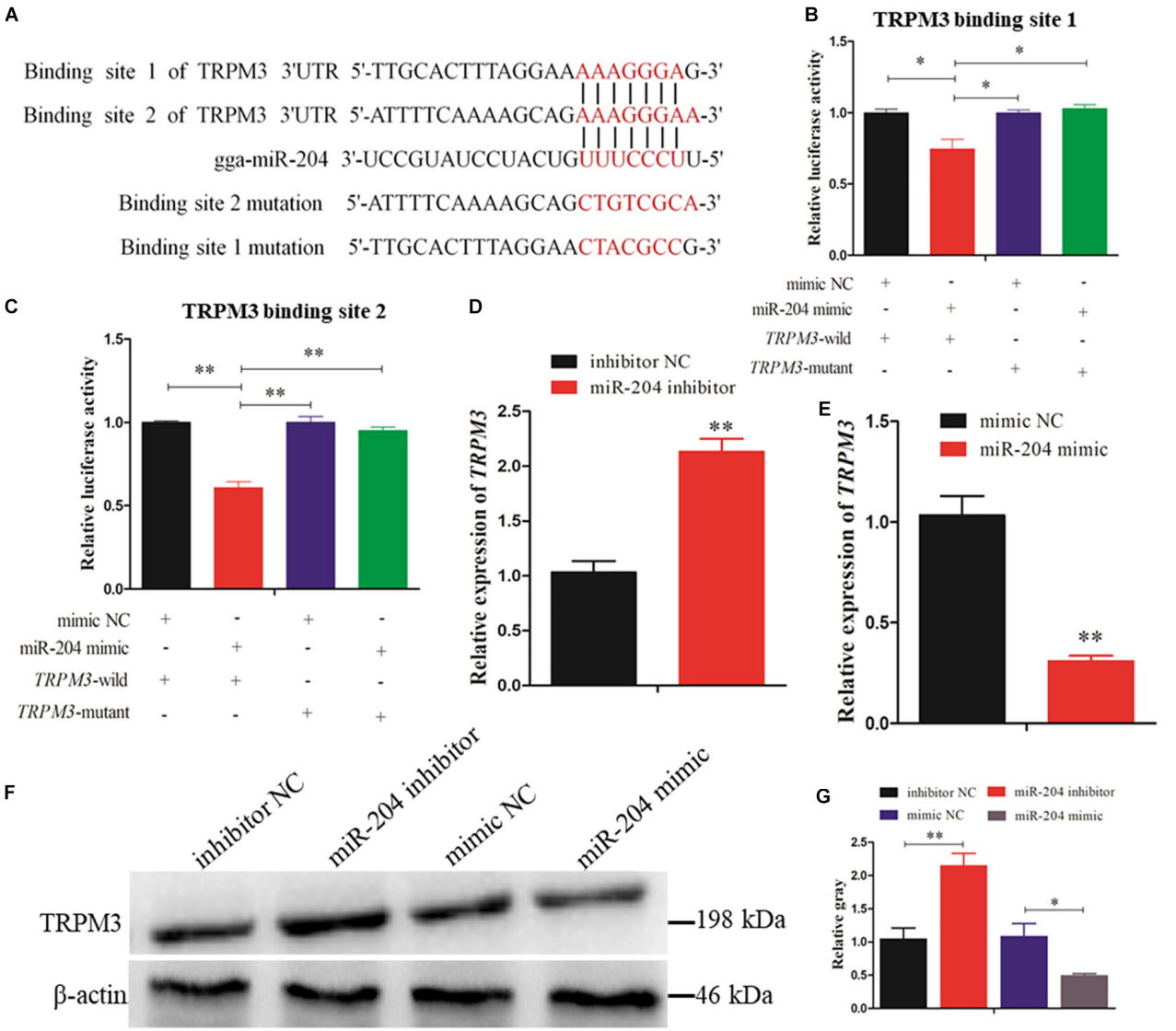

FIGURE 7 | Dual-luciferase reporter gene assays confirmed that miR-204 directly interacts with these two binding sites of transient receptor potential melastatin 3 (TRPM3). **(A)** The target positions of miR-204 seed sequence on TRPM3 and wild or mutant sequence of TRPM3-3′-untranslated region (UTR). **(B, C)** Chicken DF-1 cells were co-transfected with TRPM3-3′-UTR wild or mutant dual-luciferase vector and the miR-204 mimic or mimic negative control (NC). The relative luciferase activity was assayed 48 h later. **(D, E)** The mRNA expression of TRPM3 was detected after overexpression or inhibition of miR-204. **(F, G)** The protein levels of TRPM3 in chicken granulosa cells (GCs) were detected after transfection of overexpression or inhibition of miR-204. β-actin was used as a reference gene. Replications = 3. Data are presented as mean ± SE; $^{*}P < 0.05$ and $^{**}P < 0.01$.

GC apoptosis, which was characterized by increasing apoptotic cell numbers and gene expression of caspase-9 and caspase-3. Meanwhile, CCK-8 and EdU results indicated that a miR-204 mimic had low cell vitality and numbers of EdU-positive cells, and the gene expression of PCNA, CDK2, and cyclinD1 was decreased. Subsequently, the bioinformatics analyses and dual-luciferase reporter gene assays were performed and demonstrated that *FOXK2* is directly targeted by miR-204. Both mRNA and protein expressions of FOXK2 were suppressed by miR-204, and further functional experiments indicated that *FOXK2* had the opposite effect of miR-204 on GC proliferation and apoptosis. After *FOXK2* knockdown, we found that proliferation of GCs was inhibited and the numbers of apoptotic cells were increased. A similar result was reported in liver cells (Sakaguchi et al., 2019).

The PI3K/AKT/mTOR signaling pathway contributes to a variety of processes that are critical in mediating many aspects of cellular function, including cell proliferation and survival, gene expression, and metabolic activities (Yu and Cui, 2016). PI3K plays a key role in regulating cell proliferation, which is indispensable for cell self-renewal (Mclean et al., 2007; Zhou et al., 2011). Akt is an important downstream target in the PI3K

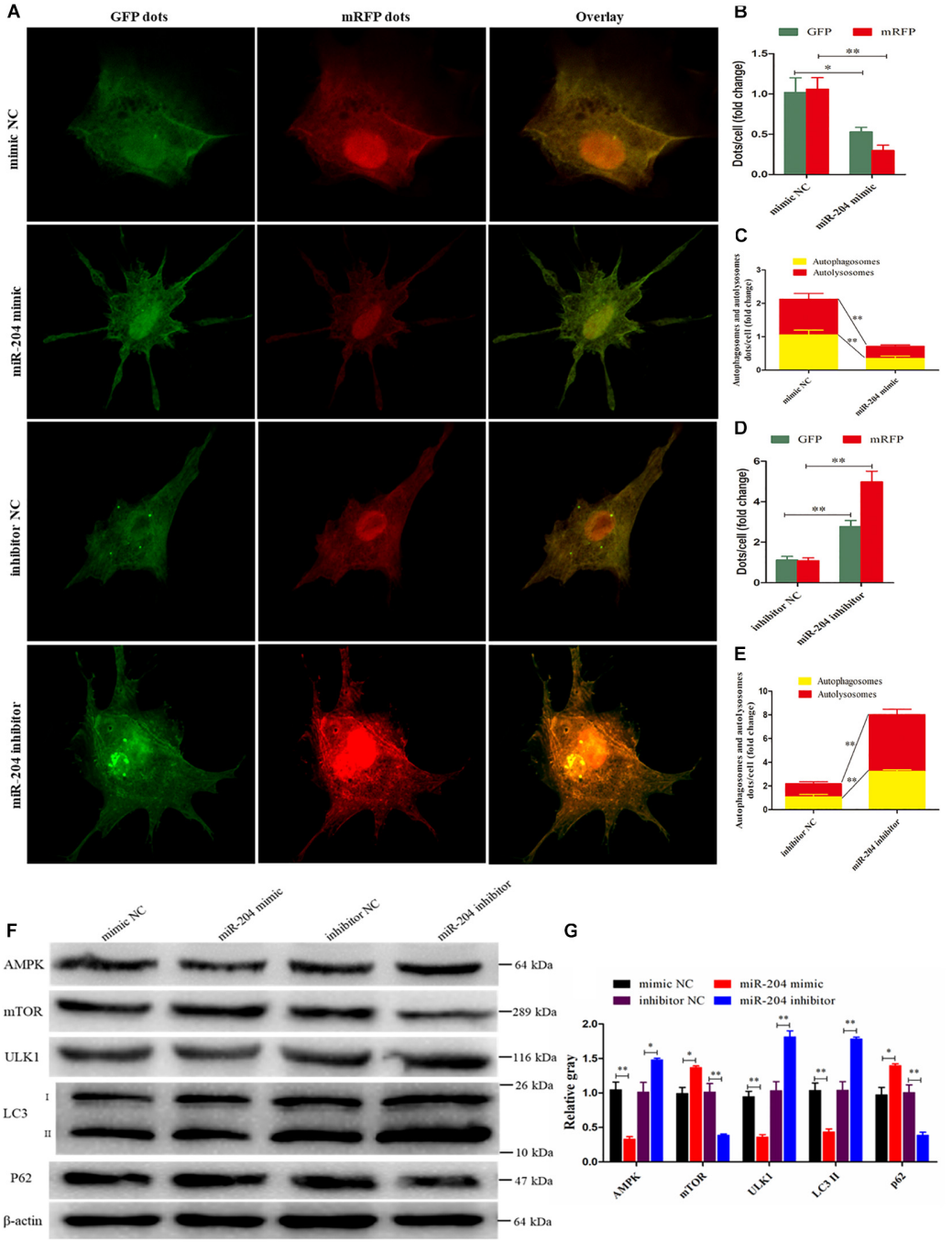

FIGURE 8 | miR-204 regulates granulosa cell (GC) autophagy *via* transient receptor potential melastatin 3 (TRPM3)/AMP-activated protein kinase (AMPK)/ULK1 pathway. **(A)** An adenovirus harboring tandem fluorescent mRFP-GFP-LC3 was used to evaluate the extent of autophagic flux after transfection of overexpression or inhibition of miR-204. **(B, D)** Mean number of green fluorescent protein (GFP) and monomeric red fluorescent protein (mRFP) dots per cell; nine cells were randomly selected to count for each field. **(C, E)** Mean number of autophagosomes and autolysosomes per cell. The autophagosomes were dotted with both green (GFP) and red (mRFP) color, and overlaid images showed with a yellow color. Autolysosomes were dotted with mRFP but not GFP, and overlaid images showed with a red color. **(F, G)** The protein levels of TRPM3/AMPK/ULK1 pathway [AMPK, mammalian target of rapamycin (mTOR), ULK, LC3-II, and p62] were detected after transfection of overexpression or inhibition of miR-204. β-actin was used as a reference gene. Replications = 3. Data are presented as mean ± SE; $^{*}P < 0.05$ and $^{**}P < 0.01$.

signal transduction pathway, which can promote cell survival and inhibit apoptosis (Tu et al., 2018). As a vital activator for Akt, mTOR plays a critical role in cell survival and differentiation (Sugatani and Hruska, 2005; Rao et al., 2010). PI3K/Akt/mTOR signaling regulated GC proliferation and apoptosis by targeting its downstream protein FOXK2 (**Figure 10**).

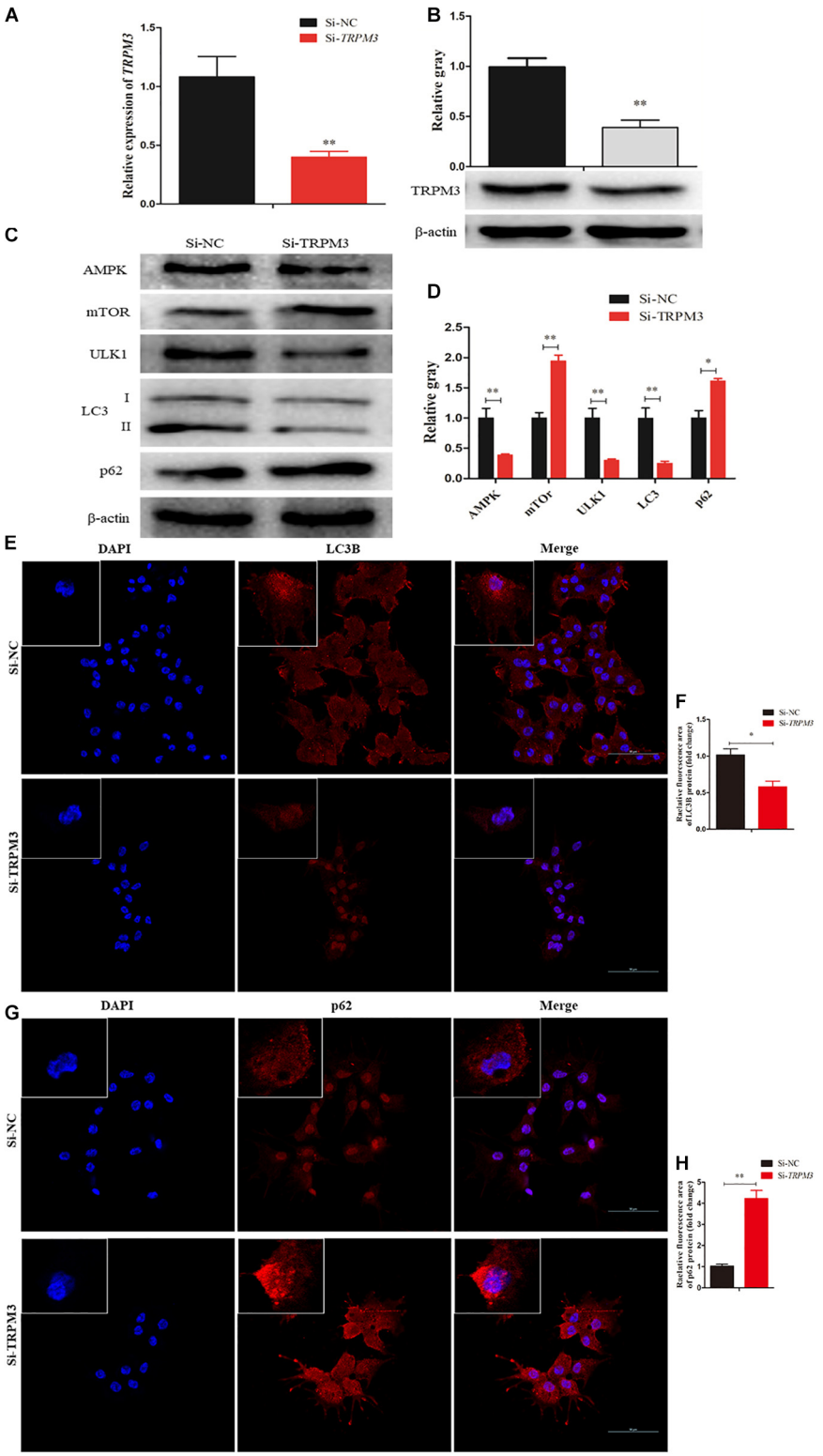

FIGURE 9 | Transient receptor potential melastatin 3 (TRPM3) promotes granulosa cell (GC) autophagy. **(A, B)** The mRNA and protein expressions of TRPM3 were detected after transfection of Si-TRPM3. **(C, D)** The protein levels of TRPM3/AMP-activated protein kinase (AMPK)/ULK1 pathway [AMPK, mammalian target of rapamycin (mTOR), ULK, LC3-II, and p62] were detected after transfection of Si-TRPM3. β-actin was used as a reference gene. **(E, F)** Immunofluorescence analysis was performed to test the fluorescence intensity of LC3B after TRPM3 silencing. **(G, H)** Immunofluorescence analysis was performed to test the fluorescence intensity of p62 after TRPM3 silencing. Replications = 3. Data are presented as mean ± SE; $^{*}P < 0.05$ and $^{**}P < 0.01$.

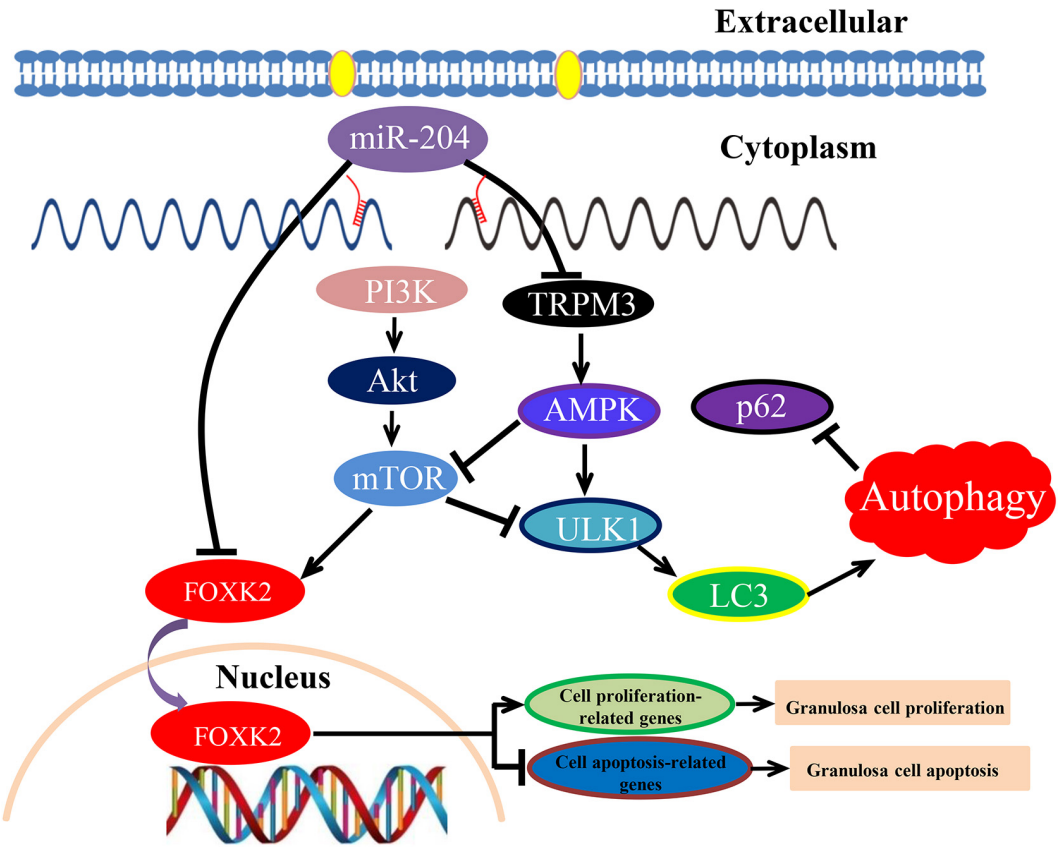

FIGURE 10 | Schematic model of miR-204-mediated regulatory mechanism in chicken granulosa cell (GC) proliferation, apoptosis, and autophagy. miR-204 promotes GC apoptosis by repressing Forkhead box K2 (FOXK2) *via* the phosphoinositide 3-kinase (PI3K)/AKT/mammalian target of rapamycin (mTOR) regulation pathway and inhibits autophagy by impeding the transient receptor potential melastatin 3 (TRPM3)/AMP-activated protein kinase (AMPK)/ULK pathway.

Increased expression of cleaved caspase-3 and caspase-9 led to the inhibition of autophagy and enhanced apoptosis (Xiong et al., 2015). We found that miR-204 regulated GC autophagy by targeting TRPM3. Autophagy is a complex cellular process that is essential for cell homeostasis (Stromhaug and Klionsky, 2001); therefore, in either extreme or less-extreme autophagy, cell death can occur (Sadoshima, 2008; Hall et al., 2014). Autophagy is regulated by many autophagy-related genes (Atgs), which are involved in autophagosome formation (Nishida et al., 2009). LC3 (microtubule-associated protein 1 light chain 3, Atg8) is essential for the formation of an autophagosome (Kabeya et al., 2000). The soluble form of LC3 (LC3-I), which transforms into the autophagic vesicle-associated form (LC3-II), is an important marker of effective autophagy (Asanuma et al., 2003). ULK1 (unc-51 like autophagy activating kinase 1, Atg1) is an autophagy-initiating kinase; therefore, it initiates autophagy (Shang and Wang, 2011).

Recently, it was established that miR-204 directly inhibits the translation of TRPM3, and a loss of miR-204 leads to a high expression of TRPM3 and stimulates autophagy (Cost and Czyzykkrzeska, 2015). Similarly, Hall et al. (2014) demonstrated that miR-204 acts as a critical regulator of autophagy by targeting TRPM3, and overexpression of TRPM3 leads to activation of AMPK and ULK1, which forms a connection with the autophagic pathway (Hall et al., 2014). In our study, we confirmed that TRPM3 is another target gene of miR-204 and regulates GC autophagy by targeting the AMPK/ULK1 pathway. AMPK and mTOR (target of rapamycin) are upstream regulators of ULK1. AMPK is involved in promoting autophagy by directly activating ULK1, while the activity of mTOR prevents the activation of ULK1 and also disrupts the interaction between ULK1 and AMPK (Kim et al., 2011). Overexpression of miR-204 attenuated autophagic flux and reduced the protein expression of TRPM3, AMPK, ULK, and LC3-II; however, it also resulted in increased protein expression of mTOR and p62. On the contrary, miR-204 inhibition enhanced autophagic flux in cultured GCs and led to increased protein expression of TRPM3, AMPK, and ULK but decreased protein expression of mTOR. miR-204 inhibition resulted in accumulation and degradation of LC3-II and p62, indicating that miR-204 inhibited autophagy by impeding the TRPM3/AMPK/ULK pathway (**Figure 10**).

In conclusion, these results show that miR-204 is highly expressed in chicken atrophic ovaries and functions in promoting GC apoptosis by repressing FOXK2 *via* the PI3K/AKT/mTOR regulation pathway and inhibiting autophagy by impeding the TRPM3/AMPK/ULK pathway.

DATA AVAILABILITY STATEMENT

The raw data supporting the conclusions of this article will be made available by the authors, without undue reservation.

ETHICS STATEMENT

The animal study was reviewed and approved by the Institutional Animal Care and Use Committee at the Sichuan Agricultural University (No. YCS-B2018102013), and all laboratory works conducted were in accordance with the Sichuan Agricultural University (SAU) Laboratory Animal Welfare and Ethics guidelines.

AUTHOR CONTRIBUTIONS

XZ, ZC, and LL conceived and designed the experiments. ZC, LL, and FK performed the experiments. ZC, FK, QZ, YW, DL, GS, and YT analyzed the data. ZC and XZ wrote the manuscript. All authors contributed to the article and approved the submitted version.

FUNDING

We would like to thank the China Agriculture Research System of Ministry of Agriculture and Rural Areas (Grant No. CARS-41), National Natural Science Foundation of China (Grant No. 31872347), and Sichuan Science and Technology Planning Project Agricultural Scientific and Technological Achievements Transformation (2018NZZJ003) for their financial support.

ACKNOWLEDGMENTS

We deeply appreciate Elizabeth R. Gilbert from the Department of Animal and Poultry Sciences, Virginia Polytechnic Institute and State University, United States, for professional suggestions on this manuscript.

SUPPLEMENTARY MATERIAL

The Supplementary Material for this article can be found online at: https://www.frontiersin.org/articles/10.3389/fcell.2020.580072/full#supplementary-material

REFERENCES

Ambros, V. R. (2004). The functions of animal microRNAs. *Nature* 431, 350–355. doi: 10.1038/nature02871

Asanuma, K., Tanida, I., Shirato, I., Ueno, T., Takahara, H., and Nishitani, T. (2003). MAP-LC3, a promising autophagosomal marker, is processed during the differentiation and recovery of podocytes from PAN nephrosis. *FASEB J.* 17, 1165–1167. doi: 10.1096/fj.02-0580fje

Bahr, J. M. (1991). The chicken ovary as a model of follicular development. *Semin. Reprod. Med.* 9, 352–359. doi: 10.1055/s-2007-1019427

Baley, J., and Li, J. (2012). MicroRNAs and ovarian function. *J. Ovarian Res.* 5, 8–8. doi: 10.1186/1757-2215-5-8

Bartel, D. P. (2004). MicroRNAs: genomics, biogenesis, mechanism, and function. *Cell* 116, 281–297.

Bernstein, E., Caudy, A. A., Hammond, S. M., and Hannon, G. J. (2001). Role for a bidentate ribonuclease in the initiation step of RNA interference. *Nature* 409, 363–366. doi: 10.1038/35053110

Bjorkoy, G., Lamark, T., Brech, A., Outzen, H., Perander, M., and Overvatn, A. (2005). p62/SQSTM1 forms protein aggregates degraded by autophagy and has a protective effect on huntingtin-induced cell death. *J. Cell Biol.* 171, 603–614. doi: 10.1083/jcb.200507002

Carletti, M. Z., Fiedler, S. D., and Christenson, L. K. (2010). MicroRNA 21 blocks apoptosis in mouse periovulatory granulosa cells. *Biol. Reprod.* 83, 286–295. doi: 10.1095/biolreprod.109.081448

Castagna, C. D., Peixoto, C. H., Bortolozzo, F. P., Wentz, I., Neto, G. B., and Ruschel, F. (2004). Ovarian cysts and their consequences on the reproductive performance of swine herds. *Anim. Reprod. Sci.* 81, 115–123. doi: 10.1016/j.anireprosci.2003.08.004

Chekulaeva, M., and Filipowicz, W. (2009). Mechanisms of miRNA-mediated post-transcriptional regulation in animal cells. *Curr. Opin. Cell Biol.* 21, 452–460. doi: 10.1016/j.ceb.2009.04.009

Chen, S., Jiang, S., Hu, F., Xu, Y., Wang, T., and Mei, Q. (2017). Foxk2 inhibits non-small cell lung cancer epithelial-mesenchymal transition and proliferation through the repression of different key target genes. *Oncol. Rep.* 37, 2335–2347. doi: 10.3892/or.2017.5461

Cost, N. G., and Czyzykkrzeska, M. F. (2015). Regulation of autophagy by two products of one gene: TRPM3 and miR-204. *Mol. Cell. Oncol.* 2:e1002712. doi: 10.1080/23723556.2014.1002712

Der Heide, L. P. V., Wijchers, P. J., Von Oerthel, L., Burbach, J. P. H., Hoekman, M. F. M., and Smidt, M. P. (2015). FoxK2 is required for cellular proliferation and survival. *J. Cell. Physiol.* 230, 1013–1023. doi: 10.1002/jcp.24828

Fredrickson, T. N. (1987). Ovarian tumors of the hen. *Environ. Health Persp.* 73, 35–51. doi: 10.1289/ehp.877335

Gebremedhn, S., Salilewwondim, D., Hoelker, M., Rings, F., Neuhoff, C., and Tholen, E. (2016). MicroRNA-183-96-182 cluster regulates bovine granulosa cell proliferation and cell cycle transition by coordinately targeting FOXO1. *Biol. Reprod.* 94:127.

Gethoffer, F., Pfarrer, C., and Siebert, U. (2018). Histology confirms that macroscopic evaluation of ovaries is a valid method for the assessment of the reproductive status in wild boar. *Theriogenology* 113, 192–196. doi: 10.1016/j.theriogenology.2018.02.019

Gilbert, A. B., Evans, A. J., Perry, M. M., and Davidson, M. H. (1977). A method for separating the granulosa cells, the basal lamina and the theca of the preovulatory ovarian follicle of the domestic fowl (*Gallus domesticus*). *Reproduction* 50, 179–181. doi: 10.1530/jrf.0.0500179

Hall, D., Cost, N. G., Hegde, S., Kellner, E., Mikhaylova, O., and Stratton, Y. (2014). TRPM3 and miR-204 establish a regulatory circuit that controls oncogenic autophagy in clear cell renal cell carcinoma. *Cancer Cell* 26, 738–753. doi: 10.1016/j.ccell.2014.09.015

Hariharan, N., Zhai, P., and Sadoshima, J. (2011). Oxidative stress stimulates autophagic flux during Ischemia/Reperfusion. *Antioxid. Redox Sign.* 14, 2179–2190. doi: 10.1089/ars.2010.3488

Huang, J., Zhao, L., Fan, Y., Liao, L., Ma, P. X., and Xiao, G. (2019). The microRNAs miR-204 and miR-211 maintain joint homeostasis and protect against osteoarthritis progression. *Nat. Commun.* 10:2876.

Imbar, T., and Eisenberg, I. (2014). Regulatory role of microRNAs in ovarian function. *Fertil. Steril.* 101, 1524–1530. doi: 10.1016/j.fertnstert.2014.04.024

Jiajie, T., Yanzhou, Y., Hoihung, A. C., Zijiang, C., and Waiyee, C. (2017). Conserved miR-10 family represses proliferation and induces apoptosis in ovarian granulosa cells. *Sci. Rep.* 7:41304.

Jian, X., Xiaoyan, Z., Bin, H., Yufeng, Z., Bo, K., and Zhinong, W. (2011). MiR-204 regulate cardiomyocyte autophagy induced by hypoxia-reoxygenation through LC3-II. *Int. J. Cardiol.* 148, 110–112. doi: 10.1016/j.ijcard.2011.01.029

Jiang, L., Huang, J., Li, L., Chen, Y., Chen, X., and Zhao, X. (2015). MicroRNA-93 promotes ovarian granulosa cells proliferation through targeting CDKN1A in polycystic ovarian syndrome. *J. Clin. Endocr. Metab.* 100:E729.

Johnson, A. L., and Woods, D. C. (2009). Dynamics of avian ovarian follicle development: cellular mechanisms of granulosa cell differentiation. *Gen. Comp. Endocr.* 163, 12–17. doi: 10.1016/j.ygcen.2008.11.012

Kabeya, Y., Mizushima, N., Ueno, T., Yamamoto, A., Kirisako, T., and Noda, T. (2000). LC3, a mammalian homologue of yeast Apg8p, is localized in autophagosome membranes after processing. *EMBO J.* 19, 5720–5728. doi: 10.1093/emboj/19.21.5720

Kim, J., Kundu, M., Viollet, B., and Guan, K. (2011). AMPK and mTOR regulate autophagy through direct phosphorylation of Ulk1. *Nat. Cell Biol.* 13, 132–141. doi: 10.1038/ncb2152

Kim, V. N. (2005). Small RNAs: classification, biogenesis, and function. *Mol. Cells* 19, 1–15.

Kim, Y. J., Ku, S., Kim, Y. Y., Liu, H. C., Chi, S. W., and Kim, S. H. (2013). MicroRNAs transfected into granulosa cells may regulate oocyte meiotic competence during in vitro maturation of mouse follicles. *Hum. Reprod.* 28, 3050–3061. doi: 10.1093/humrep/det338

Kimura, S., Noda, T., and Yoshimori, T. (2007). Dissection of the autophagosome maturation process by a novel reporter protein. Tandem Fluorescent-Tagged LC3. *Autophagy* 3, 452–460. doi: 10.4161/auto.4451

Kosaka, N., Iguchi, H., Yoshioka, Y., Takeshita, F., Matsuki, Y., and Ochiya, T. (2010). Secretory mechanisms and intercellular transfer of microRNAs in living cells. *J. Biol. Chem.* 285, 17442–17452. doi: 10.1074/jbc.m110.107821

Lee, R. C., Feinbaum, R. L., and Ambros, V. R. (1993). The *C. elegans* Heterochronic Gene lin-4 Encodes Small RNAs with antisense complementarity to lin-14. *Cell* 75, 843–854. doi: 10.1016/0092-8674(93)90529-y

Lin, M., Yang, Y., Peng, Z., Zhang, M., Liang, J., and Chen, W. (2017). FOXK2, regulted by miR-1271-5p, promotes cell growth and indicates unfavorable prognosis in hepatocellular carcinoma. *Int. J. Biochem. Cell B.* 88, 155–161. doi: 10.1016/j.biocel.2017.05.019

Liu, B., Wen, X., and Cheng, Y. (2013). Survival or death: disequilibrating the oncogenic and tumor suppressive autophagy in cancer. *Cell Death Dis.* 4:e892. doi: 10.1038/cddis.2013.422

Liu, J., Yao, W., Yao, Y., Du, X., Zhou, J., and Ma, B. (2014). MiR-92a inhibits porcine ovarian granulosa cell apoptosis by targeting Smad7 gene. *FEBS Lett.* 588, 4497–4503. doi: 10.1016/j.febslet.2014.10.021

Liu, L., Xiao, Q., Gilbert, E. R., Cui, Z., Zhao, X., and Wang, Y. (2018). Whole-transcriptome analysis of atrophic ovaries in broody chickens reveals regulatory pathways associated with proliferation and apoptosis. *Sci. Rep.* 8:7231.

Livak, K. J., and Schmittgen, T. D. (2001). Analysis of relative gene expression data using real-time quantitative PCR and the 2(-Delta Delta C(T)) Method. *Methods* 25, 402–408. doi: 10.1006/meth.2001.1262

Manabe, N., Kimura, Y., Uchio, K., Tajima, C., and Miyamoto, H. (2002). *Regulatory Mechanisms of Granulosa Cell Apoptosis in Ovarian Follicle Atresia. Animal Cell Technology: Challenges for the 21st Century*. Netherlands: Springer.

Marais, A., Ji, Z., Child, E. S., Krause, E., Mann, D. J., and Sharrocks, A. D. (2010). Cell cycle-dependent regulation of the forkhead transcription factor FOXK2 by CDK·cyclin complexes. *J. Biol. Chem.* 285, 35728–35739.

Matsudaminehata, F., Inoue, N., Goto, Y., and Manabe, N. (2006). The regulation of ovarian granulosa cell death by pro- and anti-apoptotic molecules. *J. Reprod. Dev.* 52, 695–705. doi: 10.1262/jrd.18069

Mclean, A. B., Damour, K. A., Jones, K. L., Krishnamoorthy, M., Kulik, M., Reynolds, D., et al. (2007). Activin a efficiently specifies definitive endoderm from human embryonic stem cells only when phosphatidylinositol 3-kinase signaling is suppressed. *Stem Cells* 25, 29–38. doi: 10.1634/stemcells.2006-0219

Mikhaylova, O., Stratton, Y., Hall, D., Kellner, E., Ehmer, B., and Drew, A. F. (2012). VHL-regulated MiR-204 suppresses tumor growth through inhibition of LC3B-mediated autophagy in renal clear cell carcinoma. *Cancer Cell* 21, 532–546. doi: 10.1016/j.ccr.2012.02.019

Nishida, K., Kyoi, S., Yamaguchi, O., Sadoshima, J., and Otsu, K. (2009). The role of autophagy in the heart. *Cell Death Differ.* 16, 31–38.

Pankiv, S., Clausen, T. H., Lamark, T., Brech, A., Bruun, J., and Outzen, H. (2007). p62/SQSTM1 binds directly to Atg8/LC3 to facilitate degradation of ubiquitinated protein aggregates by autophagy. *J. Biol. Chem.* 282, 24131–24145. doi: 10.1074/jbc.m702824200

Pilsworth, J. A., Cochrane, D. R., Xia, Z., Aubert, G., Farkkila, A., and Horlings, H. M. (2018). TERT promoter mutation in adult granulosa cell tumor of the ovary. *Modern Pathol.* 31, 1107–1115.

Rao, R., Li, Q., and Shrikant, P. (2010). Fine-tuning CD8(+) T cell functional responses: mTOR acts as a rheostat for regulating CD8(+) T cell proliferation, survival and differentiation? *Cell Cycle* 9, 2996–3001.

Russell, D. L. (2019). "Ovulation: the coordination of intrafollicular networks to ensure oocyte release," *The Ovary*, 3rd Edn (Amsterdam: Elsevier), 217–234. doi: 10.1016/b978-0-12-813209-8.00014-5

Sacconi, A., Biagioni, F., Canu, V., Mori, F., Benedetto, A. D., and Lorenzon, L. (2012). miR-204 targets Bcl-2 expression and enhances responsiveness of gastric cancer. *Cell Death Dis.* 3:e423. doi: 10.1038/cddis.2012.160

Sadoshima, J. (2008). The role of autophagy during ischemia/reperfusion. *Autophagy* 4, 402–403. doi: 10.4161/auto.5924

Sakaguchi, M., Cai, W., Wang, C., Cederquist, C. T., Damasio, M., and Homan, E. P. (2019). FoxK1 and FoxK2 in insulin regulation of cellular and mitochondrial metabolism. *Nat. Commun.* 10, 1582–1582.

Shan, L., Zhou, X., Liu, X., Wang, Y., Su, D., and Hou, Y. (2016). FOXK2 elicits massive transcription repression and suppresses the hypoxic response and breast cancer carcinogenesis. *Cancer Cell* 30, 708–722. doi: 10.1016/j.ccell.2016.09.010

Shang, L., and Wang, X. (2011). AMPK and mTOR coordinate the regulation of Ulk1 and mammalian autophagy initiation. *Autophagy* 7, 924–926. doi: 10.4161/auto.7.8.15860

Shelling, A. N. (2010). Premature ovarian failure. *Reproduction* 140, 633–641.

Sirotkin, A. V., Kisová, G., Brenaut, P., Ovcharenko, D., Grossmann, R., and Mlyncek, M. (2014). Involvement of MicroRNA Mir15a in control of human ovarian granulosa cell proliferation, apoptosis, steroidogenesis, and response to FSH. *Microrna* 3, 29–36. doi: 10.2174/2211536603666140227232824

Sirotkin, A. V., Makarevich, A. V., Kubovicova, E., Laurincik, J., Alwasel, S. H., and Harrath, A. H. (2018). Cow body condition affects the hormonal release of ovarian cells and their responses to gonadotropic and metabolic hormones. *Theriogenology* 110, 142–147. doi: 10.1016/j.theriogenology.2018.01.006

Stromhaug, P. E., and Klionsky, D. J. (2001). Approaching the molecular mechanism of autophagy. *Traffic* 2, 524–531. doi: 10.1034/j.1600-0854.2001.20802.x

Sugatani, T., and Hruska, K. A. (2005). Akt1/Akt2 and mammalian target of Rapamycin/Bim Play critical roles in osteoclast differentiation and survival, respectively, whereas akt is dispensable for cell survival in isolated osteoclast precursors. *J. Biol. Chem.* 280, 3583–3589. doi: 10.1074/jbc.m410480200

Tu, F., Pan, Z. X., Yao, Y., Liu, H., Liu, S. R., and Xie, Z. (2014). miR-34a targets the inhibin beta B gene, promoting granulosa cell apoptosis in the porcine ovary. *Genet. Mol. Res.* 13, 2504–2512. doi: 10.4238/2014.january.14.6

Tu, L., Wang, Y., Chen, D., Xiang, P., Shen, J., and Li, Y. (2018). Protective effects of notoginsenoside R1 via regulation of the PI3K-Akt-mTOR/JNK pathway in neonatal cerebral hypoxic–ischemic brain injury. *Neurochem. Res.* 43, 1210–1226. doi: 10.1007/s11064-018-2538-3

Valadi, H., Ekstrom, K. M., Bossios, A., Sjostrand, M., Lee, J. J., and Lotvall, J. (2007). Exosome-mediated transfer of mRNAs and microRNAs is a novel mechanism of genetic exchange between cells. *Nat. Cell Biol.* 9, 654–659. doi: 10.1038/ncb1596

Wang, W., Li, X., Lee, M., Jun, S., Aziz, K. E., and Feng, L. (2015). FOXKs Promote Wnt/β-Catenin signaling by translocating DVL into the Nucleus. *Dev. Cell* 32, 707–718. doi: 10.1016/j.devcel.2015.01.031

Wootipoom, V., Dechsukhum, C., Hanprasertpong, J., and Lim, A. (2006). Accuracy of intraoperative frozen section in diagnosis of ovarian tumors. *J. Med. Assoc.* 89, 577–582.

Wu, Z. Y., Wang, S. M., Chen, Z. H., Huv, S. X., Huang, K., and Huang, B. J. (2015). MiR-204 regulates HMGA2 expression and inhibits cell proliferation in human thyroid cancer. *Cancer Biomark.* 15, 535–542. doi: 10.3233/cbm-150492

Xiao, J., Zhu, X., He, B., Zhang, Y., Kang, B., Wang, Z., et al. (2011). MiR-204 regulates cardiomyocyte autophagy induced by ischemia-reperfusion through LC3-II. *J. Biomed. Sci.* 18:35. doi: 10.1186/1423-0127-18-35

Xiong, X., Wu, M., Zhang, H., Li, J., Lu, B., Guo, Y., et al. (2015). Atg5 siRNA inhibits autophagy and enhances norcantharidin-induced apoptosis in hepatocellular carcinoma. *Int. J. Oncol.* 47, 1321–1328. doi: 10.3892/ijo.2015.3103

Yamagami, W., Nagase, S., Takahashi, F., Ino, K., Hachisuga, T., and Aoki, D. (2017). Clinical statistics of gynecologic cancers in Japan. *J. Gynecol. Oncol.* 28:e32.

Yan, G., Zhang, L., Fang, T., Zhang, Q., Wu, S., and Jiang, Y. (2012). MicroRNA-145 suppresses mouse granulosa cell proliferation by targeting activin receptor IB. *FEBS Lett.* 586, 3263–3270. doi: 10.1016/j.febslet.2012.06.048

Yang, J., Hu, S., Rao, M., Hu, L., Lei, H., Wu, Y., et al. (2017). Copper nanoparticle-induced ovarian injury, follicular atresia, apoptosis, and gene expression alterations in female rats. *Int. J. Nanomed.* 12, 5959–5971. doi: 10.2147/ijn.s139215

Yang, X., Zhou, Y., Peng, S., Wu, L., Lin, H., and Wang, S. (2012). Differentially expressed plasma microRNAs in premature ovarian failure patients and the potential regulatory function of mir-23a in granulosa cell apoptosis. *Reproduction* 144, 235–244. doi: 10.1530/rep-11-0371

Yao, G., Yin, M., Lian, J., Tian, H., Liu, L., and Li, X. (2010). MicroRNA-224 Is involved in transforming Growth Factor-β-Mediated mouse granulosa cell proliferation and granulosa cell function by targeting Smad4. *Mol. Endocrinol.* 24, 540–551. doi: 10.1210/me.2009-0432

Yin, M., Wang, X., Yao, G., Lu, M., Liang, M., and Sun, Y. (2014). Transactivation of MicroRNA-320 by MicroRNA-383 regulates granulosa cell functions by Targeting E2F1 and SF-1 Proteins. *J. Biol. Chem.* 289, 18239–18257. doi: 10.1074/jbc.m113.546044

Yu, J. S. L., and Cui, W. (2016). Proliferation, survival and metabolism: the role of PI3K/AKT/mTOR signalling in pluripotency and cell fate determination. *Development* 143, 3050–3060. doi: 10.1242/dev.137075

Zangirolamo, A. F., Morotti, F., Silva, N. C. D., Sanches, T. K., and Seneda, M. M. (2018). Ovarian antral follicle populations and embryo production in cattle. *Anim. Reprod.* 15, 310–315. doi: 10.21451/1984-3143-ar2018-0072

Zhang, L., Wang, X., and Chen, P. (2013). MiR-204 down regulates SIRT1 and reverts SIRT1-induced epithelial-mesenchymal transition, anoikis resistance and invasion in gastric cancer cells. *BMC Cancer* 13:290. doi: 10.1186/1471-2407-13-290

Zhao, X., Wang, D., Wu, Z., Pan, B., Yang, H., and Zeng, C. (2018). Female reproductive performance in the mouse: effect of oral melatonin. *Molecules* 23:1845. doi: 10.3390/molecules23081845

Zhou, J., Liu, J., Pan, Z., Du, X., Li, X., and Ma, B. (2015). The let-7g microRNA promotes follicular granulosa cell apoptosis by targeting transforming growth factor-β type 1 receptor. *Mol. Cell. Endocrinol.* 409, 103–112. doi: 10.1016/j.mce.2015.03.012

Zhou, X., Li, L., Su, J., and Zhang, G. (2014). Decreased miR-204 in H. pylori-associated gastric cancer promotes cancer cell proliferation and invasion by targeting SOX4. *PLoS One* 9:e109057. doi: 10.1371/journal.pone.0101457

Zhou, X., Takatoh, J., and Wang, F. (2011). The mammalian class 3 PI3K (PIK3C3) is required for early embryogenesis and cell proliferation. *PLoS One* 6:e16358. doi: 10.1371/journal.pone.0016358

Conflict of Interest: The authors declare that the research was conducted in the absence of any commercial or financial relationships that could be construed as a potential conflict of interest.

frontiers in Cell and Developmental Biology

ORIGINAL RESEARCH
published: 26 November 2020
doi: 10.3389/fcell.2020.605609

HDAC6 Regulates the Fusion of Autophagosome and Lysosome to Involve in Odontoblast Differentiation

Yunyan Zhan, Haisheng Wang, Lu Zhang, Fei Pei and Zhi Chen**

The State Key Laboratory Breeding Base of Basic Science of Stomatology (Hubei-MOST) and Key Laboratory for Oral Biomedicine of Ministry of Education (KLOBM), School and Hospital of Stomatology, Wuhan University, Wuhan, China

OPEN ACCESS

Edited by:
Federica Di Sano, University of Rome Tor Vergata, Italy

Reviewed by:
Ella L. Kim, Johannes Gutenberg University Mainz, Germany
Mark J. Ranek, Johns Hopkins University, United States
Florence Carrouel, Université Claude Bernard Lyon 1, France

***Correspondence:**
Fei Pei
peifei@whu.edu.cn
Zhi Chen
zhichen@whu.edu.cn

Specialty section:
This article was submitted to Cell Death and Survival, a section of the journal Frontiers in Cell and Developmental Biology

Received: *12 September 2020*
Accepted: *06 November 2020*
Published: *26 November 2020*

Citation:
Zhan Y, Wang H, Zhang L, Pei F and Chen Z (2020) HDAC6 Regulates the Fusion of Autophagosome and Lysosome to Involve in Odontoblast Differentiation. Front. Cell Dev. Biol. 8:605609. doi: 10.3389/fcell.2020.605609

Odontoblast differentiation is an important process during tooth development in which pre-odontoblasts undergo elongation, polarization, and finally become mature secretory odontoblasts. Many factors have been found to regulate the process, and our previous studies demonstrated that autophagy plays an important role in tooth development and promotes odontoblastic differentiation in an inflammatory environment. However, it remains unclear how autophagy is modulated during odontoblast differentiation. In this study, we found that HDAC6 was involved in odontoblast differentiation. The odontoblastic differentiation capacity of human dental papilla cells was impaired upon HDAC6 inhibition. Moreover, we found that HDAC6 and autophagy exhibited similar expression patterns during odontoblast differentiation both *in vivo* and *in vitro*; the expression of HDAC6 and the autophagy related proteins ATG5 and LC3 increased as differentiation progressed. Upon knockdown of HDAC6, LC3 puncta were increased in cytoplasm and the autophagy substrate P62 was also increased, suggesting that autophagic flux was affected in human dental papilla cells. Next, we determined the mechanism during odontoblastic differentiation and found that the HDAC6 substrate acetylated-Tubulin was up-regulated when HDAC6 was knocked down, and LAMP2, LC3, and P62 protein levels were increased; however, the levels of ATG5 and Beclin1 showed no obvious change. Autophagosomes accumulated while the number of autolysosomes was decreased as determined by mRFP-GFP-LC3 plasmid labeling. This suggested that the fusion between autophagosomes and lysosomes was blocked, thus affecting the autophagic process during odontoblast differentiation. In conclusion, HDAC6 regulates the fusion of autophagosomes and lysosomes during odontoblast differentiation. When HDAC6 is inhibited, autophagosomes can't fuse with lysosomes, autophagy activity is decreased, and it leads to down-regulation of odontoblastic differentiation capacity. This provides a new perspective on the role of autophagy in odontoblast differentiation.

Keywords: differentiation, odontoblast, lysosome, autophagosome, fusion, HDAC6

INTRODUCTION

Odontogenesis is a complex process involving reciprocal interactions between the dental epithelium and mesenchymal cells (Thesleff and Nieminen, 1996). During this process, odontoblasts derived from cranial neural crest-originating mesenchyme cells produce dentin, which makes up the main portion of the tooth (Ruch et al., 1995; Kawashima and Okiji, 2016). Odontoblasts are a layer of long-living post-mitotic dental cells aligned in an ordered manner along the dental pulp (Sasaki and Garant, 1996). During odontoblast differentiation, pre-odontoblasts exit the cell cycle and then undergo cell growth, elongation, and polarization to finally become highly complex polarized secretory odontoblasts (Zhang et al., 2005; Biz et al., 2010). One major function of odontoblasts is to synthesize and secrete predentin matrix components, such as collagen type I, proteoglycans, and non-collagenous proteins like dentin sialoprotein (DSP) (Ruch et al., 1995; Sasaki and Garant, 1996). Thus, there are many activities, such as protein synthesis, protein turnover, and substance transport, taking place in odontoblasts.

Autophagy is an evolutionarily conserved homeostatic process involved in the degradation and recycling of proteins to maintain cell homeostasis and supply energy (He and Klionsky, 2009). Autophagy is initiated by the formation of double membrane vesicles that encapsulate cargo proteins or organelles to form mature autophagosomes (Hale et al., 2013). The autophagosomes go on to fuse with lysosomes to form autophagolysosomes and degrade their cargo (Zhang et al., 2013). As a recycling system, autophagy plays an important role in a variety of physiological process such as cell differentiation (Salemi et al., 2012), cell pluripotency (Sharif et al., 2017), and cell death (Denton et al., 2015). Recently, many studies have shown that autophagy is involved in various physiological process of odontoblasts. For example, the specific spatiotemporal expression pattern of LC3 in the tooth germ indicates that autophagy is involved in tooth development (Yang et al., 2013). Additionally, the autophagic-lysosomal system is involved in odontoblast longevity and aging (Couve et al., 2013). Autophagy is also thought to play a dual role in inflamed odontoblasts by modulating odontoblastic differentiation in the inflammatory microenvironment (Pei et al., 2016). However, the molecular mechanism by which autophagy regulates odontoblast differentiation remains largely unknown.

Histone deacetylases (HDACs) are a group of enzymes that remove acetyl groups from both histone and non-histone proteins (Gregoretti et al., 2004). HDAC6 is a unique member of the type II HDACs that is primarily localized in the cytoplasm; it contains two functional catalytic domains and a ubiquitin-binding zinc finger domain for the regulation of ubiquitination-mediated degradation (Hard et al., 2010). In addition to histones, the substrates of HDAC6 include acetylated-Tubulin (ac-Tubulin), Cortactin, retinoic acid inducible gene I (RIG-1), Hsp90, and β-Catenin (Zhang et al., 2015). Given its unique molecular structure and the diversity of its substrates, HDAC6 plays a vital role in cell migration, the immune response, and cell proliferation and differentiation (Hai et al., 2011; Li et al., 2013; Zheng et al., 2017). Recently, it has been found that HDAC activity plays a crucial role in osteoblast maturation (Ehnert et al., 2012). HDAC1 and HDAC3, which are type I HDACs, are thought to inhibit Runx2 expression and affect osteoblast differentiation (Schroeder et al., 2004; Liu et al., 2015). HDAC3 has been shown to interact with KLF4 during the initiation of odontoblastic induction (Tao et al., 2019). HDAC6 is also involved in human osteoblast mechanosensation (Ehnert et al., 2017). However, there are few studies of HDAC6 in odontoblasts, and the role of HDAC6 in odontoblast differentiation remains unclear.

Moreover, it has been found that autophagy and HDAC6 are closely related in many conditions. For example, in human breast cancer, HDAC6 forms complexes with CDK1 and induces its P62-dependent autophagy degradation (Galindo-Moreno et al., 2017). In pancreatic cancer, MicroRNA-221 induces autophagy through suppressing HDAC6 expression (Yang et al., 2018). During viral infection, HDAC6 induces stress granule autophagic degradation by acting as a cargo that is recognized by P62 (Zheng et al., 2020a). In Parkinson's disease, HDAC6 promotes autophagosome-lysosome fusion and autophagy (Wang et al., 2019). This indicates that HDAC6 can either induce or reduce autophagy in different pathologies. However, whether and how HDAC6 regulates autophagy in odontoblasts is unclear.

In this study, to further investigate the role of autophagy in odontoblast differentiation, we explored the role of HDAC6 in odontoblast differentiation and the relationship of HDAC6 and autophagy during this process.

MATERIALS AND METHODS

Cell Isolation and Culture

Human dental papilla cells (hDPCs) were isolated from the dental papilla tissues of the tooth germ of human third molars (Sonoyama et al., 2006). Dental papilla tissues were obtained from extracted lower third molar germ of healthy donors (12 years old) with informed consent. All procedures were performed according to the guidelines of the National Institutes of Health in regard to the use of human tissues and with permission by the Ethics Committee of the School and Hospital of Stomatology, Wuhan University (protocol No. 2018A62). After extraction, the tissue was washed three times with phosphate-buffered saline (PBS, HyClone, Logan, UT, United States) containing 2% penicillin and streptomycin (HyClone). Then, the dental papilla tissues were cut into small pieces (∼1 mm^3 in size). The tissue pieces were seeded into a T25 cell culture flask in α-modified Eagle's medium (α-MEM, HyClone) with 20% fetal bovine serum (FBS, Gibco, Thornton, NSW, Australia) and 1% penicillin and streptomycin (HyClone). The growth medium was changed once a week until the cells grew out, and then it was changed twice a week. Upon reaching confluence, cells were passaged at a 3-fold dilution. When the cells were passaged, the culture medium changed to include 10% fetal bovine serum. Cells between passage 3 and 6 were used in this study.

In vitro Odontoblastic Differentiation and Tubacin Treatment

For odontoblastic induction, cells were cultured as described previously (Chen et al., 2005; Pei et al., 2016). hDPCs were

seeded in 6-well plates at a density of 2×10^5 cells per well and cultured in mineralization-inducing medium (MM), which was α-MEM with 10% FBS, 1% penicillin and streptomycin, 10 mM sodium β-glycerophosphate (Sigma, St Louis, MO, USA), 50 mg/ml ascorbic acid (Sigma) and 10 nM dexamethasone (Sigma). MM was changed every 2 days. Cells were harvested 2 weeks after induction and underwent Alizarin Red-S staining to analyze calcified nodule formation. Proteins were harvested at different time points for western blots and were extracted at 2 weeks for alkaline phosphatase activity assays.

To inhibit the HDAC6 activity, Tubacin (Item No. 13691, Cayman Chemical Company, Michigan, United States) was added in the culture medium in a final concentration of 7.5 μmol/L of the cells with or without MM (Haggarty et al., 2003).

Small Interfering RNA and mRFP-GFP-LC3 Plasmid Transfection

For functional knock-down of HDAC6, an *HDAC6*-targeting small interfering RNA (siRNA; *siHDAC6*, Sigma) and the universal negative control siRNA were transfected into hDPCs. Cells were seeded into 6-well plates and then transfected with siRNA using Lipo2000 (Invitrogen, Thermo Fisher Scientific, Waltham, MA, United States) according to the manufacturer's instructions (Tao et al., 2019). Knockdown efficacy was confirmed by western blot. Odontoblastic differentiation was induced 48 h after transfection. For the tracing of autophagic flux, mRFP-GFP-LC3 plasmid (plasmid 21074; Addgene) was transfected into hDPCs following transfection with siRNA prior to the induction of odontoblastic differentiation using Lipo2000 according to the manufacturer's instructions(Kimura et al., 2007).

Double and Triple Immunofluorescence Staining

Double and triple immunofluorescence staining was performed as previously described (Pei et al., 2016). The lower mandibles of postnatal day 2.5 mice were dissected and fixed in 4% buffered paraformaldehyde, rinsed overnight, demineralized in 10% EDTA for 1 week, and then embedded in paraffin after being dehydrated. The paraffin block–embedded tissue was cut into 5 μm sections. After deparaffinizing, rehydrating, and undergoing antigen retrieval using a microwave, the tissues were blocked with 2.5% bovine serum albumin (BSA, Sigma–Aldrich, St Louis, MO, United States) for 1 h at 37°C, then incubated with anti-HDAC6 (1:100, Proteintech, Chicago, IL, USA) overnight at 4°C, and then incubated with Alexa Fluor 594 conjugated secondary antibody (CWBIO, Beijing, China) for 1 h. Next, the slides were again blocked with 2.5% BSA. Slides were incubated for 1 h at 37°C with primary antibodies against DSP (1:100, Santa Cruz, Biotechnology, Inc., Dallas, TX, USA) and ATG5 (1:100, Proteintech) were, followed by incubation with Alexa Fluor 488 conjugated secondary antibody following counterstaining with 4′,6-diamidino-2-phenylindole (DAPI, ZSGB-BIO, Beijing, China).

Cells were seeded on coverslips and transfected with *siHDAC6* after attachment. After inducing odontoblastic differentiation, the coverslips were washed with PBS and fixed with 4% paraformaldehyde or methyl alcohol at room temperature for 15 min. After being washed three times with PBS, the coverslips were blocked with 2.5% BSA for 1 h at 37°C, and then incubated with anti-HDAC6 primary antibody for double staining and both anti-ac-Tubulin (1:100, Proteintech) and anti-LC3 (1:100, Medical & Biological LaboratoriesCo., MBL, Nagoya, Japan) primary antibodies simultaneously for triple staining at 4°C overnight. Coverslips were then incubated with secondary antibodies conjugated with Alexa Fluor 488 or both Alexa Fluor 488 and Cy3 for 1 h. Next, the coverslips were again blocked with 2.5% BSA. After that the second primary antibodies against LC3 and HDAC6 were incubated for 1 h at 37°C, and coverslips were then incubated with Cy3- or Alexa Fluor 674-conjugated secondary antibodies, followed by counterstaining with 4′,6-diamidino-2-phenylindole (DAPI).

Tissues sections and cells were observed and photographed using a fluorescence microscope (Leica, Wetzlar, Germany) or by confocal fluorescence microscopy (Leica, Solms, Germany).

For mRFP-GFP-LC3 observation, cells were seeded on coverslips and transfected with *siHDAC6* and mRFP-GFP-LC3 plasmid after attachment. Following the induction of odontoblastic differentiation, coverslips were washed in PBS and fixed with 4% paraformaldehyde for 15 min at room temperature. After being washed three times with PBS, cells were stained with 4′,6-diamidino-2-phenylindole (DAPI) and were then directly observed by confocal fluorescence microscopy (Leica, Solms, Germany). The intensity of single red fluorescence (that not colocalized with green) and yellow fluorescence was quantified by Image Pro Plus (Media Cybernetics, Rockville, USA). The intensity was average of four random areas.

Western Blot Analysis

Cells were harvested at different time points and lysed in lysis buffer with protease and phosphatase inhibitor on ice for 3 min. Protein supernatants were harvested following centrifugation at 13,000 rpm for 10 min. Protein concentration was measured and standardized using the BCA Protein Assay Kit (Pierce Biotechnology, Rockford, IL, USA). Twenty-five microgram total protein samples were loaded and separated by 8 or 12% sodium dodecyl sulfate–polyacrylamide gel electrophoresis and then transferred to polyvinylidene fluoride membranes (Merck Millipore, Darmstadt, Germany). Membranes were immediately blocked with 5% nonfat milk for 1 h at room temperature and then incubated with the following primary antibodies: anti-HDAC6 (1:1,000, Proteintech), anti-DMP1 (1:4,000, Abcam, Cambridge, MA, USA), anti-DSP (1:1,000, Santa Cruz), anti-OSX (1:1,000, Santa Cruz), anti-GAPDH (1:8,000, Proteintech), anti-Beclin1 (1:1,000, Proteintech), anti-ATG5 (1:5,000, Abam), anti-P62 (1:1,000, Proteintech), anti-LAMP2 (1:1,000, GeneTex, Irvine, California, USA), anti-LC3 (1:1,000, MBL), anti-ac-Tubulin (1:1,000, Proteintech), and anti-Tubulin (1:1,000, Antgene, Wuhan, China) overnight at 4°C. Next, membranes were incubated with goat anti–rabbit or goat anti–mouse peroxidase–conjugated secondary antibody for 1 h at room temperature. Relative protein levels were determined by densitometry quantification using ImageJ (National Institutes of Health, Bethesda, MD, USA), and GAPDH was used as the loading control.

Alizarin Red Staining

Alizarin red staining was performed as previously described (Pei et al., 2016). Briefly, after hDPCs were cultured in MM for 14 days, the cells were fixed with 95% ethanol for 10 min after being washed with PBS. Cells were then stained with 1% Alizarin red (Sigma-Aldrich) solution for 20 min at room temperature. Then, cells were washed to remove residual Alizarin red and were photographed with an inverted phase contrast microscope (OLYMPUS IX41, Olympus, Shinjuku-ku, Tokyo, Japan) and the mineral alizarin red staining(AR-S) from each well was quantified. Stained cells were incubated in cetylpyridinium chloride (CPC, Solarbio Science Technology Co, Beijing, China) buffer (10% w/v) in 10 mM Na_2HPO_4 (PH7) at 37°C for 12 h to extract the mineralized tissue and then the OD_{550}nm was measured using a microplate reader. Mineralized nodule formation was represented as nmol AR-S per μg of total cellular protein. Total cellular protein content was determined by the BCA Protein Assay Kit. Two samples were used for each condition and the experiments were repeated three times.

Alkaline Phosphatase (ALPase) Activity Assay

Alkaline phosphatase is an enzyme produced by cells and is a marker of osteoblastic/odontogenic differentiation. Alkaline phosphatase enzyme activity of the cells in different groups was measured using the Alkaline Phosphatase Assay kit (Cat. A059-2 Jiancheng Bioengineering Institute, Nanjing, China) according to the manufacturer's instructions. The ALP substrate, the disodium phenyl phosphate, can be decomposed by the alkaline phosphatase in cell lysate and produce free phenol, free phenol can be further oxidized to red quinone derivatives which represent the amount of enzyme in cell lysate (Datta et al., 2005). Briefly, the cell lysate was added to a transparent 96-well plate with 100 μl ALP substrate solution and the plate was incubated for ∼15 min at 37°C in the dark. After incubation, 150 μl color development agent was added and the absorbance was measured at 520 nm using a multi-well plate reader. ALP activity was normalized to protein concentration (measured by the BCA Protein Assay Kit). Samples were run in triplicate and compared against phenol standards. ALP activity was calculated as 1 mol of phenol per mg protein.

Statistical Analysis

All data are presented as the mean ± SEM. GraphPad Prism 5.0 (GraphPad Software, La Jolla, CA, USA) was used to analyze and visualize the data. One-way ANOVA followed by Tukey's Multiple Comparison Test was used to analyze ALP activity and Alizarin red staining quantification in the MM, MM + siNC, MM + siHDAC6, MM + Tubacin treated hDPC groups compared to the control group. Experiments were all repeated independently three times. $P < 0.05$ was considered to be statistically significant.

RESULTS

HDAC6 Expression Increases During Odontoblast Differentiation

To observe the expression of HDAC6 during odontoblast differentiation, we first detected the protein expression pattern of HDAC6 during odontoblast differentiation in mouse molars and incisors. In mouse molars, HDAC6 was highly expressed in differentiated odontoblasts (**Figure 1A2**) when compared to undifferentiated cells in the apical region (**Figure 1A1**). HDAC6 colocalized with DSP in differentiated odontoblasts (**Figure 1A2**). In mouse incisors, which show the odontoblast differentiation process, HDAC6 exhibited a similar expression pattern. HDAC6 and the odontoblast differentiation maker DSP showed intense expression in differentiated odontoblasts (**Figure 1B**). Meanwhile, hDPCs were cultured in MM for 7 days to achieve odontoblastic differentiation *in vitro*. The protein levels of DSP, DMP1, and OSX increased during the differentiation process, and HDAC6 was also up-regulated in a time-dependent manner during odontoblastic differentiation (**Figures 1C,D**). This suggested that HDAC6 is involved in odontoblast differentiation both *in vivo* and *in vitro*.

HDAC6 Inhibition Inhibits Odontoblastic Differentiation in hDPCs

To further confirm the role of HDAC6 in odontoblast differentiation, *siHDAC6* or an inhibitor (Tubacin) was used to inhibit HDAC6 in hDPCs. Alizarin red staining revealed that the formation of mineralization nodules was clearly decreased in MM with both the *siHDAC6* (MM + *siHDAC6*) and Tubacin (MM + Tubacin) groups when compared to that of the MM group (**Figure 2A**). We then quantified the mineralized tissue using CPC buffer; the amount of mineralized tissue was increased in cells cultured in MM while it was significantly reduced following HDAC6 inhibition with *siHDAC6* or Tubacin (**Figure 2B**). Expression of the odontoblast differentiation markers DSP, DMP1, and OSX increased with MM culture, consistent with the above results. However, HDAC6 protein expression and the expression of odontoblast differentiation markers were decreased when cells were treated with *siHDAC6* or Tubacin (**Figure 2C**). ALP activity was also up-regulated in the MM group but was down-regulated upon HDAC6 inhibition (**Figure 2D**). These results demonstrated that HDAC6 played a vital role in odontoblast differentiation, and HDAC6 inhibition would inhibit the odontoblastic differentiation of hDPCs.

HDAC6 Affects Autophagic Flux in hDPCs

Given that we previously found that autophagy could regulate odontoblast differentiation for inflammatory defense (Pei et al., 2016) and in tooth development, autophagy activation was detected in differentiated odontoblasts (Yang et al., 2013). To investigate the relationship between HDAC6 and autophagy during odontoblast differentiation, we detected the expression of HDAC6 and the autophagy related molecules ATG5 and LC3 in a mouse incisor model using immunofluorescence staining. HDAC6 and ATG5 were both highly expressed in differentiated odontoblasts and were colocalized in the cytoplasm (**Figure 3A**). LC3 also colocalized with HDAC6 and was more highly expressed in differentiated odontoblasts than in undifferentiated cells (**Figure 3B**). The expression of LC3 II and ATG5 was increased during odontoblastic differentiation and peaked at 5 days (**Figure 3C**). While the expression of HDAC6 showed slightly change in the early time, its expression was also

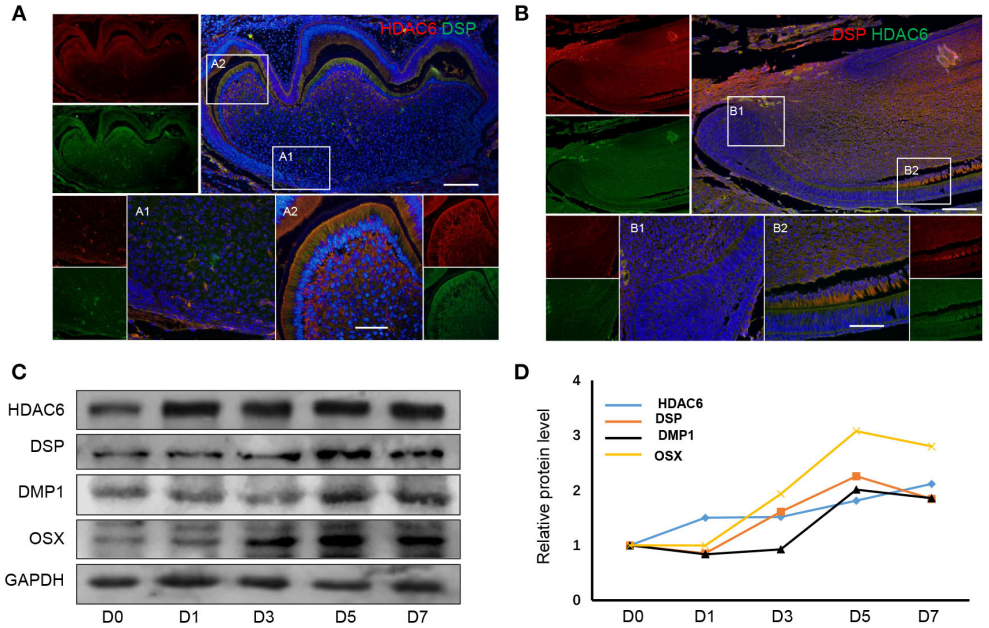

FIGURE 1 | HDAC6 expression increases during odontoblast differentiation. HDAC6 expression during odontoblast differentiation *in vivo* of mouse molar **(A)** and incisor **(B)** models as detected by HDAC6 and DSP double immunofluorescence staining. DAPI counterstaining (blue) indicates nuclei, green fluorescence represents DSP **(A)** or HDAC6 **(B)**, and red fluorescence represents HDAC6 **(A)** or DSP **(B)**. Scale bars = 25 μm. **(C,D)** The protein expression levels of HDAC6, DSP, DMP1, and OSX in hDPCs were analyzed following mineralized induction for 0–7 days.

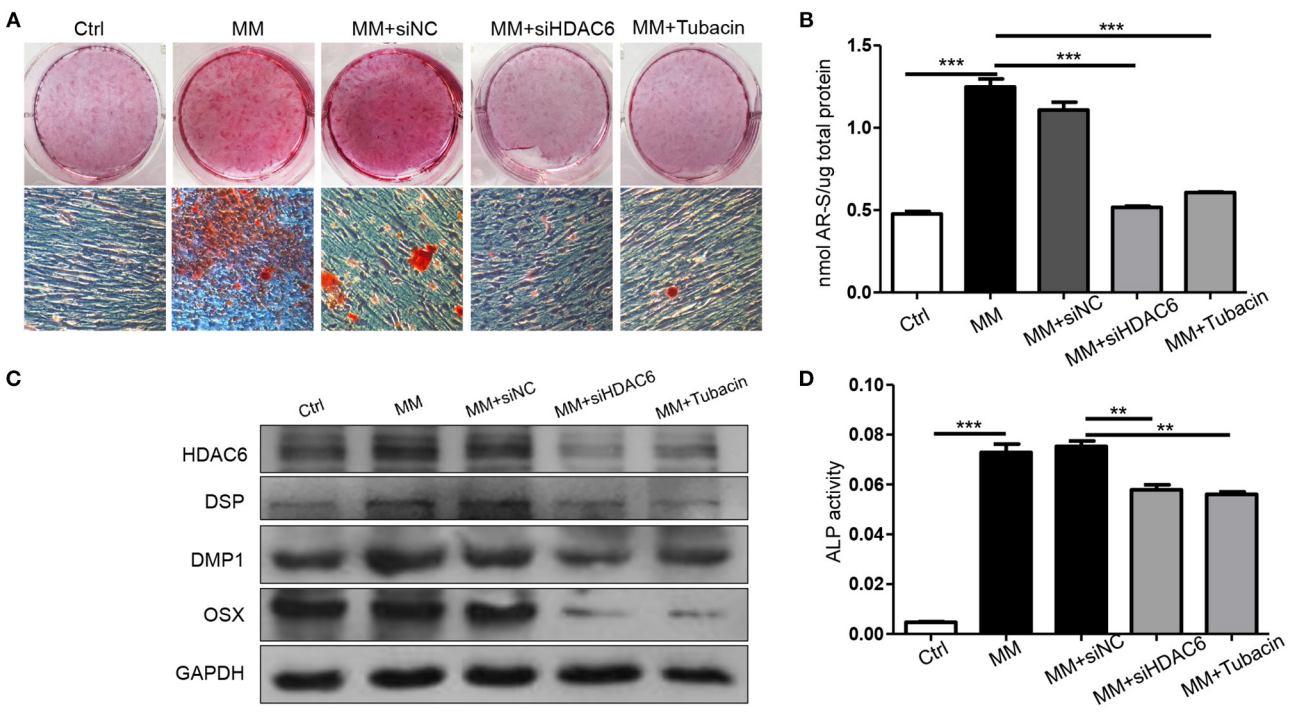

FIGURE 2 | Inhibition of HDAC6 impairs the odontoblastic differentiation of hDPCs *in vitro*. hDPCs were cultured in complete medium (Ctrl), mineralization-inducing medium (MM), MM with *siHDAC6* transfection (MM + siHDAC6), and MM with the HDAC6 inhibitor Tubacin (MM + Tubacin) for 14 days. **(A)** Alizarin red S was used to stain mineralization with red in the dishes and **(B)** cetylpyridinium chloride (CPC) was used to quantitative the relative levels of Alizarin red staining. **(C)** The expression of DSP, DMP1, and OSX was examined by western blotting. **(D)** ALP activity was tested in different groups. Results are representative of three independent experiments with similar results ± SD. Data were analyzed using one-way ANOVA with Tukey's multiple comparison test. ***$P < 0.001$, **$P < 0.01$.

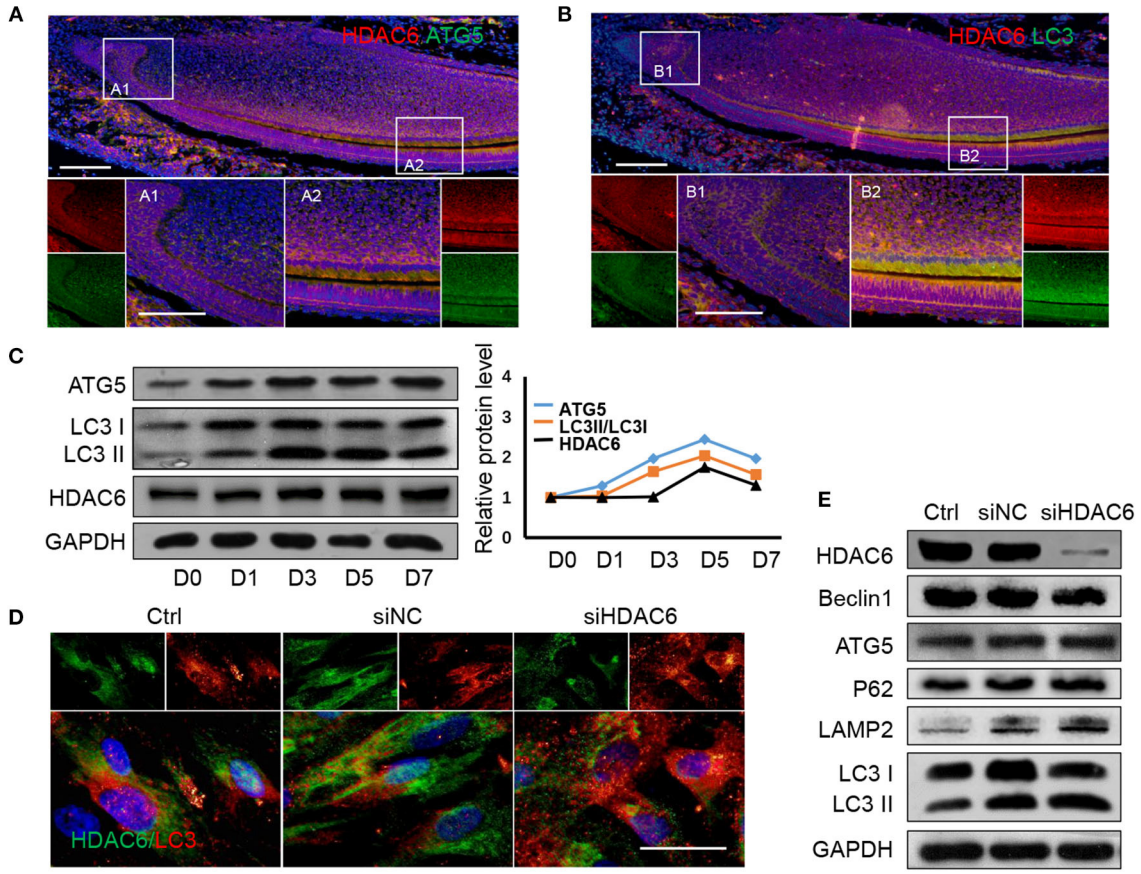

FIGURE 3 | HDAC6 and autophagy related proteins show similar expression patterns during odontoblast differentiation and HDAC6 affects autophagic flux. **(A)** The expression of HDAC6 and ATG5 in mouse incisors was detected by double immunofluorescence staining. DAPI counterstaining (blue) shows nuclei, green fluorescence represents ATG5, and red fluorescence represents HDAC6. Scale bars = 25 μm. **(B)** The expression of HDAC6 and LC3 in mouse incisors were detected by double immunofluorescence staining. DAPI counterstaining (blue) shows nuclei, green fluorescence represents LC3, and red fluorescence represents HDAC6. Scale bars = 25 μm. **(C)** The protein expression levels of HDAC6 and the autophagy related molecules ATG5 and LC3II/I were analyzed following mineralized induction for 0–7 days and were quantified using densitometry (right panel). **(D)** The expression and localizatoin of HDAC6 and LC3 were detected by double immunofluorescence staining. DAPI counterstaining (blue) shows nuclei, green fluorescence represents HDAC6, and red fluorescence represents LC3. Scale bars = 50 μm. **(E)** The expression levels of HDAC6, ATG5, Beclin1, P62, and LAMP2, and the ratio of LC3II/I were examined by western blotting. Experiments were repeated in triplicate.

increased during odontoblast differentiation and peaked at 5 days (**Figure 3C**). These suggested HDAC6 and autophagy participated in odontoblastic differentiation and had close relationship. Next, to explore the relationship between HDAC6 and autophagy, we observed autophagic flux after knocking down HDAC6 in hDPCs. We found HDAC6 expression to be reduced after transfection with *siHDAC6*, while the signal from LC3 puncta became stronger (**Figure 3D**). The ratio of LC3II/LC3I was up-regulated (**Figure 3E**). It suggested the accumulation of autophagosomes. However, more autophagosomes don't equate with increased autophagy. A block in trafficking to lysosomes will also lead to autophagosomes accumulation, which actually indicates autophagy down-regulation (Klionsky et al., 2016). So we further detected changes in protein levels to confirm the change in autophagic flux. Interestingly, the level of the autophagy degradative substrate P62 increased following HDAC6 inhibition, suggesting that autophagy degradation was inhibited. Meanwhile Beclin1 and ATG5, which are involved in the autophagy initiation and elongation stages, showed no obvious changes, and the expression of the lysosome marker LAMP2 increased (**Figure 3E**). These results revealed that knocking down HDAC6 blocked autophagic flux, autophagosomes accumulated with HDAC6 inhibition in hDPCs.

HDAC6 Deficiency Inhibits Autophagosome and Lysosome Fusion During Odontoblastic Differentiation

To investigate the mechanisms by which HDAC6 regulates autophagic flux during odontoblast differentiation, we first detected the expression of the HDAC6 substrate ac-Tubulin during odontoblast differentiation. We found that the level of ac-Tubulin increased when HDAC6 was knocked down (**Figures 4A,B**). Next, we performed multiple

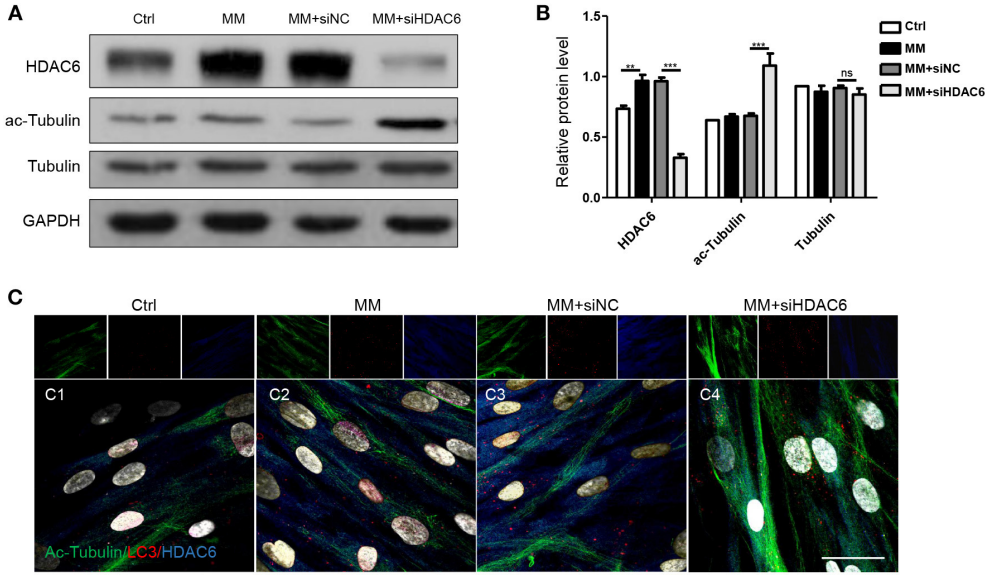

FIGURE 4 | HDAC6 regulates tubulin networks during odontoblast differentiation. hDPCs were cultured in complete medium (Ctrl), mineralization-inducing medium (MM), MM following siNC (negative control) transfection, and MM following *siHDAC6* transfection. **(A)** The protein levels of HDAC6, acetylated-tubulin (ac-Tubulin), and tubulin were detected, and their relative levels **(B)** were quantified and normalized to GAPDH using Image J. Data are presented as mean ± SD. Data were analyzed using one-way ANOVA with Tukey' multiple comparison test. $^{***}P < 0.001$, $^{**}P < 0.01$. **(C)** Triple immunofluorescence staining showed the distribution of HDAC6, ac-Tubulin, and LC3 in different conditions. DAPI counterstaining (gray) shows nuclei, green fluorescence represents ac-Tubulin, red fluorescence represents LC3, and blue fluorescence represents HDAC6. Scale bars = 25 μm.

immunofluorescence staining to visualize the distribution of HDAC6, ac-Tubulin, and LC3 during odontoblast differentiation. HDAC6 was distributed widely in the cytoplasm and its immunofluorescence signal became stronger upon mineralization induction (**Figure 4C1,C2**). Ac-Tubulin, representing the cytoskeleton, was more highly expressed and exhibited a wider distribution in the *siHDAC6* transfected group than the *siNC* transfected group (**Figure 4C3,C4**). LC3 was localized as puncta among ac-Tubulin (**Figure 4C**), and the LC3 puncta increased following HDAC6 knockdown (**Figure 4C3,C4**). These results indicated that HDAC6 regulated autophagic flux and ac-Tubulin.

To further confirm the specific stage at which HDAC6 is involved in autophagy, we detected autophagy during odontoblastic differentiation. We found the protein levels of HDAC6 and ATG5, and the ratio of LC3II/I increased when hDPCs were induced by MM (**Figures 5A,B**). This was consistent with their expression *in vivo*. Upon HDAC6 knocking down, ATG5 expression showed no obvious change, while P62 protein level increased, along with that of LAMP2 and the ratio of LC3II/I (**Figures 5A,B**). It suggested autophagsomes accumulation, and the decreased degradation. That illustrated the increased atuophagosomes was not because of increased autophagy induction, in contrast, it was due to autophagy process inhibition. Moreover, cells were transfected with mRFP-GFP-LC3 plasmid to trace autophagic flux. The GFP signal is sensitive to the acidic conditions of the lysosome lumen whereas mRFP is more stable. Therefore, colocalization of both GFP and mRFP fluorescence (yellow fluorescence) indicates autophagosmes have not fused with lysosomes, while a mRFP signal without GFP corresponds to autolysosomes (autophagosomes fused with lysosomes) (Klionsky et al., 2016). First, basic autophagy was observed in hDPCs without induction (**Figure 5C1**). Upon mineralization induction, mRFP fluorescent puncta increased, indicating that autophagy was increased and autophagic flux was occurring (**Figures 5C2**, **D**). When HDAC6 was knocked down, yellow fluorescent puncta increased in the cytoplasm, but red fluorescent (without GFP) puncta decreased (**Figures 5C3,C4**, **D**), indicating that autophagosomes were formed, but the fusion of autophagosomes and lysosomes was blocked, the autophagy activity was reduced. Ultimately, this indicated that knocking down of HDAC6 inhibited the fusion of autophagosomes and lysosomes and lead to decreased autophagy. These results indicated that HDAC6 regulated odontoblast differentiation by maintaining the fusion of autophagosomes and lysosomes through influencing the microtubule system within the cytoplasm.

DISCUSSION

HDAC6 is involved in a number of cellular processes due to its cytoplasmic localization and the various functions of its diverse substrates. HDAC6 is a component of the signaling pathway that regulates cell morphology and maturation (Destaing et al., 2005). Recently, HDAC6 has been shown to be involved in osteoblast differentiation in several osteoblastic cell lines (Ozaki et al., 2013; Wang et al., 2020) and valvular interstitial cells (Fu et al., 2019). However, there has been limited investigation

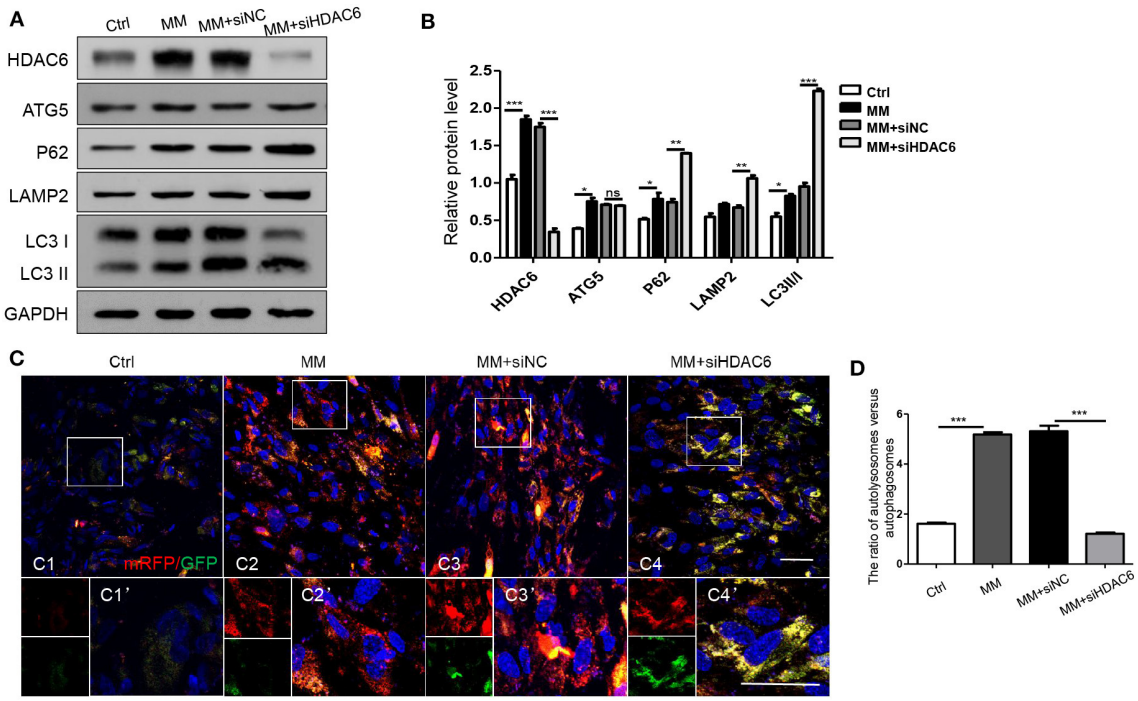

FIGURE 5 | HDAC6 affects the fusion of autophagosomes and lysosomes during odontoblast differentiation. hDPCs were cultured in complete medium (Ctrl), mineralization-inducing medium (MM), MM following siNC (negative control) transfection, and MM following *siHDAC6* transfection. The expression levels of HDAC6, ATG5, P62, LAMP2, and LC3II/I were examined **(A)** and quantified using GAPDH as a loading control with Image J **(B)**. Results are representative of three independent experiments with similar results ± SD. Data were analyzed using one-way ANOVA with Tukey's multiple comparison test. ***$P < 0.001$, **$P < 0.01$, *$P < 0.05$. **(C)** mRFP-GFP-LC3 plasmid was transfected into hDPCs prior to MM induction to trace autophagosomes and lysosomes. mRFP (red) indicated autolysosomes and yellow indicates autophagosomes. Scale bars =50 μm. **(D)** The ration of autolysosomes (sole red fluorescence without GFP) vs. autophagosomes (yellow fluorescence) was quantified by Image Pro Plus and analyzed using one-way ANOVA with Tukey's multiple comparison test. ***$P < 0.001$.

of its role in odontoblast differentiation. Our study found that HDAC6 was more highly expressed in differentiated odontoblasts *in vivo*. HDAC6 expression also increased during odontoblast differentiation of hDPCs *in vitro*. Further, we found that knocking down HDAC6 in hDPCs impaired their odontoblastic differentiation ability. This illustrates that HDAC6 is involved in odontoblast differentiation.

Autophagy is important for proteins turnover and cell homeostasis, and participates in the maintenance of stem-like features and the remodeling of cells undergoing differentiation (Sotthibundhu et al., 2018). The role of autophagy in odontoblasts has recently been explored. Autophagy was detected in differentiated odontoblasts during embryonic and postnatal stages (Yang et al., 2013). In our studies, we found ATG5 and LC3 to be highly expressed in differentiated odontoblasts in incisors. Expression of LC3 and ATG5 also increased during odontoblast differentiation *in vitro*. Additionally, recent studies have also found the autophagic machinery to be involved in autophagy-dependent secretion of many proteins, such as TGF-beta, IL-1beta and some extracellular matrix components (New and Thomas, 2019). Many activities, such as protein transport, organelle recycling, and secretory activities, occur during odontoblast differentiation that are closely with autophagy activation. It is clear that autophagy is highly activated and required during odontoblast differentiation.

Recently, HDACs were found to regulate autophagy at multiple levels, such as regulating transcription factors to modulate autophagy, modifying the acetylation status and activity of autophagy proteins, and affecting cytoskeletal proteins to modulate the autophagy environment (Bánréti et al., 2013). We found that HDAC6 exhibited a similar expression pattern as autophagy molecules during odontoblast differentiation. HDAC6, ATG5 and LC3 were colocalized in differentiated odontoblasts in mouse incisors. The expression of HDAC6, ATG5, and LC3II increased during mineralization induction of hDPCs *in vitro*, suggesting that HDAC6 was closely associated with autophagy during odontoblast differentiation. Interestingly, LC3 puncta increased in the cytoplasm following HDAC6 knocking down in hDPCs. Additionally, following HDAC6 knocking down, ATG5 and Beclin1, proteins associated with the autophagy initiation stage, showed no change, while the autophagosome and lysosome markers LC3 and LAMP2 increased, along with autophagy substrate P62. This demonstrated that autophagic flux was affected by HDAC6 inhibition.

HDAC6 exhibits special characteristics when compared with other HDACs, beyond the canonical roles in epigenetic modification of histones and transcriptional activity. The deacetylation role of HDACs has been explored in cell differentiation. Our previous study showed that acetylation was involved in dentinogenesis, and HDAC3 regulated histone acetylation during odontoblast differentiation (Tao et al., 2019). HDAC6 could also deacetylate histones related to Runx2 (Ozaki et al., 2013) and acted as a co-repressor for Runx2 transcription to suppress the osteoblastic differentiation of MC3T3 cells (Zhu et al., 2011). However, recent studies have found that HDAC6 regulates the acetylation of some proteins, such as Cortactin and ac-Tubulin, and has weak histone deacetylase activity. HDAC6 deacetylates ac-Tubulin, which is involved in the transport of cargos along microtubule tracks (Boyault et al., 2007; Valenzuela-Fernández et al., 2008). Lee point out that HDAC6 could also promote autophagy by recruiting actin-remodeling machinery and assembling the F-actin network (Lee et al., 2010). In our study, the formation and distribution of ac-Tubulin increased after HDAC6 was inhibited with siRNA during odontoblast differentiation, LC3 puncta increased and localized along ac-Tubulin, suggesting that HDAC6 regulated microtubule and autophagosome transport during odontoblastic differentiation. Our results indicated that HDAC6 could regulate autophagy through the cytoskeleton and may be involved in autophagy machinery transport.

The role of autophagy depends on the autophagic flux, which includes the formation of autophagosomes in cells, their fusion with lysosomes, and then the degradation of cargos (Zhang et al., 2013). In our study, LC3II/I ratio up-regulated and LC3 puncta increased after HDAC6 was inhibited, which suggested autophagosomes accumulation. While, the autophagy initiation protein ATG5 and Beclin1 showed no obvious change, autophagy substrate P62 increased with HDAC6 inhibition. It illustrated increased autophagsosomes was not because of increased autophagy activation, but blocked autophagy flux. We also detected autophagic flux using the mRFP-GFP-LC3 plasmid, which enabled visualization of autophagic flux during odontoblast differentiation. When HDAC6 was inhibited, the number of autolysosomes was decreased but that of autophagosomes was increased. This suggested HDAC6 inhibition would block the fusion stage of autophagosome and lysosome, then lead to decreased autophagy activity. However Zheng et al. (2020b) found that HDAC6 inhibition restored autophagy flux in axonal regeneration and Li et al. (2019) found HDAC6 inhibition induced autophagy flux in BMSCs. As HDAC6 regulates autophagy at multiple levels, it influences autophagy differently due to the cell type and the environment. It facilitated the fusion of autophagosomes to lysosomes by promting F-actin remodeling in MEFs (Lee et al., 2010). It also promoted autophagosome-lysosome fusion and autophagy by deacetylating Cortactin in mouse embryonic fibroblasts (Wang et al., 2019). What is more, it showed that HDAC6 inhibition downregulated autophagy in differentiated breast cancer cells but upregulated autophagy in cancer stem-like cells (Sharif et al., 2019). It is complex of HDAC6 in regulating autophagy. So, as we found in our study, in odontoblasts, HDAC6 could keep autophagy process by maintaining the fusion between autophagosomes and lysosomes during odontoblast differentiation.

Further, odontoblasts are able to recognize the pathogen-associated molecular patterns released by bacteria from carious lesions and produce pro-inflammatory mediators in response (Farges et al., 2013). Odontoblast is important in inflammation defense. Our previous study also found autophagy played an important role in inflammatory defense in odontoblasts (Pei et al., 2016). As such, our study on the role of HDAC6 in regulating odontoblast differentiation and the relationship of HDAC6 and autophagy during odontoblast differentiation also provides a new perspective on the treatment of caries.

In conclusion, through investigating the role of HDAC6 in odontoblast differentiation and its relationship with autophagy during this process, we find that HDAC6 affects the fusion of autophagosomes and lysosomes to maintain autophagy flux, keep autophagy activity to involve in odontoblast differentiation. When HDAC6 is inhibited, autophagosomes can't fuse with lysosome, autophagy activity is decreased, which leads to down-regulation of odontoblastic differentiation capacity.

DATA AVAILABILITY STATEMENT

The original contributions generated for the study are included in the article/supplementary materials, further inquiries can be directed to the corresponding author/s.

ETHICS STATEMENT

The studies involving human participants were reviewed and approved by the School and hospital of Stomatology, Wuhan University. Written informed consent to participate in this study was provided by the participants' legal guardian/next of kin. The animal study was reviewed and approved by Institutional Animal Care and Use Committees at the School and Hospital of Stomatology of Wuhan University.

AUTHOR CONTRIBUTIONS

YZ performed the research, collected and analyzed the data, and wrote the manuscript. HW and LZ performed the data collection and analysis. FP and ZC designed the research, supported financial support for the research, and revised the manuscript. All authors contributed to the article and approved the submitted version.

FUNDING

This work was supported by the National Natural Science Foundation of China (Grant No. 81771066) and Young Scientists Fund of the National Natural Science Foundation of China (Grant No. 81800963).

REFERENCES

Bánréti, A., Sass, M., and Graba, Y. (2013). The emerging role of acetylation in the regulation of autophagy. *Autophagy* 9, 819–829. doi: 10.4161/auto.23908

Biz, M. T., Marques, M. R., Crema, V. O., Moriscot, A. S., and dos Santos, M. F. (2010). GTPases RhoA and Rac1 are important for amelogenin and DSPP expression during differentiation of ameloblasts and odontoblasts. *Cell Tissue Res.* 340, 459–470. doi: 10.1007/s00441-010-0961-0

Boyault, C., Sadoul, K., Pabion, M., and Khochbin, S. (2007). HDAC6, at the crossroads between cytoskeleton and cell signaling by acetylation and ubiquitination. *Oncogene* 26, 5468–5476. doi: 10.1038/sj.onc.1210614

Chen, S., Rani, S., Wu, Y., Unterbrink, A., Gu, T. T., Gluhak-Heinrich, J., et al. (2005). Differential regulation of dentin sialophosphoprotein expression by Runx2 during odontoblast cytodifferentiation. *J. Biol. Chem.* 280, 29717–29727. doi: 10.1074/jbc.M502929200

Couve, E., Osorio, R., and Schmachtenberg, O. (2013). The amazing odontoblast: activity, autophagy, and aging. *J. Dental Res.* 92, 765–772. doi: 10.1177/0022034513495874

Datta, N., Holtorf, H. L., Sikavitsas, V. I., Jansen, J. A., and Mikos, A. G. (2005). Effect of bone extracellular matrix synthesized in vitro on the osteoblastic differentiation of marrow stromal cells. *Biomaterials* 26, 971–977. doi: 10.1016/j.biomaterials.2004.04.001

Denton, D., Xu, T., and Kumar, S. (2015). Autophagy as a pro-death pathway. *Immunol. Cell Biol.* 93, 35–42. doi: 10.1038/icb.2014.85

Destaing, O., Saltel, F., Gilquin, B., Chabadel, A., Khochbin, S., Ory, S., et al. (2005). A novel Rho-mDia2-HDAC6 pathway controls podosome patterning through microtubule acetylation in osteoclasts. *J. Cell Sci.* 118(Pt 13), 2901–2911. doi: 10.1242/jcs.02425

Ehnert, S., Sreekumar, V., Aspera-Werz, R. H., Sajadian, S. O., Wintermeyer, E., Sandmann, G. H., et al. (2017). TGF-β(1) impairs mechanosensation of human osteoblasts via HDAC6-mediated shortening and distortion of primary cilia. *J. Mol. Med.* 95, 653–663. doi: 10.1007/s00109-017-1526-4

Ehnert, S., Zhao, J., Pscherer, S., Freude, T., Dooley, S., Kolk, A., et al. (2012). Transforming growth factor β1 inhibits bone morphogenic protein (BMP)-2 and BMP-7 signaling via upregulation of Ski-related novel protein N (SnoN): possible mechanism for the failure of BMP therapy? *BMC Med.* 10:101. doi: 10.1186/1741-7015-10-101

Farges, J. C., Alliot-Licht, B., Baudouin, C., Msika, P., Bleicher, F., and Carrouel, F. (2013). Odontoblast control of dental pulp inflammation triggered by cariogenic bacteria. *Front. Physiol.* 4:326. doi: 10.3389/fphys.2013.00326

Fu, Z., Li, F., Jia, L., Su, S., Wang, Y., Cai, Z., et al. (2019). Histone deacetylase 6 reduction promotes aortic valve calcification via an endoplasmic reticulum stress-mediated osteogenic pathway. *J. Thorac. Cardiovasc. Surg.* 158, 408–417.e402. doi: 10.1016/j.jtcvs.2018.10.136

Galindo-Moreno, M., Giráldez, S., Sáez, C., Japón, M., Tortolero, M., and Romero, F. (2017). Both p62/SQSTM1-HDAC6-dependent autophagy and the aggresome pathway mediate CDK1 degradation in human breast cancer. *Sci Rep.* 7:10078. doi: 10.1038/s41598-017-10506-8

Gregoretti, I. V., Lee, Y. M., and Goodson, H. V. (2004). Molecular evolution of the histone deacetylase family: functional implications of phylogenetic analysis. *J. Mol. Biol.* 338, 17–31. doi: 10.1016/j.jmb.2004.02.006

Haggarty, S. J., Koeller, K. M., Wong, J. C., Grozinger, C. M., and Schreiber, S. L. (2003). Domain-selective small-molecule inhibitor of histone deacetylase 6 (HDAC6)-mediated tubulin deacetylation. *Proc. Natl. Acad. Sci. U. S. A.* 100, 4389–4394. doi: 10.1073/pnas.0430973100

Hai, T., Hao, J., Wang, L., Jouneau, A., and Zhou, Q. (2011). Pluripotency maintenance in mouse somatic cell nuclear transfer embryos and its improvement by treatment with the histone deacetylase inhibitor TSA. *Cell. Reprogram.* 13, 47–56. doi: 10.1089/cell.2010.0042

Hale, A. N., Ledbetter, D. J., Gawriluk, T. R., and Rucker, E. B. III. (2013). Autophagy: regulation and role in development. *Autophagy* 9, 951–972. doi: 10.4161/auto.24273

Hard, R. L., Liu, J., Shen, J., Zhou, P., and Pei, D. (2010). HDAC6 and Ubp-M BUZ domains recognize specific C-terminal sequences of proteins. *Biochemistry* 49, 10737–10746. doi: 10.1021/bi101014s

He, C., and Klionsky, D. J. (2009). Regulation mechanisms and signaling pathways of autophagy. *Ann. Rev. Genet.* 43, 67–93. doi: 10.1146/annurev-genet-102808-114910

Kawashima, N., and Okiji, T. (2016). Odontoblasts: specialized hard-tissue-forming cells in the dentin-pulp complex. *Congen. Anomalies* 56, 144–153. doi: 10.1111/cga.12169

Kimura, S., Noda, T., and Yoshimori, T. (2007). Dissection of the autophagosome maturation process by a novel reporter protein, tandem fluorescent-tagged LC3. *Autophagy* 3, 452–460. doi: 10.4161/auto.4451

Klionsky, D. J., Abdelmohsen, K., Abe, A., Abedin, M. J., Abeliovich, H., Acevedo Arozena, A., et al. (2016). Guidelines for the use and interpretation of assays for monitoring autophagy (3rd edition). *Autophagy* 12, 1–222. doi: 10.1080/15548627.2015.1100356

Lee, J. Y., Koga, H., Kawaguchi, Y., Tang, W., Wong, E., Gao, Y. S., et al. (2010). HDAC6 controls autophagosome maturation essential for ubiquitin-selective quality-control autophagy. *EMBO J.* 29, 969–980. doi: 10.1038/emboj.2009.405

Li, Y., Shin, D., and Kwon, S. H. (2013). Histone deacetylase 6 plays a role as a distinct regulator of diverse cellular processes. *FEBS J* 280, 775–793. doi: 10.1111/febs.12079

Li, Z., Liu, S., Fu, T., Peng, Y., and Zhang, J. (2019). Microtubule destabilization caused by silicate via HDAC6 activation contributes to autophagic dysfunction in bone mesenchymal stem cells. *Stem Cell. Res. Therapy* 10:351. doi: 10.1186/s13287-019-1441-4

Liu, T., Hou, L., Zhao, Y., and Huang, Y. (2015). Epigenetic silencing of HDAC1 by miR-449a upregulates Runx2 and promotes osteoblast differentiation. *Int. J. Mol. Med.* 35, 238–246. doi: 10.3892/ijmm.2014.2004

New, J., and Thomas, S. M. (2019). Autophagy-dependent secretion: mechanism, factors secreted, and disease implications. *Autophagy* 15, 1682–1693. doi: 10.1080/15548627.2019.1596479

Ozaki, T., Wu, D., Sugimoto, H., Nagase, H., and Nakagawara, A. (2013). Runt-related transcription factor 2 (RUNX2) inhibits p53-dependent apoptosis through the collaboration with HDAC6 in response to DNA damage. *Cell Death Dis.* 4:e610. doi: 10.1038/cddis.2013.127

Pei, F., Wang, H. S., and Chen, Z. (2016). Autophagy regulates odontoblast differentiation by suppressing NF-κB activation in an inflammatory environment. *Cell Death Dis.* 7:e2122. doi: 10.1038/cddis.2015.397

Ruch, J. V., Lesot, H., and Bègue-Kirn, C. (1995). Odontoblast differentiation. *Int. J. Dev. Biol.* 39, 51–68.

Salemi, S., Yousefi, S., Constantinescu, M. A., Fey, M. F., and Simon, H. U. (2012). Autophagy is required for self-renewal and differentiation of adult human stem cells. *Cell Res.* 22, 432–435. doi: 10.1038/cr.2011.200

Sasaki, T., and Garant, P. R. (1996). Structure and organization of odontoblasts. *Anat. Rec.* 245, 235–249. doi: 10.1002/(SICI)1097-0185(199606)245:2<235::AID-AR10>3.0.CO;2-Q

Schroeder, T. M., Kahler, R. A., Li, X., and Westendorf, J. J. (2004). Histone deacetylase 3 interacts with runx2 to repress the osteocalcin promoter and regulate osteoblast differentiation. *J. Biol. Chem.* 279, 41998–42007. doi: 10.1074/jbc.M403702200

Sharif, T., Martell, E., Dai, C., Ghassemi-Rad, M. S., Hanes, M. R., Murphy, P. J., et al. (2019). HDAC6 differentially regulates autophagy in stem-like versus differentiated cancer cells. *Autophagy* 15, 686–706. doi: 10.1080/15548627.2018.1548547

Sharif, T., Martell, E., Dai, C., Kennedy, B. E., Murphy, P., Clements, D. R., et al. (2017). Autophagic homeostasis is required for the pluripotency of cancer stem cells. *Autophagy* 13, 264–284. doi: 10.1080/15548627.2016.1260808

Sonoyama, W., Liu, Y., Fang, D., Yamaza, T., Seo, B. M., Zhang, C., et al. (2006). Mesenchymal stem cell-mediated functional tooth regeneration in swine. *PLoS ONE* 1:e79. doi: 10.1371/journal.pone.0000079

Sotthibundhu, A., Promjuntuek, W., Liu, M., Shen, S., and Noisa, P. (2018). Roles of autophagy in controlling stem cell identity: a perspective of self-renewal and differentiation. *Cell Tissue Res.* 374, 205–216. doi: 10.1007/s00441-018-2829-7

Tao, H., Lin, H., Sun, Z., Pei, F., Zhang, J., Chen, S., et al. (2019). Klf4 promotes dentinogenesis and odontoblastic differentiation via modulation of TGF-β signaling pathway and interaction with histone acetylation. *J. Bone Miner. Res.* 34, 1502–1516. doi: 10.1002/jbmr.3716

Thesleff, I., and Nieminen, P. (1996). Tooth morphogenesis and cell differentiation. *Curr. Opin. Cell Biol.* 8, 844–850. doi: 10.1016/S0955-0674(96)80086-X

Valenzuela-Fernández, A., Cabrero, J. R., Serrador, J. M., and Sánchez-Madrid, F. (2008). HDAC6: a key regulator of cytoskeleton, cell migration and cell-cell interactions. *Trends Cell Biol.* 18, 291–297. doi: 10.1016/j.tcb.2008.04.003

Wang, N., Wang, H., Chen, J., Wang, F., Wang, S., Zhou, Q., et al. (2020). ACY-1215, a HDAC6 inhibitor, decreases the dexamethasone-induced suppression of osteogenesis in MC3T3-E1 cells. *Mol. Med. Rep.* 22, 2451–2459. doi: 10.3892/mmr.2020.11319

Wang, R., Tan, J., Chen, T., Han, H., Tian, R., Tan, Y., et al. (2019). ATP13A2 facilitates HDAC6 recruitment to lysosome to promote autophagosome-lysosome fusion. *J. Cell Biol.* 218, 267–284. doi: 10.1083/jcb.201804165

Yang, J. W., Zhu, L. X., Yuan, G. H., Chen, Y. X., Zhang, L., Zhang, L., et al. (2013). Autophagy appears during the development of the mouse lower first molar. *Histochem. Cell Biol.* 139, 109–118. doi: 10.1007/s00418-012-1016-2

Yang, Y., Sun, Y., Wang, H., Li, H., Zhang, M., Zhou, L., et al. (2018). MicroRNA-221 induces autophagy through suppressing HDAC6 expression and promoting apoptosis in pancreatic cancer. *Oncol. Lett.* 16, 7295–7301. doi: 10.3892/ol.2018.9513

Zhang, L., Liu, S., Liu, N., Zhang, Y., Liu, M., Li, D., et al. (2015). Proteomic identification and functional characterization of MYH9, Hsc70, and DNAJA1 as novel substrates of HDAC6 deacetylase activity. *Protein Cell* 6, 42–54. doi: 10.1007/s13238-014-0102-8

Zhang, X. J., Chen, S., Huang, K. X., and Le, W. D. (2013). Why should autophagic flux be assessed? *Acta Pharmacol. Sin.* 34, 595–599. doi: 10.1038/aps.2012.184

Zhang, Y. D., Chen, Z., Song, Y. Q., Liu, C., and Chen, Y. P. (2005). Making a tooth: growth factors, transcription factors, and stem cells. *Cell Res.* 15, 301–316. doi: 10.1038/sj.cr.7290299

Zheng, K., Jiang, Y., He, Z., Kitazato, K., and Wang, Y. (2017). Cellular defence or viral assist: the dilemma of HDAC6. *J. Gen. Virol.* 98, 322–337. doi: 10.1099/jgv.0.000679

Zheng, Y., Zhu, G., Tang, Y., Yan, J., Han, S., Yin, J., et al. (2020a). HDAC6, a novel cargo for autophagic clearance of stress granules, mediates the repression of the type I interferon response during coxsackievirus A16 infection. *Front. Microbiol.* 11:78. doi: 10.3389/fmicb.2020.00078

Zheng, Z., Zhou, Y., Ye, L., Lu, Q., Zhang, K., Zhang, J., et al. (2020b). Histone deacetylase 6 inhibition restores autophagic flux to promote functional recovery after spinal cord injury. *Exp. Neurol.* 324:113138. doi: 10.1016/j.expneurol.2019.113138

Zhu, J., Shimizu, E., Zhang, X., Partridge, N. C., and Qin, L. (2011). EGFR signaling suppresses osteoblast differentiation and inhibits expression of master osteoblastic transcription factors Runx2 and Osterix. *J. Cell. Biochem.* 112, 1749–1760. doi: 10.1002/jcb.23094

Conflict of Interest: The authors declare that the research was conducted in the absence of any commercial or financial relationships that could be construed as a potential conflict of interest.

frontiers in Cell and Developmental Biology

REVIEW
published: 10 December 2020
doi: 10.3389/fcell.2020.602901

Autophagy in the Regulation of Tissue Differentiation and Homeostasis

*Cristiana Perrotta[1], Maria Grazia Cattaneo[2], Raffaella Molteni[2] and Clara De Palma[2]**

[1] Department of Biomedical and Clinical Sciences "Luigi Sacco" (DIBIC), Università degli Studi di Milano, Milan, Italy,
[2] Department of Medical Biotechnology and Translational Medicine (BIOMETRA), Università degli Studi di Milano, Milan, Italy

Autophagy is a constitutive pathway that allows the lysosomal degradation of damaged components. This conserved process is essential for metabolic plasticity and tissue homeostasis and is crucial for mammalian post-mitotic cells. Autophagy also controls stem cell fate and defective autophagy is involved in many pathophysiological processes. In this review, we focus on established and recent breakthroughs aimed at elucidating the impact of autophagy in differentiation and homeostasis maintenance of endothelium, muscle, immune system, and brain providing a suitable framework of the emerging results and highlighting the pivotal role of autophagic response in tissue functions, stem cell dynamics and differentiation rates.

Keywords: autophagy, tissue homeostasis, tissue differentiation, tissue remodeling, tissue pathophysiology

OPEN ACCESS

Edited by:
Federica Di Sano,
University of Rome Tor Vergata, Italy

Reviewed by:
Zengli Guo,
University of North Carolina at Chapel Hill, United States
Chunying Li,
Georgia State University, United States

***Correspondence:**
Clara De Palma
clara.depalma@unimi.it

Specialty section:
This article was submitted to Cell Death and Survival, a section of the journal Frontiers in Cell and Developmental Biology

Received: *04 September 2020*
Accepted: *20 November 2020*
Published: *10 December 2020*

Citation:
Perrotta C, Cattaneo MG, Molteni R and De Palma C (2020) Autophagy in the Regulation of Tissue Differentiation and Homeostasis. Front. Cell Dev. Biol. 8:602901. doi: 10.3389/fcell.2020.602901

INTRODUCTION

In the 1990s, the discovery of Atg genes paved the way to the awareness of the role of autophagy in embryonic differentiation and development of both invertebrates and vertebrates (Mizushima and Levine, 2010; Agnello et al., 2015). Actually, autophagy is an evolutionarily conserved process, and the orthologs of most Atg genes, originally discovered in *Saccharomyces cerevisiae* (Ohsumi, 2001), have been isolated and functionally characterized in higher eukaryotes. Genetic knockout of Atg genes has revealed the dependence on autophagy for the formation of spores in yeast (Tsukada and Ohsumi, 1993) and dauer larvae in *Caenorhabditis elegans* (Melendez et al., 2003), and for insect metamorphosis in *Lepidoptera* and *Drosophila melanogaster* (Romanelli et al., 2016). Systemic and tissue-specific knockout of Atg genes in murine models has proven the involvement of autophagy also in mammalian development and differentiation (Mizushima and Levine, 2010).

Autophagy process can be distinguished according to how cargo enters the lysosome compartment. Consistently, three different pathways can be recognized: chaperone-mediated autophagy (CMA), microautophagy and macroautophagy. In CMA, proteins with a specific motif, that are typically subjected to unfolding or denaturation, are recognized by molecular chaperones and directly driven into lysosomes. In microautophagy, cytoplasmic components are directly engulfed into the lysosomal compartment, while in macroautophagy, autophagosomes, characterized by a double membrane structure, surround the cytoplasmic components (Mizushima et al., 2008) and fuse with lysosomes, where their content is degraded. Macroautophagy, commonly and hereafter referred to as autophagy, provides amino acids and energy from the bulk degradation and recycling of intracellular components (Klionsky, 2007).

At first autophagy activation was identified as the response to starvation (Mortimore and Schworer, 1977); currently, we know that autophagy is activated in response to different cellular stressors including exercise, endoplasmic reticulum stress, infection, and hypoxia (Kroemer et al., 2010). Autophagy is a multi-step process with an ordered sequence of events that

include induction, nucleation of a phagophore structure, formation and maturation of autophagosome, and finally autophagosome fusion with lysosome to degrade and recycle nutrients (Mizushima, 2007). The proper execution of autophagy relies on the formation of two crucial protein complexes and two sequential conjugation steps. The UNC51-like kinase 1 (ULK1) kinase protein complex is responsible for the initiation step of the process and it is directly regulated by the nutrient-sensing mammalian target of rapamycin (mTOR) that, phosphorylating ULK1, prevents its interaction with the energy-sensing AMP-activated protein kinase (AMPK) and blocks the complex assembling. Moreover, AMPK can directly phosphorylate ULK1 promoting the formation of the complex (Kim et al., 2011) that additionally requires Atg13 phosphorylation and the scaffold protein FAK family kinase interacting protein of 200 kDa (FIP200) resulting in a multi-protein complex composed of ULK1-Atg13-FIP200-ATG101. This accounts for the activation of another multi-protein system, the phosphatidylinositol 3-kinase (PI3K) complex. This complex consists of VPS34, VPS15, beclin-1, Atg14L, and AMBRA1 and is involved in autophagosomes biogenesis (Simonsen and Tooze, 2009). The PI3K complex provides phosphatidylinositol 3-phosphate (PI(3)P) enrichment at specific membrane sites called omegasomes or phagophore assembly site (PAS), that are dynamically connected to the endoplasmic reticulum (ER). Omegasomes are in contact with both conjugation systems and are well-suited for nucleation step, while the connection with ER ensures a good source of the lipids that are used in the conjugation step; moreover, omegasomes are important for recruiting effectors such as Atg18, Atg20, Atg21 (Axe et al., 2008). However, not only ER but other different organelles have been suggested to supply membrane to form phagophores, including plasma membrane, Golgi, mitochondria, and recycling endosomes.

The occurrence of ubiquitin-like conjugation reactions is crucial for elongation and closure of autophagosomes. There are two ubiquitin-like Atg conjugation systems, Atg5–Atg12 and microtubule-associated protein 1 light chain 3 (LC3/Atg8). The conjugation of Atg12 and Atg5 is mediated by Atg7 and Atg10. Next, Atg12-Atg5 associates with Atg16L1 forming a complex that acts as an E3-like ligase. LC3 is first cleaved by Atg4, then in response to autophagy induction is conjugated with phosphatidylethanolamine, by Atg7 together with Atg3 and the complex Atg5–Atg12:Atg16L1. This lipidated form of LC3, also known as LC3II, is incorporated into the autophagosomes during the elongation process (Mehrpour et al., 2010) and it is a common marker of autophagy induction.

Finally, autophagosomes, carrying cytosolic components and dysfunctional organelles, fuse with lysosomes with a mechanism that requires SNARE, Rab and membrane tethering proteins; however, they can also merge with endocytic compartments before reaching the lysosomes. In the lysosomes, the content of autophagosomes is degraded and exported back to the cytosol to fuel new nutrients. Several molecular signals drive and control this complex process including the transcription factors c-Jun N-terminal kinase (JNK), NFKappaB, Hypoxia-Inducible Factor 1(HIF-1), E2F Transcription Factor 1 (E2F1), Forkhead Box proteins (FoxOs) and p53 (Mehrpour et al., 2010) that act at nuclear levels regulating the expression of genes important for autophagy.

Under normal conditions, autophagy enables long-lived protein breakdown, therefore complementing proteasomal activity on short-lived proteins and helps the cell to remove damaged organelles, such as mitochondria. However, autophagy functions can be extended beyond and here we review its essential role in maintaining cell survival and tissue homeostasis under physiological or stressed conditions focusing on how modification of its levels can be useful for tissues adaptations or detrimental, altering their functions.

In this review, we explore autophagy process in endothelium, muscle, immune system, and brain providing a suitable framework of the emerging results and highlighting the pivotal role of autophagic response in tissue differentiation, functions, and remodeling after stimuli.

AUTOPHAGY AND ENDOTHELIUM HOMEOSTASIS

The ability of autophagy to drive rapid cellular changes and tissue remodeling in response to environmental and hormonal cues favors the main role of this process in the formation of new blood vessels and vascular homeostasis. A strictly regulated cellular and tissue remodeling is indeed required either for vasculogenesis - that is the differentiation of endothelial precursor cells into endothelial cells (ECs) and *de novo* formation of a primitive vascular network that remodels to acquire tissue- and organ-specific functionality – or angiogenesis, the growth of new blood vessels from pre-existing ones *via* sprouting or intussusception. Specific ECs can also derive from local progenitors in different organs or tissues, further enhancing the complexity and diversity of the endothelial response to injury and regenerative capacity (Marcu et al., 2018). Nonetheless, albeit the phenotypical plasticity characterizing ECs is suggestive of a key role for autophagy in development, differentiation and homeostasis of the endothelium, knowledge about this issue is still sparse and incomplete. **Table 1** summarizes the present understanding on the role of autophagy in endothelial behavior, focusing on the genetic or pharmacological approaches currently available to modulate the autophagic process both *in vitro* and *in vivo*. All the data presented in **Table 1** are deeply discussed in the sections below.

Autophagy and Vasculogenesis

The formation of blood vessels *via* vasculogenesis is critical for the development of any new tissue during embryogenesis (Sweeney and Foldes, 2018). The early identifiable vessels arise in the yolk sac where primitive ECs - derived from the mesodermal layer of the embryo and expressing endothelial markers including Vascular Endothelial Growth Factor Receptor (VEGFR), VE-cadherin and CD31 (Breier et al., 1996) – aggregate to form blood islands, and then migrate to the fetus where vascular networks are formed. The expression of Atg7, Atg8, and beclin-1 has been described in the vascular plexus of the chick yolk sac and

TABLE 1 | A summary of the current knowledge on the role of autophagy in the maintenance of endothelial behavior and functions.

***In vitro* genetic or pharmacological modulation**	**Autophagy**	**Cell type**	**Biological effect**	**References**
Atg3 silencing	↓	ECs	Decrease eNOS expression, and increase ROS and inflammation	Bharath et al., 2014
Resveratrol	↑	ECs	Reduce vascular inflammation	Chen et al., 2013
Rapamycin	↑	ECs	Increase hemodynamic shear stress-induced eNOS expression	Guo et al., 2014
Atg5 overexpression	↑	ECs	Increase sprouting	Du et al., 2012
Atg5 silencing or 3-MA treatment	↓	ECs	Reduce sprouting	Du et al., 2012
ULK1 silencing	↓	ECs	Reduce VEGF- or AGGF1-induced sprouting	Lu Q. L. et al., 2016; Spengler et al., 2020
Beclin-1 silencing	↓	ECs	Reduce EC-haematopoiesis supporting ability	Lyu et al., 2020
3-MA	↓	MSCs	Favor stemness maintenance	Chang et al., 2015
Rapamycin	↑	MSCs	Exert a protective effect against senescence	Zhang et al., 2020
			Increase VEGF secretion and angiogenesis	An et al., 2018
Beclin-1 silencing	↓	MSCs	Reduce VEGF-proangiogenic effect	An et al., 2018
In vivo* genetic or *pharmacological modulation				
EC-selective Atg7 knock out	↓	Mice	Reduce postnatal microvessel brain density	Zhuang et al., 2017
		ApoE–/– mice	Favor development of atherosclerotic lesions	Torisu et al., 2016
EC-selective Atg5 knock out or chloroquine	↓	Mice	No effect in retinal vasculogenesis	Sprott et al., 2019; Zhao et al., 2019
		Mice	Larger atherosclerotic lesions in area exposed to shear stress	Vion et al., 2017
Chloroquine	↓	Melanoma mouse model	Normalize tumoral vessels	Maes et al., 2014
Preconditioning hypoxia or atorvastatin	↑	Engrafted MSCs	Promote survival	Zhang Y. et al., 2012

chorioallantoic membrane, and developing chick embryos reveal a hemorrhage phenotype – due to failure of capillary endothelium - when exposed to either inducer or inhibitor of autophagy (Lu W. H. et al., 2016). A reduced brain microvessel density has been reported in transgenic mice with endothelial-selective knockout of Atg7 (Zhuang et al., 2017). This inhibitory effect on cerebral vascular density seems to mostly rely, however, on defective postnatal angiogenesis rather than embryonal vasculogenesis (Zhuang et al., 2017). More recently, it has been observed that the physiological development of retinal vasculature is unaffected by endothelium-specific Atg5 deletion (Sprott et al., 2019) or by pharmacological inhibition of autophagy (Zhao et al., 2019). Therefore, the role of autophagy in vasculogenesis is still obscure, and further studies will be required to fully understand its impact on embryonic vascularization.

Autophagy and Angiogenesis

Blood vessels carry oxygen, nutrients, and immune cells to all the body's tissues and are crucial for tissue growth and physiology also in adult vertebrates. In healthy organisms, ECs lining blood vessels are quiescent but still retain the ability to respond to micro-environmental changes or pro-angiogenic signals to form new blood vessels. Inadequate vessel formation and maintenance as well as abnormal vascular remodeling underlie various diseases including myocardial infarct, stroke, cancer, and inflammatory disorders.

Several findings in cellular and animal models suggest that autophagy may critically regulate vascular sprouting. Overexpression of the Atg5 gene induces *in vitro* tubulogenesis whereas Atg5 silencing or drug-induced inhibition of autophagy suppress sprouting (Du et al., 2012). Functional autophagy is required for *in vitro* angiogenesis induced by VEGF (Spengler et al., 2020) or by the angiogenic factor AGGF1 (Lu Q. L. et al., 2016), even if different molecular pathways are engaged by the two factors to activate autophagy. Notably, the expression of AGGF1 is induced in ischemic myocardium, and AGGF1 knockout mice show reduced autophagy and angiogenesis and larger damaged areas after myocardial infarction (Lu Q. L. et al., 2016). Angiogenic factors can therefore induce autophagy, and autophagy, acting upstream of angiogenesis, is essential for neovascularization. Angiogenesis also relies on EC autophagy in a rat model of burn wound (Liang et al., 2018). Consequently, induction of autophagy might provide a novel approach to boost the efficacy of therapeutic angiogenesis in ischemic diseases and tissue regeneration.

Autophagy and the Angiogenic Potential of Stem Cells

Different types of stem cells (SCs), especially mesenchymal stem/stromal cells (MSCs), have been extensively investigated for proangiogenic cell therapy in hypo-vascular injuries, such as peripheral artery disease, myocardial infarction, and stroke (Bronckaers et al., 2014). A crucial issue in SC biology concerns the balance between stemness and differentiation, and accumulating evidence suggests that autophagy is critical for the maintenance of self-renewal properties of long-lived

SCs and for the differentiation of either embryonic or adult SCs (Ho et al., 2017; Boya et al., 2018; Chen X. H. et al., 2018; Chang, 2020). Likewise, stemness and differentiation are regulated by autophagy in MSCs (Sbrana et al., 2016; Jakovljevic et al., 2018) with the autophagic activity of old bone marrow-derived MSCs reduced in comparison with young MSCs (Ma et al., 2018). However, the relationship between autophagy and senescence has not been totally elucidated in MSCs (Rastaldo et al., 2020). The pharmacological inhibition of autophagy by 3-methyladenine (3-MA) maintains stemness in high glucose-treated MSCs (Chang et al., 2015). Accordingly, upregulation of autophagy in hyperglycemic conditions correlates with ROS accumulation and premature senescence (Chang et al., 2015), and increased levels of autophagy-related genes have been found in senescent MSCs (Fafian-Labora et al., 2019). At variance, a protective role for rapamycin-induced autophagy accompanied by a decrease in ROS production has been shown in a D-galactose-mediated model of MSC aging (Zhang et al., 2020), and the autophagic flux is compromised in other models of acute senescence, suggesting that functional autophagy may be required to counteract detrimental pathways whereas its negative modulation favors the establishment of cellular aging (Song et al., 2014; Capasso et al., 2015). The protective effect of autophagy may be decisive when MSCs are engrafted in regions characterized by a severe oxidative environment, such as infarcted hearts, where most of transplanted MSCs die in a few days due to hypoxic stress-induced apoptosis (Miao et al., 2017). Notably, induction of autophagy by preconditioning MSCs with brief hypoxia prior to transplantation in ischemic myocardium promotes their survival (Zhang Q. et al., 2012). Also drugs that activate autophagy, such as atorvastatin, decrease hypoxia-induced apoptosis and enhance survival of transplanted MSCs (Zhang Q. et al., 2012). Remarkably, hypoxic priming of MSCs before transplantation improves viability and pro-angiogenic potential of engrafted MSCs also in the treatment of diabetic complications such as lower limb ischemia (Qadura et al., 2018). Collectively, all these studies suggest that modulation of autophagy may be a general approach to protect MSCs from external/internal stressors, thus enhancing their survival in engrafted tissues, and finally their regenerative and therapeutic potential (Ceccariglia et al., 2020). The pro-angiogenic potential of MSCs is also controlled by their paracrine activities that are due to all the factors released from cells, collectively defined as secretome (Maacha et al., 2020). Rapamycin-induced autophagy increases VEGF secretion from MSCs and accelerates regeneration in a murine model of wound healing whereas beclin-1 silencing blunts VEGF-mediated MSC pro-angiogenic effects (An et al., 2018). Consequently, the ability of autophagy to influence secretome may represent a further level of control of the regenerative/therapeutic potential of MSCs. It is therefore possible to summarize that autophagy favors revascularization of ischemic areas either by directly promoting angiogenesis or by supporting the angiogenic potential of MSCs through multiple mechanisms.

Endothelial cells are also essential elements of the hematopoietic SC (HSC) niche by providing critical signals to support blood cell production in the bone marrow (Mendelson and Frenette, 2014). Again, autophagy has been proposed as a key regulator of this process because beclin-1 knockdown reduces the hematopoiesis-supporting ability of ECs that can be restored by beclin-1 upregulation (Lyu et al., 2020). Notably, a prospective case-control study illustrates that defective autophagy of ECs in the HSC niche may be involved in the post-allotransplant pancytopenia characteristic of poor graft function (PGF), suggesting the possibility of treating PGF patients with drugs able to promote autophagy (for example, rapamycin).

Autophagy and the Physiopathology of ECs

At variance with post-ischemic angiogenesis, that restores blood flow in hypo-vascularized areas, overgrowth of abnormal vessels results in pathological angiogenesis and underlies various diseases including retinopathies, cancer, and inflammatory disorders. Endothelium-specific deletion of Atg5 reduces pathological neo-vascularization in a mouse model of retinopathy (Sprott et al., 2019), and the retinal vascular hyper-sprouting phenotype induced by PKA deficiency is partially rescued by inhibition of autophagy or endothelium-specific Atg5 deletion (Zhao et al., 2019). Outstanding, defective autophagy does not harm physiological development of retinal vasculature in both the models. Thus, blocking autophagy may be useful to selectively target pathological neo-vascularization, at the retina as well as in tumors, where the formation of new blood vessels is essential for cancer progression. Tumor-associated blood vessels are highly permeable and unstable, and these anomalies promote a stressful environment – characterized by hypoxia, nutrient deprivation and inflammation - that results in enhanced autophagy and resistance to hypoxia-induced cell death in tumoral ECs compared to normal ECs (Filippi et al., 2018). Hypoxia drives not only autophagy but also angiogenesis *via* increased expression of VEGF due to stabilization and activation of the hypoxia-inducible factor HIF. Tumors in hemizygous beclin-1 mice show higher angiogenic potential under hypoxia in comparison to wild type animals (Lee et al., 2011), thus supporting the view that hypoxia-induced autophagy may restrain pathological angiogenesis in the tumoral microenvironment.

The aberrant structure and function of peritumoral vessels supports malignancy by establishing an abnormal tumoral microenvironment that facilitates disease progression and reduces the efficacy of antiblastic therapies. Hypoxia makes cancer cells more aggressive and favors angiogenesis and immunosuppression, while leaky vessels give tumor cells passage to metastasize. It has been hypothesized that normalization of tumor vessels can improve their functions by relieving microenvironmental hypoxia and improving delivery and outcome of anti-cancer drugs (Martin et al., 2019). Remarkably, the autophagy blocker chloroquine (CQ) normalizes tumor vessel structure and function and increases perfusion in a mouse model of melanoma (Maes et al., 2014). Through the alteration of acidic pH in endothelial late endosomes or lysosomes, CQ disrupts endosomal and autophagic cargo degradation, followed by the activation of Notch signaling and negative regulation of tip cell during sprouting angiogenesis. Notch signaling has also been

implicated in vessel stability by regulating the function of vascular mural cells (Kofler et al., 2011). In addition, the CQ-mediated reduction of tumor hypoxia favors the establishment of a less pro-angiogenic microenvironment (Maes et al., 2014). Besides autophagy, CQ improves the immunosuppressive function of the tumoral micro-environment by enhancing the switch of tumor-associated macrophages from tumor-promoting M2 to tumor-killing M1 phenotype (Chen D. et al., 2018) – a mechanism that has been related to normalization of tumor vascular network (Jarosz-Biej et al., 2018). Notably, pleiotropic effects of CQ on tumoral vessels are not phenocopied by loss of Atg5, and more generally, results obtained by genetically interfering with the expression of autophagy-related genes do not routinely overlapped to the effects of pharmacological modulation of the endo-lysosomal system (Schaaf et al., 2019). Thus, it is possible to speculate that autophagy might be modulated by complementary approaches – acting at different steps of the autophagic process – to control pathological angiogenesis. It is, however, crucial to further study whether and how these mechanisms intersect not only at the level of ECs but also in other cell types belonging to the tumoral microenvironment.

A crucial role for autophagy has also been proven in terminally differentiated cells, such as ECs lining blood vessels, where a constant renewal of cytoplasmic contents and organelles is essential for the maintenance of homeostasis and cellular health (Mizushima and Komatsu, 2011). An impairment in EC functions – the so-called endothelial dysfunction (ED) - is associated with all the common cardiovascular risk factors and stressors, such as for example aging, smoking, hypertension, diabetes, and low physical activity. ED is triggered by a loss in the endothelial Nitric Oxide Synthase (eNOS) enzymatic activity with a consequent decrease in nitric oxide (NO) availability and accumulation of damaging ROS (Li et al., 2013). Persistent oxidative stress alters mitochondrial structure and function but the efficient degradation and recycling of damaged organelles *via* autophagy/mitophagy results in cellular survival and homeostasis. At variance, the partial/incomplete degradation of mitochondria due to ineffective autophagy can cause a further increase in oxidative stress, and finally cell death (Yan and Finkel, 2017). Consequently, the activation of autophagy in response to oxidative stress, but also to other vascular stressors such as high glucose, oxidized low-density lipoproteins or advanced glycation end products, exerts a protective effect on ECs, and any alteration in the autophagic flux can elicit detrimental effects (Chen F. et al., 2014; Torisu et al., 2016; Yan and Finkel, 2017). In addition, some vasculo-protective compounds have been shown to stimulate autophagy, thereby reinforcing EC resistance to cellular stress (Chen et al., 2013; Kim H. S. et al., 2013). Hemodynamic shear stress, the mechanical force generated by blood flow on vascular ECs, is essential for endothelial homeostasis under physiological conditions (Hsieh et al., 2014). Pulsatile laminar shear stress upregulates the expression and activity of eNOS, and pretreatment with the autophagy activator rapamycin further enhances shear stress-induced eNOS expression (Guo et al., 2014). Likewise, either autophagy markers or eNOS activity increase in response to physiological levels of laminar flow, and silencing of the Atg3 protein impairs eNOS function and generates ROS and inflammatory cytokines (Bharath et al., 2014). Thus, autophagy sustains pleiotropic functions of NO in the control of barrier integrity, vessel dilation, leukocyte adhesion, platelet aggregation, and finally angiogenesis, by favoring its formation in response to physiological shear stress. In contrast, ECs exposed to low levels of shear stress are characterized by inefficient autophagy and by a proinflammatory, apoptotic, and senescent phenotype (Vion et al., 2017). Similarly, perturbed/unstable flow impairs p62-mediated clearance of autophagosomes and promotes ED (Vion et al., 2017).

The autophagy process has typically been studied in cultured ECs, which are proliferative cells at variance with quiescent cells within the vasculature. However, a protective role for autophagy has also been confirmed *in vivo* where the genetic inactivation of the Atg7 gene favors the development of atherosclerotic lesions in murine models (Torisu et al., 2016). Likewise, atherosclerosis-prone mice bearing an endothelial-specific deletion of Atg5 develop larger atherosclerotic lesions, specifically in areas exposed to high shear stress (Vion et al., 2017), that commonly remain lesion-free since atherosclerosis favorably develops at arterial bifurcations and at the inner part of curvatures where blood flow is low or disturbed (Hsieh et al., 2014). The translational relevance of these findings has been confirmed by an increase in autophagic markers and NO production in human ECs collected from the radial artery of subjects after dynamic handgrip exercises (Park et al., 2019). At variance, reduction in autophagic markers and impaired eNOS activation have been observed in peripheral venous ECs from diabetic patients showing a lower brachial artery flow-mediated dilation suggestive of ED (Fetterman et al., 2016). It can therefore be assumed that: (i) a defect in endothelial autophagy enhances pro-atherogenic responses; (ii) the activation of the autophagic flux by adequate shear stress acts as athero-protective mechanism. Enhancing endothelial autophagy within the vasculature might therefore represent a novel and attractive target for the prevention and/or treatment of atherosclerosis and cardiovascular disease (Hughes et al., 2020).

AUTOPHAGY AND SKELETAL MUSCLE HOMEOSTASIS

Skeletal muscle is a plastic tissue that is continuously adapting and changing to physical and metabolic demands. To sustain the increased energy needs or cope with catabolic conditions, skeletal muscle can mobilize proteins, reorganize organelles networks, and change the nuclei setting. Autophagy is the major reservoir of energy and the mouse model expressing fluorescent LC3 shows that muscles have one of the highest rates of autophagy during fasting (Mizushima et al., 2004). Basal autophagy is regulated by metabolic properties of muscle, indeed a negative correlation between fiber oxidative capacity and autophagy flux exists and both basal and stimulated autophagy are greater in glycolytic muscles as compared with the oxidative ones (Mofarrahi et al., 2013). These differences are associated with different activation of the AMPK pathway and inhibition of the AKT and mTOR

signaling (Mofarrahi et al., 2013) that are more evident in low oxidative muscles.

Autophagy and Muscle Mass Maintenance

Autophagy maintains healthy muscle homeostasis and physiology (Masiero et al., 2009), exerting a beneficial role in controlling muscle mass. Muscle-specific deficiencies in essential autophagy factors such as Atg5, Atg7, VPS15, ULK1, AMPK, and mTOR result in abnormal mitochondrial morphology, oxidative stress, sarcomere alterations, accumulation of ubiquitylated products, and induction of unfolded protein response that can contribute to great muscle loss and weakness leading to myofibers degeneration (Raben et al., 2008; Masiero et al., 2009; Castets et al., 2013; Nemazanyy et al., 2013; Bujak et al., 2015; Fuqua et al., 2019). Similarly, AMBRA1 deletion results in a severe myopathy with loss of muscle fibers, sarcomere disorganization, and mitochondria alterations (Skobo et al., 2014). AMBRA1 interacts with Tripartite motif-containing 32 (TRIM32) (Di Rienzo et al., 2019) that is crucial as well, and indeed its deletion causes myopathy with neurological complications, both superimposable with the phenotype observed in patients with limb-girdle muscular dystrophy 2H (LGMD2H) (Saccone et al., 2008). Recently, the autophagic lysosome reformation (ALR) pathway has also emerged as an important regulator for muscle homeostasis. Hence, the deletion of the phosphatase regulating the PI(4,5)P2 to PI(4)P conversion, i.e., the inositol polyphosphate 5-phosphatase (INPP5K), causes a progressive muscle disease associated with lysosomes depletion and autophagy impairment (McGrath et al., 2020). Whether in other systems the Transcription Factor EB (TFEB) is able to restore lysosomal homeostasis and autophagy (Spampanato et al., 2013), in this model TFEB-dependent lysosomal biogenesis is not sufficient to compensate the defective ALR, indicating its fundamental role in replenishing lysosomes during autophagy.

Interestingly, mild perturbation of autophagy does not cause a severe muscular phenotype. Muscle appears normal despite a slight, but non-significant, reduction of its mass and a small decrease in fibers size regardless of type (Paolini et al., 2018), highlighting the differences between models in which autophagy is completely blocked or only mild attenuated. In this model, muscle loss is evident after a starvation period suggesting that the absence of inducible autophagic response speeds up the process reducing protein synthesis and increasing ubiquitylated products and confirms how a normal autophagic process is essential for maintaining muscle mass (Paolini et al., 2018).

The preservation of muscle mass could be achieved by the maintenance of Sestrins levels, which appear strongly downregulated in the atrophic muscle (Segales et al., 2020) and aged-subjects (Zeng et al., 2018). Sestrins is able to enhance autophagy preserving organelles quality, and in turn muscle mass, through a double mechanism: it inhibits FoxO-dependent expression of atrogenes by increasing Akt, and sustains autophagy, by activating AMPK and blocking mTORC1 (Segales et al., 2020). Other factors are emerging as important for controlling and averting atrophy; especially, recent evidence points out that TRIM32 is required for autophagy induction in atrophic conditions promoting ULK1 activity. This improves the functional maintenance of muscle cells *via* reduction of ROS production and induction of muscle ring finger-1 (MuRF1) (Di Rienzo et al., 2019).

Of note, whether the absence of autophagy is harmful, its excessive induction is detrimental too. For instance, the upregulation of FoxO3 transcription factor enhances autophagy and is enough to induce muscle fibers atrophy (Mammucari et al., 2007). Similarly, mice lacking the nutrient-deprivation autophagy factor-1 (NAF-1), an endoplasmic reticulum (ER) protein required for blocking beclin-dependent autophagy, display muscle weakness accompanied by increased autophagy (Chang et al., 2012). Consistently, a high autophagy rate exacerbates muscle atrophy induced by several conditions. The lesson from these results is complex, indicating a dual role for autophagy and suggesting that a proper autophagic process is crucial for muscle homeostasis.

Autophagy and Exercise

Autophagy is also important for skeletal muscle remodeling after stimuli like contraction/exercise. Exercise can help to improve muscle quality in old and frail people (Cadore et al., 2014). Consistently, a recent study sheds light on the effects of acute and chronic exercise on autophagy in frail elderly subjects. The authors establish that autophagy is activated after a session of strength training in unexercised subjects. By contrast, in exercised subjects performing the same training, this response is completely blunted, suggesting that the results of this physical activity depend on the subjects' training status (Aas et al., 2020). Similarly, resistance exercise enhances autophagy in untrained young men, but it is absent in aged-subjects (Hentila et al., 2018). This last result partially contrasts the work of Aas et al. (2020), suggesting that the autophagic response to strength training needs to be further investigated.

Defective stimulation of basal autophagy impairs metabolic adaptations induced by exercise training, such as mitochondrial biogenesis and angiogenesis, without interfering with the fiber type switch distinctive of contractile adaptations (Lira et al., 2013). This confirms the existence of a link between oxidative phenotype and basal autophagy flux, as well as demonstrates that chronic contractile activity is not sufficient to affect basal autophagy flux (Lira et al., 2013).

Hence, exercise is considered a stimulus that induces autophagy *in vivo* (Grumati et al., 2011; He et al., 2012) and a described mechanism involves the disruption of the BCL2–beclin-1 complex (He et al., 2012). Knock-in mutation in BLC2 phosphorylation site generates mice with normal basal autophagy but defective stimulus-induced autophagy. These mice display normal cardiac and skeletal muscle features at baseline; conversely, they show impaired exercise-enhanced insulin sensitivity and fail to exhibit increased plasma membrane GLUT4 localization, both dictated by low AMPK activation (He et al., 2012). These mice have a much worse running performance and are not protected against high fat diet-induced glucose intolerance (He et al., 2012). However, another study reports exactly opposite results demonstrating

that muscle-specific autophagy knockout mice have an improved metabolic profile, including glucose homeostasis, associated with the release of the mitokine FGF21 triggered by dysfunctional mitochondria (Kim K. H. et al., 2013). Consistently, in the same muscle-specific inducible model, the inhibition of autophagy immediately before training does not impact on physical performance, glucose homeostasis, or PRKAA1/AMPK signaling. By contrast, autophagy accounts for the preservation of mitochondrial function during muscle contraction, revealing its important role for muscle injury repair (Lo Verso et al., 2014). Besides, these data uncover the differences between a general inhibition of autophagy with respect to tissue-specific blocking, suggesting a potential cell-autonomous regulation.

Autophagy and Muscle Regeneration

The finding that autophagy is important in muscle repair has been deeply investigated. The regenerative capacity of muscle is a crucial process that allows the recovery after damage and requires the effort of different cell types.

Autophagy is rapidly induced at the onset of regeneration process showing a role in sarcomeric disassembly but not in nutrient recycling. Autophagy inhibition causes the accumulation of sarcomeric remnants and prevents the proper organization of sarcomere during regeneration (Saera-Vila et al., 2016).

In case of injury, autophagy is required to maintain sarcolemma integrity, as demonstrated in mice with decreased Atg16 function (Atg16L1 mice) and exposed to cardiotoxin (CTX) damage. In absence of autophagy and with low CTX levels, fibers become leaky and are infiltrated by circulating immunoglobulins, but are able to buffer calcium rise preventing their necrosis and death. Otherwise, whether the local concentration of CTX is high, fibers cannot buffer calcium and die; overall, these effects result in attenuated muscle regeneration in Atg16L1 mice (Paolini et al., 2018).

Autophagy can also contribute to mitochondrial regeneration during muscle repair and chronic treatment with an autophagy inhibitor negatively affects mitochondrial activity and recovery after injury (Nichenko et al., 2016). Similarly, the muscle-specific deletion of the ULK1 gene, which is essential for mitophagy (mitochondrial-specific autophagy), causes impaired functional recovery of muscle associated with altered respiratory complexes levels (Call et al., 2017). Specifically, ULK1 is important for the reorganization of the mitochondrial network after damage and this event is crucial for the optimal recovery of muscle (Call et al., 2017).

A role for autophagy in muscle regeneration can be also drawn from the recent discoveries in satellite cells that are functional adult stem cells with the ability to proliferate and undergo myogenesis. Autophagy is essential for satellite cells to come out of their quiescent state, indeed this activation is a metabolic demanding process and autophagy can provide the required nutrients favoring the transition between quiescent to the activated state (Tang and Rando, 2014). In agreement, committed myogenic progenitors are mostly positive for LC3 in contrast to the self-renewal population, suggesting that the presence of LC3 positive satellite cells overlaps with a strong regenerative response after injury (Fiacco et al., 2016).

Autophagy is also important to control cell senescence and its decline is responsible for the rapid entry of satellite cells into senescence accounting for the exhaustion of stem cells pool and defective muscle regeneration. Physiologically, this occurs with aging: indeed, old satellite cells show autophagy decline and are more prone to senescence (Garcia-Prat et al., 2016). The link between autophagy and muscle cell senescence is challenging and it has been further expanded. Stimuli that strongly upregulate autophagy, such as repeated amino acids and serum withdrawal, do not trigger senescence features. Conversely, senescence-associated with mild toxic stress is limited in Atg7-deficient cells for increasing cell death (Bloemberg and Quadrilatero, 2020). This suggests that massive induction of autophagy prevents senescence, whereas autophagy-defective myoblasts do not develop senescence, but die (Bloemberg and Quadrilatero, 2020).

Besides, autophagy controls the effectiveness of GH-IGF1 axis in muscle affecting the proliferative capacity and the differentiation potential of satellite cells and influencing muscle development, with severe post-natal muscle growth retard in condition of autophagy disruption (Zecchini et al., 2019).

The exact role of autophagy in muscle regeneration is complex considering the different cell types involved in the process. However, the induction of autophagy seems to be beneficial for repairing after damage as well as for exercise adaptations.

Autophagy and Muscle Disorders

Another proof of concept of the role of autophagy in muscle homeostasis comes from the evidence that many pathophysiological conditions of muscle are associated with disrupted autophagic process including muscular dystrophies (Grumati et al., 2010; De Palma et al., 2012, 2014; Fiacco et al., 2016), type II diabetes mellitus and insulin resistance (He et al., 2012), sarcopenia (Fan et al., 2016) and cancer cachexia (de Castro et al., 2019). Moreover, genetic defects affecting each phase of autophagy underlie skeletal muscle illness and the severity of the phenotype depends on whether the mutation disrupts basal or inducible autophagy (Jokl and Blanco, 2016). Interestingly, upregulation as well as downregulation of autophagy, are associated with muscle disorders, confirming the importance of a proper autophagic flux. For instance, in Pompe disease, an excessive autophagic buildup occurs and compromises enzyme replacement therapy (Fukuda et al., 2006; Raben et al., 2008).

In myotonic dystrophy type 1 (DM1), which affects adults causing atrophy and myotonia, autophagy levels are enhanced (Bargiela et al., 2015) and counteracting autophagy by mTOR stimulation improves satellite cells proliferation (Song et al., 2020).

Conversely, in the Vici syndrome, the causative genetic mutation leads to an autophagic block resulting in a clearance defect with accumulation of autolysosomes (Cullup et al., 2013). Autophagy signaling is also impaired in muscular dystrophies as shown in dystrophin or collagen VI deficient muscles and the forced reactivation of the process improves both dystrophic phenotypes (Grumati et al., 2010; De Palma et al., 2012;

Fiacco et al., 2016). Specifically, in collagen VI deficient patients a dietary approach for reactivating autophagy has been attempted in a pilot clinical trial, obtaining beneficial effects (Castagnaro et al., 2016). Similarly, the administration of nutraceutical compounds, such as pterostilbene in collagen 6 null mice promotes a proper autophagic flux exerting favorable outcomes on muscle (Metti et al., 2020).

Defective autophagy is also detected in LGDM2H due to impaired interaction between mutated TRIM32 and ULK1 which results in the accumulation of autophagy cargo receptors, ROS production, and MuRF1 upregulation (Di Rienzo et al., 2019). The efficient reactivation of autophagy is also useful in Emery–Dreifuss muscular dystrophy (Ramos et al., 2012); by contrast, in laminin alpha2 chain-deficient muscle autophagy is upregulated and its inhibition has beneficial effects on dystrophic phenotype (Carmignac et al., 2011). In this regard, many other examples indicate that muscle is particularly susceptible to autophagy dysregulation (Dobrowolny et al., 2008; Sarparanta et al., 2012; Fetalvero et al., 2013). Therefore, undoubtedly, autophagy is a key process whose alteration affects development, homeostasis and remodeling of skeletal muscle and whose normalization is essential for the physiology of skeletal muscle as well as for ameliorating muscular diseases, as summarized in **Table 2**.

AUTOPHAGY AND IMMUNE SYSTEM HOMEOSTASIS

Autophagy is an essential process in the regulation of homeostasis of immune cells involved in innate and adaptive immune responses, such as monocytes, macrophages, dendritic cells (DCs), T and B lymphocytes, by influencing their proliferation, differentiation, activation, survival and cytokine release (Harris, 2011).

Monocytes and macrophages are pivotal effectors and regulators of the innate immune response (Italiani and Boraschi, 2014). DCs, as antigen-presenting cells (APCs), trigger and modulate the activation of naive T cells, and have a central role in the development and maintenance of immune tolerance (Patente et al., 2018). T cells have diverse jobs: (i) they activate other immune cells (T helper cells) (Glimcher and Murphy, 2000); (ii) they detect and destroy infected and tumor cells (cytotoxic T cells) (Andersen et al., 2006); (iii) they can "remember" a previous encounter with a specific microbe and start a quick response upon pathogen re-exposure (memory T cells) (Omilusik and Goldrath, 2017); (iv) they can regulate or suppress other cells in the immune system (regulatory T cells: Treg) (Vignali et al., 2008). B cells are mainly responsible for mediating the production of antigen-specific antibodies directed against invasive pathogens (Eibel et al., 2014). Autophagy has been demonstrated to be central in all these cells, as it modulates cell signaling and metabolism, antigen presentation, proteostasis, mitochondrial function and reactive oxygen species (ROS) production and ER stress (Rathmell, 2012; Gkikas et al., 2018; Smith, 2018; Valecka et al., 2018; Macian, 2019). An overview of the effects of autophagy changes on immune cells is reported in **Table 3** and discussed in the sections below.

Autophagy and Macrophages

Autophagy plays a key role in different stages of macrophage life, including differentiation from monocytes and polarization into pro-inflammatory and anti-inflammatory and tissue repairing macrophages (i.e., M1 and M2 cells) (Vergadi et al., 2017). Monocytes originate in the bone marrow from a myeloid progenitor and then they are released into the peripheral blood. In response to inflammation, monocytes migrate into tissues and can differentiate into macrophages or die by caspase-dependent apoptosis. Both the cytokines colony-stimulating factor 1 and 2 (CSF1 – CSF2) are able to promote monocyte survival and differentiation into macrophages via autophagy (Jacquel et al., 2012; Zhang Y. et al., 2012). CSF1 contributes to increased induction of autophagy by activating the ULK1 pathway (Jacquel et al., 2012; Obba et al., 2015), while CSF2 acts through JNK/beclin-1 and the block of Atg5 cleavage (Zhang Y. et al., 2012). Of note, the pharmacological blockade of autophagy in CSF2 treated monocytes by 3-MA and CQ leads to the promotion of apoptosis and the inhibition of differentiation and cytokine release, thus corroborating the role of autophagy in these events (Zhang Y. et al., 2012).

To date, it is clear that autophagy is also fundamental in macrophage polarization, i.e., the process by which macrophages develop a peculiar functional phenotype as a reaction to specific signals. Depending on the stimulus that macrophages receive they can acquire an M1 or an M2 phenotype (Murray et al., 2014); however, how autophagy affects these events, especially M1 polarization, is still under debate, because of discrepancy in published data that can be explained by differences in the backgrounds of the macrophages studied and in the experimental settings. The first study addressing directly this issue demonstrated that molecular inhibition of autophagy, by targeting Atg5 gene in C57Bl/6 mice, boosts M1 polarization *in vitro* by significantly increasing M1 markers and proinflammatory cytokine release including TNF-alpha, CCL5, IL6, CCL2, and IL1beta (Liu et al., 2015). These data were confirmed by a following paper showing a lower activation of autophagy in M1 macrophages when compared with M2 and demonstrating that the pharmacological inhibitor of autophagy CQ repolarizes M2 macrophages to an M1 phenotype (Guo et al., 2019). Of notice, once acquired an M1 phenotype, macrophages reduce autophagy and increase glycolysis (Matta and Kumar, 2015). In this context, the role of AKT/mTOR pathway seems to be significant in both autophagy and metabolism. Indeed, in M1 polarized macrophages AKT activation mediates the switch to glycolytic metabolism that leads to suppression of autophagy (Matta and Kumar, 2015). However, in 2017 Esteban-Martinez and collaborators by using a different mouse model (i.e., peritoneal elicited macrophages in CD1 mice) stated that mitophagy contributes to macrophage polarization toward the proinflammatory and more glycolytic M1 phenotype by eliminating mitochondria, but not to M2 macrophage polarization that relies mainly on oxidative phosphorylation (Esteban-Martinez et al., 2017). On the other hand, it seems clear that induction of autophagy supports M2 polarization involving AKT/PI3K pathway, STAT6 and Atg7 (Kapoor et al., 2015;

TABLE 2 | A summary of the current knowledge on the role of autophagy in the maintenance of muscle behavior and functions.

***In vitro* genetic or pharmacological modulation**	**Autophagy**	**Model**	**Biological effect**	**References**
3-MA or Chloroquine Atg5 or Atg7 silencing	↓	SC	Inhibition of SC activation	Tang and Rando, 2014
In vivo* genetic or *pharmacological modulation				
Muscle-specific knock out models for: Atg5-Atg7-VPS15-ULK1-AMPK-mTOR-AMBRA1	↓	Mice	Mitochondria dysfunctions, sarcomere alterations, muscle loss, weakness, and myofibers degeneration.	Raben et al., 2008; Masiero et al., 2009; Castets et al., 2013; Nemazanyy et al., 2013; Skobo et al., 2014; Bujak et al., 2015; Fuqua et al., 2019
Muscle-specific TRIM32 knockout	↓	Mice	Myopathy with neurological alterations. Mutations in TRIM32 are responsible for LGMD2H	Saccone et al., 2008
Muscle-specific INPP5K knockout	↓	Mice	INPP5K deletion causes muscular dystrophy	McGrath et al., 2020
Muscle-specific FoxO3 upregulation	↑	Mice	Muscle atrophy	Mammucari et al., 2007
Muscle-specific NAF-1 knockout	↑	Mice	Muscle weakness	Chang et al., 2012
Muscle-specific Atg16L1	↓ (mild)	Mice	Impaired regeneration after injury	Paolini et al., 2018
Muscle-specific Ulk1 knockout	↓ (mitophagy)	Mice	Impaired regeneration after injury	Call et al., 2017
Muscle stem cell-specific Atg7 knockout	↓	Mice	Impairment of GH-IGF1 axis and severe muscle growth retard. Altered proliferation and differentiation of muscle stem cells	Zecchini et al., 2019
Atg6 knockout	Defective stimulus-induced autophagy	Mice	Defective adaptations to endurance exercise training	Lira et al., 2013
Knock-in mutations in BCL2 phosphorylation sites ($Bcl2^{AAA}$)	Defective stimulus-induced autophagy	Mice	Decreased performance and altered glucose metabolism during acute exercise. Impaired exercise-mediated protection against high-fat-diet-induced glucose intolerance	He et al., 2012
3-MA	↓	Mice	Impaired mitochondrial activity and muscle regeneration after injury	Nichenko et al., 2016
Low protein diet	↑	COLL6 deficient patients mdx mice	Autophagy recovery and amelioration of dystrophic phenotype. Autophagy recovery and amelioration of dystrophic phenotype	De Palma et al., 2012; Castagnaro et al., 2016
Pterostilbene	↑	COLL6 knockout mice	Autophagy recovery and amelioration of dystrophic phenotype	Metti et al., 2020

Vergadi et al., 2017; Sanjurjo et al., 2018; Wen et al., 2019; Bo et al., 2020).

Recently, it has been demonstrated that autophagy plays a key role in cytokine production by macrophages. The lack of autophagy, obtained by the genetic depletion of Atg16L1, beclin-1, and LC3, indeed enhances the secretion of interleukin 1beta (IL-1beta) and IL-18 in response to lipopolysaccharide (LPS) and other pathogen-associated molecular patterns (Saitoh et al., 2008; Nakahira et al., 2011). In macrophages, the secretion of IL-1beta and IL-18 is controlled by the signaling platform known as the inflammasome via the release of mitochondrial DNA (mtDNA) and ROS production and the ensuing cleavage and activation of caspase-1. Autophagy by controlling the elimination of dysfunctional mitochondria and the translocation of mtDNA into the cytosol inhibits mitochondrial ROS generation and exerts an anti-inflammatory effect (Nakahira et al., 2011).

Autophagy and Dendritic Cells

Little is known about the role of autophagy in the generation of DCs. While it does not seem to have a role in the development of immature DCs, however, it seems to contribute to the activation and function of mature DCs, thus indicating autophagy as a key player in the physiological and pathological processes that rely on DCs. Targeting of Atg16L1, a gene associated with inflammatory bowel disease has been demonstrated to boost the immunostimulatory capability of murine mature DCs by increasing the expression of co-stimulatory molecules on the cell surface (Hubbard-Lucey et al., 2014). Autophagy dependent degradation of intracellular materials, including phagocytosed antigens, has been described as a key route for endogenous and exogenous antigens to reach the MHC-II presentation machinery in DCs and activate CD4+ T cells (Dengjel et al., 2005; Munz, 2009; Lee et al., 2010; Keller et al., 2017). Thus autophagy, by regulating MHC-II presentation in DCs, might shape the self-tolerance of CD4+ T cells and trigger CD4+ T cell responses against pathogens and tumors. Moreover, it is clear that autophagy in DCs is required for Treg homeostasis and function both in normal and pathological conditions, as for instance in the development of autoimmune diseases (Niven et al., 2019). In this context, it has to be noted that Treg cells themselves may suppress CD4+ T cell-dependent autoimmune responses through inhibition of autophagy in DCs

TABLE 3 | A summary of the current knowledge on the role of autophagy in the maintenance of immune cells behavior and functions.

***In vitro* genetic or pharmacological modulation**	**Autophagy**	**Model**	**Biological effect**	**References**
3-MA or chloroquine	↓	Monocytes	Promotion of apoptosis, inhibition of differentiation and of cytokine release	Zhang Y. et al., 2012
Chloroquine	↓	Macrophages	M2 repolarization to M1	Guo et al., 2019
3-MA or cyclosporine A	↓	Macrophages	M1 polarization	Esteban-Martinez et al., 2017
3-MA	↓	Macrophages	Inhibition of M2 polarization	Bo et al., 2020
3-MA or beclin-1 and Atg7 silencing	↓	T cells	Resistance to cell death of Th2 cells	Li et al., 2006
Beclin-1 silencing	↓	ECs	Reduce EC-haematopoiesis supporting ability	Lyu et al., 2020
In vivo* genetic or *pharmacological modulation				
Atg5 knock out	↓	Macrophages	Increase of M1 marker expression and cytokine release	Liu et al., 2015
3-MA	↓	Macrophages	Inhibition of M2 polarization	Bo et al., 2020
Atg16L1 knock out	↓	Macrophages	Increase of secretion of IL-1β and IL-18	Saitoh et al., 2008
Beclin-1 knock out or LC3 knock out	↓	Macrophages	Increase of secretion of IL-1β and IL-18	Nakahira et al., 2011
Atg16L1 knock out	↓	Dendritic cells	Boost of the immunostimulatory capability of murine mature DCs	Hubbard-Lucey et al., 2014
Atg5 knock out	↓	T cells	Inhibition of cell survival and proliferation	Pua et al., 2007
Beclin-1 knock out	↓	T cells	Increase of cell death	Kovacs et al., 2012
Plasma cells Atg5 selective knock out	↓	B cells	Plasma cells maintenance and humoral immunity	Pengo et al., 2013
Plasma cells Atg5 selective knock out	↓	B cells	B cell receptor trafficking	Arbogast et al., 2019

in a cytotoxic T-lymphocyte-associated protein 4-dependent (CTLA4-dependent) manner (Alissafi et al., 2017).

Autophagy and T Cells

Lymphocytes (T and B cells) are the essential mediators of the adaptive immune system. All lymphocytes originate from a common progenitor [common lymphoid progenitor (CLP)], derived from the hematopoietic stem cell. In naïve T cells, macroautophagy is active and constitutes a key mechanism for preserving cells homeostasis and survival and adapting cells to intracellular or extracellular environment modifications (Li et al., 2006; Pua et al., 2007). This has been addressed in autophagy gene-deficient T cells, such as cell lacking Atg5, Atg7, beclin-1, or VPS34 (Li et al., 2006; Pua et al., 2007, 2009; Kovacs et al., 2012; Willinger and Flavell, 2012). Indeed, mice with autophagy-deficient T cells displayed a strong decrease in both mature CD4+ and CD8+ cells and the remaining T cells failed to proliferate upon T cell receptor (TCR) stimulation (Pua et al., 2009). In T cells, autophagy acts as a pro-survival process also by eliminating the excess of organelles such as mitochondria and ER. Defective mitophagy in T cells contributes to increase of mitochondrial mass and the ensuing ROS production, therefore prompting the cells to cell death via apoptosis (Pua et al., 2009; Jia and He, 2011). Moreover, the genetic deletion of Atg3, Atg5, and Atg7 results in expanded ER compartments containing increased calcium stores that cannot be depleted properly, thus causing defective calcium influx inside the cells (Jia and He, 2011; Jia et al., 2011). Several studies provided evidence that TCR engagement in CD4+ and CD8+ T cells triggers autophagy activation to support energetic demands for proliferation and cytokines production (Li et al., 2006; Arnold et al., 2014; Botbol et al., 2015; Bantug et al., 2018). Pharmacological or genetic (Atg3, Atg5, or Atg7) inhibition of autophagy has been reported to affect proliferative responses in both CD4+ and CD8+ T cells (Pua et al., 2007; Hubbard et al., 2010). The molecular mechanisms that may induce autophagy in activated T cells are still not completely understood, but multiple pathways seem to be involved. Li et al. (2006) demonstrated that autophagy in TCR activated T cells is affected by 3-MA, an inhibitor of PI3K, as well as JNK inhibitors, and can be enhanced by rapamycin (inhibitor of the mTOR pathway) and zVAD (inhibitor of caspase activity), suggesting a role for all these pathways. More recently, Botbol et al. (2015) reported that intracellular signaling of cytokines such as IL2, IL4, IL7, and IL15 can induce autophagy in CD4+ T cells and demonstrated the involvement of Janus kinase 3 (JAK3). Autophagy has been shown to control also Treg stability and function (Wei et al., 2016). Treg cells have higher autophagy activity than naive CD4+ T cells and Treg cells- specific deletion of Atg7 or Atg5, results in increased cell apoptosis and therefore in the development of autoimmune and inflammatory disorders or tumor resistance (Zhang et al., 2019).

Autophagy and B Cells

Autophagy has recently emerged as crucial for the maintenance of memory B cells and plasma cells, while its role in the development and survival of naïve B cells needs further elucidation. By using two new mouse models of conditional Atg5 deletion, one under the control of a promoter active early during B-cell development and the other active in mature B cells, Arnold and collaborators drawn the conclusion that basal levels of autophagy are necessary to maintain a normal number of peripheral B cells and central during development of B-1a B cells, tissue-resident, innate-like

B cells (Arnold et al., 2016). Subsequently, it has been also demonstrated that B1a B cells have active glycolysis and fatty acid synthesis and depend on autophagy to survive and self-renew (Clarke et al., 2018). Following appropriate stimulation, peripheral B cells in lymphoid follicles may differentiate in the germinal center (GC) B cells, which generate either plasma cells or memory B cells. It has been recently reported that GC B cells are the most active B cells in processing autophagy, which appears to be non-canonical autophagy independent of Atg genes (Martinez-Martin et al., 2017).

Both plasma cells and memory B cells display high levels of autophagy. The elevated secretory activity of plasma cells makes them particularly susceptible to ER stress thus determining the activation of the unfolded protein response (UPR), whose principal aim is to restore ER homeostasis (Li et al., 2019). In response to the challenge of misfolded proteins, autophagy may function as an adaptive 'self-eating' process by which excessive intracellular components are encapsulated within autophagosomes and degraded. Pengo et al. (2013), in autophagy-deficient (Atg5f/fCD19-Cre) plasma cells, discovered that autophagy is required for plasma cells maintenance and humoral immunity, by limiting ER expansion and immunoglobulin synthesis while sustaining energy metabolism and viability. In memory B cells autophagy deficiency leads to a significant decline of cell number accompanied by accumulation of abnormal mitochondria, excessive ROS production and oxidative damage and Ab-dependent immunological memory (Chen M. et al., 2014; Chen et al., 2015). Of notice, autophagy is dispensable for the initial formation of memory B cells, but it is necessary for their long-term maintenance, via the upregulation of the expression of BCL2 and autophagy genes, starting from the transcription factors FoxO1 and FoxO3 (Chen et al., 2015). Finally, autophagy has been demonstrated to be central in MHC-II-dependent antigen presentation by B cells to CD4+ T cells. In their role of APCs B cells can induce T cell tolerance and, in case of presenting self-antigens, they can be involved in the development of autoimmune diseases. Moreover, priming of helper T cells by B cells provides instructive signals for B cells terminal differentiation into memory or plasma cells secreting high-affinity antibodies (Rodriguez-Pinto, 2005). In B cells as APCs, autophagy is indeed implicated in the processing of viral antigens for MHC-II-mediated presentation (Paludan et al., 2005), and optimizes B cell receptor signaling in response to nucleic acid antigens (Chaturvedi et al., 2008). Recently, it has been reported that Atg5 is involved in B cell receptor trafficking and in the recruitment of lysosomes and MHC-II compartment in B cells, thus suggesting that autophagy may control the B cell activation steps required for the humoral immune response against particulate antigens (Arbogast et al., 2019).

AUTOPHAGY AND BRAIN HOMEOSTASIS

It is well known that the development, survival and function of nervous system strongly depend on autophagy, which plays a crucial role to maintain neuronal homeostasis and functioning (Yamamoto and Yue, 2014; Ariosa and Klionsky, 2016). In fact, as post-mitotic cells, neurons cannot remove dysfunctional cellular components by cell division. Conversely, they require specific processes aimed to preserve their viability during lifetime. To better understand the importance of autophagy for neurons, we have to consider that differently from frequently replaced cells, most of the neurons are generated during embryogenesis and have to maintain their functionality for the entire lifespan of the individual. The critical relationship between neurons and autophagy is demonstrated by the detrimental impact of the deletion from the neural lineage of specific Atg genes, which results in cytoplasmic inclusions and increased risk of neurodegeneration, even without concomitant pathological processes. Moreover, growing evidence suggests the involvement of autophagy in several pathologies characterized by neuronal dysfunction without cell death. In line with these observations, a better knowledge of the mechanisms underlying autophagy in neurons would be crucial to develop potential therapeutic strategies able to preserve and/or protect neuronal health. Although in this review we aim to specifically describe the involvement of autophagy in neuronal health and function, we have to be aware that other cells of the nervous systems such as glial populations, i.e., astrocytes, oligodendrocytes, Schwann cells and microglia cells are under the control of this process [for review (Kulkarni et al., 2018)]. The comprehension of the mechanisms by which autophagy occurs within the nervous system, both in neurons and in non-neuronal cells, may provide crucial information to address autophagy as potential therapeutic target. **Table 4** summarizes the present understanding on the role of autophagy in brain homeostasis, focusing on the genetic or pharmacological approaches used to modulate the autophagic process both *in vitro* and *in vivo*. All the data presented in **Table 4** are deeply discussed in the sections below.

Autophagy and Neuronal Survival

The role of autophagy in neuronal survival has been demonstrated by using mice and/or other models with whole-body or conditional/selective knockouts of Atg genes. For example, deletion of genes codifying proteins involved in the formation of autophagosome within the nervous system such as Atg5 and Atg7 caused axon swelling and neuron death (Hara et al., 2006; Komatsu et al., 2006). Specifically, neuronal loss was detected in the Purkinje cell layer of the cerebellum as well as in the pyramidal cells of cerebral cortex and hippocampus (Hara et al., 2006; Komatsu et al., 2006). Interestingly, inhibition of autophagy was paralleled by increased ubiquitin-positive aggregates, an effect restricted to neurons with no impact on the surrounding glia (Hara et al., 2006; Komatsu et al., 2006). It is important to note that the loss of autophagy differently affects the various brain regions. For example, despite their susceptibility to the consequences of compromised autophagy, Purkinje cells were not characterized by aggregates (Hara et al., 2006). Degeneration and death of Purkinje cells have been also observed in response to neural-specific deletion of FIP200, a protein required for the initiation of autophagosome formation (Hara et al., 2008). The negative impact of autophagy loss was associated with behavioral alterations such as cerebellar ataxia, motor deficits and even

TABLE 4 | A summary of the current knowledge on the role of autophagy in the maintenance of brain behavior and functions.

***In vitro* genetic or pharmacological modulation**	**Autophagy**	**Cell type**	**Biological effect**	**References**
FIP200–/– mouse embryonic fibroblasts	↓	Embryonic fibroblasts	Reduced autophagosome formation, cell degeneration	Hara et al., 2008
Lymphoblastoid cell lines of ataxia patients	↓	Lymphoblastoid cell lines	ATG5 mutation	Kim et al., 2016
ATG5 silencing	↓	Cortical neural progenitor cells	Inhibited differentiation	Lv et al., 2014
ATG7 or ATG16L1 silencing	↓	HEK cells	Modulation of Notch signaling and stem cell differentiation	Wu et al., 2016
In vivo* genetic or *pharmacological modulation				
Brain ATG5–/– mice	↓	Several brain regions	Cerebral cortex atrophy, neuronal loss, motor and behavioral deficits	Komatsu et al., 2006
Neural-cell-specific ATG5–/– mice	↓	Several brain regions	Cell degeneration, protein aggregation, neurological phenotype	Hara et al., 2006
Neural-specific conditional FIP200–/– mice	↓	Cerebellum	Reduced autophagosome formation, cell degeneration, apoptosis, neuronal loss, protein aggregation, mitochondrial impairment, cerebellar ataxia, animal lethality	Liang et al., 2010
Purkinje cell-specific conditional ATG5–/– mice	↓	Purkinje cell	Axonal swelling, autophagosome-like vesicles accumulation, cell degeneration, ataxia	Nishiyama et al., 2007
Purkinje cell-specific conditional ATG7–/– mice	↓	Cerebellum, Purkinje cell	Axonal dystrophy, cell death, locomotion and motor coordination impairment	Komatsu et al., 2007
ATG3–/– mice, *ATG12–/– mice*, ATG16L1 mutant mice	↓	–	Animal lethality	Saitoh et al., 2008; Sou et al., 2008; Malhotra et al., 2015
ATG5–/– mice with re-expression of ATG5 in the brain	–	Brain	Rescue of ATG5–/– mice	Yoshii et al., 2016
Eva1a–/– mice	↓	Brain	Impaired neurogenesis	Wu et al., 2016
WDFY3 mutant mice	↓	Mitochondria	Mitophagy, impaired mitochondrial function	Napoli et al., 2018
Brain of ASds patients	↓	Temporal lobe, layer V pyramidal neurons	Increased dendritic spine density, reduced developmental spine pruning	Tang et al., 2014
Conditional neuronal ATG7–/– mice	↓	Pyramidal neurons	Spine pruning defect, increased dendritic spines	Tang et al., 2014
Dopamine neuron-specific ATG7–/– mice	↓	Corticostriatal slices, dopaminergic neurons	Abnormally large dopaminergic axonal profiles, increased neurotransmitter release, rapid presynaptic recovery	Hernandez et al., 2012
Microglia-specific ATG7–/– mice	↓	Brain	ASDs-like phenotype, increased dendritic spines and synaptic markers, altered connectivity between brain regions	Kim et al., 2017
Systemic administration of young plasma into aged mice	↑	Hippocampal neurons	Recovery memory deficits	Glatigny et al., 2019
Drosophila brain	↓	Drosophila learning center (mushroom body)	Memory impairment, increased metaplasticity	Bhukel et al., 2019
Amitriptyline treated mice	↓	Hippocampal lysosomes	Sphingomyelin accumulation, ceramide increase	Gulbins et al., 2018

animal lethality (Hara et al., 2006; Komatsu et al., 2006; Liang et al., 2010). Since Atg5 or Atg7 deletion affects both neuron and glial cell precursors, neuron-specific knockout mice were developed. Specifically, Atg5 or Atg7 genetic inactivation within Purkinje cells caused gradual axon degeneration and neuronal death paralleled by deficit in motor coordination (Komatsu et al., 2007; Nishiyama et al., 2007). One of the most frequent behavioral consequences of neuronal autophagy deficiency in mice is neonatal lethality, an effect observed not only in response to Atg5 deletion, but also in Atg3, Atg7, Atg12, and Atg16L1 null mice (Komatsu et al., 2005; Saitoh et al., 2008; Sou et al., 2008; Malhotra et al., 2015). Recently, it has been demonstrated that an almost complete rescue from neonatal lethality was possible by re-expressing Atg5 only in neuron, suggestive of neuronal dysfunction as the primary cause of neonatal lethality (Yoshii et al., 2016).

As previously mentioned, in human autophagy deficiency cell death has been associated with neurodegenerative disorders. For example, childhood ataxia, a movement disorder linked with degeneration of cerebellar Purkinje cells has been recently demonstrated to be caused by a mutation in Atg5 that is able to reduce autophagic flux (Kim et al., 2016). Similarly, mutations in autophagy receptors and/or regulatory proteins have been linked to several neurodegenerative diseases (Frake et al., 2015). Most of these disorders such as Amyotrophic Lateral Sclerosis, Alzheimer's, Parkinson's, and Huntington's Diseases have been characterized by neuronal autophagosomes accumulation (Nixon et al., 2005; Son et al., 2012; Menzies et al., 2017). This effect might be due to an unbalance between autophagosome formation and clearance. Although the specific mechanism is currently unknown, the latter hypothesis seems more feasible. Indeed, neurodegenerative experimental models showed compromised

axonal transport and defective lysosomal function, alterations that may affect the clearance ability leading to neuronal death (Millecamps and Julien, 2013; Maday and Holzbaur, 2014; Gowrishankar et al., 2015).

Autophagy and Neurogenesis

In the last years, there has been a growing interest in the role of autophagy in the maintenance of neuronal stem cells as well as in the proliferation of neural progenitors. In particular, it has been reported that the developing central nervous system (CNS) expresses core autophagy genes (Wu et al., 2013) and that neurogenesis in the developing embryo is regulated by autophagy (Kuma et al., 2017). Specifically, neural progenitor cells (NPCs) in the embryonic mouse cortex express Atg genes, whose silencing results in reduced neuronal proliferation, altered growth and branching of cortical neurons, increased cells in the subventricular (SVZ) and ventricular zones (Lv et al., 2014). A similar effect was found in another study using Atg16L1 mice, in which reduced cortical plate and enlarged SVZ were observed (Wu et al., 2016). Several mediators are thought potential players of these effects. Specifically, it has been suggested the involvement of the lysosome and ER- associated protein EVA1 (transmembrane protein 166, TMEM166 protein) largely distributed in the brain during neurogenesis and involved in autophagy and apoptosis (Li et al., 2016). Loss of Nestin-expressing neuronal stem cells (NSCs) and decreased self-renewal and differentiation were observed in the cortex of EVA1 conditional knockout mice, effect due to the activation of mTOR pathway (Li et al., 2016).

The role of autophagy in neurogenesis is supported by the autosomal dominant human microcephaly observed in response to mutations of specific autophagy genes (Kadir et al., 2016). Specifically, the mutations are identified on a scaffolding protein responsible for the degradation of ubiquitinated aggregate-prone proteins by autophagy (Filimonenko et al., 2010) and clearance of mitochondria via mitophagy (Napoli et al., 2018). Interestingly, studies in Drosophila, reported that the expression of the mutant protein is paralleled by a marked reduction of the brain volume (Kadir et al., 2016).

Moreover, mild non-specific neurodevelopmental delay has been associated with further mutations that result in truncated proteins or missense heterozygous mutations and may lead to microcephaly or macrocephaly, autism spectrum disorder, and attention deficit hyperactivity disorder depending on the protein domain in which the mutation occurs (Le Duc et al., 2019).

Interestingly, the main clinical abnormalities associated with genetic mutations in autophagy genes are developmental delay, cognitive decline, and functional deficits while only minor structural alterations were observed [for detailed examination, (Fleming and Rubinsztein, 2020)]. Nevertheless, further studies are demanded to clarify the mechanisms underlying the impact of these mutations.

Autophagy and Neuronal Plasticity

Despite the contribution of autophagy in the regulation of developing nervous system, this process is critical also for the mature nervous system. In particular, autophagy exerts an important role in the maintenance of the so-called neuronal plasticity: the ability of the neuronal cells to perceive, respond and adapt to any internal or external, beneficial, or detrimental stimulus. It is well-known that a variety of functions require this capability: learning and memory, cognition, several intellectual abilities, adaptive behaviors, injury repair. All these behaviors involve structural remodeling of the neuron itself and the circuits in which is involved trough axonal growth, synaptic assembly, dendritic spine formation, and pruning (Lieberman and Sulzer, 2020).

Again, major findings on the role of autophagy in neuronal plasticity derive from studies with mutant animals for core autophagy genes. For example, conditional knockout mice with neuronal Atg7 deletion display pyramidal neurons with increased dendritic spines due to spine pruning defect (Tang et al., 2014). Moreover, Atg7 deletion in mouse dopaminergic neurons induces not only structural alteration such as larger axonal profiles but also enhanced stimulus-evoked dopamine release and rapid presynaptic recovery, suggesting a potential regulation of synaptic vesicle turnover (Hernandez et al., 2012). As previously mentioned, given the mutual regulation between neurons and glia, glial cells are involved in the synaptic effect of autophagy.

Specifically, conditional Atg7-knockout mice shown impaired synaptosome degradation, increased dendritic spines and synaptic markers, and altered connectivity paralleled by loss of microglial autophagy (Kim et al., 2017). The mutual influence between autophagy and synaptic machinery has been demonstrated by studies indicating that gain of function or loss of function of the synaptic protein Bassoon may suppress or enhance autophagy through direct interaction with Atg5 (Okerlund et al., 2017; Vanhauwaert et al., 2017). Moreover, blockade of autophagy at the presynaptic terminal may be obtained by deletion of the synaptic protein synaptojanin (Okerlund et al., 2017; Vanhauwaert et al., 2017).

In support of the involvement of autophagy in memory, it has been reported that it is possible to partially recover memory deficit in aged animals by inducing autophagy. In particular, the administration to old animals of plasma obtained from young animals improved memory decline with the involvement of bone-derived osteocalcin, a hormonal regulator of hippocampal memory (Glatigny et al., 2019). A similar effect was observed in Drosophila, where autophagy protects from the memory impairment associated with the expansion of the presynaptic active zone (Bhukel et al., 2019). Despite these observations, exaggerate increased autophagy may be deleterious, as suggested by the loss of pre- and post-synaptic markers – index of proper synaptic function – in response to the hyperactivation of the positive autophagy regulator, AMPK (Domise et al., 2019). Further studies could be important to clarify this issue, however, we have to keep in mind that autophagy proteins may have a non-canonical function leading to microtubule instability that may affect synaptic structural plasticity (Negrete-Hurtado et al., 2020).

Given the role of compromised neuronal plasticity in the etiopathology of several psychiatric disorders, deficit

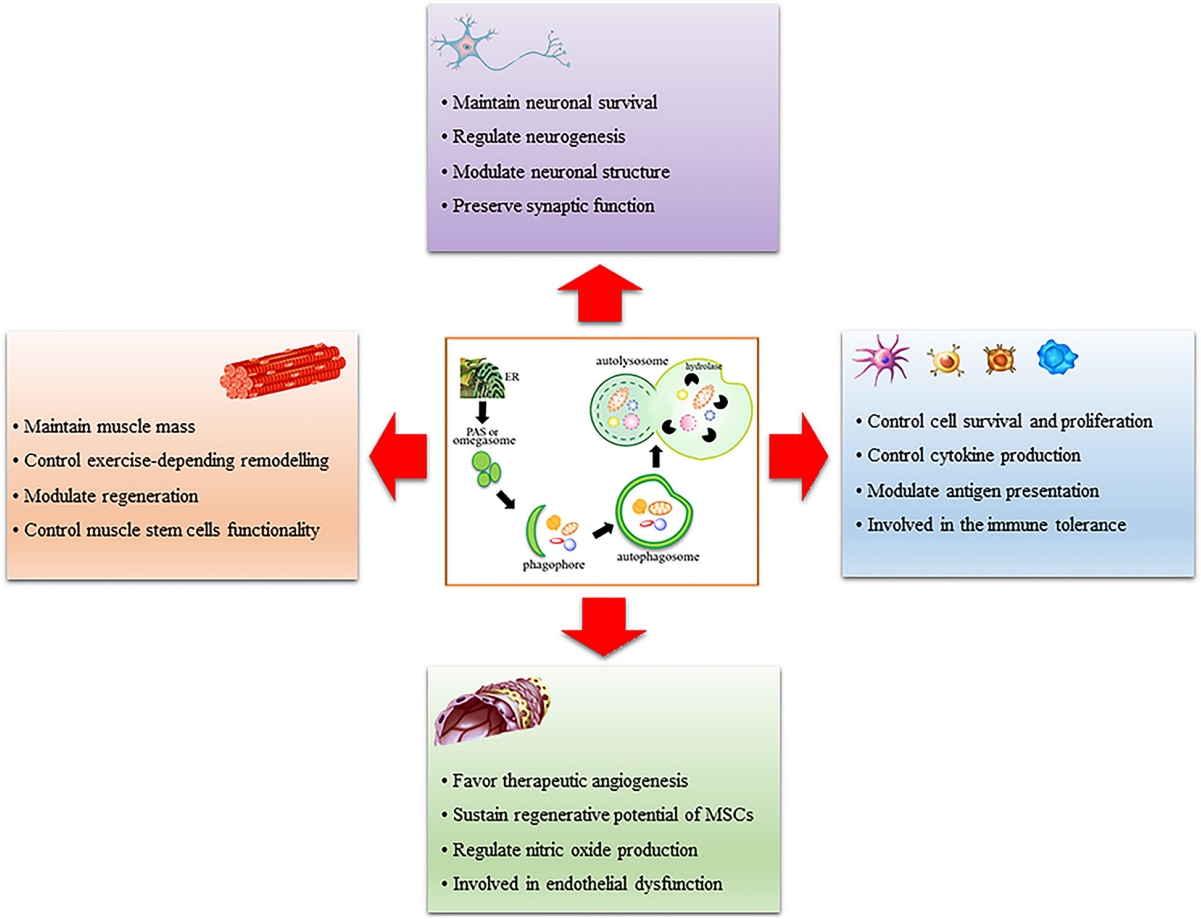

FIGURE 1 | Schematic representation of the role of autophagy in muscle, immune system, endothelium, and brain. Autophagy is a multi-step process that involves phagophore formation from the endoplasmic reticulum-associated structure called omegasome or phagophore assembly site (PAS). This structure grows around the material to be eliminated and forms a characteristic double-membrane vesicle called autophagosome. Mature autophagosome fuses with lysosomes to form autolysosome wherein the material is digested by lysosomal hydrolases. Autophagy regulates many functions in each tissue analyzed, it is important for their remodeling after stimuli or stress conditions and it is altered in many pathologic conditions.

in autophagy has been postulated to contribute to these diseases. In this context, it has been evaluated the ability of antidepressant drugs to modulate autophagy in different preclinical settings. For example, it has been reported that the Selective Serotonin Reuptake Inhibitor (SSRI) fluoxetine, as well as the TriCyclic Antidepressant (TCA) amitriptyline, stimulate autophagy through a mechanism involving the accumulation of sphingomyelin in lysosomes and Golgi membranes and ceramide in the ER (Gulbins et al., 2018). On the other hand, drugs able to induce autophagy display in mice antidepressant properties, suggesting that the ability to modulate the mood action might also depend on autophagy (Kara et al., 2013). Other drugs, able to reduce IP3 such as the mood stabilizers valproate, lithium, and carbamazepine, induce autophagy via the same mechanism (Sarkar et al., 2005).

As previously mentioned, this evidence clearly supports the potential of autophagy as pharmacological target for several diseases of the nervous systems, not only neurodegenerative but also psychiatric.

CONCLUSIONS

Autophagy is often considered as a cell death mechanism in the mammalian system, however, in the last decade, the thorough characterization of macroautophagy at molecular level and the development of reliable methods to monitor and manipulate autophagic activity both *in vitro* and *in vivo* have led to outstanding results in understanding the role of autophagy on tissue pathophysiology.

As reported in this review, it is now clear that autophagy is an essential process for the homeostasis of several tissues driving their development, differentiation and ability to remodel after stimuli or under stress conditions. Of note, autophagy alterations are associated with many diseases in each tissue analyzed uncovering the cardinal importance of both basal and inducible autophagy for the maintenance of tissue homeostasis. With this review, we provide a suitable framework of the importance of autophagy in endothelium, muscle, immune systems and brain, as schematically reported in **Figure 1**. These are very different

tissues with a diverse organization and activity and it is worth mentioning that, in each of these, autophagy is relevant and crucial; thereby this should drive scientists to continue studying autophagy in still unexplored fields or deepen some preliminary observations to fully understand autophagy's role.

AUTHOR CONTRIBUTIONS

CDP conceptualized the review and wrote the introduction, conclusions, and Section "Autophagy and Skeletal Muscle Homeostasis." CP wrote and revised Section "Autophagy and Immune System Homeostasis." MGC wrote and revised Section "Autophagy and Endothelium Homeostasis." RM wrote and revised Section "Autophagy and Brain Homeostasis." All authors read and approved the final manuscript.

FUNDING

This work was supported by AFM-Telethon (n° 20568).

REFERENCES

Aas, S. N., Tommerbakke, D., Godager, S., Nordseth, M., Armani, A., Sandri, M., et al. (2020). Effects of acute and chronic strength training on skeletal muscle autophagy in frail elderly men and women. *Exp. Gerontol.* 142:111122. doi: 10.1016/j.exger.2020.111122

Agnello, M., Bosco, L., Chiarelli, R., Martino, C., and Roccheri, M. C. (2015). "The role of autophagy and apoptosis during embryo development," in *Cell Death - Autophagy, Apoptosis and Necrosis*, ed. T. M. Ntuli (Reijeka: InTech), 83–112. doi: 10.5772/61765

Alissafi, T., Banos, A., Boon, L., Sparwasser, T., Ghigo, A., Wing, K., et al. (2017). Tregs restrain dendritic cell autophagy to ameliorate autoimmunity. *J. Clin. Invest.* 127, 2789–2804. doi: 10.1172/JCI92079

An, Y., Liu, W. J., Xue, P., Ma, Y., Zhang, L. Q., Zhu, B., et al. (2018). Autophagy promotes MSC-mediated vascularization in cutaneous wound healing via regulation of VEGF secretion. *Cell Death Dis.* 9:58. doi: 10.1038/s41419-017-0082-8

Andersen, M. H., Schrama, D., Thor Straten, P., and Becker, J. C. (2006). Cytotoxic T cells. *J. Invest. Dermatol.* 126, 32–41. doi: 10.1038/sj.jid.5700001

Arbogast, F., Arnold, J., Hammann, P., Kuhn, L., Chicher, J., Murera, D., et al. (2019). ATG5 is required for B cell polarization and presentation of particulate antigens. *Autophagy* 15, 280–294. doi: 10.1080/15548627.2018.1516327

Ariosa, A. R., and Klionsky, D. J. (2016). Autophagy core machinery: overcoming spatial barriers in neurons. *J. Mol. Med.* 94, 1217–1227. doi: 10.1007/s00109-016-1461-9

Arnold, C. R., Pritz, T., Brunner, S., Knabb, C., Salvenmoser, W., Holzwarth, B., et al. (2014). T cell receptor-mediated activation is a potent inducer of macroautophagy in human CD8(+)CD28(+) T cells but not in CD8(+)CD28(−) T cells. *Exp. Gerontol.* 54, 75–83. doi: 10.1016/j.exger.2014.01.018

Arnold, J., Murera, D., Arbogast, F., Fauny, J. D., Muller, S., and Gros, F. (2016). Autophagy is dispensable for B-cell development but essential for humoral autoimmune responses. *Cell Death Differ.* 23, 853–864. doi: 10.1038/cdd.2015.149

Axe, E. L., Walker, S. A., Manifava, M., Chandra, P., Roderick, H. L., Habermann, A., et al. (2008). Autophagosome formation from membrane compartments enriched in phosphatidylinositol 3-phosphate and dynamically connected to the endoplasmic reticulum. *J. Cell Biol.* 182, 685–701. doi: 10.1083/jcb.200803137

Bantug, G. R., Galluzzi, L., Kroemer, G., and Hess, C. (2018). The spectrum of T cell metabolism in health and disease. *Nat. Rev. Immunol.* 18, 19–34. doi: 10.1038/nri.2017.99

Bargiela, A., Cerro-Herreros, E., Fernandez-Costa, J. M., Vilchez, J. J., Llamusi, B., and Artero, R. (2015). Increased autophagy and apoptosis contribute to muscle atrophy in a myotonic dystrophy type 1 *Drosophila* model. *Dis. Model Mech.* 8, 679–690. doi: 10.1242/dmm.018127

Bharath, L. P., Mueller, R., Li, Y. Y., Ruan, T., Kunz, D., Goodrich, R., et al. (2014). Impairment of autophagy in endothelial cells prevents shear-stress-induced increases in nitric oxide bioavailability. *Can. J. Physiol. Pharmacol.* 92, 605–612. doi: 10.1139/cjpp-2014-0017

Bhukel, A., Beuschel, C. B., Maglione, M., Lehmann, M., Juhasz, G., Madeo, F., et al. (2019). Autophagy within the mushroom body protects from synapse aging in a non-cell autonomous manner. *Nat. Commun.* 10:1318. doi: 10.1038/s41467-019-09262-2

Bloemberg, D., and Quadrilatero, J. (2020). Autophagy displays divergent roles during intermittent amino acid starvation and toxic stress-induced senescence in cultured skeletal muscle cells. *J. Cell Physiol.* doi: 10.1002/jcp.30079 [Epub ahead of print].

Bo, Q., Shen, M., Xiao, M., Liang, J., Zhai, Y., Zhu, H., et al. (2020). 3-Methyladenine alleviates experimental subretinal fibrosis by inhibiting macrophages and M2 polarization through the PI3K/Akt Pathway. *J. Ocul. Pharmacol. Ther.* 36, 618–628. doi: 10.1089/jop.2019.0112

Botbol, Y., Patel, B., and Macian, F. (2015). Common gamma-chain cytokine signaling is required for macroautophagy induction during CD4+ T-cell activation. *Autophagy* 11, 1864–1877. doi: 10.1080/15548627.2015.1089374

Boya, P., Codogno, P., and Rodriguez-Muela, N. (2018). Autophagy in stem cells: repair, remodelling and metabolic reprogramming. *Development* 145:dev146506. doi: 10.1242/dev.146506

Breier, G., Breviario, F., Caveda, L., Berthier, R., Schnurch, H., Gotsch, U., et al. (1996). Molecular cloning and expression of murine vascular endothelial cadherin in early stage development of cardiovascular system. *Blood* 87, 630–641. doi: 10.1182/blood.v87.2.630.bloodjournal872630

Bronckaers, A., Hilkens, P., Martens, W., Gervois, P., Ratajczak, J., Struys, T., et al. (2014). Mesenchymal stem/stromal cells as a pharmacological and therapeutic approach to accelerate angiogenesis. *Pharmacol. Ther.* 143, 181–196. doi: 10.1016/j.pharmthera.2014.02.013

Bujak, A. L., Crane, J. D., Lally, J. S., Ford, R. J., Kang, S. J., Rebalka, I. A., et al. (2015). AMPK activation of muscle autophagy prevents fasting-induced hypoglycemia and myopathy during aging. *Cell Metab.* 21, 883–890. doi: 10.1016/j.cmet.2015.05.016

Cadore, E. L., Casas-Herrero, A., Zambom-Ferraresi, F., Idoate, F., Millor, N., Gomez, M., et al. (2014). Multicomponent exercises including muscle power training enhance muscle mass, power output, and functional outcomes in institutionalized frail nonagenarians. *Age* 36, 773–785. doi: 10.1007/s11357-013-9586-z

Call, J. A., Wilson, R. J., Laker, R. C., Zhang, M., Kundu, M., and Yan, Z. (2017). Ulk1-mediated autophagy plays an essential role in mitochondrial remodeling and functional regeneration of skeletal muscle. *Am. J. Physiol. Cell Physiol.* 312, C724–C732. doi: 10.1152/ajpcell.00348.2016

Capasso, S., Alessio, N., Squillaro, T., Di Bernardo, G., Melone, M. A., Cipollaro, M., et al. (2015). Changes in autophagy, proteasome activity and metabolism to determine a specific signature for acute and chronic senescent mesenchymal stromal cells. *Oncotarget* 6, 39457–39468. doi: 10.18632/oncotarget.6277

Carmignac, V., Svensson, M., Korner, Z., Elowsson, L., Matsumura, C., Gawlik, K. I., et al. (2011). Autophagy is increased in laminin alpha2 chain-deficient muscle and its inhibition improves muscle morphology in a mouse model of MDC1A. *Hum. Mol. Genet.* 20, 4891–4902. doi: 10.1093/hmg/ddr427

Castagnaro, S., Pellegrini, C., Pellegrini, M., Chrisam, M., Sabatelli, P., Toni, S., et al. (2016). Autophagy activation in COL6 myopathic patients by a low-protein-diet pilot trial. *Autophagy* 12, 2484–2495. doi: 10.1080/15548627.2016.1231279

Castets, P., Lin, S., Rion, N., Di Fulvio, S., Romanino, K., Guridi, M., et al. (2013). Sustained activation of mTORC1 in skeletal muscle inhibits constitutive and starvation-induced autophagy and causes a severe, late-onset myopathy. *Cell Metab.* 17, 731–744. doi: 10.1016/j.cmet.2013.03.015

Ceccariglia, S., Cargnoni, A., Silini, A. R., and Parolini, O. (2020). Autophagy: a potential key contributor to the therapeutic action of mesenchymal stem cells. *Autophagy* 16, 28–37. doi: 10.1080/15548627.2019.1630223

Chang, N. C., Nguyen, M., Bourdon, J., Risse, P. A., Martin, J., Danialou, G., et al. (2012). Bcl-2-associated autophagy regulator Naf-1 required for maintenance of skeletal muscle. *Hum, Mol. Genet.* 21, 2277–2287. doi: 10.1093/hmg/dds048

Chang, N. T. C. (2020). Autophagy and stem cells: self-eating for self-renewal. *Front. Cell Dev. Biol.* 8:138. doi: 10.3389/Fcell.2020.00138

Chang, T. C., Hsu, M. F., and Wu, K. K. (2015). High glucose induces bone marrow-derived mesenchymal stem cell senescence by upregulating autophagy. *PLoS One* 10:e0126537. doi: 10.1371/journal.pone.0126537

Chaturvedi, A., Dorward, D., and Pierce, S. K. (2008). The B cell receptor governs the subcellular location of Toll-like receptor 9 leading to hyperresponses to DNA-containing antigens. *Immunity* 28, 799–809. doi: 10.1016/j.immuni.2008.03.019

Chen, D., Xie, J., Fiskesund, R., Dong, W., Liang, X., Lv, J., et al. (2018). Chloroquine modulates antitumor immune response by resetting tumor-associated macrophages toward M1 phenotype. *Nat. Commun,* 9:873. doi: 10.1038/s41467-018-03225-9

Chen, X. H., He, Y. F., and Lu, F. (2018). Autophagy in stem cell biology: a perspective on stem cell self-renewal and differentiation. *Stem Cells Int.* 2018:9131397. doi: 10.1155/2018/9131397

Chen, F., Chen, B., Xiao, F. Q., Wu, Y. T., Wang, R. H., Sun, Z. W., et al. (2014). Autophagy protects against senescence and apoptosis via the RAS-mitochondria in high-glucose-induced endothelial cells. *Cell Physiol. Biochem.* 33, 1058–1074. doi: 10.1159/000358676

Chen, M., Hong, M. J., Sun, H., Wang, L., Shi, X., Gilbert, B. E., et al. (2014). Essential role for autophagy in the maintenance of immunological memory against influenza infection. *Nat. Med.* 20, 503–510. doi: 10.1038/nm.3521

Chen, M., Kodali, S., Jang, A., Kuai, L., and Wang, J. (2015). Requirement for autophagy in the long-term persistence but not initial formation of memory B cells. *J. Immunol.* 194, 2607–2615. doi: 10.4049/jimmunol.1403001

Chen, M. L., Yi, L., Jin, X., Liang, X. Y., Zhou, Y., Zhang, T., et al. (2013). Resveratrol attenuates vascular endothelial inflammation by inducing autophagy through the cAMP signaling pathway. *Autophagy* 9, 2033–2045. doi: 10.4161/auto.26336

Clarke, A. J., Riffelmacher, T., Braas, D., Cornall, R. J., and Simon, A. K. (2018). B1a B cells require autophagy for metabolic homeostasis and self-renewal. *J. Exp. Med.* 215, 399–413. doi: 10.1084/jem.20170771

Cullup, T., Kho, A. L., Dionisi-Vici, C., Brandmeier, B., Smith, F., Urry, Z., et al. (2013). Recessive mutations in EPG5 cause Vici syndrome, a multisystem disorder with defective autophagy. *Nat. Genet.* 45, 83–87. doi: 10.1038/ng.2497

de Castro, G. S., Simoes, E., Lima, J., Ortiz-Silva, M., Festuccia, W. T., Tokeshi, F., et al. (2019). Human cachexia induces changes in mitochondria, autophagy and apoptosis in the skeletal muscle. *Cancers* 11:1264. doi: 10.3390/cancers11091264

De Palma, C., Morisi, F., Cheli, S., Pambianco, S., Cappello, V., Vezzoli, M., et al. (2012). Autophagy as a new therapeutic target in Duchenne muscular dystrophy. *Cell Death Dis.* 3:e418.

De Palma, C., Perrotta, C., Pellegrino, P., Clementi, E., and Cervia, D. (2014). Skeletal muscle homeostasis in duchenne muscular dystrophy: modulating autophagy as a promising therapeutic strategy. *Front. Aging Neurosci.* 6:188. doi: 10.3389/fnagi.2014.00188

Dengjel, J., Schoor, O., Fischer, R., Reich, M., Kraus, M., Muller, M., et al. (2005). Autophagy promotes MHC class II presentation of peptides from intracellular source proteins. *Proc. Natl. Acad. Sci. U.S.A.* 102, 7922–7927. doi: 10.1073/pnas.0501190102

Di Rienzo, M., Antonioli, M., Fusco, C., Liu, Y., Mari, M., Orhon, I., et al. (2019). Autophagy induction in atrophic muscle cells requires ULK1 activation by TRIM32 through unanchored K63-linked polyubiquitin chains. *Sci. Adv.* 5:eaau8857. doi: 10.1126/sciadv.aau8857

Dobrowolny, G., Aucello, M., Rizzuto, E., Beccafico, S., Mammucari, C., Boncompagni, S., et al. (2008). Skeletal muscle is a primary target of SOD1G93A-mediated toxicity. *Cell Metab.* 8, 425–436. doi: 10.1016/j.cmet.2008.09.002

Domise, M., Sauve, F., Didier, S., Caillerez, R., Begard, S., Carrier, S., et al. (2019). Neuronal AMP-activated protein kinase hyper-activation induces synaptic loss by an autophagy-mediated process. *Cell Death Dis.* 10:221. doi: 10.1038/s41419-019-1464-x

Du, J. H., Teng, R. J., Guan, T. J., Eis, A., Kaul, S., Konduri, G. G., et al. (2012). Role of autophagy in angiogenesis in aortic endothelial cells. *Am. J. Physiol. Cell Physiol.* 302, C383–C391. doi: 10.1152/ajpcell.00164.2011

Eibel, H., Kraus, H., Sic, H., Kienzler, A. K., and Rizzi, M. (2014). B cell biology: an overview. *Curr. Allergy Asthma Rep.* 14:434. doi: 10.1007/s11882-014-0434-8

Esteban-Martinez, L., Sierra-Filardi, E., McGreal, R. S., Salazar-Roa, M., Marino, G., Seco, E., et al. (2017). Programmed mitophagy is essential for the glycolytic switch during cell differentiation. *EMBO J.* 36, 1688–1706. doi: 10.15252/embj.201695916

Fafian-Labora, J. A., Morente-Lopez, M., and Arufe, M. C. (2019). Effect of aging on behaviour of mesenchymal stem cells. *World J. Stem Cells* 11, 337–346. doi: 10.4252/wjsc.v11.i6.337

Fan, J., Kou, X., Jia, S., Yang, X., Yang, Y., and Chen, N. (2016). Autophagy as a potential target for sarcopenia. *J. Cell Physiol.* 231, 1450–1459. doi: 10.1002/jcp.25260

Fetalvero, K. M., Yu, Y., Goetschkes, M., Liang, G., Valdez, R. A., Gould, T., et al. (2013). Defective autophagy and mTORC1 signaling in myotubularin null mice. *Mol. Cell Biol.* 33, 98–110. doi: 10.1128/MCB.01075-12

Fetterman, J. L., Holbrook, M., Flint, N., Feng, B., Breton-Romero, R., Linder, E. A., et al. (2016). Restoration of autophagy in endothelial cells from patients with diabetes mellitus improves nitric oxide signaling. *Atherosclerosis* 247, 207–217. doi: 10.1016/j.atherosclerosis.2016.01.043

Fiacco, E., Castagnetti, F., Bianconi, V., Madaro, L., De Bardi, M., Nazio, F., et al. (2016). Autophagy regulates satellite cell ability to regenerate normal and dystrophic muscles. *Cell Death Differ.* 23, 1839–1849. doi: 10.1038/cdd.2016.70

Filimonenko, M., Isakson, P., Finley, K. D., Anderson, M., Jeong, H., Melia, T. J., et al. (2010). The selective macroautophagic degradation of aggregated proteins requires the PI3P-binding protein Alfy. *Mol. Cell* 38, 265–279. doi: 10.1016/j.molcel.2010.04.007

Filippi, I., Saltarella, I., Aldinucci, C., Carraro, F., Ria, R., Vacca, A., et al. (2018). Different adaptive responses to hypoxia in normal and multiple myeloma endothelial cells. *Cell. Physiol. Biochem.* 46, 203–212. doi: 10.1159/000488423

Fleming, A., and Rubinsztein, D. C. (2020). Autophagy in neuronal development and plasticity. *Trends Neurosci.* 43, 767–779. doi: 10.1016/j.tins.2020.07.003

Frake, R. A., Ricketts, T., Menzies, F. M., and Rubinsztein, D. C. (2015). Autophagy and neurodegeneration. *J. Clin. Invest.* 125, 65–74. doi: 10.1172/JCI73944

Fukuda, T., Roberts, A., Ahearn, M., Zaal, K., Ralston, E., Plotz, P. H., et al. (2006). Autophagy and lysosomes in Pompe disease. *Autophagy* 2, 318–320. doi: 10.4161/auto.2984

Fuqua, J. D., Mere, C. P., Kronemberger, A., Blomme, J., Bae, D., Turner, K. D., et al. (2019). ULK2 is essential for degradation of ubiquitinated protein aggregates and homeostasis in skeletal muscle. *FASEB J.* 33, 11735–11745. doi: 10.1096/fj.201900766R

Garcia-Prat, L., Martinez-Vicente, M., Perdiguero, E., Ortet, L., Rodriguez-Ubreva, J., Rebollo, E., et al. (2016). Autophagy maintains stemness by preventing senescence. *Nature* 529, 37–42. doi: 10.1038/nature16187

Gkikas, I., Palikaras, K., and Tavernarakis, N. (2018). The Role of mitophagy in innate immunity. *Front. Immunol.* 9:1283. doi: 10.3389/fimmu.2018.01283

Glatigny, M., Moriceau, S., Rivagorda, M., Ramos-Brossier, M., Nascimbeni, A. C., Lante, F., et al. (2019). Autophagy is required for memory formation and reverses age-related memory decline. *Curr Biol.* 29, 435.e8–448.e8 doi: 10.1016/j.cub.2018.12.021

Glimcher, L. H., and Murphy, K. M. (2000). Lineage commitment in the immune system: the T helper lymphocyte grows up. *Genes Dev.* 14, 1693–1711.

Gowrishankar, S., Yuan, P., Wu, Y., Schrag, M., Paradise, S., Grutzendler, J., et al. (2015). Massive accumulation of luminal protease-deficient axonal lysosomes at Alzheimer's disease amyloid plaques. *Proc. Natl. Acad. Sci. U.S.A.* 112, E3699–E3708.

Grumati, P., Coletto, L., Sabatelli, P., Cescon, M., Angelin, A., Bertaggia, E., et al. (2010). Autophagy is defective in collagen VI muscular dystrophies, and its reactivation rescues myofiber degeneration. *Nat. Med.* 16, 1313–1320. doi: 10.1038/nm.2247

Grumati, P., Coletto, L., Schiavinato, A., Castagnaro, S., Bertaggia, E., Sandri, M., et al. (2011). Physical exercise stimulates autophagy in normal skeletal muscles

but is detrimental for collagen VI-deficient muscles. *Autophagy* 7, 1415–1423. doi: 10.4161/auto.7.12.17877

Gulbins, A., Schumacher, F., Becker, K. A., Wilker, B., Soddemann, M., Boldrin, F., et al. (2018). Antidepressants act by inducing autophagy controlled by sphingomyelin-ceramide. *Mol. Psychiatry* 23, 2324–2346. doi: 10.1038/s41380-018-0090-9

Guo, F. X., Li, X. H., Peng, J., Tang, Y. L., Yang, Q., Liu, L. S., et al. (2014). Autophagy regulates vascular endothelial cell eNOS and ET-1 expression induced by laminar shear stress in an Ex Vivo perfused system. *Ann. Biomed. Eng.* 42, 1978–1988. doi: 10.1007/s10439-014-1033-5

Guo, Y., Feng, Y., Cui, X., Wang, Q., and Pan, X. (2019). Autophagy inhibition induces the repolarisation of tumour-associated macrophages and enhances chemosensitivity of laryngeal cancer cells to cisplatin in mice. *Cancer Immunol. Immunother.* 68, 1909–1920. doi: 10.1007/s00262-019-02415-8

Hara, T., Nakamura, K., Matsui, M., Yamamoto, A., Nakahara, Y., Suzuki-Migishima, R., et al. (2006). Suppression of basal autophagy in neural cells causes neurodegenerative disease in mice. *Nature* 441, 885–889. doi: 10.1038/nature04724

Hara, T., Takamura, A., Kishi, C., Iemura, S., Natsume, T., Guan, J. L., et al. (2008). FIP200, a ULK-interacting protein, is required for autophagosome formation in mammalian cells. *J. Cell Biol.* 181, 497–510. doi: 10.1083/jcb.200712064

Harris, J. (2011). Autophagy and cytokines. *Cytokine* 56, 140–144. doi: 10.1016/j.cyto.2011.08.022

He, C., Bassik, M. C., Moresi, V., Sun, K., Wei, Y., Zou, Z., et al. (2012). Exercise-induced BCL2-regulated autophagy is required for muscle glucose homeostasis. *Nature* 481, 511–515. doi: 10.1038/nature10758

Hentila, J., Ahtiainen, J. P., Paulsen, G., Raastad, T., Hakkinen, K., Mero, A. A., et al. (2018). Autophagy is induced by resistance exercise in young men, but unfolded protein response is induced regardless of age. *Acta Physiol.* 224:e13069. doi: 10.1111/apha.13069

Hernandez, D., Torres, C. A., Setlik, W., Cebrian, C., Mosharov, E. V., Tang, G., et al. (2012). Regulation of presynaptic neurotransmission by macroautophagy. *Neuron* 74, 277–284. doi: 10.1016/j.neuron.2012.02.020

Ho, T. T., Warr, M. R., Adelman, E. R., Lansinger, O. M., Flach, J., Verovskaya, E. V., et al. (2017). Autophagy maintains the metabolism and function of young and old stem cells. *Nature* 543, 205–210. doi: 10.1038/nature21388

Hsieh, H. J., Liu, C. A., Huang, B., Tseng, A. H. H., and Wang, D. L. (2014). Shear-induced endothelial mechanotransduction: the interplay between reactive oxygen species (ROS) and nitric oxide (NO) and the pathophysiological implications. *J. Biomed. Sci.* 21:3. doi: 10.1186/1423-0127-21-3

Hubbard, V. M., Valdor, R., Patel, B., Singh, R., Cuervo, A. M., and Macian, F. (2010). Macroautophagy regulates energy metabolism during effector T cell activation. *J. Immunol.* 185, 7349–7357. doi: 10.4049/jimmunol.1000576

Hubbard-Lucey, V. M., Shono, Y., Maurer, K., West, M. L., Singer, N. V., Ziegler, C. G., et al. (2014). Autophagy gene Atg16L1 prevents lethal T cell alloreactivity mediated by dendritic cells. *Immunity* 41, 579–591. doi: 10.1016/j.immuni.2014.09.011

Hughes, W. E., Beyer, A. M., and Gutterman, D. D. (2020). Vascular autophagy in health and disease. *Basic Res. Cardiol.* 115:41. doi: 10.1007/s00395-020-0802-6

Italiani, P., and Boraschi, D. (2014). From Monocytes to M1/M2 macrophages: phenotypical vs. functional differentiation. *Front. Immunol.* 5:514. doi: 10.3389/fimmu.2014.00514

Jacquel, A., Obba, S., Boyer, L., Dufies, M., Robert, G., Gounon, P., et al. (2012). Autophagy is required for CSF-1-induced macrophagic differentiation and acquisition of phagocytic functions. *Blood* 119, 4527–4531. doi: 10.1182/blood-2011-11-392167

Jakovljevic, J., Harrell, C. R., Fellabaum, C., Arsenijevic, A., Jovicic, N., and Volarevic, V. (2018). Modulation of autophagy as new approach in mesenchymal stem cell-based therapy. *Biomed. Pharmacother.* 104, 404–410. doi: 10.1016/j.biopha.2018.05.061

Jarosz-Biej, M., Kaminska, N., Matuszczak, S., Cichon, T., Pamula-Pilat, J., Czapla, J., et al. (2018). M1-like macrophages change tumor blood vessels and microenvironment in murine melanoma. *PLoS One* 13:e0191012. doi: 10.1371/journal.pone.0191012

Jia, W., and He, Y. W. (2011). Temporal regulation of intracellular organelle homeostasis in T lymphocytes by autophagy. *J. Immunol.* 186, 5313–5322. doi: 10.4049/jimmunol.1002404

Jia, W., Pua, H. H., Li, Q. J., and He, Y. W. (2011). Autophagy regulates endoplasmic reticulum homeostasis and calcium mobilization in T lymphocytes. *J. Immunol.* 186, 1564–1574. doi: 10.4049/jimmunol.1001822

Jokl, E. J., and Blanco, G. (2016). Disrupted autophagy undermines skeletal muscle adaptation and integrity. *Mamm Genome* 27, 525–537. doi: 10.1007/s00335-016-9659-2

Kadir, R., Harel, T., Markus, B., Perez, Y., Bakhrat, A., Cohen, I., et al. (2016). ALFY-Controlled DVL3 autophagy regulates Wnt signaling, determining human brain size. *PLoS Genet.* 12:e1005919. doi: 10.1371/journal.pgen

Kapoor, N., Niu, J., Saad, Y., Kumar, S., Sirakova, T., Becerra, E., et al. (2015). Transcription factors STAT6 and KLF4 implement macrophage polarization via the dual catalytic powers of MCPIP. *J. Immunol.* 194, 6011–6023. doi: 10.4049/jimmunol.1402797

Kara, N. Z., Toker, L., Agam, G., Anderson, G. W., Belmaker, R. H., and Einat, H. (2013). Trehalose induced antidepressant-like effects and autophagy enhancement in mice. *Psychopharmacology* 229, 367–375. doi: 10.1007/s00213-013-3119-4

Keller, C. W., Sina, C., Kotur, M. B., Ramelli, G., Mundt, S., Quast, I., et al. (2017). ATG-dependent phagocytosis in dendritic cells drives myelin-specific CD4(+) T cell pathogenicity during CNS inflammation. *Proc. Natl. Acad. Sci. U.S.A.* 114, E11228–E11237. doi: 10.1073/pnas.1713664114

Kim, H. J., Cho, M. H., Shim, W. H., Kim, J. K., Jeon, E. Y., Kim, D. H., et al. (2017). Deficient autophagy in microglia impairs synaptic pruning and causes social behavioral defects. *Mol. Psychiatry* 22, 1576–1584. doi: 10.1038/mp.2016.103

Kim, H. S., Montana, V., Jang, H. J., Parpura, V., and Kim, J. A. (2013). Epigallocatechin Gallate (EGCG) stimulates autophagy in vascular endothelial cells A POTENTIAL ROLE FOR REDUCING LIPID ACCUMULATION. *J. Biol. Chem.* 288, 22693–22705. doi: 10.1074/jbc.M113.477505

Kim, K. H., Jeong, Y. T., Oh, H., Kim, S. H., Cho, J. M., Kim, Y. N., et al. (2013). Autophagy deficiency leads to protection from obesity and insulin resistance by inducing Fgf21 as a mitokine. *Nat. Med.* 19, 83–92. doi: 10.1038/nm.3014

Kim, J., Kundu, M., Viollet, B., and Guan, K. L. (2011). AMPK and mTOR regulate autophagy through direct phosphorylation of Ulk1. *Nat. Cell Biol.* 13, 132–141. doi: 10.1038/ncb2152

Kim, M., Sandford, E., Gatica, D., Qiu, Y., Liu, X., Zheng, Y., et al. (2016). Mutation in ATG5 reduces autophagy and leads to ataxia with developmental delay. *eLife* 5:e12245. doi: 10.7554/eLife.12245

Klionsky, D. J. (2007). Autophagy: from phenomenology to molecular understanding in less than a decade. *Nat. Rev. Mol. Cell Biol.* 8, 931–937. doi: 10.1038/nrm2245

Kofler, N. M., Shawber, C. J., Kangsamaksin, T., Reed, H. O., Galatioto, J., and Kitajewski, J. (2011). Notch signaling in developmental and tumor angiogenesis. *Genes Cancer* 2, 1106–1116. doi: 10.1177/1947601911423030

Komatsu, M., Waguri, S., Chiba, T., Murata, S., Iwata, J., Tanida, I., et al. (2006). Loss of autophagy in the central nervous system causes neurodegeneration in mice. *Nature* 441, 880–884. doi: 10.1038/nature04723

Komatsu, M., Waguri, S., Ueno, T., Iwata, J., Murata, S., Tanida, I., et al. (2005). Impairment of starvation-induced and constitutive autophagy in Atg7-deficient mice. *J. Cell Biol.* 169, 425–434. doi: 10.1083/jcb.200412022

Komatsu, M., Wang, Q. J., Holstein, G. R., Friedrich, V. L. Jr., Iwata, J., Kominami, E., et al. (2007). Essential role for autophagy protein Atg7 in the maintenance of axonal homeostasis and the prevention of axonal degeneration. *Proc. Natl. Acad. Sci. U.S.A.* 104, 14489–14494. doi: 10.1073/pnas.0701311104

Kovacs, J. R., Li, C., Yang, Q., Li, G., Garcia, I. G., Ju, S., et al. (2012). Autophagy promotes T-cell survival through degradation of proteins of the cell death machinery. *Cell Death Differ.* 19, 144–152. doi: 10.1038/cdd.2011.78

Kroemer, G., Marino, G., and Levine, B. (2010). Autophagy and the integrated stress response. *Mol. Cell* 40, 280–293. doi: 10.1016/j.molcel.2010.09.023

Kulkarni, A., Chen, J., and Maday, S. (2018). Neuronal autophagy and intercellular regulation of homeostasis in the brain. *Curr. Opin. Neurobiol.* 51, 29–36. doi: 10.1016/j.conb.2018.02.008

Kuma, A., Komatsu, M., and Mizushima, N. (2017). Autophagy-monitoring and autophagy-deficient mice. *Autophagy* 13, 1619–1628. doi: 10.1080/15548627.2017.1343770

Le Duc, D., Giulivi, C., Hiatt, S. M., Napoli, E., Panoutsopoulos, A., Harlan De Crescenzo, A., et al. (2019). Pathogenic WDFY3 variants cause neurodevelopmental disorders and opposing effects on brain size. *Brain* 142, 2617–2630. doi: 10.1093/brain/awz198

Lee, H. K., Mattei, L. M., Steinberg, B. E., Alberts, P., Lee, Y. H., Chervonsky, A., et al. (2010). In vivo requirement for Atg5 in antigen presentation by dendritic cells. *Immunity* 32, 227–239. doi: 10.1016/j.immuni.2009.12.006

Lee, S. J., Kim, H. P., Jin, Y., Choi, A. M. K., and Ryter, S. W. (2011). Beclin 1 deficiency is associated with increased hypoxia-induced angiogenesis. *Autophagy* 7, 829–839. doi: 10.4161/auto.7.8.15598

Li, A., Song, N. J., Riesenberg, B. P., and Li, Z. (2019). The emerging roles of endoplasmic reticulum stress in balancing immunity and tolerance in health and diseases: mechanisms and opportunities. *Fron.t Immunol.* 10:3154. doi: 10.3389/fimmu.2019.03154

Li, C., Capan, E., Zhao, Y., Zhao, J., Stolz, D., Watkins, S. C., et al. (2006). Autophagy is induced in CD4+ T cells and important for the growth factor-withdrawal cell death. *J. Immunol.* 177, 5163–5168. doi: 10.4049/jimmunol.177.8.5163

Li, H., Horke, S., and Forstermann, U. (2013). Oxidative stress in vascular disease and its pharmacological prevention. *Trends Pharmacol. Sci.* 34, 313–319. doi: 10.1016/j.tips.2013.03.007

Li, M., Lu, G., Hu, J., Shen, X., Ju, J., Gao, Y., et al. (2016). EVA1A/TMEM166 regulates embryonic neurogenesis by autophagy. *Stem Cell Rep.* 6, 396–410. doi: 10.1016/j.stemcr.2016.01.011

Liang, C. C., Wang, C., Peng, X., Gan, B., and Guan, J. L. (2010). Neural-specific deletion of FIP200 leads to cerebellar degeneration caused by increased neuronal death and axon degeneration. *J. Biol. Chem.* 285, 3499–3509. doi: 10.1074/jbc.M109.072389

Liang, P., Jiang, B., Li, Y., Liu, Z., Zhang, P., Zhang, M., et al. (2018). Autophagy promotes angiogenesis via AMPK/Akt/mTOR signaling during the recovery of heat-denatured endothelial cells. *Cell Death Dis.* 9:1152. doi: 10.1038/s41419-018-1194-5

Lieberman, O. J., and Sulzer, D. (2020). The synaptic autophagy cycle. *J. Mol. Biol.* 432, 2589–2604. doi: 10.1016/j.jmb.2019.12.028

Lira, V. A., Okutsu, M., Zhang, M., Greene, N. P., Laker, R. C., Breen, D. S., et al. (2013). Autophagy is required for exercise training-induced skeletal muscle adaptation and improvement of physical performance. *FASEB J.* 27, 4184–4193. doi: 10.1096/fj.13-228486

Liu, K., Zhao, E., Ilyas, G., Lalazar, G., Lin, Y., Haseeb, M., et al. (2015). Impaired macrophage autophagy increases the immune response in obese mice by promoting proinflammatory macrophage polarization. *Autophagy* 11, 271–284. doi: 10.1080/15548627.2015.1009787

Lo Verso, F., Carnio, S., Vainshtein, A., and Sandri, M. (2014). Autophagy is not required to sustain exercise and PRKAA1/AMPK activity but is important to prevent mitochondrial damage during physical activity. *Autophagy* 10, 1883–1894. doi: 10.4161/auto.32154

Lu, Q. L., Yao, Y. F., Hu, Z. K., Hu, C. Q., Song, Q. X., Ye, J., et al. (2016). Angiogenic factor AGGF1 activates autophagy with an essential role in therapeutic angiogenesis for heart disease. *PLoS Biol.* 14:e1002529. doi: 10.1371/journal.pbio.1002529

Lu, W. H., Shi, Y. X., Ma, Z. L., Wang, G., Liu, L. X., Chuai, M. L., et al. (2016). Proper autophagy is indispensable for angiogenesis during chick embryo development. *Cell Cycle* 15, 1742–1754. doi: 10.1080/15384101.2016.1184803

Lv, X., Jiang, H., Li, B., Liang, Q., Wang, S., Zhao, Q., et al. (2014). The crucial role of Atg5 in cortical neurogenesis during early brain development. *Sci. Rep.* 4:6010. doi: 10.1038/srep06010

Lyu, Z. S., Cao, X. N., Wen, Q., Mo, X. D., Zhao, H. Y., Chen, Y. H., et al. (2020). Autophagy in endothelial cells regulates their haematopoiesis-supporting ability. *Ebiomedicine* 53:102677. doi: 10.1016/J.Ebiom.2020.102677

Ma, Y., Qi, M., An, Y., Zhang, L. Q., Yang, R., Doro, D. H., et al. (2018). Autophagy controls mesenchymal stem cell properties and senescence during bone aging. *Aging Cell* 17:e12709. doi: 10.1111/acel.12709

Maacha, S., Sidahmed, H., Jacob, S., Gentilcore, G., Calzone, R., Grivel, J. C., et al. (2020). Paracrine mechanisms of mesenchymal stromal cells in angiogenesis. *Stem Cells Int.* 2020:4356359. doi: 10.1155/2020/4356359

Macian, F. (2019). Autophagy in T Cell function and aging. *Front. Cell Dev. Biol.* 7:213. doi: 10.3389/fcell.2019.00213

Maday, S., and Holzbaur, E. L. (2014). Autophagosome biogenesis in primary neurons follows an ordered and spatially regulated pathway. *Dev. Cell* 30, 71–85. doi: 10.1016/j.devcel.2014.06.001

Maes, H., Kuchnio, A., Peric, A., Moens, S., Nys, K., De Bock, K., et al. (2014). Tumor vessel normalization by chloroquine independent of autophagy. *Cancer Cell* 26, 190–206. doi: 10.1016/j.ccr.2014.06.025

Malhotra, R., Warne, J. P., Salas, E., Xu, A. W., and Debnath, J. (2015). Loss of Atg12, but not Atg5, in pro-opiomelanocortin neurons exacerbates diet-induced obesity. *Autophagy* 11, 145–154. doi: 10.1080/15548627.2014.998917

Mammucari, C., Milan, G., Romanello, V., Masiero, E., Rudolf, R., Del Piccolo, P., et al. (2007). FoxO3 controls autophagy in skeletal muscle in vivo. *Cell Metab.* 6, 458–471. doi: 10.1016/j.cmet.2007.11.001

Marcu, R., Choi, Y. J., Xue, J., Fortin, C. L., Wang, Y. L., Nagao, R. J., et al. (2018). Human Organ-Specific Endothelial Cell Heterogeneity. *Iscience* 4, 20–35. doi: 10.1016/j.isci.2018.05.003

Martin, J. D., Seano, G., and Jain, R. K. (2019). Normalizing function of tumor vessels: progress. Opportunities, and Challenges. *Annu. Rev. Physiol.* 81, 505–534. doi: 10.1146/annurev-physiol-020518-114700

Martinez-Martin, N., Maldonado, P., Gasparrini, F., Frederico, B., Aggarwal, S., Gaya, M., et al. (2017). A switch from canonical to noncanonical autophagy shapes B cell responses. *Science* 355, 641–647. doi: 10.1126/science.aal3908

Masiero, E., Agatea, L., Mammucari, C., Blaauw, B., Loro, E., Komatsu, M., et al. (2009). Autophagy is required to maintain muscle mass. *Cell Metab.* 10, 507–515. doi: 10.1016/j.cmet.2009.10.008

Matta, S. K., and Kumar, D. (2015). AKT mediated glycolytic shift regulates autophagy in classically activated macrophages. *Int. J. Biochem. Cell Biol.* 66, 121–133. doi: 10.1016/j.biocel.2015.07.010

McGrath, M. J., Eramo, M. J., Gurung, R., Sriratana, A., Gehrig, S. M., Lynch, G. S., et al. (2020). Defective lysosome reformation during autophagy causes skeletal muscle disease. *J. Clin. Invest.* 135124. doi: 10.1172/JCI135124 [Epub ahead of print].

Mehrpour, M., Esclatine, A., Beau, I., and Codogno, P. (2010). Overview of macroautophagy regulation in mammalian cells. *Cell Res.* 20, 748–762. doi: 10.1038/cr.2010.82

Melendez, A., Talloczy, Z., Seaman, M., Eskelinen, E. L., Hall, D. H., and Levine, B. (2003). Autophagy genes are essential for dauer development and life-span extension in *C-elegans*. *Science* 301, 1387–1391. doi: 10.1126/science.1087782

Mendelson, A., and Frenette, P. S. (2014). Hematopoietic stem cell niche maintenance during homeostasis and regeneration. *Nat. Med.* 20, 833–846. doi: 10.1038/nm.3647

Menzies, F. M., Fleming, A., Caricasole, A., Bento, C. F., Andrews, S. P., Ashkenazi, A., et al. (2017). Autophagy and neurodegeneration: pathogenic mechanisms and therapeutic opportunities. *Neuron* 93, 1015–1034. doi: 10.1016/j.neuron.2017.01.022

Metti, S., Gambarotto, L., Chrisam, M., Baraldo, M., Braghetta, P., Blaauw, B., et al. (2020). The polyphenol pterostilbene ameliorates the myopathic phenotype of collagen VI deficient mice via autophagy induction. *Front. Cell Dev. Biol.* 8:580933. doi: 10.3389/fcell.2020.580933

Miao, C., Lei, M., Hu, W., Han, S., and Wang, Q. (2017). A brief review: the therapeutic potential of bone marrow mesenchymal stem cells in myocardial infarction. *Stem Cell Res. Ther.* 8:242. doi: 10.1186/s13287-017-0697-9

Millecamps, S., and Julien, J. P. (2013). Axonal transport deficits and neurodegenerative diseases. *Nat. Rev. Neurosci.* 14, 161–176. doi: 10.1038/nrn3380

Mizushima, N. (2007). Autophagy: process and function. *Genes Dev.* 21, 2861–2873. doi: 10.1101/gad.1599207

Mizushima, N., and Komatsu, M. (2011). Autophagy: renovation of cells and tissues. *Cell* 147, 728–741. doi: 10.1016/j.cell.2011.10.026

Mizushima, N., and Levine, B. (2010). Autophagy in mammalian development and differentiation. *Nat. Cell Biol.* 12, 823–830. doi: 10.1038/Ncb0910-823

Mizushima, N., Levine, B., Cuervo, A. M., and Klionsky, D. J. (2008). Autophagy fights disease through cellular self-digestion. *Nature* 451, 1069–1075. doi: 10.1038/nature06639

Mizushima, N., Yamamoto, A., Matsui, M., Yoshimori, T., and Ohsumi, Y. (2004). In vivo analysis of autophagy in response to nutrient starvation using transgenic mice expressing a fluorescent autophagosome marker. *Mol. Biol. Cell* 15, 1101–1111. doi: 10.1091/mbc.e03-09-0704

Mofarrahi, M., Guo, Y., Haspel, J. A., Choi, A. M., Davis, E. C., Gouspillou, G., et al. (2013). Autophagic flux and oxidative capacity of skeletal muscles during acute starvation. *Autophagy* 9, 1604–1620. doi: 10.4161/auto.25955

Mortimore, G. E., and Schworer, C. M. (1977). Induction of autophagy by amino-acid deprivation in perfused rat liver. *Nature* 270, 174–176. doi: 10.1038/270174a0

Munz, C. (2009). Enhancing immunity through autophagy. *Annu. Rev. Immunol.* 27, 423–449. doi: 10.1146/annurev.immunol.021908.132537

Murray, P. J., Allen, J. E., Biswas, S. K., Fisher, E. A., Gilroy, D. W., Goerdt, S., et al. (2014). Macrophage activation and polarization: nomenclature and experimental guidelines. *Immunity* 41, 14–20. doi: 10.1016/j.immuni.2014.06.008

Nakahira, K., Haspel, J. A., Rathinam, V. A., Lee, S. J., Dolinay, T., Lam, H. C., et al. (2011). Autophagy proteins regulate innate immune responses by inhibiting the release of mitochondrial DNA mediated by the NALP3 inflammasome. *Nat. Immunol.* 12, 222–230. doi: 10.1038/ni.1980

Napoli, E., Song, G., Panoutsopoulos, A., Riyadh, M. A., Kaushik, G., Halmai, J., et al. (2018). Beyond autophagy: a novel role for autism-linked Wdfy3 in brain mitophagy. *Sci. Rep.* 8:11348. doi: 10.1038/s41598-018-29421-7

Negrete-Hurtado, A., Overhoff, M., Bera, S., De Bruyckere, E., Schatzmuller, K., Kye, M. J., et al. (2020). Autophagy lipidation machinery regulates axonal microtubule dynamics but is dispensable for survival of mammalian neurons. *Nat. Commun.* 11:1535. doi: 10.1038/s41467-020-15287-9

Nemazanyy, I., Blaauw, B., Paolini, C., Caillaud, C., Protasi, F., Mueller, A., et al. (2013). Defects of Vps15 in skeletal muscles lead to autophagic vacuolar myopathy and lysosomal disease. *EMBO Mol. Med.* 5, 870–890. doi: 10.1002/emmm.201202057

Nichenko, A. S., Southern, W. M., Atuan, M., Luan, J., Peissig, K. B., Foltz, S. J., et al. (2016). Mitochondrial maintenance via autophagy contributes to functional skeletal muscle regeneration and remodeling. *Am. J. Physiol. Cell Physiol.* 311, C190–C200. doi: 10.1152/ajpcell.00066.2016

Nishiyama, J., Miura, E., Mizushima, N., Watanabe, M., and Yuzaki, M. (2007). Aberrant membranes and double-membrane structures accumulate in the axons of Atg5-null Purkinje cells before neuronal death. *Autophagy* 3, 591–596. doi: 10.4161/auto.4964

Niven, J., Madelon, N., Page, N., Caruso, A., Harle, G., Lemeille, S., et al. (2019). Macroautophagy in dendritic cells controls the homeostasis and stability of regulatory T Cells. *Cell Rep.* 28, 21.e6–29.e26. doi: 10.1016/j.celrep.2019.05.110

Nixon, R. A., Wegiel, J., Kumar, A., Yu, W. H., Peterhoff, C., Cataldo, A., et al. (2005). Extensive involvement of autophagy in Alzheimer disease: an immuno-electron microscopy study. *J. Neuropathol. Exp. Neurol.* 64, 113–122. doi: 10.1093/jnen/64.2.113

Obba, S., Hizir, Z., Boyer, L., Selimoglu-Buet, D., Pfeifer, A., Michel, G., et al. (2015). The PRKAA1/AMPKalpha1 pathway triggers autophagy during CSF1-induced human monocyte differentiation and is a potential target in CMML. *Autophagy* 11, 1114–1129. doi: 10.1080/15548627.2015.1034406

Ohsumi, Y. (2001). Molecular dissection of autophagy: two ubiquitin-like systems. *Nat. Rev. Mol. Cell Biol.* 2, 211–216. doi: 10.1038/35056522

Okerlund, N. D., Schneider, K., Leal-Ortiz, S., Montenegro-Venegas, C., Kim, S. A., Garner, L. C., et al. (2017). Bassoon controls presynaptic autophagy through Atg5. *Neuron* 93, 897.e7–913.e7. doi: 10.1016/j.neuron.2017.01.026

Omilusik, K. D., and Goldrath, A. W. (2017). The origins of memory T cells. *Nature* 552, 337–339. doi: 10.1038/d41586-017-08280-8

Paludan, C., Schmid, D., Landthaler, M., Vockerodt, M., Kube, D., Tuschl, T., et al. (2005). Endogenous MHC class II processing of a viral nuclear antigen after autophagy. *Science* 307, 593–596. doi: 10.1126/science.1104904

Paolini, A., Omairi, S., Mitchell, R., Vaughan, D., Matsakas, A., Vaiyapuri, S., et al. (2018). Attenuation of autophagy impacts on muscle fibre development, starvation induced stress and fibre regeneration following acute injury. *Sci. Rep.* 8:9062. doi: 10.1038/s41598-018-27429-7

Park, S. K., La Salle, D. T., Cerbie, J., Cho, J. M., Bledsoe, A., Nelson, A., et al. (2019). Elevated arterial shear rate increases indexes of endothelial cell autophagy and nitric oxide synthase activation in humans. *Am. J. Physiol. Heart Circ. Physiol.* 316, H106–H112. doi: 10.1152/ajpheart.00561.2018

Patente, T. A., Pinho, M. P., Oliveira, A. A., Evangelista, G. C. M., Bergami-Santos, P. C., and Barbuto, J. A. M. (2018). Human dendritic cells: their heterogeneity and clinical application potential in cancer immunotherapy. *Front. Immunol.* 9:3176. doi: 10.3389/fimmu.2018.03176

Pengo, N., Scolari, M., Oliva, L., Milan, E., Mainoldi, F., Raimondi, A., et al. (2013). Plasma cells require autophagy for sustainable immunoglobulin production. *Nat. Immunol.* 14, 298–305. doi: 10.1038/ni.2524

Pua, H. H., Dzhagalov, I., Chuck, M., Mizushima, N., and He, Y. W. (2007). A critical role for the autophagy gene Atg5 in T cell survival and proliferation. *J. Exp. Med.* 204, 25–31. doi: 10.1084/jem.20061303

Pua, H. H., Guo, J., Komatsu, M., and He, Y. W. (2009). Autophagy is essential for mitochondrial clearance in mature T lymphocytes. *J. Immunol.* 182, 4046–4055. doi: 10.4049/jimmunol.0801143

Qadura, M., Terenzi, D. C., Verma, S., Al-Omran, M., and Hess, D. A. (2018). Concise review: cell therapy for critical limb ischemia: an integrated review of preclinical and clinical studies. *Stem Cells* 36, 161–171. doi: 10.1002/stem.2751

Raben, N., Hill, V., Shea, L., Takikita, S., Baum, R., Mizushima, N., et al. (2008). Suppression of autophagy in skeletal muscle uncovers the accumulation of ubiquitinated proteins and their potential role in muscle damage in Pompe disease. *Hum. Mol. Genet.* 17, 3897–3908. doi: 10.1093/hmg/ddn292

Ramos, F. J., Chen, S. C., Garelick, M. G., Dai, D. F., Liao, C. Y., Schreiber, K. H., et al. (2012). Rapamycin reverses elevated mTORC1 signaling in lamin A/C-deficient mice, rescues cardiac and skeletal muscle function, and extends survival. *Sci. Transl. Med.* 4:144ra103. doi: 10.1126/scitranslmed.3003802

Rastaldo, R., Vitale, E., and Giachino, C. (2020). Dual role of autophagy in regulation of mesenchymal stem cell senescence. *Front. Cell Dev. Biol.* 8:276. doi: 10.3389/Fcell.2020.00276

Rathmell, J. C. (2012). Metabolism and autophagy in the immune system: immunometabolism comes of age. *Immunol. Rev.* 249, 5–13. doi: 10.1111/j.1600-065X.2012.01158.x

Rodriguez-Pinto, D. (2005). B cells as antigen presenting cells. *Cell Immunol.* 238, 67–75. doi: 10.1016/j.cellimm.2006.02.005

Romanelli, D., Casartelli, M., Cappellozza, S., de Eguileor, M., and Tettamanti, G. (2016). Roles and regulation of autophagy and apoptosis in the remodelling of the lepidopteran midgut epithelium during metamorphosis. *Sci. Rep.* 6:32939. doi: 10.1038/Srep32939

Saccone, V., Palmieri, M., Passamano, L., Piluso, G., Meroni, G., Politano, L., et al. (2008). Mutations that impair interaction properties of TRIM32 associated with limb-girdle muscular dystrophy 2H. *Hum. Mutat.* 29, 240–247. doi: 10.1002/humu.20633

Saera-Vila, A., Kish, P. E., Louie, K. W., Grzegorski, S. J., Klionsky, D. J., and Kahana, A. (2016). Autophagy regulates cytoplasmic remodeling during cell reprogramming in a zebrafish model of muscle regeneration. *Autophagy* 12, 1864–1875. doi: 10.1080/15548627.2016.1207015

Saitoh, T., Fujita, N., Jang, M. H., Uematsu, S., Yang, B. G., Satoh, T., et al. (2008). Loss of the autophagy protein Atg16L1 enhances endotoxin-induced IL-1beta production. *Nature* 456, 264–268. doi: 10.1038/nature07383

Sanjurjo, L., Aran, G., Tellez, E., Amezaga, N., Armengol, C., Lopez, D., et al. (2018). CD5L Promotes M2 macrophage polarization through autophagy-mediated upregulation of ID3. *Front. Immunol.* 9:480. doi: 10.3389/fimmu.2018.00480

Sarkar, S., Floto, R. A., Berger, Z., Imarisio, S., Cordenier, A., Pasco, M., et al. (2005). Lithium induces autophagy by inhibiting inositol monophosphatase. *J. Cell Biol,* 170, 1101–1111. doi: 10.1083/jcb.200504035

Sarparanta, J., Jonson, P. H., Golzio, C., Sandell, S., Luque, H., Screen, M., et al. (2012). Mutations affecting the cytoplasmic functions of the co-chaperone DNAJB6 cause limb-girdle muscular dystrophy. *Nat. Genet.* 44, S451–S452. doi: 10.1038/ng.1103

Sbrana, F. V., Cortini, M., Avnet, S., Perut, F., Columbaro, M., De Milito, A., et al. (2016). The role of autophagy in the maintenance of stemness and differentiation of mesenchymal stem cells. *Stem Cell Rev. Rep.* 12, 621–633. doi: 10.1007/s12015-016-9690-4

Schaaf, M. B., Houbaert, D., Mece, O., and Agostinis, P. (2019). Autophagy in endothelial cells and tumor angiogenesis. *Cell Death Differ.* 26, 665–679. doi: 10.1038/s41418-019-0287-8

Segales, J., Perdiguero, E., Serrano, A. L., Sousa-Victor, P., Ortet, L., Jardi, M., et al. (2020). Sestrin prevents atrophy of disused and aging muscles by integrating anabolic and catabolic signals. *Nat. Commun.* 11:189. doi: 10.1038/s41467-019-13832-9

Simonsen, A., and Tooze, S. A. (2009). Coordination of membrane events during autophagy by multiple class III PI3-kinase complexes. *J. Cell Biol.* 186, 773–782. doi: 10.1083/jcb.200907014

Skobo, T., Benato, F., Grumati, P., Meneghetti, G., Cianfanelli, V., Castagnaro, S., et al. (2014). Zebrafish ambra1a and ambra1b knockdown impairs skeletal muscle development. *PLoS One* 9:e99210. doi: 10.1371/journal.pone.0099210

Smith, J. A. (2018). Regulation of cytokine production by the unfolded protein response. Implications for infection and autoimmunity. *Front. Immunol.* 9:422. doi: 10.3389/fimmu.2018.00422

Son, J. H., Shim, J. H., Kim, K. H., Ha, J. Y., and Han, J. Y. (2012). Neuronal autophagy and neurodegenerative diseases. *Exp. Mol. Med.* 44, 89–98. doi: 10.3858/emm.2012.44.2.031

Song, C., Song, C., and Tong, F. (2014). Autophagy induction is a survival response against oxidative stress in bone marrow-derived mesenchymal stromal cells. *Cytotherapy* 16, 1361–1370. doi: 10.1016/j.jcyt.2014.04.006

Song, K. Y., Guo, X. M., Wang, H. Q., Zhang, L., Huang, S. Y., Huo, Y. C., et al. (2020). MBNL1 reverses the proliferation defect of skeletal muscle satellite cells in myotonic dystrophy type 1 by inhibiting autophagy via the mTOR pathway. *Cell Death Dis.* 11:545. doi: 10.1038/s41419-020-02756-8

Sou, Y. S., Waguri, S., Iwata, J., Ueno, T., Fujimura, T., Hara, T., et al. (2008). The Atg8 conjugation system is indispensable for proper development of autophagic isolation membranes in mice. *Mol. Biol. Cell* 19, 4762–4775. doi: 10.1091/mbc.e08-03-0309

Spampanato, C., Feeney, E., Li, L., Cardone, M., Lim, J. A., Annunziata, F., et al. (2013). Transcription factor EB (TFEB) is a new therapeutic target for Pompe disease. *EMBO Mol. Med.* 5, 691–706. doi: 10.1002/emmm.201202176

Spengler, K., Kryeziu, N., Grosse, S., Mosig, A. S., and Heller, R. (2020). VEGF triggers transient induction of autophagy in endothelial cells via AMPK alpha 1. *Cells* 9:687. doi: 10.3390/Cells9030687

Sprott, D., Poitz, D. M., Korovina, I., Ziogas, A., Phieler, J., Chatzigeorgiou, A., et al. (2019). Endothelial-specific deficiency of ATG5 (Autophagy Protein 5) attenuates ischemia-related angiogenesis. *Arteriosc. Thromb. Vasc. Biol.* 39, 1137–1148. doi: 10.1161/ATVBAHA.119.309973

Sweeney, M., and Foldes, G. (2018). It takes two: endothelial-perivascular cell cross-talk in vascular development and disease. *Front. Cardiovasc. Med.* 5:154. doi: 10.3389/fcvm.2018.00154

Tang, A. H., and Rando, T. A. (2014). Induction of autophagy supports the bioenergetic demands of quiescent muscle stem cell activation. *EMBO J.* 33, 2782–2797. doi: 10.15252/embj.201488278

Tang, G., Gudsnuk, K., Kuo, S. H., Cotrina, M. L., Rosoklija, G., Sosunov, A., et al. (2014). Loss of mTOR-dependent macroautophagy causes autistic-like synaptic pruning deficits. *Neuron* 83, 1131–1143. doi: 10.1016/j.neuron.2014.0

Torisu, K., Singh, K. K., Torisu, T., Lovren, F., Liu, J., Pan, Y., et al. (2016). Intact endothelial autophagy is required to maintain vascular lipid homeostasis. *Aging Cell* 15, 187–191. doi: 10.1111/acel.12423

Tsukada, M., and Ohsumi, Y. (1993). Isolation and characterization of autophagy-defective mutants of saccharomyces-cerevisiae. *Febs Lett.* 333, 169–174. doi: 10.1016/0014-5793(93)80398-E

Valecka, J., Almeida, C. R., Su, B., Pierre, P., and Gatti, E. (2018). Autophagy and MHC-restricted antigen presentation. *Mol. Immunol.* 99, 163–170. doi: 10.1016/j.molimm.2018.05.009

Vanhauwaert, R., Kuenen, S., Masius, R., Bademosi, A., Manetsberger, J., Schoovaerts, N., et al. (2017). The SAC1 domain in synaptojanin is required for autophagosome maturation at presynaptic terminals. *EMBO J.* 36, 1392–1411. doi: 10.15252/embj.201695773

Vergadi, E., Ieronymaki, E., Lyroni, K., Vaporidi, K., and Tsatsanis, C. (2017). akt signaling pathway in macrophage activation and M1/M2 polarization. *J. Immunol.* 198, 1006–1014. doi: 10.4049/jimmunol.1601515

Vignali, D. A., Collison, L. W., and Workman, C. J. (2008). How regulatory T cells work. *Nat. Rev. Immunol.* 8, 523–532. doi: 10.1038/nri2343

Vion, A. C., Kheloufi, M., Hammoutene, A., Poisson, J., Lasselin, J., Devue, C., et al. (2017). Autophagy is required for endothelial cell alignment and atheroprotection under physiological blood flow. *Proc. Natl. Acad. Sci. U.S.A.* 114, E8675–E8684. doi: 10.1073/pnas.1702223114

Wei, J., Long, L., Yang, K., Guy, C., Shrestha, S., Chen, Z., et al. (2016). Autophagy enforces functional integrity of regulatory T cells by coupling environmental cues and metabolic homeostasis. *Nat. Immunol.* 17, 277–285. doi: 10.1038/ni.3365

Wen, Y. T., Zhang, J. R., Kapupara, K., and Tsai, R. K. (2019). mTORC2 activation protects retinal ganglion cells via Akt signaling after autophagy induction in traumatic optic nerve injury. *Exp. Mol. Med.* 51, 1–11. doi: 10.1038/s12276-019-0298-z

Willinger, T., and Flavell, R. A. (2012). Canonical autophagy dependent on the class III phosphoinositide-3 kinase Vps34 is required for naive T-cell homeostasis. *Proc. Natl. Acad. Sci. U.S.A.* 109, 8670–8675. doi: 10.1073/pnas.1205305109

Wu, X., Fleming, A., Ricketts, T., Pavel, M., Virgin, H., Menzies, F. M., et al. (2016). Autophagy regulates Notch degradation and modulates stem cell development and neurogenesis. *Nat. Commun.* 7:10533. doi: 10.1038/ncomms10533

Wu, X., Won, H., and Rubinsztein, D. C. (2013). Autophagy and mammalian development. *Biochem. Soc. Trans,* 41, 1489–1494. doi: 10.1042/BST20130185

Yamamoto, A., and Yue, Z. (2014). Autophagy and its normal and pathogenic states in the brain. *Annu. Rev. Neurosci.* 37, 55–78. doi: 10.1146/annurev-neuro-071013-014149

Yan, Y., and Finkel, T. (2017). Autophagy as a regulator of cardiovascular redox homeostasis. *Free Radic. Biol. Med.* 109, 108–113. doi: 10.1016/j.freeradbiomed.2016.12.003

Yoshii, S. R., Kuma, A., Akashi, T., Hara, T., Yamamoto, A., Kurikawa, Y., et al. (2016). Systemic analysis of Atg5-null mice rescued from neonatal lethality by transgenic ATG5 expression in neurons. *Dev. Cell* 39, 116–130. doi: 10.1016/j.devcel.2016.09.001

Zecchini, S., Giovarelli, M., Perrotta, C., Morisi, F., Touvier, T., Di Renzo, I., et al. (2019). Autophagy controls neonatal myogenesis by regulating the GH-IGF1 system through a NFE2L2- and DDIT3-mediated mechanism. *Autophagy* 15, 58–77. doi: 10.1080/15548627.2018.1507439

Zeng, N., D'Souza, R. F., Mitchell, C. J., and Cameron-Smith, D. (2018). Sestrins are differentially expressed with age in the skeletal muscle of men: a cross-sectional analysis. *Exp. Gerontol.* 110, 23–34. doi: 10.1016/j.exger.2018.05.006

Zhang, D. Y., Chen, Y. F., Xu, X. B., Xiang, H. Y., Shi, Y. Z., Gao, Y., et al. (2020). Autophagy inhibits the mesenchymal stem cell aging induced by D-galactose through ROS/JNK/p38 signalling. *Clin. Exp. Pharmacol. Physiol.* 47, 466–477. doi: 10.1111/1440-1681.13207

Zhang, J., Chen, L., Xiong, F., Zhang, S., Huang, K., Zhang, Z., et al. (2019). Autophagy in regulatory T cells: a double-edged sword in disease settings. *Mol. Immunol.* 109, 43–50. doi: 10.1016/j.molimm.2019.02.004

Zhang, Q., Yang, Y. J., Wang, H., Dong, Q. T., Wang, T. J., Qian, H. Y., et al. (2012). Autophagy activation: a novel mechanism of atorvastatin to protect mesenchymal stem cells from hypoxia and serum deprivation via AMP-activated protein kinase/mammalian target of rapamycin pathway. *Stem Cells Dev.* 21, 1321–1332. doi: 10.1089/scd.2011.0684

Zhang, Y., Morgan, M. J., Chen, K., Choksi, S., and Liu, Z. G. (2012). Induction of autophagy is essential for monocyte-macrophage differentiation. *Blood* 119, 2895–2905. doi: 10.1182/blood-2011-08-372383

Zhao, X. C., Nedvetsky, P., Stanchi, F., Vion, A. C., Popp, O., Zuhlke, K., et al. (2019). Endothelial PKA activity regulates angiogenesis by limiting autophagy through phosphorylation of ATG16L1. *eLife* 8:e46380. doi: 10.7554/eLife.46380

Zhuang, S. F., Liu, D. X., Wang, H. J., Zhang, S. H., Wei, J. Y., Fang, W. G., et al. (2017). Atg7 regulates brain angiogenesis via NF-kappaB-Dependent IL-6 production. *Int. J. Mol. Sci.s* 18:968. doi: 10.3390/ijms18050968

Conflict of Interest: The authors declare that the research was conducted in the absence of any commercial or financial relationships that could be construed as a potential conflict of interest.

frontiers in Cell and Developmental Biology

MINI REVIEW
published: 07 January 2021
doi: 10.3389/fcell.2020.599048

ATM Kinase-Dependent Regulation of Autophagy: A Key Player in Senescence?

Venturina Stagni[1,2], Alessandra Ferri[2,3], Claudia Cirotti[2,3] and Daniela Barilà[2,3]**

[1] Institute of Molecular Biology and Pathology, National Research Council (CNR), Rome, Italy, [2] Laboratory of Cell Signaling, Istituto di Ricovero e Cura a Carattere Scientifico (IRCCS) Fondazione Santa Lucia, Rome, Italy, [3] Department of Biology, University of Rome Tor Vergata, Rome, Italy

Increasing evidence suggests a strong interplay between autophagy and genomic stability. Recently, several papers have demonstrated a molecular connection between the DNA Damage Response (DDR) and autophagy and have explored how this link influences cell fate and the choice between apoptosis and senescence in response to different stimuli. The aberrant deregulation of this interplay is linked to the development of pathologies, including cancer and neurodegeneration. Ataxia-telangiectasia mutated kinase (ATM) is the product of a gene that is lost in Ataxia-Telangiectasia (A-T), a rare genetic disorder characterized by ataxia and cerebellar neurodegeneration, defects in the immune response, higher incidence of lymphoma development, and premature aging. Importantly, ATM kinase plays a central role in the DDR, and it can finely tune the balance between senescence and apoptosis: activated ATM promotes autophagy and in particular sustains the lysosomal-mitochondrial axis, which in turn promotes senescence and inhibits apoptosis. Therefore, ATM is the key factor that enables cells to escape apoptosis by entering senescence through modulation of autophagy. Importantly, unlike apoptotic cells, senescent cells are viable and have the ability to secrete proinflammatory and mitogenic factors, thus influencing the cellular environment. In this review we aim to summarize recent advances in the understanding of molecular mechanisms linking DDR and autophagy to senescence, pointing out the role of ATM kinase in these cellular responses. The significance of this regulation in the pathogenesis of Ataxia-Telangiectasia will be discussed.

Keywords: ATM kinase, autophagy, senescence, ataxia-telangiectasia, DDR

OPEN ACCESS

Edited by:
Lucia Latella,
Institute of Traslational Pharmacology, Italian National Research Council, Italy

Reviewed by:
Ella L. Kim,
Johannes Gutenberg University Mainz, Germany
Shaochun Yuan,
Sun Yat-sen University, China

****Correspondence:***
Venturina Stagni
venturina.stagni@cnr.it
Daniela Barilà
daniela.barila@uniroma2.it

Specialty section:
This article was submitted to Cell Death and Survival, a section of the journal Frontiers in Cell and Developmental Biology

Received: *26 August 2020*
Accepted: *24 November 2020*
Published: *07 January 2021*

Citation:
Stagni V, Ferri A, Cirotti C and Barilà D (2021) ATM Kinase-Dependent Regulation of Autophagy: A Key Player in Senescence? Front. Cell Dev. Biol. 8:599048. doi: 10.3389/fcell.2020.599048

INTRODUCTION

Autophagy is a highly conserved catabolic pathway necessary for the maintenance of cellular homeostasis (Rubinsztein et al., 2011). Physiologically, autophagy acts as a quality control pathway that eliminates damaged proteins and organelles. Instead, under stress conditions, it could induce a programmed cell death called "autophagy-dependent cell death" (ADCD) (Rubinsztein et al., 2011). Among autophagic pathways, selective mitochondrial degradation (mitophagy) and selective peroxisome degradation (pexophagy), have emerged as important homeostatic mechanisms (Wang and Wang, 2019). Overall, the autophagic pathway deregulation appears to be related

to many biologic processes as cancer, cardiovascular diseases, aging, and neurodegeneration, (Levine and Kroemer, 2008).

DNA damage response (DDR) is another essential pathway in the control of cellular homeostasis (Jackson and Bartek, 2009). In response to DNA damage, cells activate a highly conserved and complex kinase-based signaling network, to safeguard genomic integrity (Jackson and Bartek, 2009). The DDR pathway consists of a series of tightly regulated events, starting from the detection of DNA damage, accumulation of DNA repair factors at the site of damage, and finally physical repair of the lesion. When DNA repair is unsuccessful, the same DDR network that directs repair can induce senescence or cell death (d'Adda di Fagagna, 2008; Ribezzo et al., 2016). Deficiency of the DDR pathway underlies many human diseases, including developmental disorders, neurodegeneration, cancer, and immune disorders. Moreover, pharmacological inhibition of DDR is often used in cancer treatment (Helleday et al., 2008).

Accumulating evidence has demonstrated a strong connection between autophagy and DDR in the maintenance of cellular homeostasis (Eliopoulos et al., 2016). Autophagy acts as a source of energy during cell cycle arrest and during repair mechanisms, under DNA damage conditions (Eliopoulos et al., 2016). On the other hand, alterations in autophagy can enhance DNA damage and can promote the onset of neurodegenerative disorders as well as tumor development, highlighting the importance of the crosstalk between autophagy and DDR pathways in the maintenance of genomic stability (Eliopoulos et al., 2016). In particular, activation of autophagy during DDR seems to play an essential role in the outcome of senescence, disfavoring the apoptotic response (Herranz and Gil, 2018). Conversely, autophagy defects are linked to alteration of DDR, in particular in senescence response (Hewitt and Korolchuk, 2017).

Ataxia-telangiectasia mutated (ATM) protein, a 350 kDa evolutionarily conserved serine/threonine protein kinase, was first identified as a central player in the DDR pathway (Shiloh and Ziv, 2013). Now it is well known that ATM kinase is activated also by several stimuli different from DNA damage such as reactive oxygen species (ROS), reactive nitrogen species (RNS), and starvation (Shiloh, 2014). Consistently, recent evidence demonstrates critical cytoplasmic functions of ATM, in addition to the classical functions in the nucleus in response to DDR (Ditch and Paull, 2012). In the cytoplasm, ATM has been shown to be located in peroxisomes, mitochondria, and endosomes, and it participates in sensing oxidative stress and in regulating cell metabolism and autophagy (Lee and Paull, 2020). Consistently, among DDR kinases, the ATM protein kinase has a unique, intriguing connection to autophagy (Stagni et al., 2018; Liang et al., 2019). ATM regulates autophagy not only upon DDR induction but also in ROS-induced autophagy, mitophagy, and pexophagy (Stagni et al., 2018). Interestingly, accumulating evidence shows that ATM regulates cellular homeostasis upon DDR and ROS induction through the autophagy-senescence axis (Liang et al., 2019).

Here, we focus on the link between DDR and senescence, pointing out the role of ATM kinase in the modulation of autophagy as a bridging point between these cellular responses. The significance of the deregulation of this equilibrium in the pathogenesis of Ataxia Telangiectasia will also be discussed.

CROSSTALK BETWEEN DDR AND AUTOPHAGY

As described above, it is well documented that autophagy is induced by DNA damage, and it is required for several functional outcomes of the DDR, such as DNA repair, senescence, and cytokine secretion (Hewitt and Korolchuk, 2017). On the other hand, alterations of autophagy have been shown to increase DNA damage and to promote cancer and neurodegenerative disease occurrence (Hewitt and Korolchuk, 2017).

On the molecular level, it is well demonstrated that the DDR can trigger a rapid early induction of autophagy mediated by posttranslational modifications (PTMs), such as phosphorylation, ubiquitination, and acetylation (McEwan and Dikic, 2011). Interestingly, recent papers also report a slower, later induction of autophagy by DDR, mediated by transcriptional or posttranscriptional programs (Chen et al., 2020).

The first molecular player to be discovered between the DDR and autophagy was p53 (White, 2016). p53 is a well-known actor in the DDR pathway, and its role in this pathway has been largely reviewed elsewhere (Shiloh and Ziv, 2013), so it will not be discussed in this review. Recently, it has been discovered that p53 has a dual function in the control of autophagy: it can either activate or repress autophagy (White, 2016), depending on p53's subcellular localization (Maiuri et al., 2010). Nuclear p53 can induce autophagy through the inhibition of mTOR by transcriptional upregulation of targets such as AMPK, PTEN, and Sestrins (Tang et al., 2015). Conversely, cytoplasmic p53 may inhibit autophagy through activation of AMP-dependent kinase (AMPK) and the consequent activation of mTOR independently of its transcriptional activity (Tasdemir et al., 2008a,b). Autophagy, in turn, represses p53 levels and function, significantly promoting tumorigenesis (White et al., 2015). For example, in a mouse model of hereditary breast cancer, allelic loss of *Atg6/Beclin1* extends mouse survival and suppresses tumor development, only when p53 is functional (Huo et al., 2013).

Another important player of the DDR that is also strongly involved in autophagy regulation is ATM kinase. Activation of ATM after exposure to genotoxic and oxidizing agents causes the repression of mTORC1 and the subsequent induction of autophagy (Alexander et al., 2010a,b). Moreover, upon DNA damage, ATM phosphorylates PTEN, promoting its nuclear localization and inducing autophagy as well (Chen et al., 2015). In addition, ATM sustains autophagy in breast cancer stem cells as it can promote the expression of ATG4C mRNA and protein (Antonelli et al., 2017). Consistent with the positive role of ATM on autophagy induction, ATM phosphorylates CHK2 and promotes FOXK nuclear export, following DNA damage, as has been recently demonstrated. In the process, phosphorylation prevents the inhibitory effect of ATM on the expression of autophagic genes and provides

a novel mechanism that activates transcription of ATGs (Chen et al., 2020).

Interestingly, it has been demonstrated that the activation of ATM in the cytosol plays an essential role in the regulation of the autophagic response as well (Stagni et al., 2018). ATM is activated in the cytosol by ROS and hypoxia and can modulate autophagy through multiple molecular mechanisms. For example, in hypoxic conditions ATM inhibits mTORC1 by the regulation of the hypoxia-inducible factor (HIF-1α) transcription factor (Cam et al., 2010), while in response to ROS ATM can regulate pexophagy, through the phosphorylation of Pex5 (Zhang et al., 2015), and mitophagy through the modulation of Beclin-1 (Valentin-Vega et al., 2012; Guo et al., 2020). Overall, this evidence suggests that cytosolic functions of ATM are more related to autophagy regulation than to the canonical nuclear role, but how the balance between nuclear and cytosolic ATM functions is regulated is still unknown.

While the regulation of autophagy by DDR proteins is well documented, the molecular mechanisms behind the regulation of DDR protein functions by autophagy still remain a matter of debate (Eliopoulos et al., 2016). Some evidence suggests that autophagy inhibits the DDR by eliminating misfolded protein and damaged organelles (like mitochondria and peroxisome) that could trigger DNA damage, genome instability, and metabolic stress (Eliopoulos et al., 2016). Consistently, autophagy-deficient cells accumulate ROS and mitochondrial dysfunction together with DNA replication stress (Gomes et al., 2017). Moreover, defective autophagy sensitizes cells to metabolic stress and increases DNA damage (Rabinowitz and White, 2010; Gomes et al., 2017). At the molecular level it has been shown that loss of autophagy increases proteasomal activity resulting in an enhanced degradation of checkpoint kinase 1 (CHK1), a key enzyme for homologous recombination (HR) and increased micronuclei and sub-G1 DNA, markers of diminished genomic integrity (Liu et al., 2015). In addition, autophagy impairment-dependent accumulation of p62 promotes a direct binding of p62 to DDR proteins to inhibit the recruitment of the DNA repair proteins (Wang et al., 2016). Although the detailed molecular mechanism involved in autophagy-dependent regulation of DDR proteins is still largely unknown, a strong crosstalk occurs between DDR signaling and autophagy in the regulation of cellular homeostasis.

THE AUTOPHAGY-SENESCENCE CONNECTION IN THE DDR: ROLE OF ATM KINASE

The link between the DDR and senescence was first associated with replication exhaustion at the end of the cellular lifespan, a process called replicative senescence (d'Adda di Fagagna, 2008; Rossiello et al., 2014). Telomere shortening is sensed by the cells as a double strand of DNA breaks and thereby triggers the activation of the ATM-p53 axis to elicit cell-cycle arrest and to execute senescence. The same link was identified also during persistent oncogenic signaling that triggers a powerful senescence response, known as oncogene-induced senescence (OIS) (Herranz and Gil, 2018). Enforced DNA replication induced by oncogene activation results in DDR and ATM kinase activation followed by activation of senescence, which must be considered a barrier to transformation (Liu et al., 2018). Interestingly, persistent DDR signaling mediated by ATM activation has been reported to contribute also to the acquisition of a proinflammatory senescence-associated secretory phenotype (SASP). It has been recently demonstrated in a model of naturally aged mice that activation of the ATM-NEMO-NF-κB axis is necessary for senescence induction and SASP, which in turn elicits DDR and SASP activation also in neighboring cells, thereby creating a proinflammatory environment (Zhao et al., 2020). Genetic or pharmacological inhibition of ATM reduces the adverse effects of chronic DNA damage, impinging on cellular senescence, improving stem cell functionality and extending health span. Consistently, by using high-throughput screening (HTS), the ATM inhibitor KU-60019 has been identified as an inhibitor of senescence in normal aging cells, which shows the importance of ATM kinase as an essential modulator of senescence (Kang et al., 2017; Kuk et al., 2019).

It is clear that ATM kinase plays a central role in connecting DDR to autophagy and DDR to senescence response, but whether autophagy is connected to senescence through ATM kinase is still debated. It has been demonstrated that the ATM-autophagy axis is responsible for the induction of senescence and the protection of cells against apoptosis upon DDR induction by anti-cancer drugs (Beauvarlet et al., 2019). Indeed, ATM activation upon G-quadruplex ligands (G4L) treatment drives cells to senescence to prevent cell death through activation of the autophagic pathway, pointing out the importance of ATM kinase as a modulator of senescence response through the regulation of autophagy (Beauvarlet et al., 2019). Consistently, disruption of either ATM or autophagy following G4L treatment impairs the induction of senescence and drives cells to apoptotic cell death (Beauvarlet et al., 2019).

Conversely, ATM was demonstrated to promote the acquisition of a senescent-associated secretory phenotype, SASP, by inhibiting the selective autophagy of the transcription factor GATA4 (Kang et al., 2015). Therefore, ATM could promote cell senescence through activation or inhibition of autophagy, probably depending on the cell type and on upstream stimuli (**Figure 1**).

Interestingly, another point of complexity in this regulation is that ATM kinase is essential for the regulation of autophagy not only upon DDR but also upon oxidative stress, as described above. The intracellular accumulation of oxidative damage triggered by ROS is considered a major determinant of senescence (Chandrasekaran et al., 2017). Recently it has been reported that ATM could be necessary in ROS-dependent senescence response induced by inhibitors of Vascular Endothelial Growth Factor (Mongiardi et al., 2019). Interestingly, autophagy is essential for the regulation of senescence upon ROS induction (Cordani et al., 2019). High ROS levels induce mitochondrial dysfunction and autophagy inhibition, which in turn promote cell senescence and generate vicious loop cycles in ROS production (Cordani et al., 2019). Given the central role of ATM in autophagy regulation upon ROS induction we

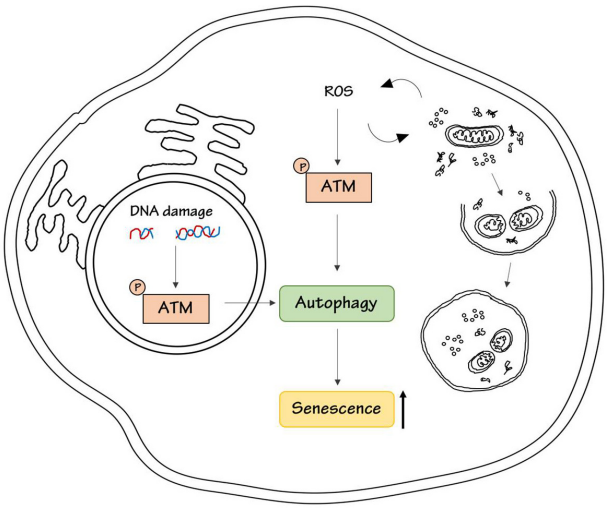

FIGURE 1 | ATM kinase induces senescence. DNA damage or ROS stimulation activates ATM kinase respectively in the nucleus, to repair DNA damage, and in the cytoplasm, to maintain intracellular homeostasis by promoting the removal of damaged proteins and organelles. Both nuclear and cytoplasmic ATM has been shown to be involved in the regulation of autophagy either in a positive or negative way. ATM-dependent autophagy results in senescence induction.

could speculate that this ATM-autophagy axis could regulate senescence response also upon oxidative stress, but there is still no experimental evidence about this possible connection.

In conclusion, ATM kinase could link DNA damage and oxidative stress to autophagy, and this could be responsible for the senescence outcome (**Figure 1**).

CONCLUSION

Ataxia-telangiectasia mutated is functionally inactivated in a genetic rare disorder called Ataxia-telangiectasia (A-T) (OMIM:208900). As we discussed above, it is clear that ATM kinase, by regulating autophagy, plays a central role in the induction of senescence and the suppression of apoptosis, both upon DNA damage and oxidative stress. What is the role of these pathways and of senescence in the development of the A-T pathology?

Ataxia-Telangiectasia (A-T) is an autosomal recessive disorder characterized by cancer susceptibility, radiation sensitivity, cerebellar degeneration, and telangiectasia (Shiloh and Ziv, 2013). Importantly, neurodegeneration and immune system defects in A-T have been regarded as a reflection of premature aging observed in A-T patients [reviewed in Shiloh and Lederman (2017)]. Evidence is growing that senescent cells accumulate during aging, promote chronic inflammation, and are associated with many age-related pathologies, including cancer and neurodegenerative disorders. Despite the fact that ATM kinase has been shown to promote senescence, the loss of ATM expression in A-T cells triggers a senescent-like phenotype as well (**Table 1**), including decreased replication

TABLE 1 | Summary of the key characteristics of senescent cells in A-T.

Senescent phenotype in A-T	References
Decreased replication	Shiloh et al., 1982; Metcalfe et al., 1996; Xia et al., 1996; Smilenov et al., 1997; Wood et al., 2001; Naka et al., 2004; Shiloh and Lederman, 2017
Telomeres shortening	Shiloh et al., 1982; Metcalfe et al., 1996; Xia et al., 1996; Smilenov et al., 1997; Wood et al., 2001; Naka et al., 2004; Shiloh and Lederman, 2017
Increased IL-6, IL-8	McGrath-Morrow et al., 2016
Elevated Type-I interferon levels	McGrath-Morrow et al., 2018
Chronic inflammation	Zaki-Dizaji et al., 2018
SASP phenotype	Gatei et al., 2001; Stern et al., 2002; Weizman et al., 2003; Rashi-Elkeles et al., 2006.

capacity and shortening telomeres, as reported by several studies (Shiloh et al., 1982; Metcalfe et al., 1996; Xia et al., 1996; Smilenov et al., 1997; Wood et al., 2001; Naka et al., 2004; Shiloh and Lederman, 2017). In addition, A-T patients show increased levels of cytokines including IL-6 and IL-8 (McGrath-Morrow et al., 2016), elevated levels of Type I interferons (McGrath-Morrow et al., 2018), and chronic inflammation (Zaki-Dizaji et al., 2018). More recently, the upregulation of several genes associated with senescence and malignancy in A-T cells has been reported (McGrath-Morrow et al., 2020), consistently with the SASP phenotype and with premature senescence in A-T (Gatei et al., 2001; Stern et al., 2002; Weizman et al., 2003; Rashi-Elkeles et al., 2006; Shiloh and Lederman, 2017; **Table 1**). Interestingly, anti-inflammatory agents, such as betamethasone, can generate short-term improvement in A-T symptoms (Leuzzi et al., 2015; Hui et al., 2018).

Why do A-T cells show a senescent phenotype? The apparent paradox between the role of ATM in the promotion of senescence and the senescent phenotype of A-T cells may be explained by the central role of ATM in the maintenance of cellular homeostasis upon different stress induction, as previously outlined.

The senescent phenotype could be explained in part by the fact that ATM-deficient tissues and cultured cells exhibit signs of chronic stress and low-level DDR that could contribute to SASP and senescence (Shiloh and Lederman, 2017; Sunderland et al., 2020). In addition, although A-T is considered a genome instability or DNA damage response syndrome and ATM is predominantly present in the nucleus of most mammalian cells, where it acts as an essential regulator of the DDR (Shiloh, 2014); several studies also supported the presence of ATM in the cytoplasmic compartment, including cytoplasmic vesicles, mitochondria, and peroxisomes, where ATM acts as a major regulator of proteostasis upon its oxidative stress-dependent cytosolic activation (Ditch and Paull, 2012; Lee and Paull, 2020). Given the role of ATM in the regulation of autophagy upon ROS induction (Stagni et al., 2018), we could hypothesize that not only persistent DNA damage, but also high ROS in A-T cells could contribute to premature senescence. The loss of ATM expression in A-T, resulting in an aberrant response to stress, dramatically

breaks the ATM-autophagy axis and therefore unbalances this equilibrium, causing an accumulation of ROS, DNA damage, and senescence. These features may contribute to the overall loss of proteostasis and homeostasis control associated to this disorder (Lee and Paull, 2020).

The investigation of the molecular interconnection between ATM-autophagy and senescence will therefore support the comprehension of A-T pathogenesis and may also contribute to identify novel strategies to ameliorate patient's management.

AUTHOR CONTRIBUTIONS

VS and DB: conceptualization. VS: writing – original draft preparation. DB, VS, AF, and CC: writing – review and editing. DB and VS: supervision. DB: funding acquisition. All authors have read and agreed to the published version of the manuscript.

FUNDING

This research was funded by the Associazione Italiana per la Ricerca sul Cancro (AIRC)-IG2016- n.19069, MIUR-JPI-HDHL-NUTRICOG-MiTyrAge, PRIN_2015LZE9944_005, and the Italian Ministry of Health, RF-2016-02362022 to DB. AF is supported by the Ph.D. program in Molecular and Cellular Biology, University of Rome Tor Vergata. CC is supported by FIRC-AIRC fellowship for Italy "Filomena Todini." The study was supported for VS by a research grant from Italian Ministry of Health RF-2016-02363460.

ACKNOWLEDGMENTS

We acknowledge all our laboratory members for critical reading of the manuscript.

REFERENCES

Alexander, A., Cai, S. L., Kim, J., Nanez, A., Sahin, M., MacLean, K. H., et al. (2010a). ATM signals to TSC2 in the cytoplasm to regulate mTORC1 in response to ROS. *Proc. Natl. Acad. Sci. U.S.A.* 107, 4153–4158. doi: 10.1073/pnas.0913860107

Alexander, A., Kim, J., and Walker, C. L. (2010b). ATM engages the TSC2/mTORC1 signaling node to regulate autophagy. *Autophagy* 6, 672–673. doi: 10.4161/auto.6.5.12509

Antonelli, M., Strappazzon, F., Arisi, I., Brandi, R., D'Onofrio, M., Sambucci, M., et al. (2017). ATM kinase sustains breast cancer stem-like cells by promoting ATG4C expression and autophagy. *Oncotarget* 8, 21692–21709. doi: 10.18632/oncotarget.15537

Beauvarlet, J., Mergny, J. L., and Djavaheri-Mergny, M. (2019). Activation of the Ataxia Telangiectasia Mutated/Autophagy pathway by a G-quadruplex ligand links senescence with apoptosis. *Mol. Cell Oncol.* 6:1604047. doi: 10.1080/23723556.2019.1604047

Cam, H., Easton, J. B., High, A., and Houghton, P. J. (2010). mTORC1 signaling under hypoxic conditions is controlled by ATM-dependent phosphorylation of HIF-1α. *Mol. Cell* 40, 509–520. doi: 10.1016/j.molcel.2010.10.030

Chandrasekaran, A., Idelchik, M. D. P. S., and Melendez, J. A. (2017). Redox control of senescence and age-related disease. *Redox Biol.* 11, 91–102. doi: 10.1016/j.redox.2016.11.005

Chen, J. H., Zhang, P., Chen, W. D., Li, D. D., Wu, X. Q., Deng, R., et al. (2015). ATM-mediated PTEN phosphorylation promotes PTEN nuclear translocation and autophagy in response to DNA-damaging agents in cancer cells. *Autophagy* 11, 239–252. doi: 10.1080/15548627.2015.1009767

Chen, Y., Wu, J., Liang, G., Geng, G., Zhao, F., Yin, P., et al. (2020). CHK2-FOXK axis promotes transcriptional control of autophagy programs. *Sci. Adv.* 6:eaax5819. doi: 10.1126/sciadv.aax5819

Cordani, M., Donadelli, M., Strippoli, R., Bazhin, A. V., and ánchez-Álvarez, M. S. (2019). Interplay between ROS and autophagy in cancer and aging: from molecular mechanisms to novel therapeutic approaches. *Oxid. Med. Cell. Longev.* 2019:8794612.

d'Adda di Fagagna, F. (2008). Living on a break: cellular senescence as a DNA-damage response. *Nat. Rev. Cancer* 8, 512–522. doi: 10.1038/nrc2440

Ditch, S., and Paull, T. T. (2012). The ATM protein kinase and cellular redox signaling: beyond the DNA damage response. *Trends Biochem. Sci.* 37, 15–22. doi: 10.1016/j.tibs.2011.10.002

Eliopoulos, A. G., Havaki, S., and Gorgoulis, V. G. (2016). DNA damage response and autophagy: a meaningful partnership. *Front. Genet.* 7:204. doi: 10.3389/fgene.2016.00204

Gatei, M., Shkedy, D., Khanna, K. K., Uziel, T., Shiloh, Y., Pandita, T. K., et al. (2001). Ataxia-telangiectasia: chronic activation of damage-responsive functions is reduced by alpha-lipoic acid. *Oncogene* 20, 289–294. doi: 10.1038/sj.onc.1204111

Gomes, L. R., Menck, C. F. M., and Leandro, G. S. (2017). Autophagy roles in the modulation of DNA repair pathways. *Int. J. Mol. Sci.* 18:2351. doi: 10.3390/ijms18112351

Guo, Q. Q., Wang, S. S., Zhang, S. S., Xu, H. D., Li, X. M., Guan, Y., et al. (2020). ATM-CHK2-Beclin 1 axis promotes autophagy to maintain ROS homeostasis under oxidative stress. *EMBO J.* 39:e103111.

Helleday, T., Petermann, E., Lundin, C., Hodgson, B., and Sharma, R. A. (2008). DNA repair pathways as targets for cancer therapy. *Nat. Rev. Cancer* 8, 193–204. doi: 10.1038/nrc2342

Herranz, N., and Gil, J. (2018). Mechanisms and functions of cellular senescence. *J. Clin. Invest.* 128, 1238–1246. doi: 10.1172/jci95148

Hewitt, G., and Korolchuk, V. I. (2017). Repair. reuse, recycle: the expanding role of autophagy in genome maintenance. *Trends Cell. Biol.* 27, 340–351. doi: 10.1016/j.tcb.2016.11.011

Hui, C. W., Song, X., Ma, F., Shen, X., and Herrup, K. (2018). Ibuprofen prevents progression of ataxia telangiectasia symptoms in ATM-deficient mice. *J. Neuroinflammation* 15:308.

Huo, Y., Cai, H., Teplova, I., Bowman-Colin, C., Chen, G., Price, S., et al. (2013). Autophagy opposes p53-mediated tumor barrier to facilitate tumorigenesis in a model of PALB2-associated hereditary breast cancer. *Cancer Discov.* 3, 894–907. doi: 10.1158/2159-8290.cd-13-0011

Jackson, S. P., and Bartek, J. (2009). The DNA-damage response in human biology and disease. *Nature* 461, 1071–1078. doi: 10.1038/nature08467

Kang, C., Xu, Q., Martin, T. D., Li, M. Z., Demaria, M., Aron, L., et al. (2015). The DNA damage response induces inflammation and senescence by inhibiting autophagy of GATA4. *Science* 349:aaa5612. doi: 10.1126/science.aaa5612

Kang, H. T., Park, J. T., Choi, K., Kim, Y., Choi, H. J. C., Jung, C. W., et al. (2017). Chemical screening identifies ATM as a target for alleviating senescence. *Nat. Chem. Biol.* 13, 616–623. doi: 10.1038/nchembio.2342

Kuk, M. U., Kim, J. W., Lee, Y. S., Cho, K. A., Park, J. T., and Park, S. C. (2019). Alleviation of senescence via ATM inhibition in accelerated aging models. *Mol. Cells* 42, 210–217.

Lee, J. H., and Paull, T. T. (2020). Mitochondria at the crossroads of ATM-mediated stress signaling and regulation of reactive oxygen species. *Redox Biol.* 32:101511. doi: 10.1016/j.redox.2020.101511

Leuzzi, V., Micheli, R., D'Agnano, D., Molinaro, A., Venturi, T., Plebani, A., et al. (2015). Positive effect of erythrocyte-delivered dexamethasone in ataxia-telangiectasia. *Neurol. Neuroimmunol. Neuroinflamm.* 2:e98. doi: 10.1212/nxi.0000000000000098

Levine, B., and Kroemer, G. (2008). Autophagy in the pathogenesis of disease. *Cell* 132, 27–42. doi: 10.1016/j.cell.2007.12.018

Liang, N., He, Q., Liu, X., and Sun, H. (2019). Multifaceted roles of ATM in autophagy: from nonselective autophagy to selective autophagy. *Cell. Biochem. Funct.* 37, 177–184. doi: 10.1002/cbf.3385

Liu, E. Y., Xu, N., O'Prey, J., Lao, L. Y., Joshi, S., Long, J. S., et al. (2015). Loss of autophagy causes a synthetic lethal deficiency in DNA repair. *Proc. Natl. Acad. Sci. U.S.A.* 112, 773–778. doi: 10.1073/pnas.1409563112

Liu, X. L., Ding, J., and Meng, L. H. (2018). Oncogene-induced senescence: a double edged sword in cancer. *Acta Pharmacol. Sin.* 39, 1553–1558. doi: 10.1038/aps.2017.198

Maiuri, M. C., Galluzzi, L., Morselli, E., Kepp, O., Malik, S. A., and Kroemer, G. (2010). Autophagy regulation by p53. *Curr. Opin. Cell Biol.* 22, 181–185.

McEwan, D. G., and Dikic, I. (2011). The three musketeers of autophagy: phosphorylation, ubiquitylation and acetylation. *Trends Cell Biol.* 21, 195–201. doi: 10.1016/j.tcb.2010.12.006

McGrath-Morrow, S. A., Collaco, J. M., Detrick, B., and Lederman, H. M. (2016). Serum Interleukin-6 Levels and Pulmonary Function in Ataxia-Telangiectasia. *J. Pediatr.* 171, 256–61.e1.

McGrath-Morrow, S. A., Ndeh, R., Collaco, J. M., Rothblum-Oviatt, C., Wright, J., O'Reilly, M. A., et al. (2018). Inflammation and transcriptional responses of peripheral blood mononuclear cells in classic ataxia telangiectasia. *PLoS One* 13:e0209496. doi: 10.1371/journal.pone.0209496

McGrath-Morrow, S. A., Ndeh, R., Helmin, K. A., Khuder, B., Rothblum-Oviatt, C., Collaco, J. M., et al. (2020). DNA methylation and gene expression signatures are associated with ataxia-telangiectasia phenotype. *Sci. Rep.* 10:7479.

Metcalfe, J. A., Parkhill, J., Campbell, L., Stacey, M., Biggs, P., Byrd, P. J., et al. (1996). Accelerated telomere shortening in ataxia telangiectasia. *Nat. Genet.* 13, 350–353. doi: 10.1038/ng0796-350

Mongiardi, M. P., Radice, G., Piras, M., Stagni, V., Pacioni, S., Re, A., et al. (2019). Axitinib exposure triggers endothelial cells senescence through ROS accumulation and ATM activation. *Oncogene* 38, 5413–5424. doi: 10.1038/s41388-019-0798-2

Naka, K., Tachibana, A., Ikeda, K., and Motoyama, N. (2004). Stress-induced premature senescence in hTERT-expressing ataxia telangiectasia fibroblasts. *J. Biol. Chem.* 279, 2030–2037. doi: 10.1074/jbc.m309457200

Rabinowitz, J. D., and White, E. (2010). Autophagy and metabolism. *Science* 330, 1344–1348.

Rashi-Elkeles, S., Elkon, R., Weizman, N., Linhart, C., Amariglio, N., Sternberg, G., et al. (2006). Parallel induction of ATM-dependent pro- and antiapoptotic signals in response to ionizing radiation in murine lymphoid tissue. *Oncogene* 25, 1584–1592. doi: 10.1038/sj.onc.1209189

Ribezzo, F., Shiloh, Y., and Schumacher, B. (2016). Systemic DNA damage responses in aging and diseases. *Semin. Cancer Biol.* 37–38, 26–35. doi: 10.1016/j.semcancer.2015.12.005

Rossiello, F., Herbig, U., Longhese, M. P., Fumagalli, M., and d'Adda di Fagagna, F. (2014). Irreparable telomeric DNA damage and persistent DDR signalling as a shared causative mechanism of cellular senescence and ageing. *Curr. Opin. Genet. Dev.* 26, 89–95. doi: 10.1016/j.gde.2014.06.009

Rubinsztein, D. C., Mariño, G., and Kroemer, G. (2011). Autophagy and aging. *Cell* 146, 682–695.

Shiloh, Y. (2014). ATM: expanding roles as a chief guardian of genome stability. *Exp. Cell Res.* 329, 154–161. doi: 10.1016/j.yexcr.2014.09.002

Shiloh, Y., and Lederman, H. M. (2017). Ataxia-telangiectasia (A-T): an emerging dimension of premature ageing. *Ageing Res. Rev.* 33, 76–88. doi: 10.1016/j.arr.2016.05.002

Shiloh, Y., Tabor, E., and Becker, Y. (1982). Colony-forming ability of ataxia-telangiectasia skin fibroblasts is an indicator of their early senescence and increased demand for growth factors. *Exp. Cell Res.* 140, 191–199. doi: 10.1016/0014-4827(82)90169-0

Shiloh, Y., and Ziv, Y. (2013). The ATM protein kinase: regulating the cellular response to genotoxic stress, and more. *Nat. Rev. Mol. Cell Biol.* 14, 197–210. doi: 10.1038/nrm3546

Smilenov, L. B., Morgan, S. E., Mellado, W., Sawant, S. G., Kastan, M. B., and Pandita, T. K. (1997). Influence of ATM function on telomere metabolism. *Oncogene* 15, 2659–2665. doi: 10.1038/sj.onc.1201449

Stagni, V., Cirotti, C., and Barilà, D. (2018). Ataxia-telangiectasia mutated kinase in the control of oxidative stress, mitochondria, and autophagy in cancer: a maestro with a large orchestra. *Front. Oncol.* 8:73. doi: 10.3389/fonc.2018.00073

Stern, N., Hochman, A., Zemach, N., Weizman, N., Hammel, I., Shiloh, Y., et al. (2002). Accumulation of DNA damage and reduced levels of nicotine adenine dinucleotide in the brains of Atm-deficient mice. *J. Biol. Chem.* 277, 602–608. doi: 10.1074/jbc.m106798200

Sunderland, P., Augustyniak, J., Lenart, J., Bużańska, L., Carlessi, L., Delia, D., et al. (2020). ATM-deficient neural precursors develop senescence phenotype with disturbances in autophagy. *Mech. Ageing Dev.* 190:111296. doi: 10.1016/j.mad.2020.111296

Tang, J., Di, J., Cao, H., Bai, J., and Zheng, J. (2015). p53-mediated autophagic regulation: a prospective strategy for cancer therapy. *Cancer Lett.* 363, 101–107. doi: 10.1016/j.canlet.2015.04.014

Tasdemir, E., Chiara Maiuri, M., Morselli, E., Criollo, A., D'Amelio, M., Djavaheri-Mergny, M., et al. (2008a). A dual role of p53 in the control of autophagy. *Autophagy* 4, 810–814. doi: 10.4161/auto.6486

Tasdemir, E., Maiuri, M. C., Galluzzi, L., Vitale, I., Djavaheri-Mergny, M., D'Amelio, M., et al. (2008b). Regulation of autophagy by cytoplasmic p53. *Nat. Cell Biol.* 10, 676–687.

Valentin-Vega, Y. A., Maclean, K. H., Tait-Mulder, J., Milasta, S., Steeves, M., Dorsey, F. C., et al. (2012). Mitochondrial dysfunction in ataxia-telangiectasia. *Blood* 119, 1490–1500.

Wang, R., and Wang, G. (2019). Autophagy in mitochondrial quality control. *Adv. Exp. Med. Biol.* 1206, 421–434. doi: 10.1007/978-981-15-0602-4_19

Wang, Y., Zhang, N., Zhang, L., Li, R., Fu, W., Ma, K., et al. (2016). Autophagy regulates chromatin ubiquitination in DNA damage response through elimination of SQSTM1/p62. *Mol. Cell* 63, 34–48. doi: 10.1016/j.molcel.2016.05.027

Weizman, N., Shiloh, Y., and Barzilai, A. (2003). Contribution of the Atm protein to maintaining cellular homeostasis evidenced by continuous activation of the AP-1 pathway in Atm-deficient brains. *J. Biol. Chem.* 278, 6741–6747. doi: 10.1074/jbc.m211168200

White, E. (2016). Autophagy and p53. *Cold Spring Harb. Perspect. Med.* 6:a026120.

White, E., Mehnert, J. M., and Chan, C. S. (2015). Autophagy, metabolism, and cancer. *Clin. Cancer Res.* 21, 5037–5046. doi: 10.1158/1078-0432.ccr-15-0490

Wood, L. D., Halvorsen, T. L., Dhar, S., Baur, J. A., Pandita, R. K., Wright, W. E., et al. (2001). Characterization of ataxia telangiectasia fibroblasts with extended life-span through telomerase expression. *Oncogene* 20, 278–288. doi: 10.1038/sj.onc.1204072

Xia, S. J., Shammas, M. A., and Shmookler Reis, R. J. (1996). Reduced telomere length in ataxia-telangiectasia fibroblasts. *Mutat. Res.* 364, 1–11. doi: 10.1016/0921-8777(96)00015-8

Zaki-Dizaji, M., Akrami, S. M., Azizi, G., Abolhassani, H., and Aghamohammadi, A. (2018). Inflammation, a significant player of Ataxia-Telangiectasia pathogenesis? *Inflamm. Res.* 67, 559–570. doi: 10.1007/s00011-018-1142-y

Zhang, J., Tripathi, D. N., Jing, J., Alexander, A., Kim, J., Powell, R. T., et al. (2015). ATM functions at the peroxisome to induce pexophagy in response to ROS. *Nat. Cell. Biol.* 17, 1259–1269. doi: 10.1038/ncb3230

Zhao, J., Zhang, L., Lu, A., Han, Y., Colangelo, D., Bukata, C., et al. (2020). ATM is a key driver of NF-κB-dependent DNA-damage-induced senescence, stem cell dysfunction and aging. *Aging (Albany N.Y.)* 12, 4688–4710. doi: 10.18632/aging.102863

Conflict of Interest: The authors declare that the research was conducted in the absence of any commercial or financial relationships that could be construed as a potential conflict of interest.

frontiers in Cell and Developmental Biology

METHODS
published: 21 January 2021
doi: 10.3389/fcell.2020.620409

Assessing Autophagy in Muscle Stem Cells

Silvia Campanario[1,2], Ignacio Ramírez-Pardo[1,2], Xiaotong Hong[1,2], Joan Isern[1,2] and Pura Muñoz-Cánoves[1,2,3]**

[1] Centro Nacional de Investigaciones Cardiovasculares (CNIC), Madrid, Spain, [2] Department of Experimental and Health Sciences, Pompeu Fabra University (UPF), CIBER on Neurodegenerative Diseases (CIBERNED), Barcelona, Spain, [3] ICREA, Barcelona, Spain

The skeletal muscle tissue in the adult is relatively stable under normal conditions but retains a striking ability to regenerate by its resident stem cells (satellite cells). Satellite cells exist in a quiescent (G0) state; however, in response to an injury, they reenter the cell cycle and start proliferating to provide sufficient progeny to form new myofibers or undergo self-renewal and returning to quiescence. Maintenance of satellite cell quiescence and entry of satellite cells into the activation state requires autophagy, a fundamental degradative and recycling process that preserves cellular proteostasis. With aging, satellite cell regenerative capacity declines, correlating with loss of autophagy. Enhancing autophagy in aged satellite cells restores their regenerative functions, underscoring this proteostatic activity's relevance for tissue regeneration. Here we describe two strategies for assessing autophagic activity in satellite cells from GFP-LC3 reporter mice, which allows direct autophagosome labeling, or from non-transgenic (wild-type) mice, where autophagosomes can be immunostained. Treatment of GFP-LC3 or WT satellite cells with compounds that interfere with autophagosome-lysosome fusion enables measurement of autophagic activity by flow cytometry and immunofluorescence. Thus, the methods presented permit a relatively rapid assessment of autophagy in stem cells from skeletal muscle in homeostasis and in different pathological scenarios such as regeneration, aging or disease.

Keywords: autophagy, stem cell, satellite cell, skeletal muscle, regeneration, quiescence, flow cytometry, immunofluorescence

OPEN ACCESS

Edited by:
Lucia Latella,
Institute of Traslational Pharmacology, Italian National Research Council, Italy

Reviewed by:
Marco Segatto,
University of Molise, Italy
Luca Madaro,
Sapienza University of Rome, Italy

****Correspondence:***
Pura Muñoz-Cánoves
pura.munoz@upf.edu
Joan Isern
jisern@cnic.es

Specialty section:
This article was submitted to Cell Death and Survival, a section of the journal Frontiers in Cell and Developmental Biology

Received: *22 October 2020*
Accepted: *31 December 2020*
Published: *21 January 2021*

Citation:
Campanario S, Ramírez-Pardo I, Hong X, Isern J and Muñoz-Cánoves P (2021) Assessing Autophagy in Muscle Stem Cells. Front. Cell Dev. Biol. 8:620409. doi: 10.3389/fcell.2020.620409

INTRODUCTION

Skeletal muscle is formed by multinucleated myofibers and exhibits a remarkable capacity to regenerate thanks to its resident stem cells, also called satellite cells (SCs) (Mauro, 1961). These cells are characterized by the expression of the paired-box transcription factor Pax7 (Seale et al., 2004), and constitute the main source of new myonuclei for myofiber growth and regeneration. In homeostasis, SCs are in a reversible G_0 arrest state called quiescence and present low transcriptional and metabolic activities. In response to muscle injury, SCs activate and orchestrate a myogenic program to regenerate the damaged muscle (see detailed myogenic states and markers in **Figure 1**). Activated SCs rapidly proliferate, and differentiate and fuse to form new regenerating myofibers and reconstitute the muscle tissue. Alternatively, SCs undergo self-renewal to replenish the quiescent stem-cell pool (revised in Evano and Tajbakhsh, 2018; Feige et al., 2018).

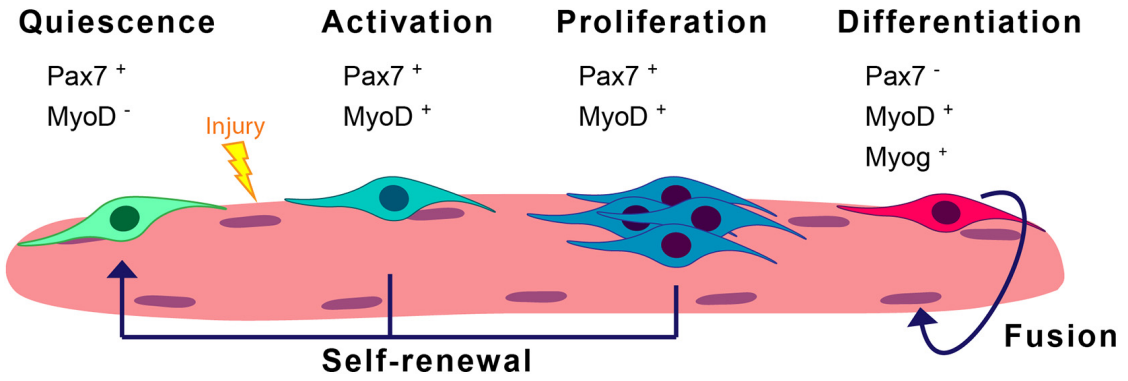

FIGURE 1 | Scheme of the satellite cell myogenic program. SCs are normally in quiescence and enter a myogenic cycle upon stress conditions such as injury. In the steady-state, they express Pax7. Activation of SCs can be determined by the co-expression of Pax7 and the myogenic regulatory factor MyoD. Proliferating SCs later differentiate into differentiated/committed progenitors characterized by the downregulation of Pax7 expression and the induction of Myog expression. These differentiated cells will eventually fuse into myofibers. A subset of the proliferating SCs will return to quiescence through the process of self-renewal.

SC regenerative functions decline with aging, and this decline is maximal at geriatric age (Sousa-Victor et al., 2014). Likewise, SC functions are altered in muscle diseases such as in the severe Duchene muscular dystrophy (DMD) (Dumont et al., 2015; Chang et al., 2018). Maintenance of the SC quiescent state needs basal surveillance mechanisms to maintain the cell's proteome quality and overall homeostasis. The entrance of SCs into an activated state in response to local muscle damage requires rapid protein composition changes, eliminating proteins involved in maintaining the quiescent state and supplying new proteins involved in cell-cycle regulation and differentiation. In particular, SC quiescence and activation after injury both require macroautophagy (Tang and Rando, 2014; García-Prat et al., 2016). Macroautophagy (hereafter called autophagy) is a regulated recycling mechanism that dismantles unnecessary or dysfunctional cell components, ranging from small macromolecules to full-sized organelles (Mizushima and Komatsu, 2011).

The autophagy process is divided into sequential steps: initiation and nucleation, elongation, maturation, fusion and degradation (**Figure 2**). At the initiation of autophagy, a flat membrane sheet known as phagophore surrounds cytosolic components. This phagophore then elongates and seals itself forming a double-membrane bound vesicle called the autophagosome. Upon subsequent fusion with the lysosome, it gives rise to the autolysosome, whose intracellular components are rapidly degraded by the lysosomal hydrolases (Kroemer et al., 2010; Pyo et al., 2012). Several autophagy-related genes (Atg) products including the Atg8/Map1lc3b protein (microtubule-associated protein 1 light-chain 3, hereafter referred to as LC3) regulate autophagosome formation and maturation into autolysosomes. LC3 is a cytosolic protein that is cleaved and conjugated to phosphatidylethanolamine (PE) giving rise to the membrane-bound form of LC3, also referred to as LC3-II, the level of which is known to be correlated with the number of autophagosomes (Lee and Lee, 2016). Moreover, LC3-II in the autophagosome interacts with autophagy adaptors, such as p62/Sqstm1, Ndp52, Optn, Nbr1, or Tax1bp1, that act as a linkage between autophagosome and the substrate (Kirkin and Rogov, 2019). In sum, through the autophagy process, targeted cytoplasmic constituents are degraded in lysosomes.

Under metabolic stress, autophagy-mediated degradation of cytoplasmic constituents supports energy balance (Klionsky, 2005; Klionsky et al., 2010; Mizushima and Komatsu, 2011). Although autophagy was described in the beginning as a cellular process induced by stress, it also functions at baseline under quiescence in resting SCs, and this constitutive autophagic activity appears to be indispensable for maintaining stemness (García-Prat et al., 2016). Disruption of the autophagic capacity by Atg7 genetic deletion in young SCs leads to an increased accumulation of impaired mitochondria that cause high ROS levels, provoking further damage to proteins and DNA (García-Prat et al., 2016). Of interest, autophagy induction is also observed during SC activation *in vivo*, and blocking autophagy delays cell-cycle entry from the quiescent state, with consequences for muscle regeneration (Tang and Rando, 2014). Notably, the reported phenotype in autophagy-deficient murine SCs from young animals partly recapitulates the one observed in chronologically aged SCs (García-Prat et al., 2016). In fact, in contrast to young SCs, old SCs show defective autophagic activity. This autophagy failure ends up in a progressive accumulation of harmful intracellular waste, mainly composed of altered mitochondrial material, which produces high oxidative stress and DNA damage, leading to muscle stem cell senescence in very old (geriatric) mice (Sousa-Victor et al., 2014; García-Prat et al., 2016). Fiacco et al., recently showed that autophagy is induced during the early, compensatory regenerative stages of DMD. A gradual decline was observed throughout disease progression in dystrophic *mdx* mice, coinciding with the functional exhaustion of SC-mediated regeneration and accumulation of fibrosis. Furthermore, pharmacological modulation of autophagy could influence disease progression in *mdx* mutant mice. In support of this notion, interventions that prolong the activation of autophagy might be beneficial in treating DMD (Fiacco et al., 2016).

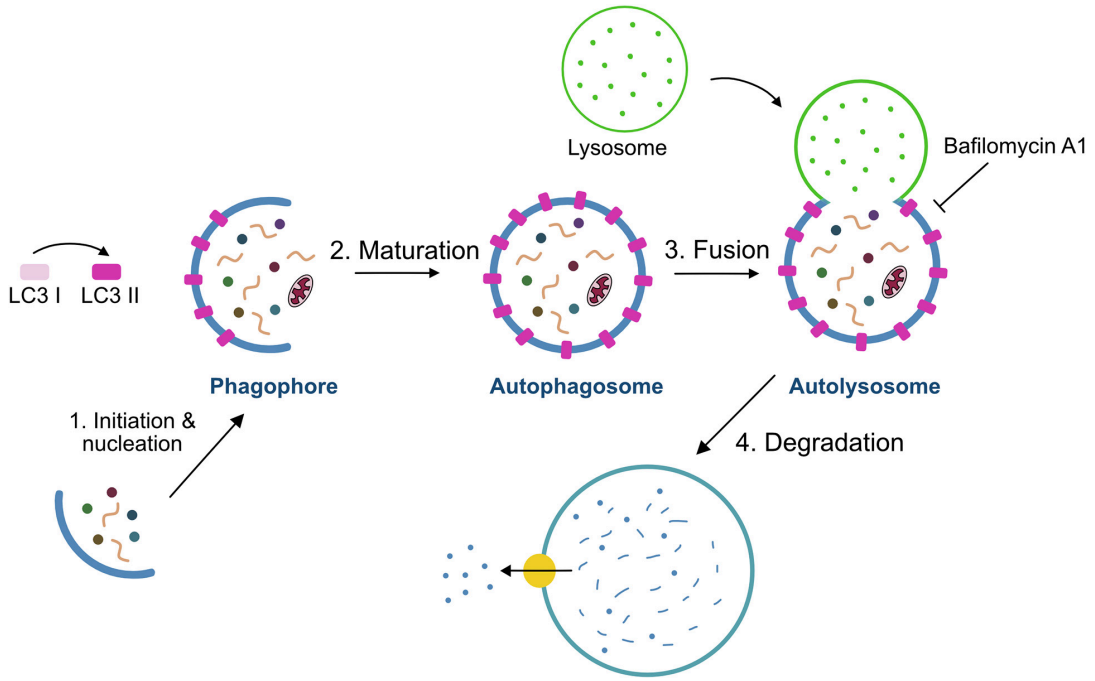

FIGURE 2 | Schematic model of the autophagy process. The process of autophagy includes four steps: (i) initiation/nucleation where the phagophore is formed and starts engulfing the cargo, (ii) formation of the phagosome by elongation and maturation of the phagophore, (iii) fusion of the phagosome with the lysosome, and (iv) degradation of the internal material by lysosomal hydrolases. Bafilomycin A1 is used to measure autophagy flux through the inhibition of autophagolysosome formation.

Because quiescent SCs exist in low numbers in resting muscles, are small in size, and have a low proportion of cytoplasm/nucleus (consistent with their quiescent state), the study of dynamic cytoplasmic processes, such as autophagy, in these cells is therefore challenging. Here, we show different methods to study autophagy in SCs, focusing on their quiescence state.

MATERIALS AND METHODS

Mice

C57BL/6 (wild type, WT) and GFP-LC3 (Mizushima et al., 2004) mice were used in this study. All experiments were carried in young (3–4 months old) male mice. Mice were kept in standard cages with food and water *ad libitum*. All animals were sacrificed between 9:00 and 10:00 am by cervical dislocation to avoid circadian changes in autophagy (Solanas et al., 2017). All animal experiments were approved by the Ethics Committee of the Barcelona Biomedical Research Park (PRBB) and by the Catalan Government, by the Animal Care and Ethics Committee of the Spanish National Cardiovascular Research Center (CNIC) and, by the Regional Authorities.

Satellite Cell Isolation by Fluorescence-Activated Cell Sorting

Muscles were collected from fore and hind limbs in cold DMEM (Gibco 41965-039) with 1% Penicillium/Streptomycin (P/S) (15140-122) into 50 mL Falcon tubes. Any visible fat and connective tissue were removed before mincing muscles with scissors. Cleaned and minced muscles were collected into a M tube (Miltelnyi Biotec, GentleMACS^{TM}) and digestion medium (8 mL) was added. Digestion medium was freshly prepared with DMEM containing Liberase 0.1 mg/g muscle weight (Roche, 5401127001), Dispase 0.3% (Sigma-Aldrich, D4693-1G), 1% P/S, 0.4 μM $CaCl_2$ and 5 μM $MgCl_2$. M tubes were placed onto Miltelnyi tissue dissociator under the program 37C_mr_SMDK_1. Once it finished, tubes were kept 5 min on ice to sediment the sample and 5 mL of FBS (Sigma-Aldrich F7524) was added to block the enzymatic digestion. Next, digested muscles were transferred to a 50 mL Falcon tube and rinsed up to 40 mL with cold DMEM 1% P/S (Optional: cold DMEM can be used to rinse M tubes in order to collect leftovers and transferred to the same Falcon tube). Muscle homogenates were filtered through 100 and 70 μm cell strainers (SPL Lifescience, 93100 and 93070) consecutively and centrifuged at 50 × *g* for 10 min at 4°C. The supernatant was collected in a new Falcon tube and centrifuged at 600 × *g* for 10 min at 4°C. The supernatant was then discarded and the pellet was incubated for 10 min on ice (protected from light) with 1 mL of 1X RBC lysis buffer (eBioscience, 00-4333-57) to eliminate the excess of erythrocytes. To stop the lysis, 30 mL of 1X PBS was added and filtered through a 40 μm cell strainer (SPL Lifescience, 93040. Filtered cell suspension was centrifuged at 600 × *g* for 10 min at 4°C and after discarding the supernatant, the cell pellet was resuspended in 1 mL of DMEM with 1% P/S to count the number of cells for each sample.

For antibody staining, cell suspension was centrifuged at 600 × *g* for 10 min at 4°C and resuspended in cold FACS buffer (1% P/S, 5% Goat Serum (Gibco, 16210-064) in 1X PBS) containing antibody mixture at a ratio of 1 × 10^6 cells/100 μL antibody mixture for 1 h at 4°C (protected from light). The antibody mixture contained antibodies for negative and positive selection of QSCs in FACS buffer. PE-Cy7-conjugated anti-CD45 (Biolegend 103114), anti-Sca-1 (Biolegend 108114) and anti-CD31 (Biolegend 102418) antibodies were used for lineage-negative selection at a ratio of 0.5 μL antibody/100 μL FACS buffer. Alexa Fluor 647-conjugated anti-CD34 (BD Pharmigen 560230) and PE-conjugated anti-α7-integrin (AbLab AB10STMW215) were used for double-positive staining of QSCs at a ratio of 3 μL/100 μL and 1 μL/100 μL FACS buffer respectively. Optionally, single staining and FMO controls can be included to set up correctly the gates. After staining, samples were rinsed up to 30 mL of FACS buffer and centrifuged at 600 × *g* for 10 min at 4°C to wash the excess of antibodies. Samples were then resuspended in 300 μL FACS buffer with DAPI (1 μg/mL) (Invitrogen, D1306) to exclude dead cells. Finally, $Sca1^-/CD31^-/CD45^-/CD34^+/\alpha7\text{-integrin}^+$ SCs were collected into Eppendorf tubes containing 100 μL of collection medium (Ham's F10 (Biowest L0140-500), 1% P/S, 1% Glutamine (Lonza, 17-605E), 20% FBS) at 4°C using a FACS Aria II (BD Biosciences).

Drug Treatment for Autophagy Flux Determination in Quiescent Satellite Cells

Prior to antibody staining and quiescent SC isolation by FACS, samples (already resuspended in 1 mL of DMEM with 1% P/S) were centrifuged at 600 × *g* for 10 min at 4°C. The cell pellet was resuspended in 1 mL of collection medium. Each sample was split into two new 2 mL Eppendorf tubes for Bafilomycin A1 (10 nM; Sigma, B1793) or DMSO (vehicle; Sigma, D2540) treatment for 4 h at 37°C 5% CO_2. After drug treatment, antibody staining for SC isolation was performed as mentioned above.

Drug Treatment for Autophagic Flux Determination in Activated and Proliferating Satellite Cells

Freshly sorted SCs were cultured on 15-well plastic slides (μ-Slide Angiogenesis ibiTreat: Ibidi, 81506) previously coated with collagen type I (Corning, 354236) in growth medium [GM; collection medium supplemented with recombinant bFGF (Preprotech, 100-18B, 0.0025 μg/mL)]. A total number of 3000 SCs per well were homogenously distributed plated. After 20 or 68 h in culture, cells were treated with Bafilomycin A1 at 10 nM or DMSO during the last 4 h for activation and proliferation SCs states. Cells were then fixed at 24 and 72 h respectively.

Flow Cytometry Analysis of Autophagy in Quiescent Satellite Cells

Using GFP-LC3 reporter mice, GFP fluorescence signal was recorded from at least 10.000 $Sca1^-/CD31^-/CD45^-/CD34^+/\alpha7\text{-integrin}^+$ SCs in each sample. GFP-LC3 fluorescence positive signal was determined comparing to the corresponding negative control sample (wild-type sample without GFP fluorescence). Median fluorescence intensity (MFI) of the whole GFP histogram signal for SCs was analyzed. Autophagy flux was determined as the relative change of GFP-LC3 MFI between DMSO and Bafilomycin A1 treated samples.

Immunofluorescence and Image Acquisition of Satellite Cells

Isolated quiescent SCs were plated onto 15-well plastic slides (μ-Slide Angiogenesis ibiTreat: Ibidi, 81506). Prior to SC plating, slides were coated with 0.1% Poli-L-Lysin (Sigma, P8920) in distilled water (it can be reused) for 30 min at room temperature (RT) and air-dried. For each sample, 3000 SCs per well were seeded into the 15-well slides. Eventually, 1X PBS can be added to the wells in order to ensure that the cell suspension is equally distributed. To cytospin the cells, the slides were then centrifuged at 50 × *g* for 10 min.

For both cultured and quiescent SCs, the supernatant was removed and cells were fixed with 30 μL of 4% PFA for 10 min at RT. After fixation, two washes with 1X PBS were performed. At this time point, slides can be stored with 1X PBS 0.05% azide at 4°C. It is recommended to fill completely each well and cover them with parafilm to avoid PBS evaporation.

After fixation, slides were permeabilized with 0.5% Triton X-100 (Sigma, T8787) for 15 min at RT and washed three times with 1X PBS. Next, wells were incubated 30 min at RT with blocking solution containing BSA (Sigma, A7906, 3 mg/mL) in 1X PBS. Primary antibodies (**Table 1**) were diluted in blocking solution and incubated for 2 h at RT or overnight (O/N) at 4°C. Antibodies were removed and wells were washed three times with 1X PBS. Slides were incubated with secondary antibody solution for 1 h at RT (**Table 1**). DAPI (1 μg/mL) or Sytox™ Green (Invitrogen, S7020, 1/15000) were used for nuclear staining. Each well was extensively washed three times with 1X PBS and finally

TABLE 1 | List of antibodies used in this article.

Antibody	Company	Reference	Source	Dilution
Anti-CD45 PE-Cy7	Biolegend	103114	Rat	0.5/100*
Anti-Sca-1 PE-Cy7	Biolegend	108114	Rat	0.5/100*
Anti-CD31 PE-Cy7	Biolegend	102418	Rat	0.5/100*
Anti-CD34 Alexa Fluor-647	BD Pharmigen	560230	Rat	3/100*
Anti- α7-integrin PE	AbLab	AB10STMW215	Rat	1/100*
Anti-GFP	Aves labs	GFP-1020	Chicken	1/200
Anti-LC3	Nanotools	5F10	Mouse	1/100
Anti-MyoD	Dako	M3512	Mouse	1/200
Anti-Ki67	Abcam	ab15580	Rabbit	1/200
Anti-Chicken FITC	Aves Labs	F-1005	Goat	1/500
Anti-Chicken Alexa Fluor-405	Life Technologies	Ab175674	Goat	1/500
Anti-Mouse Alexa Fluor-647	Life Technologies	A-31571	Donkey	1/500
Anti-Rabbit Alexa Fluor-647	Life Technologies	A-21245	Donkey	1/500

**SCs were previously diluted in a ratio of 1 × 10^6 cells/100 μL.*

Fluoromount-G® (SouthernBiotech, 0100-01) mounting media was added. Optionally, a drop of mineral oil can be added to the top of the well for long-term storage.

Image Acquisition and Analysis of Autophagy in Satellite Cells

Digital images were acquired using a Zeiss LSM 700 confocal microscope with a Plan-Apochromat 63x/1.4 NA oil objective. At least 25–30 SCs per sample were imaged using confocal z-stack (0.5 μm interval). Zeiss LSM software Zen Black was used for digital acquisition and Fiji software was used for further image processing. As image preprocessing, gaussian smoothing (radius = 0.4) and background subtraction (ball radius = 20) were applied to the whole z-stack. Then, autophagosomes per cell defined as GFP-LC3$^+$ puncta were identified as individual 3D objects using the 3D Roi Manager plugin (Ollion et al., 2013). Whenever possible, measurements were performed blindly.

Statistical Analysis

GraphPad Prism (GraphPad Software, Inc) software was used for all statistical analysis. Data are presented as the mean ± the standard deviation of the mean. Sample size (n) of each experimental group was described in the corresponding figure legend and all experiments were done with at least three biological replicates. Normality was analyzed in each experiment using Shapiro-Wilk tests and homoscedasticity to test variances distribution was checked using the Fisher test. For normally distributed data, two-tail unpaired Student's t-test was performed. Statistical significance was set at $^*p < 0.05$, $^{**}p < 0.01$, $^{***}p < 0.001$, $^{****}p < 0.0001$.

RESULTS AND DISCUSSION

Satellite Cell Isolation by FACS

The proper isolation of SCs is crucial for characterizing the mechanisms involved in stem-cell quiescence maintenance and/or regenerative functions. Several methods based on fluorescence-activated cell sorting (FACS) using different cell surface markers for positive and negative cell selection have been optimized to isolate SCs (Sherwood et al., 2004; Joe et al., 2010; Pasut et al., 2012; Liu et al., 2013). Here, we used a FACS protocol based on CD45/CD31/Sca1 negative (Lin$^-$) cells and α7-integrin/CD34 double positive cells (Lin$^-$/α7-integrin$^+$/CD34$^+$) to isolate quiescent SCs from resting muscle (**Figure 3A**).

Autophagy Flux Determination in Quiescent Satellite Cells

As autophagy is a multistep process (see **Figure 2**), identification and quantification of autophagosomes within a cell at a given time-point is insufficient to report this dynamic process. Instead, the balance between the rate of autophagosome generation and its incorporation into autolysosomes (i.e., autophagic flux) is the optimal way to assess autophagy (Mizushima et al., 2010). Autophagy flux assays use inhibitors of autophagosome incorporation into the lysosome to discern between autophagosome formation and clearance. We have used Bafilomycin A1 (BafA1), a vacuolar H$^+$-ATPase inhibitor that blocks vesicle acidification as well as fusion between autophagosomes and lysosomes (Mauvezin et al., 2015).

The autophagy flux can be assessed by measuring relative levels of p62 or measuring the ratio between the lipidated form of LC3 (LC3-II) and the unconjugated form (LC3-I) (Kabeya, 2004) from protein extracts (granted that enough material is available to perform standard Western blotting). Unfortunately, the low numbers of freshly isolated SCs per mg of muscle tissue and their reduced cytoplasmic content, and therefore, low protein content, make this option unfeasible unless the starting material is scaled up (pooling tissue from several mice per experiment).

As quiescent SCs have a low cytoplasmic content, the identification of autophagosomes within the cytoplasm is a challenging task. We have set up an autophagy flux protocol in SCs isolated from a GFP-LC3 reporter mouse line, in which autophagosomes are labeled with GFP (green florescent protein). Although freshly isolated SCs from steady-state skeletal muscle are considered quiescent cells, one important point to consider when studying the quiescent state *ex vivo* is the potential changes induced in freshly isolated cells during the tissue's mechano-enzymatic disruption and subsequent isolation procedures, particularly at the transcriptional level (Machado et al., 2017; van Velthoven et al., 2017). Digested muscle was treated with BafA1 or vehicle (DMSO) for 4 h prior to quiescent SC isolation by FACS (see "Drug Treatment for Autophagy Flux Determination in Quiescent Satellite Cells" and scheme in **Figure 3A** for further details). After SC isolation, the autophagy flux in quiescent SCs was determined by monitoring the GFP-LC3 fluorescence levels by flow cytometry. We observed an increase in the GFP-LC3 intensity upon BafA1 treatment (**Figure 3B**). To assess whether this increase is due to an accumulation of autophagosomes, we quantified the number of GFP$^+$-autophagosomes in BafA1-treated quiescent SCs by immunofluorescence, and found that the number of GFP$^+$-autophagosomes was increased in BafA1-treated compared to vehicle-treated quiescent SCs (**Figure 4A**).

As GFP-LC3 reporter mouse strains may not be always available, we determined the autophagy flux in quiescent SCs isolated from WT mice by immunostaining the endogenous LC3 in cells treated or not with BafA1 (**Figure 4B**). As for GFP-LC3 reporter SCs, the number of autophagosomes was increased in BafA1-treated compared to vehicle-treated quiescent SCs (**Figure 4C**); moreover, similar autophagy flux ratios were found in GFP-LC3 reporter and WT quiescent SCs (**Figure 4C**) despite the higher background observed in endogenous LC3-staining conditions. Of note, it should be feasible to combine the GFP-LC3 fluorescence or the endogenous LC3 staining with other autophagy markers such as p62 (adaptor protein) and ubiquitin (in the cargo) aggregates to assess their potential colocalization. Since p62 is a marker of damaged organelles to be eliminated by autophagy and ubiquitin marks substrates for elimination by autophagy or the ubiquitin-proteasome system (UPS) (reviewed in Liu et al., 2016), the colocalization of LC3 with these markers may serve to further assess autophagy defects or autophagy flux impairments. Other lysosomal inhibitors can also be used for the assessment of autophagy flux, including lysosomal

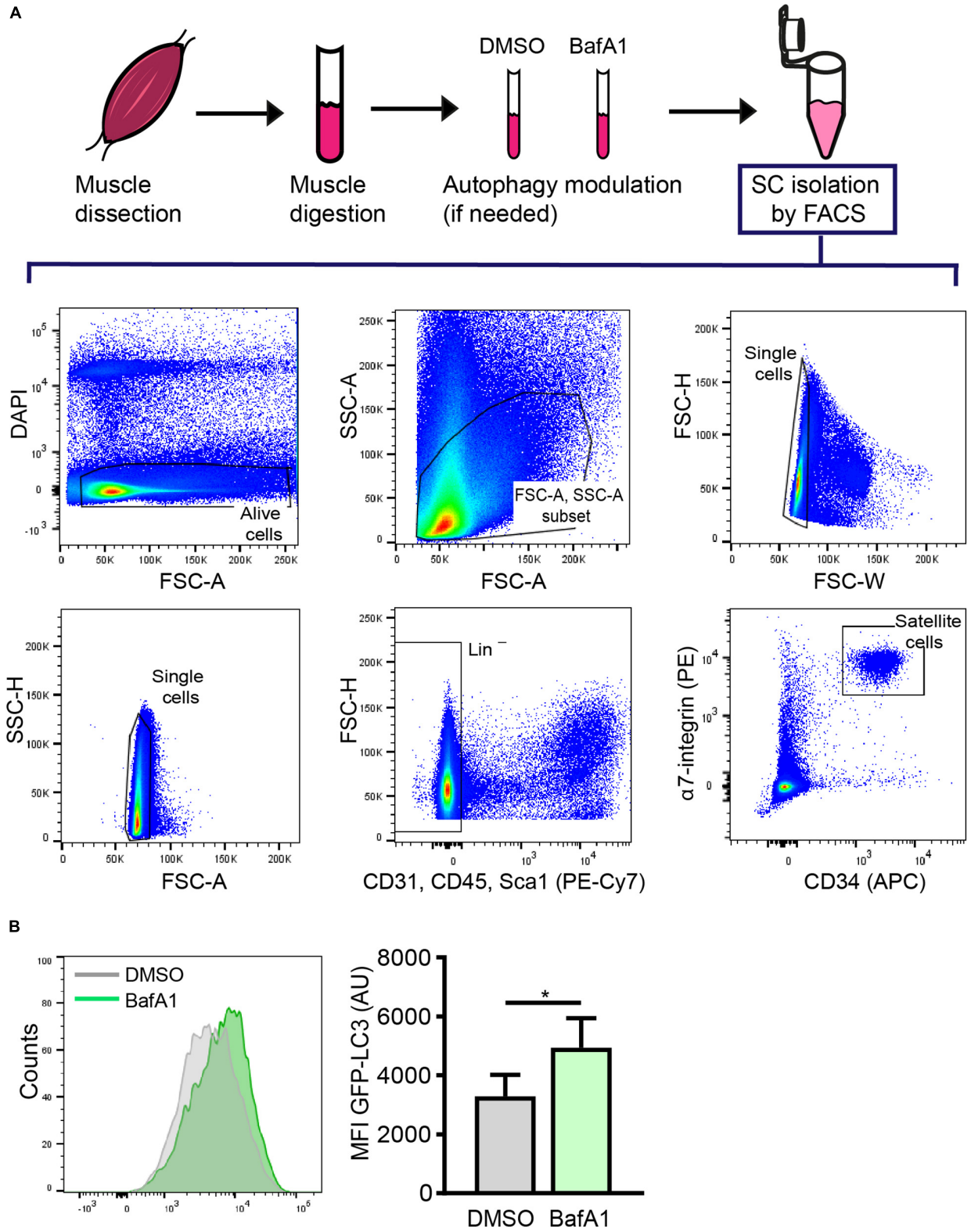

FIGURE 3 | Satellite cell isolation by FACS and subsequent analysis of autophagy through flow cytometry. **(A)** Representative example of the FACS strategy and gating scheme to isolate quiescent SCs (QSCs) rom resting muscles. **(B)** Representative example of histogram of LC3-GFP intensity (left panel) and analysis of the mean fluorescence intensity (MFI) by flow cytometry (right panel) in QSCs treated for 4 h with vehicle (DMSO) or BafA1 prior to their isolation by FACS ($n = 4$). Mean ± SD; two-tailed unpaired *t*-test. $^*p < 0.05$.

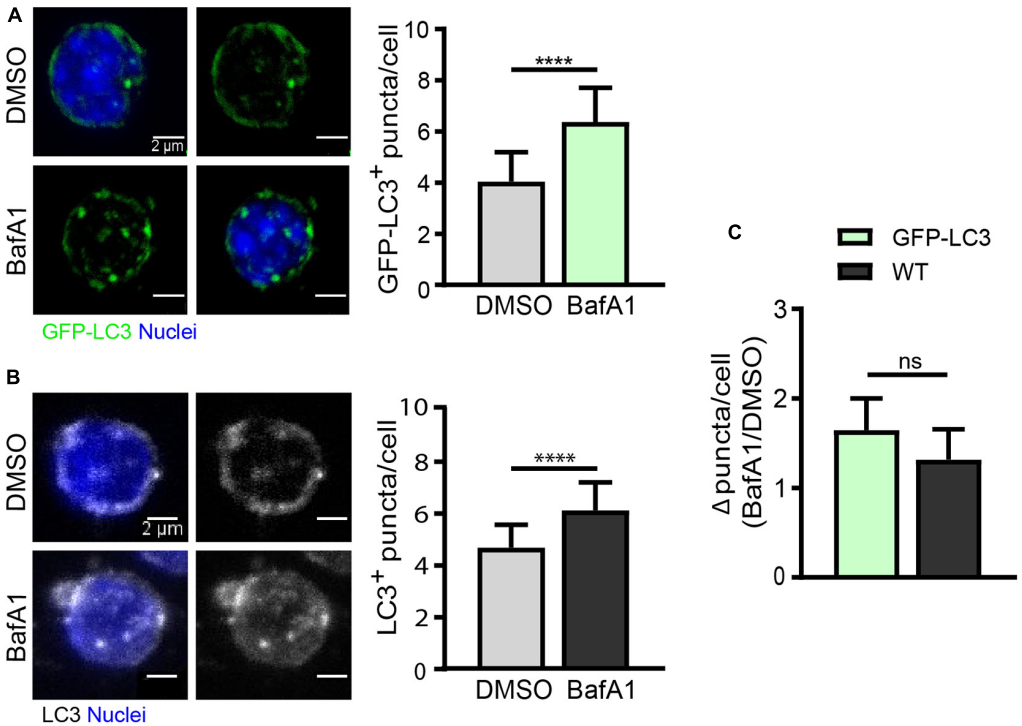

FIGURE 4 | Autophagy flux analysis in quiescent satellite cells by immunofluorescence. **(A)** Representative images of GFP$^+$-autophagosomes (green) and nuclei (blue) in freshly isolated QSCs from GFP-LC3 reporter mice (left panel) with the corresponding quantification of GFP-LC3$^+$ puncta per cell (right panel). Treatment with vehicle (DMSO) or BafA1 was performed for 4 h prior QSC isolation by FACS (n = 4). Scale bar, 2 μm. **(B)** Representative images of LC3-stained autophagosomes and nuclei (blue) in freshly isolated QSCs from WT mice (left panel) with its corresponding quantification of LC3$^+$ puncta per cell (right panel). Treatment with vehicle (DMSO) or BafA1 was performed for 4 h prior QSC isolation by FACS (n = 3). Scale bar, 2 μm. **(C)** Comparison of autophagy flux in GFP-LC3 or WT QSCs. Autophagy flux was determined as the ratio of the number of autophagosome puncta in BafA1 treated QSCs divided by the number of autophagosome puncta in vehicle (DMSO) treated QSCs (for GFP-LC3: n = 4; for WT: n = 3). Means ± SD; two-tailed unpaired t-test. ****$p < 0.0001$.

lumen "alkalizers" such as chloroquine or NH4Cl, as well as acid protease inhibitors such as leupeptin (Yang et al., 2013).

Autophagy Flux Determination in Activated and Proliferating Satellite Cells

We next analyzed the differences in autophagy flux in activated and proliferating SCs compared to quiescent cells. Freshly FACS-isolated SCs carrying the GFP-LC3 reporter were cultured for 24 and 72 h, corresponding to activation and proliferation states, respectively (**Figure 5A**). At 24 h, the cell cycle marker Ki67 is only expressed in around 10% of SCs, indicating that most SCs have not yet achieved the full proliferation state at this time point. Concurrently, SCs start to express the myogenic regulatory factor MyoD (**Figure 5A**). In contrast, at 72 h, most SCs (95%) are actively proliferating and become immunopositive for Ki67 (**Figure 5A**). Cells were treated with vehicle or BafA1 for 4 h prior to fixation and autophagy flux was measured by counting GFP-LC3 autophagosomes in activated SCs (MyoD$^+$ cells, after 24 h culture) and in proliferating SCs (Ki67$^+$ cells, after 72 h culture) (**Figures 5B,C**). Autophagy flux was estimated as the difference between autophagosome formation and degradation at a given time-window. Since SCs differ in their cellular size along the distinct myogenic stages, the number of autophagosomes upon BafA1 treatment was divided by the number of autophagosomes upon DMSO treatment for autophagy flux normalization, thus reducing cell size-induced variability. We found that autophagy flux was increased upon SC activation from quiescence, and this increase was even higher at the proliferation stage (**Figure 5D**).

Autophagy flux was also analyzed in WT freshly FACS-isolated SCs cultured for 24 and 72 h following the approach described in **Figure 5A**. Immunostaining of endogenous LC3 was performed for autophagosome detection and autophagy flux measurement in SCs treated with vehicle or BafA1, showing an increase in the number of autophagosomes in BafA1-treated SCs (**Figures 5E,F**). Moreover, similar to what is observed in transgenic SCs expressing the GFP-LC3 reporter, the highest autophagy flux was found at the proliferation stage (**Figures 5D,G**). However, although WT SCs showed a trend to increase their autophagy flux upon activation, we did not obtain significant differences in activated SCs with respect to their quiescent state (**Figure 5G**). Of note, the ratios for autophagy flux during activation and proliferation were smaller in WT SCs compared to transgenic SCs (**Figures 5D,G**).

GFP-LC3 can be incorporated into protein aggregates (Hara et al., 2006; Komatsu et al., 2006), and given that protein synthesis (and probably protein aggregates) increases upon cell division, the transgene would be more prone to be incorporated into

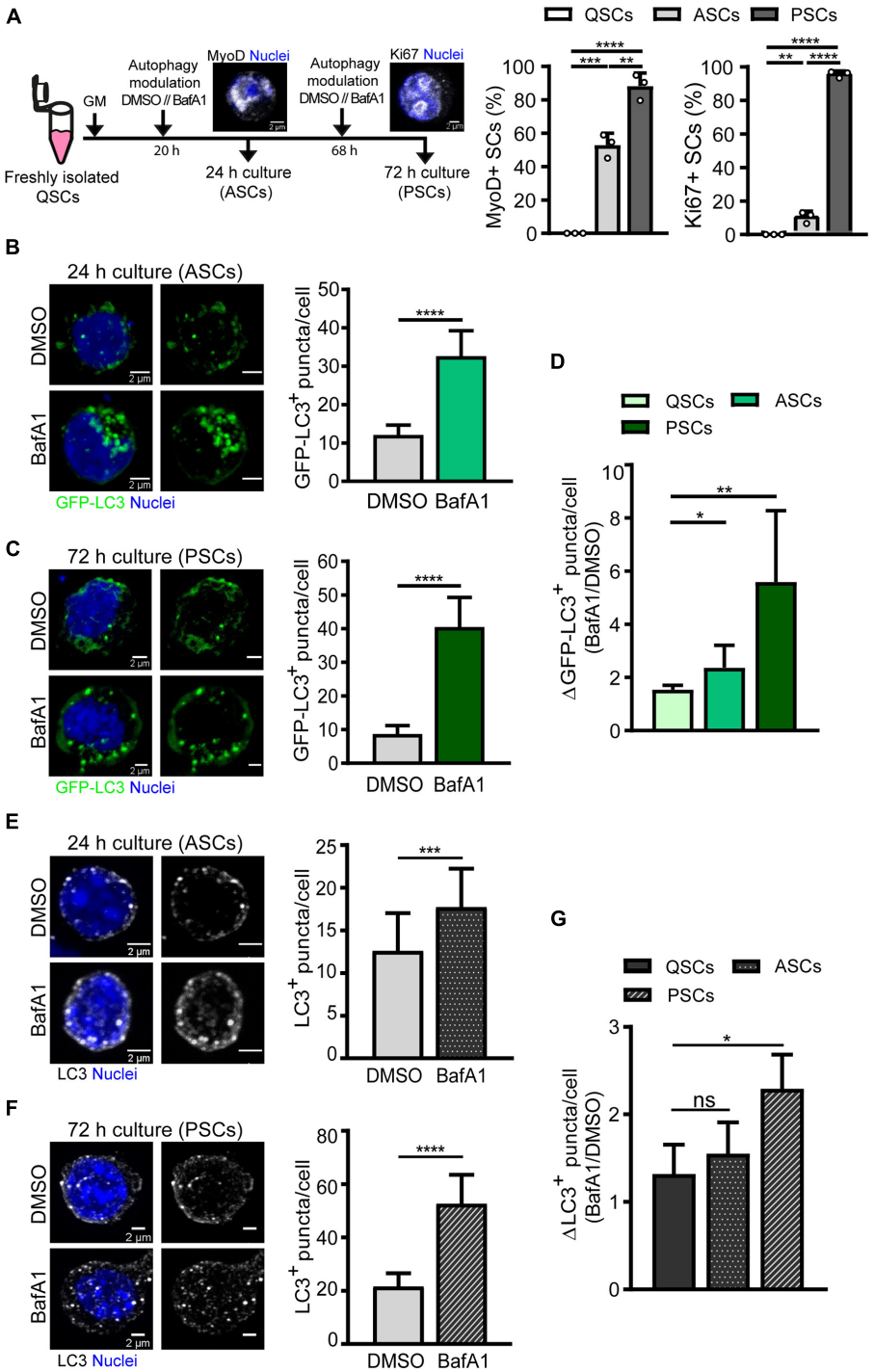

FIGURE 5 | Autophagy flux analysis in activated and proliferating satellite cells by immunofluorescence. **(A)** Right panel: Scheme of the process followed for autophagy flux assessment in (1) activated SCs (ASCs), characterized by the presence of MyoD protein and still lacking cell-cycle proteins such as Ki67, and (2) proliferating SCs (PSCs), marked by the expression of the proliferative marker Ki67. Left panels: quantification of the percentage of MyoD$^+$ and Ki67$^+$ cultured SCs at 24 and 72 h time points. **(B,C)** Representative images of GFP$^+$-autophagosomes (green) and nuclei (blue) in ASCs **(B)** and PSCs **(C)** from GFP-LC3 reporter mice (left panels) with the corresponding quantification of GFP-LC3$^+$ puncta per cell (right panels). Treatment with vehicle (DMSO) or BafA1 was performed for 4 h prior fixation (n = 3). Scale bar, 2 μm. **(D)** Autophagy flux represented as the ratio of GFP-LC3$^+$ puncta in BafA1 and vehicle (DMSO) along SC myogenesis *in vitro* (n = 3–6). **(E,F)** Representative images of LC3 + -autophagosomes (gray scale) and nuclei (blue) in ASCs **(E)** and PSCs **(F)** from WT mice (left panels) with the corresponding quantification of LC3$^+$ puncta per cell (right panels). Treatment with vehicle (DMSO) or BafA1 was performed as in panels **(B,C)** (n = 4). Scale bar, 2 μm. **(G)** Autophagy flux, depicted as the ratio of LC3$^+$ puncta in BafA1 and vehicle (DMSO), along SC myogenesis *in vitro* (n = 4). Means ± SD; two-tail unpaired t-test. *$p < 0.05$, **$p < 0.01$, ***$p < 0.001$, and ****$p < 0.0001$.

these aggregates in activated and proliferating SCs, mainly if the reporter's cellular levels are high. This possibility could explain why the differences in autophagy flux ratios in WT and transgenic SCs are higher upon SC cell cycle entry while remaining more similar at quiescence. Moreover, the distinct background observed with endogenous LC3 staining may also influence autophagosome detection and subsequent ratio determinations.

In summary, despite the slight differences in determining autophagy flux with both approaches, the autophagy activity increases upon SC activation and consequent proliferation. Therefore, the use of either GFP-LC3 reporter or endogenous LC3 staining provides an easy and robust way to analyze autophagy during SC myogenesis *in vitro*. Indeed, these results are in agreement with previous observations demonstrating a role for autophagy in quiescence maintenance and in supporting cell survival and metabolic demands upon stem-cell exit from quiescence and entrance into proliferation to ensure successful muscle regeneration (Tang and Rando, 2014; García-Prat et al., 2016).

CONCLUSION

The small proportion of SCs present in steady-state skeletal muscle and their reduced cytoplasm in the quiescent state after sorting, challenges the monitoring of autophagy in these cells. The protocols reported here enable quiescent SC isolation by FACS from resting murine skeletal muscle tissue using standard laboratory equipment and allows us to study their autophagy activity at distinct myogenic stages. We describe different experimental strategies for autophagy flux determination by either flow cytometry or immunofluorescence in quiescent SCs and their activated and proliferating progeny. These methods provide the scientific community with useful approaches for assessing autophagy in scenarios in which autophagy is genetically altered or in aging and disease conditions.

DATA AVAILABILITY STATEMENT

The raw data supporting the conclusions of this article will be made available by the authors, without undue reservation.

ETHICS STATEMENT

This study was carried out in accordance with the EU Directive 86/609/EEC and approved by the National and Regional Animal Care and Ethics Committees.

AUTHOR CONTRIBUTIONS

SC and IR-P performed the experimental work. SC, IR-P, and PM-C wrote the manuscript. SC, IR-P, and XH assembled the figures. SC, JI, and PM-C supervised the manuscript. PM-C approved the final version of the manuscript. All the authors contributed to the data analysis and interpretation and discussed the results.

FUNDING

Work in the authors' laboratory has been supported by MINECO-Spain (RTI2018-096068), ERC-2016-AdG-741966, LaCaixa-HEALTH-HR17-00040, MDA, Fundació LaMarató/TV3, MDA, UPGRADE-H2020-825825, AFM and DPP-Spain, as well as María-de-Maeztu-Program for Units of Excellence to UPF (MDM-2014-0370), Severo-Ochoa-Program for Centers of Excellence to CNIC (SEV-2015-0505). SC was supported by a Predoctoral Fellowship from Ayudas para la formación y contratación de personal investigador novel (FI) – AGAUR (Barcelona, Spain), IR-P was supported by a Predoctoral Fellowship from Programa de Formación de Personal Investigador (Spain), and XH was supported by a Severo-Ochoa Pre-doctoral Fellowship (Spain).

ACKNOWLEDGMENTS

We thank L. García-Prat for initial protocol set-up, G. Mariño for the GFP-LC3 transgenic mouse strain, A. Pollán and J. Ballestero for technical support, and the Microscopy and Cellomic facilities at CNIC for their support.

REFERENCES

Chang, N. C., Sincennes, M.-C., Chevalier, F. P., Brun, C. E., Lacaria, M., Segalés, J., et al. (2018). The Dystrophin Glycoprotein Complex Regulates the Epigenetic Activation of Muscle Stem Cell Commitment. *Cell Stem Cell* 22, 755–768.e6. doi: 10.1016/j.stem.2018.03.022

Dumont, N. A., Wang, Y. X., von Maltzahn, J., Pasut, A., Bentzinger, C. F., Brun, C. E., et al. (2015). Dystrophin expression in muscle stem cells regulates their polarity and asymmetric division. *Nat. Med.* 21, 1455–1463. doi: 10.1038/nm.3990

Evano, B., and Tajbakhsh, S. (2018). Skeletal muscle stem cells in comfort and stress. *NPJ Regen. Med.* 3, 1–13. doi: 10.1038/s41536-018-0062-3

Feige, P., Brun, C. E., Ritso, M., and Rudnicki, M. A. (2018). Orienting Muscle Stem Cells for Regeneration in Homeostasis, Aging, and Disease. *Cell Stem Cell* 23, 653–664. doi: 10.1016/j.stem.2018.10.006

Fiacco, E., Castagnetti, F., Bianconi, V., Madaro, L., De Bardi, M., Nazio, F., et al. (2016). Autophagy regulates satellite cell ability to regenerate normal and dystrophic muscles. *Cell Death Differ.* 23, 1839–1849. doi: 10.1038/cdd.2016.70

García-Prat, L., Martínez-Vicente, M., Perdiguero, E., Ortet, L., Rodríguez-Ubreva, J., Rebollo, E., et al. (2016). Autophagy maintains stemness by preventing senescence. *Nature* 529, 37–42. doi: 10.1038/nature16187

Hara, T., Nakamura, K., Matsui, M., Yamamoto, A., Nakahara, Y., Suzuki-Migishima, R., et al. (2006). Suppression of basal autophagy in neural cells causes neurodegenerative disease in mice. *Nature* 441, 885–889. doi: 10.1038/nature04724

Joe, A. W. B., Yi, L., Natarajan, A., Le Grand, F., So, L., Wang, J., et al. (2010). Muscle injury activates resident fibro/adipogenic progenitors that facilitate myogenesis. *Nat. Cell Biol.* 12, 153–163. doi: 10.1038/ncb2015

Kabeya, Y. (2004). LC3, GABARAP and GATE16 localize to autophagosomal membrane depending on form-II formation. *J. Cell Sci.* 117, 2805–2812. doi: 10.1242/jcs.01131

Kirkin, V., and Rogov, V. V. (2019). A Diversity of Selective Autophagy Receptors Determines the Specificity of the Autophagy Pathway. *Mol. Cell* 76, 268–285. doi: 10.1016/j.molcel.2019.09.005

Klionsky, D. J. (2005). Autophagy. *Curr. Biol.* 15, 282–283. doi: 10.1016/j.cub.2005.04.013

Klionsky, D. J., Codogno, P., Cuervo, A. M., Deretic, V., Elazar, Z., Fueyo-Margareto, J., et al. (2010). A comprehensive glossary of autophagy-related molecules and processes. *Autophagy* 6, 438–448. doi: 10.4161/auto.6.4.12244

Komatsu, M., Waguri, S., Chiba, T., Murata, S., Iwata, J., Tanida, I., et al. (2006). Loss of autophagy in the central nervous system causes neurodegeneration in mice. *Nature* 441, 880–884. doi: 10.1038/nature04723

Kroemer, G., Mariño, G., and Levine, B. (2010). Autophagy and the Integrated Stress Response. *Mol. Cell* 40, 280–293. doi: 10.1016/j.molcel.2010.09.023

Lee, Y. K., and Lee, J. A. (2016). Role of the mammalian ATG8/LC3 family in autophagy: Differential and compensatory roles in the spatiotemporal regulation of autophagy. *BMB Rep.* 49, 424–430. doi: 10.5483/BMBRep.2016.49.8.081

Liu, L., Cheung, T. H., Charville, G. W., Hurgo, B. M. C., Leavitt, T., Shih, J., et al. (2013). Chromatin Modifications as Determinants of Muscle Stem Cell Quiescence and Chronological Aging. *Cell Rep.* 4, 189–204. doi: 10.1016/j.celrep.2013.05.043

Liu, W. J., Ye, L., Huang, W. F., Guo, L. J., Xu, Z. G., Wu, H. L., et al. (2016). P62 Links the Autophagy Pathway and the Ubiqutin-Proteasome System Upon Ubiquitinated Protein Degradation. *Cell. Mol. Biol. Lett.* 21, 1–14. doi: 10.1186/s11658-016-0031-z

Machado, L., Esteves, de Lima, J., Fabre, O., Proux, C., Legendre, R., et al. (2017). In Situ Fixation Redefines Quiescence and Early Activation of Skeletal Muscle Stem Cells. *Cell Rep.* 21, 1982–1993. doi: 10.1016/j.celrep.2017.10.080

Mauro, A. (1961). Satellite cell of skeletal muscle fibers. *J. Biophys. Biochem. Cytol.* 9, 493–495. doi: 10.1083/jcb.9.2.493

Mauvezin, C., Nagy, P., Juhász, G., and Neufeld, T. P. (2015). Autophagosome-lysosome fusion is independent of V-ATPase-mediated acidification. *Nat. Commun.* 6:7007. doi: 10.1038/ncomms8007

Mizushima, N., and Komatsu, M. (2011). Autophagy: Renovation of cells and tissues. *Cell* 147, 728–741. doi: 10.1016/j.cell.2011.10.026

Mizushima, N., Yamamoto, A., Matsui, M., Yoshimori, T., and Ohsumi, Y. (2004). In Vivo Analysis of Autophagy in Response to Nutrient Starvation Using Transgenic Mice Expressing a Fluorescent Autophagosome Marker. *Mol. Biol. Cell* 15, 1101–1111. doi: 10.1091/mbc.e03-09-0704

Mizushima, N., Yoshimori, T., and Levine, B. (2010). Methods in Mammalian Autophagy Research. *Cell* 140, 313–326. doi: 10.1016/j.cell.2010.01.028

Ollion, J., Cochennec, J., Loll, F., Escudé, C., and Boudier, T. (2013). TANGO: A generic tool for high-throughput 3D image analysis for studying nuclear organization. *Bioinformatics* 29, 1840–1841. doi: 10.1093/bioinformatics/btt276

Pasut, A., Oleynik, P., and Rudnicki, M. A. (2012). Isolation of Muscle Stem Cells by Fluorescence Activated Cell Sorting Cytometry. *Methods Mol Biol.* 798, 53–64. doi: 10.1007/978-1-61779-343-1_3

Pyo, J. O., Nah, J., and Jung, Y. K. (2012). Molecules and their functions in autophagy. *Exp. Mol. Med.* 44, 73–80. doi: 10.3858/emm.2012.44.2.029

Seale, P., Ishibashi, J., Scimè, A., and Rudnicki, M. A. (2004). Pax7 is necessary and sufficient for the myogenic specification of CD45+:Sca1+ stem cells from injured muscle. *PLoS Biol.* 2:E130. doi: 10.1371/journal.pbio.0020130

Sherwood, R. I., Christensen, J. L., Conboy, I. M., Conboy, M. J., Rando, T. A., Weissman, I. L., et al. (2004). Isolation of adult mouse myogenic progenitors: Functional heterogeneity of cells within and engrafting skeletal muscle. *Cell* 119, 543–554. doi: 10.1016/j.cell.2004.10.021

Solanas, G., Peixoto, F. O., Perdiguero, E., Jardí, M., Ruiz-Bonilla, V., Datta, D., et al. (2017). Aged Stem Cells Reprogram Their Daily Rhythmic Functions to Adapt to Stress. *Cell* 170, 678–692.e. doi: 10.1016/j.cell.2017.07.035

Sousa-Victor, P., Gutarra, S., García-Prat, L., Rodriguez-Ubreva, J., Ortet, L., Ruiz-Bonilla, V., et al. (2014). Geriatric muscle stem cells switch reversible quiescence into senescence. *Nature* 506, 316–321. doi: 10.1038/nature13013

Tang, A. H., and Rando, T. A. (2014). Induction of autophagy supports the bioenergetic demands of quiescent muscle stem cell activation. *EMBO J.* 33, 2782–2797. doi: 10.15252/embj.201488278

van Velthoven, C. T. J., de Morree, A., Egner, I. M., Brett, J. O., and Rando, T. A. (2017). Transcriptional Profiling of Quiescent Muscle Stem Cells In Vivo. *Cell Rep.* 21, 1994–2004. doi: 10.1016/j.celrep.2017.10.037

Yang, Y. P., Hu, L. F., Zheng, H. F., Mao, C. J., Hu, W. D., Xiong, K. P., et al. (2013). Application and interpretation of current autophagy inhibitors and activators. *Acta Pharmacol. Sin.* 34, 625–635. doi: 10.1038/aps.2013.5

Conflict of Interest: The authors declare that the research was conducted in the absence of any commercial or financial relationships that could be construed as a potential conflict of interest.

frontiers in Cell and Developmental Biology

ORIGINAL RESEARCH
published: 05 February 2021
doi: 10.3389/fcell.2021.629182

Anti-tumor Effect of Oleic Acid in Hepatocellular Carcinoma Cell Lines *via* Autophagy Reduction

Federico Giulitti, Simonetta Petrungaro, Sara Mandatori†, Luana Tomaipitinca†, Valerio de Franchis, Antonella D'Amore, Antonio Filippini, Eugenio Gaudio, Elio Ziparo and Claudia Giampietri**

Department of Anatomical, Histological, Forensic Medicine, and Orthopedic Sciences, Sapienza University of Rome, Rome, Italy

OPEN ACCESS

Edited by:
Lucia Latella, Italian National Research Council, Italy

Reviewed by:
Emanuele Berardi, Universiteit Hasselt, Belgium
Laura Belloni, Sapienza University of Rome, Italy

***Correspondence:**
Claudia Giampietri
claudia.giampietri@uniroma1.it
Antonio Filippini
antonio.filippini@uniroma1.it

†Present address:
Sara Mandatori, Neuroinflammation Unit, Faculty of Health and Medical Sciences, Biotech Research and Innovation Centre (BRIC), Copenhagen Biocentre, University of Copenhagen, Copenhagen, Denmark
Luana Tomaipitinca, Department of Molecular Medicine, Sapienza University of Rome, Laboratory Affiliated to Istituto Pasteur Italia - Fondazione Cenci Bolognetti, Rome, Italy

Specialty section:
This article was submitted to Cell Death and Survival, a section of the journal Frontiers in Cell and Developmental Biology

Received: *13 November 2020*
Accepted: *14 January 2021*
Published: *05 February 2021*

Citation:
Giulitti F, Petrungaro S, Mandatori S, Tomaipitinca L, de Franchis V, D'Amore A, Filippini A, Gaudio E, Ziparo E and Giampietri C (2021) Anti-tumor Effect of Oleic Acid in Hepatocellular Carcinoma Cell Lines via Autophagy Reduction. Front. Cell Dev. Biol. 9:629182. doi: 10.3389/fcell.2021.629182

Oleic acid (OA) is a component of the olive oil. Beneficial health effects of olive oil are well-known, such as protection against liver steatosis and against some cancer types. In the present study, we focused on OA effects in hepatocellular carcinoma (HCC), investigating responses to OA treatment (50–300 μM) in HCC cell lines (Hep3B and Huh7.5) and in a healthy liver-derived human cell line (THLE-2). Upon OA administration higher lipid accumulation, perilipin-2 increase, and autophagy reduction were observed in HCC cells as compared to healthy cells. OA in the presence of 10% FBS significantly reduced viability of HCC cell lines at 300 μM through Alamar Blue staining evaluation, and reduced cyclin D1 expression in a dose-dependent manner while it was ineffective on healthy hepatocytes. Furthermore, OA increased cell death by about 30%, inducing apoptosis and necrosis in HCC cells but not in healthy hepatocytes at 300 μM dosage. Moreover, OA induced senescence in Hep3B, reduced P-ERK in both HCC cell lines and significantly inhibited the antiapoptotic proteins c-Flip and Bcl-2 in HCC cells but not in healthy hepatocytes. All these results led us to conclude that different cell death processes occur in these two HCC cell lines upon OA treatment. Furthermore, 300 μM OA significantly reduced the migration and invasion of both HCC cell lines, while it has no effects on healthy cells. Finally, we investigated autophagy role in OA-dependent effects by using the autophagy inducer torin-1. Combined OA/torin-1 treatment reduced lipid accumulation and cell death as compared to single OA treatment. We therefore concluded that OA effects in HCC cells lines are, at least, in part dependent on OA-induced autophagy reduction. In conclusion, we report for the first time an autophagy dependent relevant anti-cancer effect of OA in human hepatocellular carcinoma cell lines.

Keywords: lipid droplets, autophagy, fatty acids, cell death, cancer

INTRODUCTION

In the last years different research groups investigated the relationships between fatty acids and solid tumors. Fatty acids are major components of biological membranes and play important roles in the intracellular signaling pathways. They are chemically classified as saturated and unsaturated (monounsaturated and polyunsaturated) fatty acids and their structure affects their biological effects. One of the most abundant fatty acid is the monounsaturated fatty

acid Oleic Acid (OA), representing the main component of olive oil (70–80%). Olive oil has beneficial effects in counteracting liver steatosis and cardiovascular diseases (Perez-Martinez et al., 2011; Perdomo et al., 2015; Zeng et al., 2020). OA effects on cancer cells are not completely elucidated although they seem to be different depending on cancer cell types (Sales-Campos et al., 2013; Maan et al., 2018). Upon OA administration in *in vitro* set up, lipid droplets (LD) formation occurs within the cells (Rohwedder et al., 2014) and inside these compartments neutral lipids are concentrated with mechanisms still largely unclear (Fujimoto et al., 2006). Most eukaryotic cells can store excess neutral lipids within LD (consisting mainly of triglycerides and cholesteryl esters), and release them when necessary, depending on cellular needs. This property is particularly important in cells exposed to feeding periods followed by starvation periods, such as cancer cells (Jarc and Petan, 2019). In the present study we investigated *in vitro* the effects of OA in HCC models. Previous works have shown that OA treatment leads to a massive lipid accumulation in hepatocytes cell lines (i.e., LO2 and HepG2 cells) associated with cell viability reduction (Yao et al., 2011). We tested whether OA affects lipid accumulation, autophagy and cell death in different HCC cell lines compared to immortalized healthy hepatocytes. Autophagy is a catabolic process essential to maintain cellular homeostasis; it allows the turnover of cellular components including LD (Giampietri et al., 2017). In the autophagy-mediated lipolytic process, LD are associated with the autophagosome protein microtubule-associated protein light chain 3 (LC3) and then are delivered to lysosomes (Singh et al., 2009). Therefore, autophagy plays a crucial role in LD degradation regulating fatty acids mobilization. On the contrary, autophagy impairment, achieved by genetic knockdown of autophagy genes (i.e., atg5 or atg7), significantly increases hepatic lipid stores (Amir and Czaja, 2011). Autophagy is the main cellular response to nutrients deprivation (Denton et al., 2012) and plays a dual role in neoplastic transformations (Mizushima, 2007; D'Arcangelo et al., 2018). Autophagy upregulation under chemotherapy treatment may increase cancer cell survival (Ding et al., 2011). Autophagy inhibition leads to cell death promotion and cell growth inhibition, and its activation induces cell proliferation in HCC (Chava et al., 2017). For such reasons inhibiting the autophagy pathways might be crucial to induce cancer cell death (Tomaipitinca et al., 2019). Relatively little is known about the molecular mechanisms underlying the OA effects in liver cancer cells and the role of autophagy (Li et al., 2014; Maan et al., 2018). Evidences exist showing an inverse relation in liver between levels of autophagy and perilipin-2, a constitutive protein of LD. High levels of Perilipin-2 inhibit LD degradation by decreasing autophagy while perilipin-2 deficiency increases autophagy leading to LD breakdown (Singh et al., 2009; Sanchez-Martinez et al., 2015; Tsai et al., 2017). Further evidences demonstrated a direct relationship between OA and perilipin-2 accumulation in tumors such as glioblastoma, confirming the relationship between OA and LD storage (Taib et al., 2019). Conversely, the role LD store plays on controlling HCC growth is still partially unknown. In the present work we investigated LD accumulation in HCC cell lines (Hep3B and Huh7.5) vs. immortalized healthy hepatocytes (THLE-2) after OA treatment, with a focus on autophagy role. We report an anti-tumor action of OA in HCC and a specific OA effect on lipid accumulation, viability, proliferation, migration and invasion, at least partially dependent on reduced autophagy.

MATERIALS AND METHODS

Cells Culture and Reagents

Hep3B and Huh7.5 cell lines were kindly donated by Professor Maria Rosa Ciriolo "Tor Vergata" University of Rome.

The two HCC cell lines display respectively deletion (i.e., Hep3B) or point p53 mutation (i.e., Huh7.5) as tumor suppressor *p53* is one of the most frequently mutated genes in liver cancer (Rebouissou and Nault, 2020). Cells were cultured in DMEM (Gibco-Invitrogen, Carlsbad, CA, USA) containing high glucose enriched with 10% fetal bovine serum, glutamine (2 mmol/l), in presence of penicillin (100 U/ml) and streptomycin (100 μg/ml). Cells were maintained at 37°C in a humidified 5% CO_2 atmosphere. OA was purchased from Sigma-Aldrich (Milano, Italy) and diluted with 0.1% NaOH, 10% delipidated BSA (Sigma-Aldrich).

Control cell line (THLE-2) was purchased from the American Type Culture Collection (ATCC, Manasses, VA, USA). THLE-2 cells show phenotypic characteristics of normal adult hepatocytes, are non-tumorigenic when injected into athymic nude mice and do not express alpha-fetoprotein (Pfeifer et al., 1993). THLE-2 were cultured with BEGM Bullet Kit (Catalog No. CC-3170) from Lonza (East Rutherford, NJ, USA). The Bullet Kit contains BEBM Basal Medium (CC-3171 Lonza) and supplements. The final growth medium consists of BEBM supplemented with 10% FCS, bovine pituitary gland extract, hydrocortisone, epidermal growth factor (EGF), insulin, triiodothyronine, transferrin, retinoic acid, 6 ng/ml human recombinant EGF (Sigma-Aldrich) and 80 ng/ml o-phosphorylethanolamine (Sigma-Aldrich). THLE-2 cells require a special flask coating medium that consists of the following reagents: a mixture of 0.01 mg/mL fibronectin from human plasma (Sigma-Aldrich), 0.03 mg/mL bovine collagen type I (Sigma-Aldrich) and 0.01 mg/mL bovine serum albumin (Sigma-Aldrich) in BEBM medium.Before seeding, 3 ml of coating medium for a T-75 flask and 1 ml of coating medium for one 6-well plate were applied for 2 min and then aspirated.

ATCC guidelines for culturing THLE-2 are available at: https://www.lgcstandards-atcc.org/products/all/CRL-2706.aspx?geo_country=it#culturemethod.

Hep3B, Huh7.5 and THLE-2 cells were cultured in T-75 flasks and experiments were performed in 6-well plates. The day after plating, cells were treated with OA at different concentration (50, 150, and 300 μM OA) for the indicated time. Bafilomycin A1 was purchased from Sigma-Aldrich and was used at 100 nM during the last 3 h treatment. Torin-1 was purchased from (Tocris, Bristol, UK) and was used during the last 4 h treatment at the concentration of 250 nM for Hep3B and 500 nM for Huh7.5 cell lines.

Western Blotting

Cells were washed two times with pre-chilled PBS (Phosphate Buffered Saline) purchased from Sigma-Aldrich and lysed. Lysis Buffer 10x (Cell Signaling, Danvers, MA, USA) was diluted

in the presence of 2% SDS (Sodium Dodecyl Sulfate) and proteases' inhibitors (Sigma-Aldrich). Lysates were also sonicated through a sonicator (Branson, Danbury, USA) for 10 s at 50% amplitude. Lysates were then incubated for 10 min on ice and then centrifuged at 4°C for 15 min at 14,000 g to remove cell debris.

Protein concentration was determined by micro BCA assay (Pierce, Thermo Scientific, Rockford, IL, USA) and samples were boiled at 95°C for 5 min following Laemmli Buffer addition (0,04% Bromophenol blue, 40% Glycerol, 2% SDS, 20% ß-mercaptoethanol, 250 mM Tris HCl pH.6.8, all purchased from Sigma-Aldrich) (Giampietri et al., 2006).

Proteins were separated by SDS–PAGE and transferred on Polyvinylidene fluoride (PVDF) or Nitrocellulose membranes (Amersham Bioscience, Piscataway, NJ, USA). Membranes were probed using the following antibodies: anti-β-Actin-HRP (Sigma-Aldrich 1:10,000); anti-Tubulin (Sigma-Aldrich 1:10,000); anti-LC3 (Cell Signaling 1:1,000); anti-Perilipin-2 (Sigma-Aldrich 1:500); anti-Cleaved caspase-3 (Cell Signaling 1:700); anti-PARP (Cell Signaling 1:1,000); anti-pERK (Cell Signaling 1:1,000); anti-ERK2 (Santa Cruz, Santa Cruz, CA, USA 1:1,000); anti-Bcl-2 (Santa Cruz 1:500); anti-Flip (Cell Signaling 1:1,000); anti-Cyclin D1 (Santa Cruz 1:500); anti-PCNA (Santa Cruz 1:500); anti-Srebp-1 (Santa Cruz sc-13551 1:50); anti PPAR-gamma (Cell Signaling 2443 1:500).

Secondary antibodies were horseradish peroxidase-conjugated anti-mouse or anti-rabbit (Bio-Rad, Hercules, CA, USA). Membranes were washed with Tris-buffered saline (Medicago, Uppsala, Sweden) with 0.1% Tween-20 (Sigma-Aldrich) and developed through the chemiluminescence system (Amersham Bioscience) on the ChemiDoc image analyser (Bio-Rad, Hercules, CA, USA), Image lab software was used for densitometric quantifications.

Oil-Red O Staining

Briefly, a stock oil red solution was prepared diluting 0.7 g Oil Red O with 200 mL isopropanol. A working dilution was then obtained by mixing 6 parts Oil-Red O stock with 4 parts dH_2O. Cells were fixed with 10% formalin 5 min at room temperature. Then fresh formalin was added and incubated 1 h. After formalin removal, cells were washed with 60% isopropanol 5 min at room temperature. After isopropanol removal, oil red working solution was added for 10 min. Cells were then washed with H_2O and analyzed immediately by light microscopy. The Axioskop 2 plus microscope (Carl Zeiss Microimaging, Inc., Milan, Italy) was used. Images were obtained at room temperature using AxioCamHRC camera (Carl Zeiss Microimaging, Inc.) by Axiovision software (version 3.1, Carl Zeiss Microimaging, Inc.). Then, the stained lipid droplets were dissolved in 1.5 ml 100% isopropanol 5 min at room temperature and the absorbance was measured at 500 nm to quantify neutral lipid accumulation.

Alamar Blue Assay

Alamar blue assay was performed using Resazurin sodium salt solution (Sigma-Aldrich). Cells were cultured and treated in 96-well plates as previously described, washed and then Resazurin sodium salt solution was added for 4 h. The solution was collected and detected using a luminometer (Promega, Madison, WIS, USA) using 580–640 nm emission filter and 520 nm excitation filter.

Cell Viability Assay

Cell viability was performed by counting cells in the presence of trypan blue. Cells were seeded on 6-well plates and incubated at 37°C in 5% CO_2 overnight, then treated with different doses of OA. After OA incubation, cells were detached, volume mixed 1:1 with trypan blue and counted. The percentage of trypan blue positive-dead cells respect to the total cell number was expressed as the viability rate.

Flow Cytometry Cell Cycle and Cell Death Analysis

For cell cycle analysis, cells were treated with OA at a concentration of 300 μM for 48 h and then the cells were fixed with 70% ethanol, washed three times with PBS and stained for 3 h at room temperature with PBS containing 20 μg/mL RNase A and 50 μg/mL propidium iodide (PI). Around 10,000 cells were analyzed using a CyAn ADP flow cytometer (Beckman Coulter, Brea, CA, USA) and FCS express 5 (*De Novo* software, Glendale, CA, USA). The experiment was performed three times with consistent results.

Annexin Pacific Blue /PI kit (Termo Fisher Scientific, Rockford, IL, USA) was employed for the detection of percentage of cell death according to manufacturer's instructions. Cells were treated with OA at the different concentrations into a 6-well plate at the density of 1×10^5 cells/well for 24 h. Double staining was used to identify the cell membrane phosphatidylserine externalization and PI uptake. The results are from three independent experiments ($n = 3$). Samples were run on the CyAn ADP flow cytometer (Beckman Coulter) and analyzed with FlowJo software, version 10.5.3.

Wound-Healing Assay

To evaluate cell migration we performed the wound-healing assay using double well culture inserts (Ibidi GmbH, Martinsried, Germany). Each insert was placed in a 24-well plate, 3.5×10^4 cells were plated into both wells of each insert with 70 μL medium containing 10% FBS. When cells were confluent, the culture inserts were gently removed and cells were fed with 1% FBS DMEM (CTRL) or treated with OA 300 μM (in the presence of 1% FBS DMEM). Each well was photographed at 10× magnification immediately after insert removal, for the measurement of the wound (cell-free) area (T0 area considered as 100%), and after 24 and 48 h with a Nikon DS-Fi1 camera (Nikon Corporation, Tokyo, Japan). The mean percentage of residual open area compared with the respective cell-free space taken at T0 was calculated using ImageJ v 1.47 h software. For each experimental condition, three independent experiments were performed.

Invasion Assay

To determine the invasion ability of HCC cell lines, transwell membrane filters (8 μM pore size) (Falcon, Corning, NY, USA) coated by reduced growth factor matrigel (BD, Franklin Lakes,

NJ, USA) were used. 1×10^5 cells were seeded in the upper chamber with 1% FBS medium, 20% FBS medium was added to the bottom chamber. Following 48 h incubation, the cells were removed from the top surface of the membrane. The invasive cells adhering to the bottom surface of the membrane were fixed using 4% paraformaldehyde (Electron Microscopy Sciences, Hatfield, PA, USA) and stained with 600 nM DAPI (Thermo Fisher Scientific, Rockford, IL, USA). The total number of DAPI-stained nuclei of invading cells were counted under a fluorescence microscopy by using ImageJ software in five randomly chosen macroscopic fields per membrane. Each experiment was performed in triplicate and was repeated at least three times.

β-galactosidase Assay

All the experiments were performed using the beta-galactosidase staining kit according to manufacturer's instructions (Cell Signaling Technologies - USA, Danvers, MA).

Briefly, 100,000 cells were plated on 35 mm Petri dishes at 37°C in 5% CO_2 overnight, then treated with 300 μM OA for up to 48 h. Cells were fixed at 48 h, then 1 ml of beta-galactosidase staining solution was applied to each dish. Cells were incubated overnight in a dry, CO_2-free incubator, then were examined under light microscope at 200x magnification. For the quantification of β-galactosidase positive cells, a score from 1 to 3 was assigned to each cell based on color intensity. The average of the scores of three microscopic fields from each Petri dish was calculated and the values were divided by the overall number of analyzed cells. Each experiment was performed in triplicate and was repeated at least three times.

Statistical Analysis

All the experiments were repeated at least 3 times. Statistical analysis was performed using Prism software (GraphPad). Values are expressed as mean, with individual experiments data points plotting. The statistical significance was determined performing unpaired Student *t*-tests or One-Way Analysis of variance (ANOVA). Student's *t*-test was used for statistical comparison between means where appropriate (two groups) and One-Way

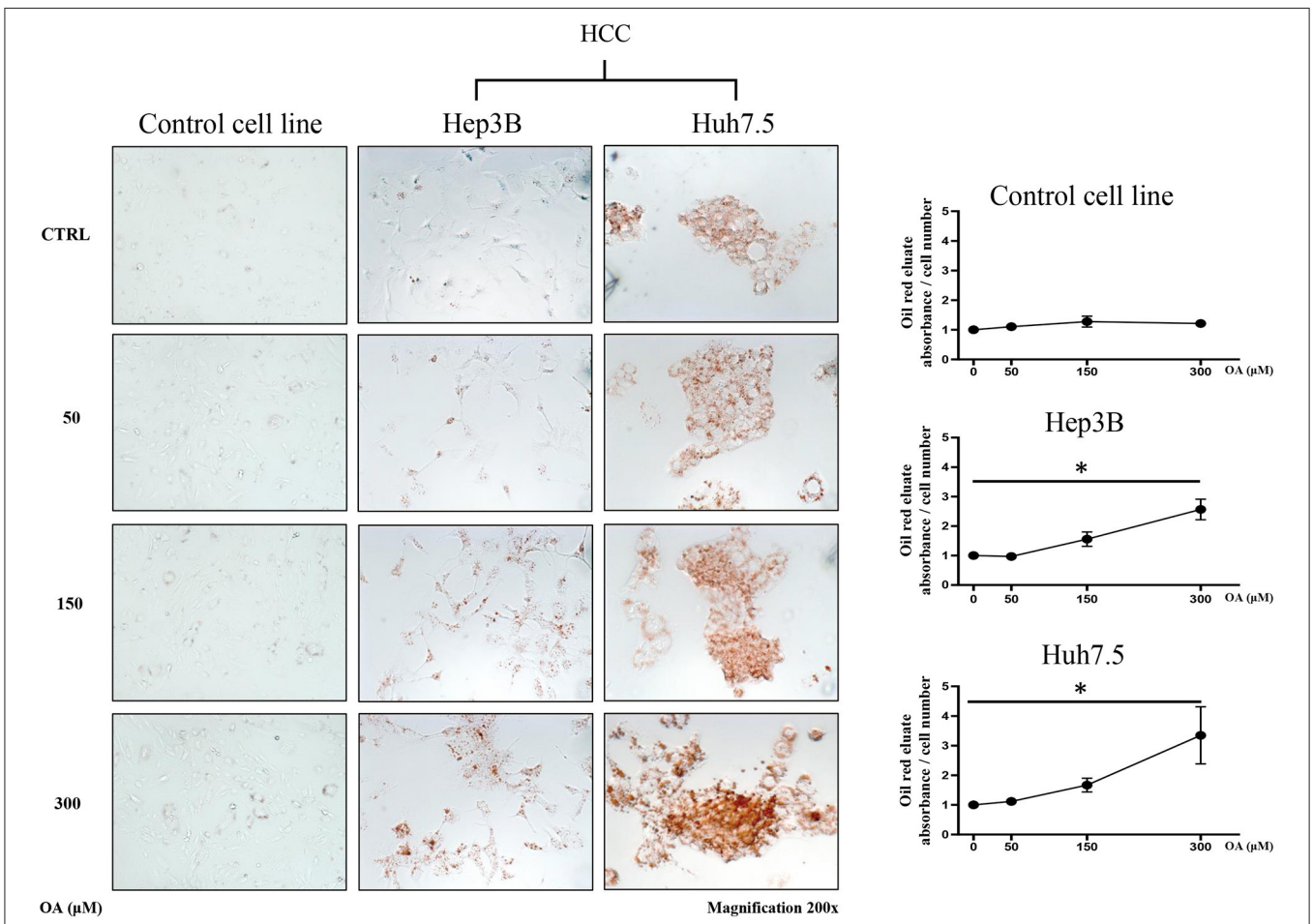

FIGURE 1 | Neutral lipid accumulation upon OA treatment. Control (THLE-2), Hep3B and Huh7.5 cell lines treated with OA. In the left panels: images of the three cell lines: Control, Hep3B and Huh7.5 stained with Oil-Red O after treatment with increasing doses of OA (50, 150, and 300 μM). In the right end panels: quantification of Oil-Red O eluates/cell number, upon treatment with increasing doses of OA ($n = 3$; $^*p < 0.05$).

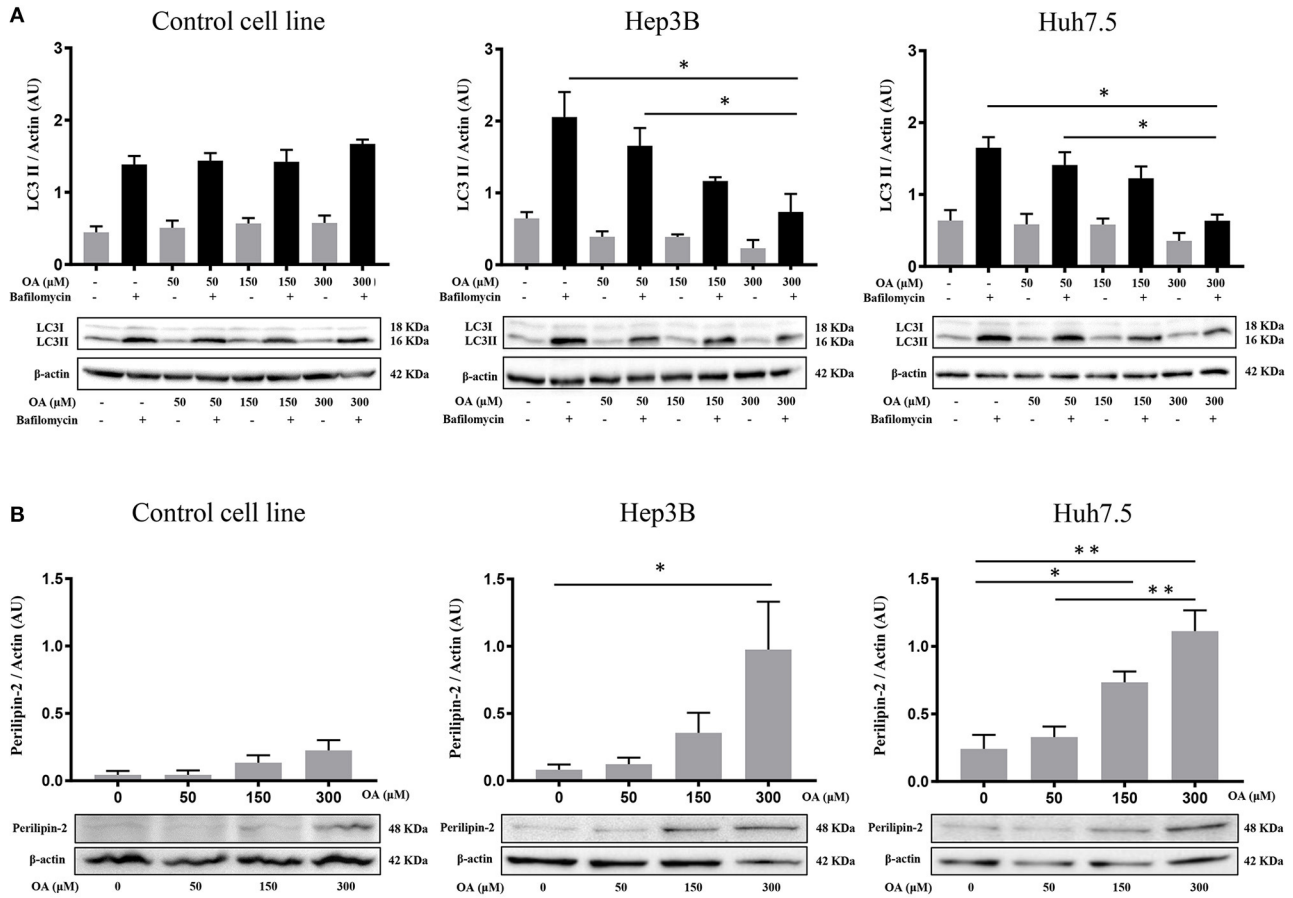

FIGURE 2 | Autophagic flux and perilipin-2 modulation upon OA treatment in Hep3B, Huh7.5 and THLE-2 cell lines. **(A)** Control (THLE-2), Hep3B and Huh7.5 and cell lines treated with OA increasing doses in the presence of bafilomycin A1. LC3II quantification reveals a significant reduction of autophagic flux upon high OA doses in both HCC cell lines, but not in the healthy hepatocyte cell line. **(B)** Western blot analyses for perilipin-2, were performed. Perilipin-2 levels in both HCC cell lines are increased in a dose dependent manner, while in Control cells perilipin-2 levels do not significantly increase upon 48 h OA treatment ($n = 3$; $^{*}p < 0.05$; $^{**}p < 0.01$).

ANOVA (three or more groups); $P \leq 0.05$ was considered statistically significant.

RESULTS

Lipid Accumulation Induced by OA Administration

In order to evaluate the involvement of OA in the modulation of neutral lipid accumulation in human hepatocellular carcinoma and hepatocyte cell lines, we treated Control cell line (THLE-2), Hep3B and Huh7.5 with increasing doses of OA (50, 150, and 300 μM). Upon 24 h treatment, cells were fixed and stained with Oil-Red O dye, which binds neutral lipids, such as triglycerides and cholesterol esters. As shown by optical microscopy analyses, the treatment with increasing doses of OA induced a consistent relevant and dose-dependent Oil-Red O accumulation compared to the basal level into the cytoplasm of both HCC cell lines. Only a slight Oil-Red O staining increase was observed in the control cell line (**Figure 1**). Oil-Red O quantification by eluate absorbance normalized by cell number, showed a dose dependent increase with a significant value at 300 μM OA vs. untreated cells in HCC.

Supplementary Figure 1 shows a similar increase of oil-red staining at 48 h, suggesting that there is not a delay in lipid accumulation, rather, a permanent increase is present in cancer cells at 24 and 48 h.

Autophagic Flux and Perilipin-2 Modulation Upon OA Treatment

Since autophagy is known to be involved in tumor metabolism and in LD break-down, we investigated OA effect on autophagy. We treated Control, Hep3B, Huh7.5 with increasing doses of OA and bafilomycin A1. The presence of bafilomycin A1 allows to evaluate the autophagic flux (Klionsky et al., 2016) by blocking the fusion between autophagosome and lysosome and inducing autophagosomes accumulation. As shown in **Figure 2A**, increasing doses of OA reduce the autophagic flux in a dose dependent manner, in both HCC cell lines. On the contrary, in the control cell line (THLE-2) OA shows no effect. We speculate that the reduction observed in **Figure 2** on Hep3B

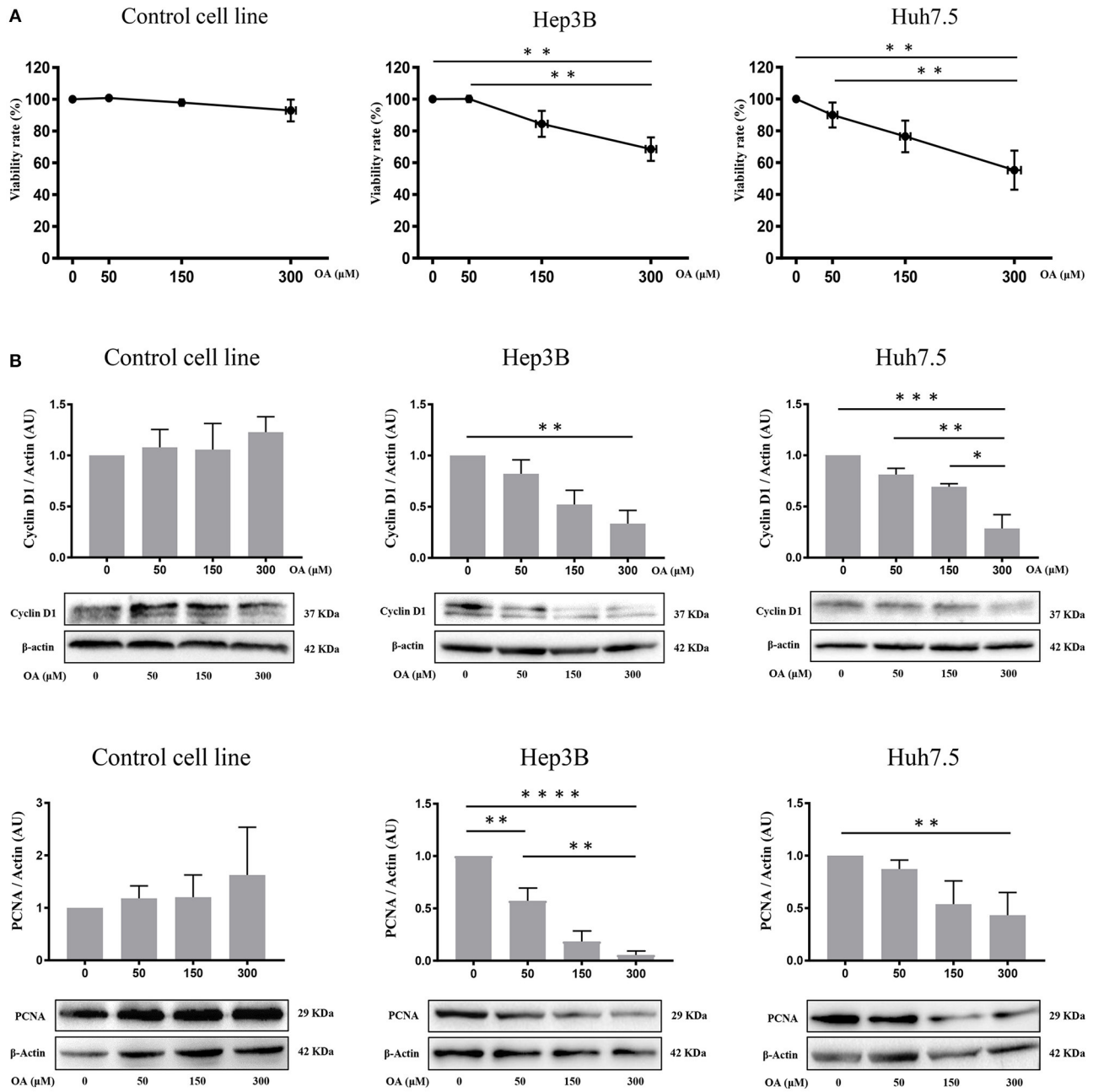

FIGURE 3 | OA reduces viability, cyclin D1 and PCNA in HCC cell lines. Cell viability assays and western blot analyses for Cyclin D1 and PCNA were performed. **(A)** OA induced a significant dose-dependent reduction of cellular viability in HCC cell lines but not in healthy hepatocyte cell line, measured by Alamar Blue assay. **(B)** Western blot Cyclin D1 and PCNA analyses showed that OA treatment induced a significant reduction of Cyclin D1 and PCNA levels in HCC cell lines, but not in healthy hepatocytes cell line ($n = 3$; $^{*}p < 0.05$; $^{**}p < 0.01$; $^{***}p < 0.001$; $^{****}p < 0.0001$).

and Huh7.5 may be associated with the parallel increase observed in **Figure 1**, while the lack of effect in control cell line is consistent in **Figures 1**, **2**. In order to better understand the relation between LD accumulation and autophagy, the levels of perilipin-2 were investigated by western blot analyses upon 48 h OA administration. Perilipin-2 is located in LD peripheral zone and its abundance is inversely related to autophagy level in liver (Tsai et al., 2017). In **Figure 2B** perilipin-2 levels in Control, Hep3B, and Huh7.5 cell lines are shown. 48 h OA treatment led to a significant and dose-dependent increase of perilipin-2 levels in both HCC cell lines. Metabolic and inflammation related targets (Zhong et al., 2018; Gnoni et al., 2019) were differently modulated in HCC cells as compared to control cells thus indicating that OA exerts different effects in healthy vs. HCC cells as a consequence of different lipid accumulation (**Supplementary Figure 2**).

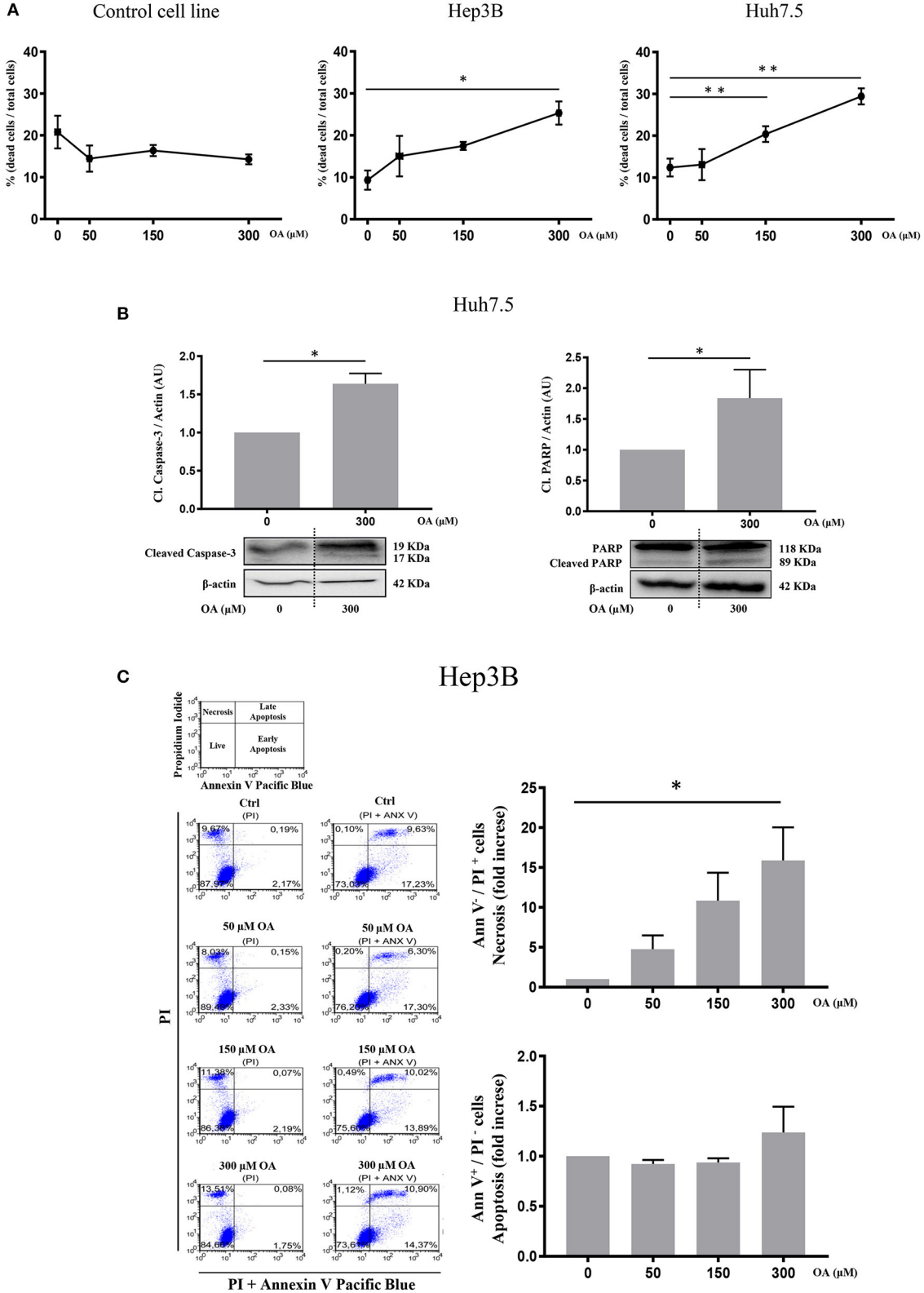

FIGURE 4 |

(Continued)

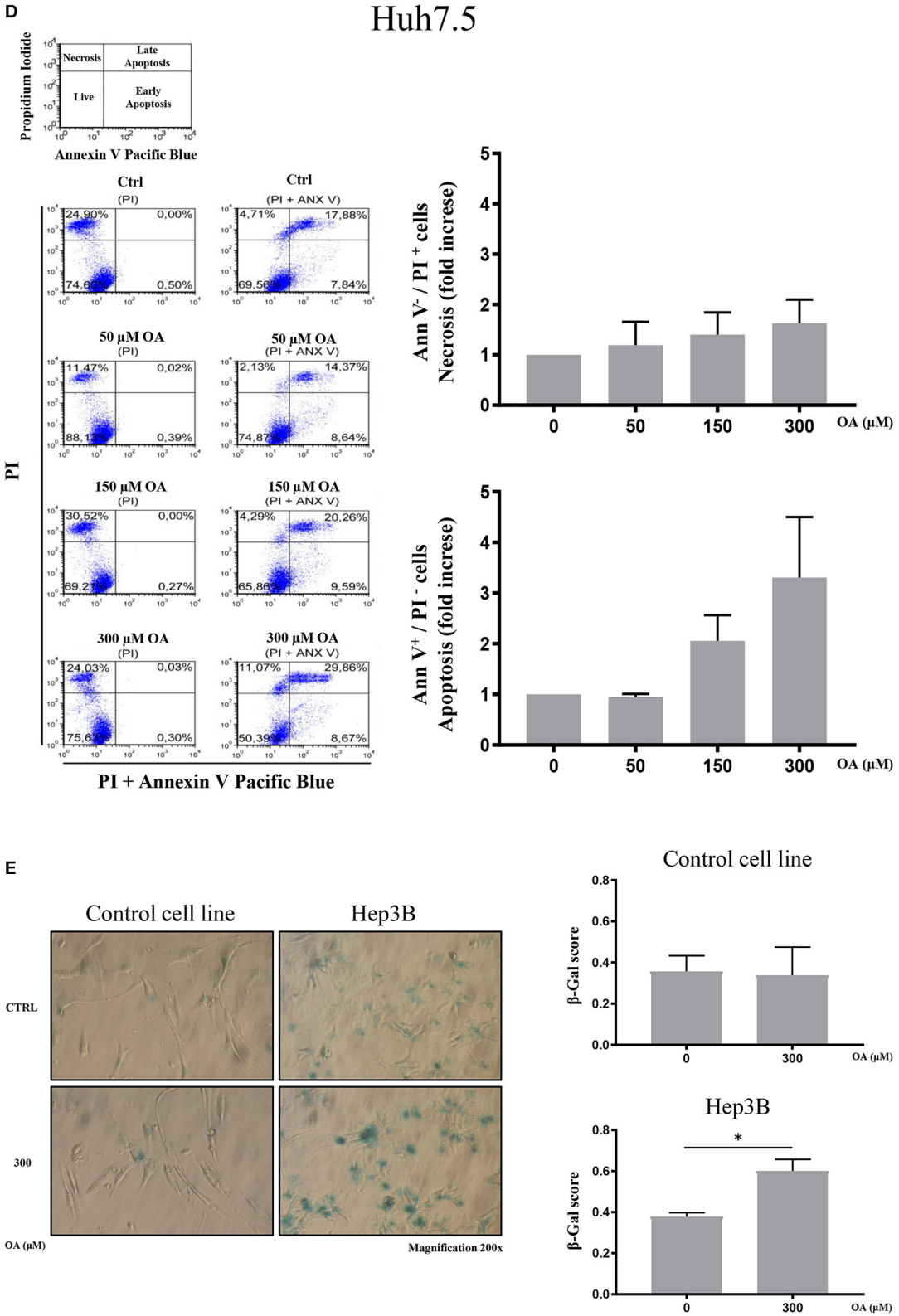

FIGURE 4 | OA increases cell death in HCC cell lines but not in healthy hepatocyte cell line. Dead/total cells percentage ratio, western blot analysis for the cleaved forms of caspase-3 and PARP, cytofluorimetric analysis for Ann V/PI as well as β-galactosidase staining were performed. **(A)** Trypan blue staining showed that OA treatment induced cell death in both HCC cell lines, but not in healthy hepatocytes cell line. **(B)** Western blot analysis for the cleaved forms of caspase-3 and PARP

(Continued)

FIGURE 4 | proteins showed that 300 μM OA induced apoptotic cell death in Huh7.5 cell line. **(C,D)** Cytofluorimetric analysis for Ann V/PI staining of Hep3B and Huh7.5 cell lines cultured with different concentration of OA (50, 150, and 300 μM). The strategy of cytometric analysis is showed on the left: representative dot plots from five different experiments, by using PI staining alone for gating Ann V + / PI + cells. On the right, histograms of Ann V – / PI + necrotic cells (fold increase) of Hep3B and Huh7.5 cell lines showed that 300 μM OA significantly induces necrosis in Hep3B ($n = 3$; $^*p < 0.05$; $^{**}p < 0.01$). **(E)** β-galactosidase staining for Control cell line and Hep3B was performed. Images and graphs revealed that 300 μM OA treatment induced significant increase of senescence phenotype in Hep3B but not in Control ($n = 3$; $^*p < 0.05$).

These results show that OA treatment directly affects perilipin-2 expression in hepatocellular carcinoma cell lines, correlating with both neutral lipid accumulation and autophagic flux reduction.

Viability and Cell Death Upon OA Treatment

Control, Hep3B and Huh7.5 cells were treated with OA for 48 h to investigate OA effects on viability and cell death. Alamar Blue assay showed a specific dose-dependent reduction of cellular viability in both HCC cell lines (**Figure 3A**). Also, OA-dose-dependently reduced the expression of the proliferation markers cyclin D1 and PCNA in both HCC cell lines but not in healthy controls (**Figure 3B**).

Then, we evaluated cell death by trypan blue cell staining. Forty-eight hours OA treatment induced a significant cell death in both HCC cell lines, but not in the Control cell line (**Figure 4A**). Finally, we investigated two markers of the apoptotic pathway, namely, caspase-3 and PARP. Western blot analyses show that both Caspase-3 and PARP are activated by cleavage in Huh7.5 cell line upon 300 μM OA treatment (**Figure 4B**). Conversely in Hep3B and in Control cells no increase of the active form of Caspase-3 proteins has been observed. Nevertheless, a small sub-G1 population is observed through Flow Cytometry cell cycle analysis after PI staining, suggesting a week apoptotic response in Hep3B (**Supplementary Figure 3**).

We also carried out cytofluorimetric analyses with Annexin V-FITC/PI. As shown in **Figures 4C,D**, increasing doses of OA significantly increase necrosis in Hep3B but not in in Huh7.5. Necrosis appears as a dose dependent effect of OA treatment in Hep3B but not in Huh7.5. Finally, as shown in **Figure 4E**, 300 μM OA treatment significantly induced a senescence phenotype in Hep3B cell line, but not in Control cell line.

We therefore concluded that OA may induce cell death and senescence pathways in HCC cell lines.

p-ERK and Anti-apoptotic Proteins Modulation Upon OA Treatment

We then investigated p44/p42 MAPK (ERK1/2) phosphorylation after 48 h OA treatment since reduction of ERK phosphorylation in the Thr202/Tyr204 has been related to reduced proliferation and increased cell death (Hennig et al., 2010). Western blot analyses (**Figure 5A**) show that increasing OA concentrations dose-dependently reduce p-ERK in both HCC cell lines but not in the healthy controls.

To further investigate OA-induced cell death pathways, we treated Control, Hep3B and Huh7.5 cell lines for 48 h with 300 μM OA. Western blot analyses revealed that OA significantly down-regulated the expression of anti-apoptotic proteins c-Flip (**Figure 5B**) and Bcl-2 (**Figure 5C**) in both HCC cell lines but not in the heathy cells. These data highlight OA as a possible inducer of cell death processes in HCC by modulating cell death regulators (Tsujimoto et al., 1997; Giampietri et al., 2014). Our results are in agreement and extend previous results obtained in different cellular models showing Bcl-2 reduction upon OA treatment (Jiang et al., 2017).

OA Reduces Migration and Invasion of Both HCC Cell Lines

We then performed wound-healing assays to evaluate cell migration. Representative images are shown in **Figure 6** at different times after wound scratch. The percentage of uncovered area at different time points represents the different wound recovery ability of Control, Hep3B and Huh7.5 cell lines. Hep3B cells display higher ability to cover the plate as compared to Huh7.5. Such result is in agreement with previous data demonstrating higher Hep3B cell line aggressiveness as compared to other HCC cell lines (Slany et al., 2010; Qiu et al., 2015). OA (300 μM) significantly reduces the migration of both HCC cell lines (**Figures 6B,C**) as compared to healthy cells (**Figure 6A**). OA appears to be more potent on Hep3B cells, thus indicating the potential utility of OA in aggressive setup.

We then evaluated the OA effect on invasiveness in transwell invasion assays. As shown in **Figure 6D**, a significant 70-to-80% reduction of invasion after 300 μM OA treatment is observed in both HCC cell lines.

The Autophagy Activator Torin-1 Reduces OA-Induced Lipid Accumulation and Cell Death

We then further analyzed the autophagy under OA treatment. Hep3B and Huh7.5 cells were treated with OA combined with torin-1 in the presence of bafilomycin A1. As expected, combined OA/torin-1 treatment increases the autophagic marker LC3II in both HCC cell lines as compared to OA alone (**Figure 7A**). A significant reduction of neutral lipid accumulation was observed, as compared to single OA treatment in HCC cell lines (**Figure 7B**). Interestingly, the neutral lipid storage reduction parallels the significant cell death decrease (**Figure 7C**).

We concluded that OA-induced neutral lipid accumulation and cell death are both dependent on autophagy impairment since the combined OA/torin-1 treatment is able to reduce lipid accumulation and cell death; therefore, OA-dependent anti-tumor effects are dependent, at least in part, on autophagy reduction in HCC cell lines.

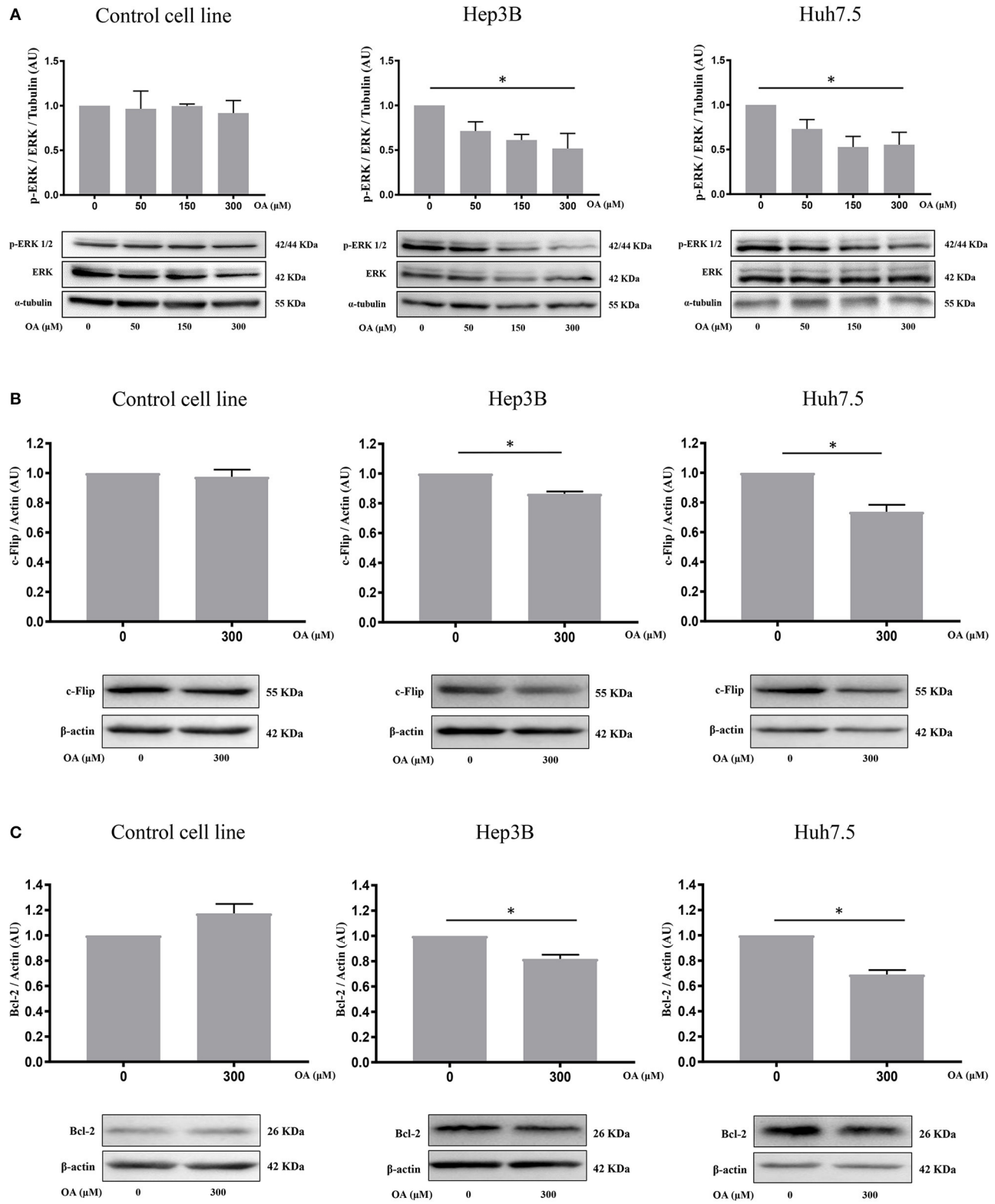

FIGURE 5 | OA significantly reduces ERK phosphorylation and anti-apoptotic proteins in HCC cell lines. **(A)** Western blot analyses show that p-ERK levels are significantly decreased upon 300 μM OA treatment in both HCC cell lines, but not in Control cell line. **(B)** c-Flip levels are significantly reduced in both HCC cell lines, but not in the healthy cells. **(C)** Bcl-2 protein expression is significantly decreased in both HCC cell lines but not in the healthy cells. ($n = 3$; $^*p < 0.05$).

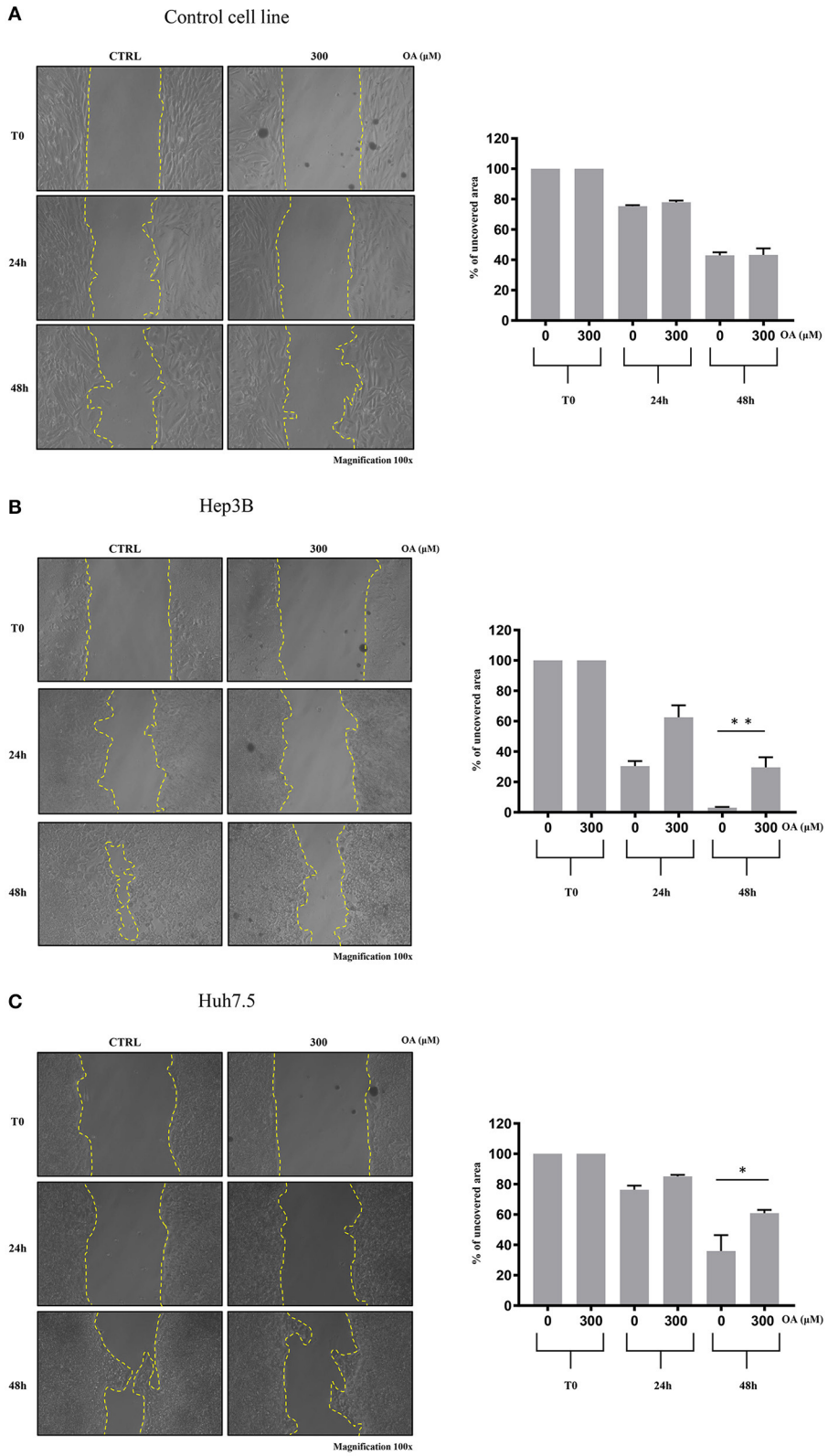

FIGURE 6 |

(Continued)

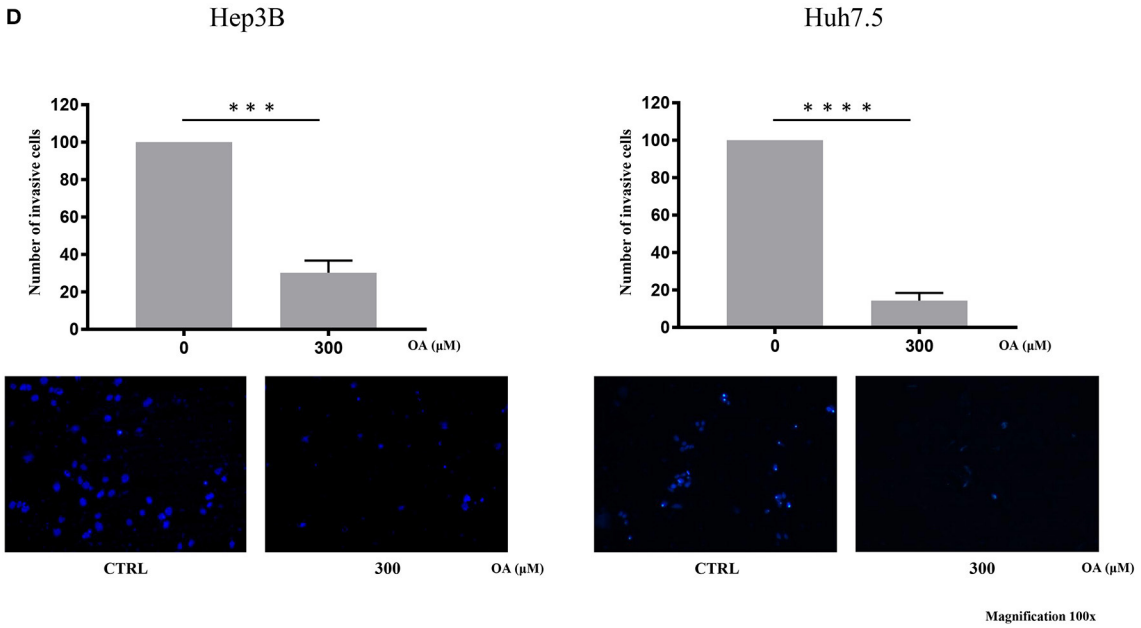

FIGURE 6 | OA reduces migration and invasion of both hepatocarcinoma cell lines. Wound-healing assay on Control **(A)**, Hep3B **(B)**, and Huh7.5 **(C)** cell lines were performed. Representative phase-contrast images wound-healing assay (scratch test) taken at different time points (0, 24, and 48 h) after 300 μM OA treatment are shown. Quantitative analysis of the percentage of uncovered area at 48 h revealed a statistical significance difference in both HCC cell lines after OA treatment, while no differences in Control cell line were observed upon OA treatment ($n = 3$; $^{*}p < 0.05$; $^{**}p < 0.01$). **(D)** Invasion assay of Hep3B and Huh7.5 cell lines was performed. Top: significant reduction of invading cells percentage after 48 h OA treatment in both HCC cell lines. Bottom: Representative images of Hep3b and Huh7.5 DAPI-stained nuclei after 300 μM OA treatment are shown ($n = 3$; $^{***}p < 0.001$; $^{****}p < 0.0001$).

DISCUSSION

In the last recent years different studies highlighted the role of lipids in tumor progression, namely, in hepatocellular carcinoma. This cancer type, like other tumors, exploits lipid reservoirs to promote its progression (Borchers and Pieler, 2010). OA displays important beneficial effects on the liver, by reducing hepatic steatosis and fibrogenesis. OA plays a positive role in the primary prevention of non-alcoholic fatty liver disease (NAFLD). Intake of monounsaturated fatty acids such as OA, may be beneficial for NAFLD patients, as opposed to the intake of carbohydrates, thus reducing the potential risk to develop HCC (Assy et al., 2009). In addition, the effects of OA in different cancer processes are well-known. OA promotes the growth of highly metastatic tumors (Li et al., 2014) while it induces cell death in low metastatic tumors (Carrillo et al., 2012). OA has been also shown to exert anti-cancer effects in tumors inducing lipotoxicity (Yao et al., 2011). In the present study we investigated the involvement of OA in counteracting HCC growth with a particular focus on autophagy. We addressed this issue on two different HCC cell lines vs. healthy hepatocytes. The two HCC cell lines differ in their morphology, growth and cisplatin sensitivity (Qin and Ng, 2002).

Since fatty acids are able to determine LD accumulation in HCC (Jarc and Petan, 2019), we evaluated neutral lipids and LD content. Surprisingly, we observed (**Figure 1**) a significant increase in neutral lipid storage in both HCC cell lines, but not in the healthy hepatocyte cell line at 300 μM OA, assayed through Oil-Red O staining. We therefore concluded that HCC cell lines display higher attitude to accumulate neutral lipids in LD as compared to healthy cells. As shown in **Figure 2** we also found a specific reduction of autophagy marker LC3II and increased LD marker perilipin-2 in HCC thus hypothesizing that autophagy reduction underlies higher LD and neutral lipid accumulation in HCC upon OA administration. An inverse relationship between perilipin-2 and autophagy levels is known to occur in the liver (Tsai et al., 2017) in agreement with our OA-induced effects.

Reduced Alamar Blue staining in both HCC cell lines upon OA treatment as well as significant cyclin-D1 and PCNA decrease in both HCC cell lines (**Figure 3**) suggest the role of OA as a negative regulator of proliferation in HCC cell lines. Previous studies reported cell proliferation inhibition and apoptosis induction after OA administration in carcinoma cells (Carrillo et al., 2012). In previous works unsaturated fatty acid oleate (an oleic acid-derived salt) induces (Vinciguerra et al., 2009; Park et al., 2018) or inhibits (Arous et al., 2011; Li et al., 2013) HepG2 cell proliferation in a concentration-dependent manner, with a mechanism only partially elucidated. We report here that increasing doses of OA reduce viability and increase cell death (**Figure 4**) in both HCC cell lines. OA activates the apoptotic process in Huh7.5 but not in Hep3B and increases necrotic cell percentage in Hep3B but not in Huh7.5. Such data agree with previous observations indicating that OA, among many beneficial functions, can induce cell death through apoptotic (Jiang et al., 2017) and non-apoptotic pathways (Yamakami et al., 2014). Remarkably, as described by Magtanong et al. (2016) there are several non-apoptotic cell death pathways activated

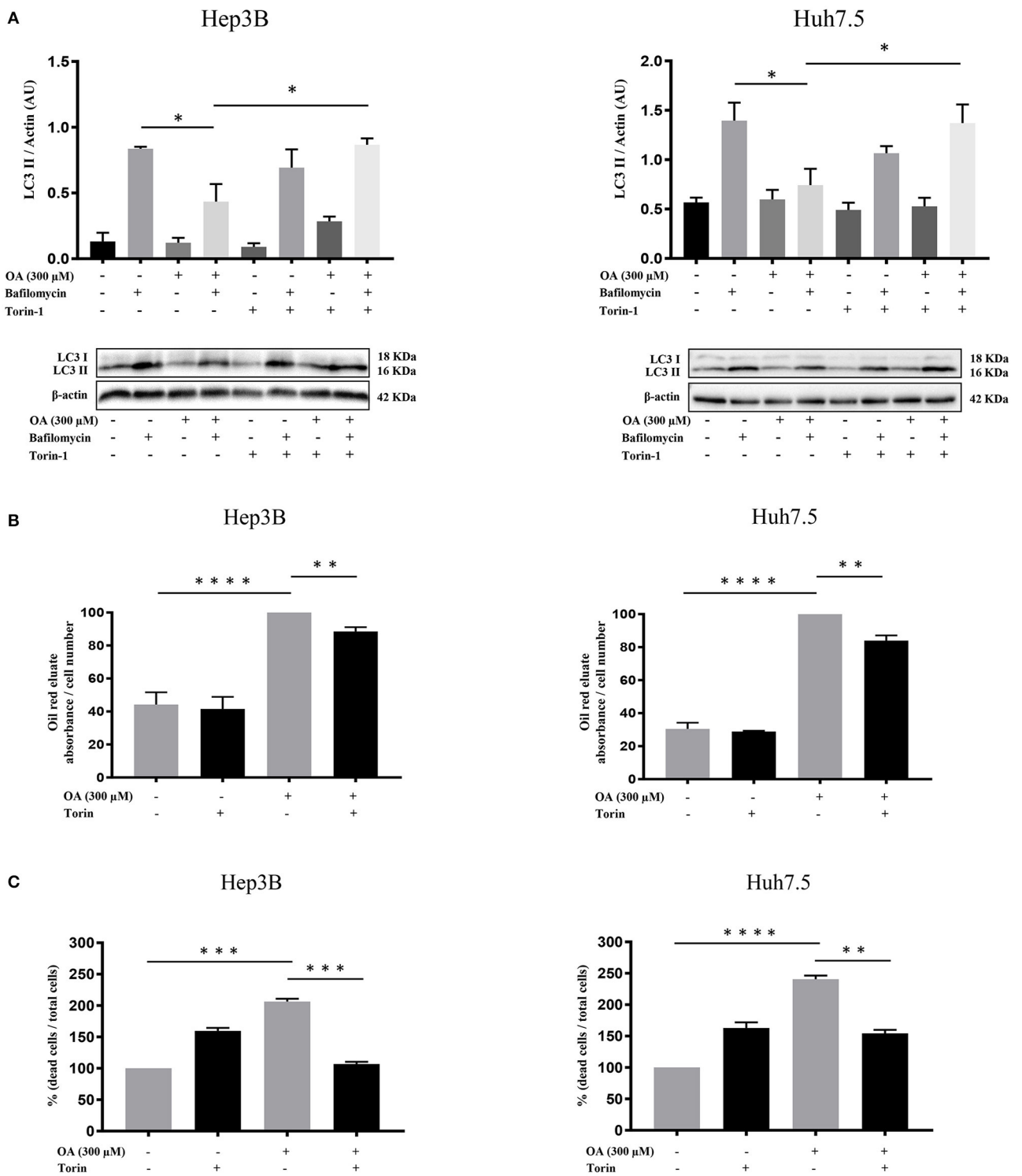

FIGURE 7 | Torin-1 partially reverts the OA-induced effects in HCC cell lines. **(A)** Autophagic flux modulation upon combined OA and torin-1 treatment in both HCC cell lines. Western blot analyses for HCC cell lines treated with 300 μM OA plus torin-1 in the presence of bafilomycin A1 were performed. LC3II quantification confirms that torin-1 activates the autophagic flux after OA treatment in both HCC cell lines. **(B)** Hep3B and Huh7.5 cell lines were treated with OA (300 μM) and torin-1. Oil-Red O-eluates/cell number of Hep3B and Huh7.5 cell lines are shown. OA induced a significant accumulation of neutral lipids in both HCC cell lines; the simultaneous presence of torin-1 significantly decreased the accumulation in both HCC cell lines. **(C)** Cell counts with trypan blue staining were performed. Dead/total cell percentage ratio showed that OA treatment induced cell death in both HCC cell lines; the simultaneous presence of torin-1 significantly reduced the percentage of dead cells in both HCC cell lines ($n = 3$; $^{*}p < 0.05$; $^{**}p < 0.01$; $^{***}p < 0.001$; $^{****}p < 0.0001$).

by OA, such as necroptosis. OA is known to modulate cell death by altering lipid metabolism or by altering membrane lipid composition (Fontana et al., 2013; Ning et al., 2019).

Recently, Bosc et al. (2020) demonstrated that autophagy regulates fatty acids availability through mitochondria-endoplasmic reticulum contact sites and this event occurs mainly in cancer cells. The metastatic potential of cancer cells is related to genes involved in fatty acids synthesis and intracellular lipids storage. Therefore, modulation of lipid accumulation, function of enzymes dedicated to LD digestion, and fatty acids availability play together a role in tumor progression (Sanchez-Martinez et al., 2015; Giampietri et al., 2020). In fact, lipid metabolism generates a high energy support used by cancer cells to grow and metastasize. It is important to note that OA accumulates inside the cell as triglycerides and cholesterol esters, resulting in LD formation, i.e., cellular organelles important in lipotoxicity control (Wen et al., 2013; Petan et al., 2018). Interfering with LD accumulation leads to cell death in fibroblasts exposed to the otherwise non-toxic oleate (Listenberger et al., 2003).

We report here a senescent phenotype in β-galactosidase stained Hep3B after OA treatment (**Figure 4**). This result is in accordance with our data showing that Hep3B cell line does not undergo apoptosis but necrosis after OA treatment. Different factors are known to regulate cellular senescence and cells displaying G1 or G2 phase increase with S-phase reduction may enter a senescent state becoming resistant to apoptotic signals and undergoing necrosis (Kastan and Bartek, 2004; Gire and Dulic, 2015). Furthermore, senescence observed on OA-treated Hep3B is in accordance with previous reports demonstrating OA as a mild senescence inducer (Iwasa et al., 2003; Yamakami et al., 2014). Further studies are underway to further evaluate cell death processes induced by OA in HCC cell lines. We therefore concluded that in our experimental setup OA activates both apoptotic (Jiang et al., 2017) and non-apoptotic pathways (Assy et al., 2009), depending on cell type.

We observed that OA treatment displays significant reduction of c-Flip and Bcl-2 in both HCC cell lines but not in the healthy hepatocyte cell line (**Figure 5**). Wang et al. described the anti-apoptotic role of both these proteins in the liver (Wang, 2015). It is well-known that c-Flip has multiple roles, modulating apoptosis, autophagy and necrosis (Safa, 2013). Its up-regulation was correlated with a poor clinical outcome in many pathological conditions including cancer. Moreover, agents or molecules able to inhibit c-Flip expression are of potential therapeutic interest (Safa, 2013). Bcl-2 is known for its properties in cell death modulation and OA has been shown to reduce Bcl-2 expression levels in tongue squamous carcinoma cells (Jiang et al., 2017). In accordance with our results showing OA-dependent cyclin D1 decrease and cell death activation, we also found dose-dependent OA p-ERK reduction, reported in **Figure 5**. This finding parallels results obtained in tongue squamous cell carcinoma cells, where dose-dependent OA treatment reduced p-ERK1/2 (Jiang et al., 2017). In the present study OA significantly reduced the migratory capability of HCC cells as compared to Control cells (THLE-2) and reduced the number of invading cells in both HCC cell lines (**Figure 6**). Hep3B cells display higher ability to cover the scratch respect to Huh7.5 cells. This difference between the two cell lines is in agreement with previous data indicating higher aggressiveness of Hep3B cell line vs. other HCC cell lines. Taken together these data supported the hypothesis that OA, by negatively modulating the autophagic flux, counteracts the aggressiveness and invasiveness of Hep3B and Huh7.5 cell lines.

OA treatment in hepatic cell lines like HepG2 or immortalized hepatocytes induces lipid accumulation and represents an *in vitro* model of liver disease (Lim et al., 2020). Under our experimental conditions, OA treatment induces lipid accumulation as expected in healthy cells (THLE-2), although at a lower extent as compared to cancer cells (Hep3B and Huh7.5). This suggests a beneficial role of OA in cancers cells since the higher lipid accumulation observed in cancer cells leads to cell death and to reduced proliferation, migration, and invasion. We demonstrate that this is likely related to autophagy flux reduction in cancer cells. These results agree with Li et al. (2013), who demonstrated that reduced invasiveness of HCC cells (HepG2 and BEL7402) is related to a negative modulation of autophagy. To verify the role of autophagy in OA-dependent effects, HCC cells were treated with OA and analyzed for LD content in the presence of the autophagy inducer Torin-1 (a mTOR kinase inhibitor). The results shown in **Figure 7** led us to conclude that 300 μM OA-induced LD accumulation and cell death are both, at least partially, dependent on autophagy impairment since the combined torin-1/OA treatment reduces LD and cell death. Previous studies demonstrated that OA treatment reduces autophagy in Hepa1c1c7 mouse hepatoma cell line (Ning et al., 2019); also the saturated palmitic acid (PA) impairs autophagic-flux in a time-dependent manner in liver HepG2 cells (Korovila et al., 2020). Furthermore, OA was previously shown to exert different effects in HepG2 cells at different concentrations (Pang et al., 2018). In particular LD accumulation and apoptosis induction was reported at concentrations ranging from 0.1 to 2 mM OA while LD reduction was found at 400 μM OA treatment. The Authors concluded that these concentration-dependent effects are strictly related to autophagy since autophagy is able to prevent 400 μM OA-induced HepG2 apoptosis.

Results of the present study achieved on three human cell lines-based *in vitro* systems, confirm the pivotal role of autophagy reduction in promoting OA-dependent LD accumulation, cell death and reduced aggressiveness/invasiveness. Additional studies are needed to further clarify the underlying molecular mechanisms. We conclude that OA stimulates HCC cell death via autophagy reduction while it does not impair autophagy level in healthy cells thus leading us to hypothesize that fine autophagy regulation preserves healthy hepatocytes resistance to toxicity caused by high levels of neutral lipids. LD accumulation in association with autophagic flux reduction after OA treatments in Hep3B and Huh7.5 cell lines, promote cell death through apoptosis in Huh7.5

and also non-apoptotic pathway in Hep3B cell line. Such differences in cell death mechanisms are currently under further investigation.

In conclusion, we present here several evidences indicating OA specific antitumor effects in HCC in an autophagy-dependent manner.

DATA AVAILABILITY STATEMENT

The raw data supporting the conclusions of this article will be made available by the authors, without undue reservation.

AUTHOR CONTRIBUTIONS

FG, SP, and CG conceived the study. FG performed the majority of the experiments and analyzed the data. SM and AD'A performed flow cytometry analyses. LT and VF supported FG in performing some experiments. FG and CG wrote the manuscript supervised by AF, EG, and EZ. All authors contributed to the article and approved the submitted version.

FUNDING

This work was supported by Progetti di Ricerca di Ateneo (Sapienza University of Rome, Italy).

ACKNOWLEDGMENTS

The authors are grateful to Prof. Cinzia Fabrizi and Dr. Silvia Sideri from the Department of Anatomical, Histological, Forensic Medicine and Orthopedic Sciences, Sapienza University of Rome, Rome, Italy for suggestions and technical support. The authors are also grateful to Prof. Federica Barbagallo from Department of Experimental Medicine, Sapienza University of Rome, for her helpful insights and kind support.

SUPPLEMENTARY MATERIAL

The Supplementary Material for this article can be found online at: https://www.frontiersin.org/articles/10.3389/fcell.2021.629182/full#supplementary-material

REFERENCES

Amir, M., and Czaja, M. J. (2011). Autophagy in nonalcoholic steatohepatitis. *Expert Rev. Gastroenterol. Hepatol.* 5, 159–166. doi: 10.1586/egh.11.4

Arous, C., Naimi, M., and Van Obberghen, E. (2011). Oleate-mediated activation of phospholipase D and mammalian target of rapamycin (mTOR) regulates proliferation and rapamycin sensitivity of hepatocarcinoma cells. *Diabetologia* 54, 954–964. doi: 10.1007/s00125-010-2032-1

Assy, N., Nassar, F., Nasser, G., and Grosovski, M. (2009). Olive oil consumption and non-alcoholic fatty liver disease. *World J. Gastroenterol.* 15, 1809–1815. doi: 10.3748/wjg.15.1809

Borchers, A., and Pieler, T. (2010). Programming pluripotent precursor cells derived from Xenopus embryos to generate specific tissues and organs. *Genes* 1, 413–426. doi: 10.3390/genes1030413

Bosc, C., Broin, N., Fanjul, M., Saland, E., Farge, T., Courdy, C., et al. (2020). Autophagy regulates fatty acid availability for oxidative phosphorylation through mitochondria-endoplasmic reticulum contact sites. *Nat. Commun.* 11:4056. doi: 10.1038/s41467-020-17882-2

Carrillo, C., Cavia Mdel, M., and Alonso-Torre, S. R. (2012). Antitumor effect of oleic acid; mechanisms of action: a review. *Nutr. Hosp.* 27, 1860–1865.

Chava, S., Lee, C., Aydin, Y., Chandra, P. K., Dash, A., Chedid, M., et al. (2017). Chaperone-mediated autophagy compensates for impaired macroautophagy in the cirrhotic liver to promote hepatocellular carcinoma. *Oncotarget* 8, 40019–40036. doi: 10.18632/oncotarget.16685

D'Arcangelo, D., Giampietri, C., Muscio, M., Scatozza, F., Facchiano, F., and Facchiano, A. (2018). WIPI1, BAG1, and PEX3 autophagy-related genes are relevant melanoma markers. *Oxid. Med. Cell. Longev.* 2018:1471682. doi: 10.1155/2018/1471682

Denton, D., Nicolson, S., and Kumar, S. (2012). Cell death by autophagy: facts and apparent artefacts. *Cell Death Differ.* 19, 87–95. doi: 10.1038/cdd.2011.146

Ding, Z. B., Hui, B., Shi, Y. H., Zhou, J., Peng, Y. F., Gu, C. Y., et al. (2011). Autophagy activation in hepatocellular carcinoma contributes to the tolerance of oxaliplatin via reactive oxygen species modulation. *Clin. Cancer Res.* 17, 6229–6238. doi: 10.1158/1078-0432.CCR-11-0816

Fontana, A., Spolaore, B., and Polverino De Laureto, P. (2013). The biological activities of protein/oleic acid complexes reside in the fatty acid. *Biochim. Biophys. Acta* 1834, 1125–1143. doi: 10.1016/j.bbapap.2013.02.041

Fujimoto, Y., Onoduka, J., Homma, K. J., Yamaguchi, S., Mori, M., Higashi, Y., et al. (2006). Long-chain fatty acids induce lipid droplet formation in a cultured human hepatocyte in a manner dependent of acyl-coa synthetase. *Biol. Pharm. Bull.* 29, 2174–2180. doi: 10.1248/bpb.29.2174

Giampietri, C., Petrungaro, S., Coluccia, P., Antonangeli, F., Paone, A., Padula, F., et al. (2006). c-Flip(L) is expressed in undifferentiated mouse male germ cells. *FEBS Lett.* 580, 6109–6114. doi: 10.1016/j.febslet.2006.10.010

Giampietri, C., Petrungaro, S., Cordella, M., Tabolacci, C., Tomaipitinca, L., Facchiano, A., et al. (2017). Lipid storage and autophagy in melanoma cancer cells. *Int. J. Mol. Sci.* 18:1271. doi: 10.3390/ijms18061271

Giampietri, C., Starace, D., Petrungaro, S., Filippini, A., and Ziparo, E. (2014). Necroptosis: molecular signalling and translational implications. *Int. J. Cell Biol.* 2014:490275. doi: 10.1155/2014/490275

Giampietri, C., Tomaipitinca, L., Scatozza, F., and Facchiano, A. (2020). Expression of genes related to lipid handling and the obesity paradox in melanoma: database analysis. *JMIR Cancer* 6:e16974. doi: 10.2196/16974

Gire, V., and Dulic, V. (2015). Senescence from G2 arrest, revisited. *Cell Cycle* 14, 297–304. doi: 10.1080/15384101.2014.1000134

Gnoni, A., Siculella, L., Paglialonga, G., Damiano, F., and Giudetti, A. M. (2019). 3,5-diiodo-L-thyronine increases de novo lipogenesis in liver from hypothyroid rats by SREBP-1 and ChREBP-mediated transcriptional mechanisms. *IUBMB Life* 71, 863–872. doi: 10.1002/iub.2014

Hennig, M., Yip-Schneider, M. T., Wentz, S., Wu, H., Hekmatyar, S. K., Klein, P., et al. (2010). Targeting mitogen-activated protein kinase kinase with the inhibitor PD0325901 decreases hepatocellular carcinoma growth *in vitro* and in mouse model systems. *Hepatology* 51, 1218–1225. doi: 10.1002/hep.23470

Iwasa, H., Han, J., and Ishikawa, F. (2003). Mitogen-activated protein kinase p38 defines the common senescence-signalling pathway. *Genes Cells* 8, 131–144. doi: 10.1046/j.1365-2443.2003.00620.x

Jarc, E., and Petan, T. (2019). Lipid droplets and the management of cellular stress. *Yale J. Biol. Med.* 92, 435–452.

Jiang, L., Wang, W., He, Q., Wu, Y., Lu, Z., Sun, J., et al. (2017). Oleic acid induces apoptosis and autophagy in the treatment of tongue squamous cell carcinomas. *Sci. Rep.* 7:11277. doi: 10.1038/s41598-017-11842-5

Kastan, M. B., and Bartek, J. (2004). Cell-cycle checkpoints and cancer. *Nature* 432, 316–323. doi: 10.1038/nature03097

Klionsky, D. J., Abdelmohsen, K., Abe, A., Abedin, M. J., Abeliovich, H., Acevedo Arozena, A., et al. (2016). Guidelines for the use and interpretation of assays for monitoring autophagy (3rd edition). *Autophagy* 12, 1–222. doi: 10.1080/15548627.2015.1100356

Korovila, I., Jung, T., Deubel, S., Grune, T., and Ott, C. (2020). Punicalagin attenuates palmitate-induced lipid droplet content by simultaneously

improving autophagy in hepatocytes. *Mol. Nutr. Food Res.* 64:e2000816. doi: 10.1002/mnfr.202000816

Li, J., Yang, B., Zhou, Q., Wu, Y., Shang, D., Guo, Y., et al. (2013). Autophagy promotes hepatocellular carcinoma cell invasion through activation of epithelial-mesenchymal transition. *Carcinogenesis* 34, 1343–1351. doi: 10.1093/carcin/bgt063

Li, S., Zhou, T., Li, C., Dai, Z., Che, D., Yao, Y., et al. (2014). High metastaticgastric and breast cancer cells consume oleic acid in an AMPK dependent manner. *PLoS ONE* 9:e97330. doi: 10.1371/journal.pone.0097330

Lim, D. W., Jeon, H., Kim, M., Yoon, M., Jung, J., Kwon, S., et al. (2020). Standardized rice bran extract improves hepatic steatosis in HepG2 cells and ovariectomized rats. *Nutr. Res. Pract.* 14, 568–579. doi: 10.4162/nrp.2020.14.6.568

Listenberger, L. L., Han, X., Lewis, S. E., Cases, S., Farese, R. V., Jr Ory, D. S., et al. (2003). Triglyceride accumulation protects against fatty acid-induced lipotoxicity. *Proc. Natl. Acad. Sci. U. S. A.* 100, 3077–3082. doi: 10.1073/pnas.0630588100

Maan, M., Peters, J. M., Dutta, M., and Patterson, A. D. (2018). Lipid metabolism and lipophagy in cancer. *Biochem. Biophys. Res. Commun.* 504, 582–589. doi: 10.1016/j.bbrc.2018.02.097

Magtanong, L., Ko, P. J., and Dixon, S. J. (2016). Emerging roles for lipids in non-apoptotic cell death. *Cell Death Differ.* 23, 1099–1109. doi: 10.1038/cdd.2016.25

Mizushima, N. (2007). Autophagy: process and function. *Genes Dev.* 21, 2861–2873. doi: 10.1101/gad.1599207

Ning, J., Zhao, C., Chen, J. X., and Liao, D. F. (2019). Oleate inhibits hepatic autophagy through p38 mitogen-activated protein kinase (MAPK). *Biochem. Biophys. Res. Commun.* 514, 92–97. doi: 10.1016/j.bbrc.2019.04.073

Pang, L., Liu, K., Liu, D., Lv, F., Zang, Y., Xie, F., et al. (2018). Differential effects of reticulophagy and mitophagy on nonalcoholic fatty liver disease. *Cell Death Dis.* 9:90. doi: 10.1038/s41419-017-0136-y

Park, S., Park, J. H., Jung, H. J., Jang, J. H., Ahn, S., Kim, Y., et al. (2018). A secretome profile indicative of oleate-induced proliferation of HepG2 hepatocellular carcinoma cells. *Exp. Mol. Med.* 50:93. doi: 10.1038/s12276-018-0120-3

Perdomo, L., Beneit, N., Otero, Y. F., Escribano, O., Diaz-Castroverde, S., Gomez-Hernandez, A., et al. (2015). Protective role of oleic acid against cardiovascular insulin resistance and in the early and late cellular atherosclerotic process. *Cardiovasc. Diabetol.* 14:75. doi: 10.1186/s12933-015-0237-9

Perez-Martinez, P., Garcia-Rios, A., Delgado-Lista, J., Perez-Jimenez, F., and Lopez-Miranda, J. (2011). Mediterranean diet rich in olive oil and obesity, metabolic syndrome and diabetes mellitus. *Curr. Pharm. Des.* 17, 769–777. doi: 10.2174/138161211795428948

Petan, T., Jarc, E., and Jusovic, M. (2018). Lipid droplets in cancer: guardians of fat in a stressful world. *Molecules* 23:1941. doi: 10.3390/molecules23081941

Pfeifer, A. M., Cole, K. E., Smoot, D. T., Weston, A., Groopman, J. D., Shields, P. G., et al. (1993). Simian virus 40 large tumor antigen-immortalized normal human liver epithelial cells express hepatocyte characteristics and metabolize chemical carcinogens. *Proc. Natl. Acad. Sci. U. S. A.* 90, 5123–5127. doi: 10.1073/pnas.90.11.5123

Qin, L. F., and Ng, I. O. (2002). Induction of apoptosis by cisplatin and its effect on cell cycle-related proteins and cell cycle changes in hepatoma cells. *Cancer Lett.* 175, 27–38. doi: 10.1016/S0304-3835(01)00720-0

Qiu, G. H., Xie, X., Xu, F., Shi, X., Wang, Y., and Deng, L. (2015). Distinctive pharmacological differences between liver cancer cell lines HepG2 and Hep3B. *Cytotechnology* 67, 1–12. doi: 10.1007/s10616-014-9761-9

Rebouissou, S., and Nault, J. C. (2020). Advances in molecular classification and precision oncology in hepatocellular carcinoma. *J. Hepatol.* 72, 215–229. doi: 10.1016/j.jhep.2019.08.017

Rohwedder, A., Zhang, Q., Rudge, S. A., and Wakelam, M. J. (2014). Lipid droplet formation in response to oleic acid in Huh-7 cells is mediated by the fatty acid receptor FFAR4. *J. Cell Sci.* 127 (Pt 14), 3104–3115. doi: 10.1242/jcs.145854

Safa, A. R. (2013). Roles of c-FLIP in apoptosis, necroptosis, and autophagy. *J. Carcinog. Mutagen.* (Suppl. 6):003. doi: 10.4172/2157-2518.S6-003

Sales-Campos, H., Souza, P. R., Peghini, B. C., Da Silva, J. S., and Cardoso, C. R. (2013). An overview of the modulatory effects of oleic acid in health and disease. *Mini. Rev. Med. Chem.* 13, 201–210. doi: 10.2174/138955713804805193

Sanchez-Martinez, R., Cruz-Gil, S., Gomez de Cedron, M., Alvarez-Fernandez, M., Vargas, T., Molina, S., et al. (2015). A link between lipid metabolism and epithelial-mesenchymal transition provides a target for colon cancer therapy. *Oncotarget* 6, 38719–38736. doi: 10.18632/oncotarget.5340

Singh, R., Kaushik, S., Wang, Y., Xiang, Y., Novak, I., Komatsu, M., et al. (2009). Autophagy regulates lipid metabolism. *Nature* 458, 1131–1135. doi: 10.1038/nature07976

Slany, A., Haudek, V. J., Zwickl, H., Gundacker, N. C., Grusch, M., Weiss, T. S., et al. (2010). Cell characterization by proteome profiling applied to primary hepatocytes and hepatocyte cell lines Hep-G2 and Hep-3B. *J. Proteome. Res.* 9, 6–21. doi: 10.1021/pr900057t

Taib, B., Aboussalah, A. M., Moniruzzaman, M., Chen, S., Haughey, N. J., Kim, S. F., et al. (2019). Lipid accumulation and oxidation in glioblastoma multiforme. *Sci. Rep.* 9:19593. doi: 10.1038/s41598-019-55985-z

Tomaipitinca, L., Mandatori, S., Mancinelli, R., Giulitti, F., Petrungaro, S., Moresi, V., et al. (2019). The role of autophagy in liver epithelial cells and its impact on systemic homeostasis. *Nutrients* 11:827. doi: 10.3390/nu11040827

Tsai, T. H., Chen, E., Li, L., Saha, P., Lee, H. J., Huang, L. S., et al. (2017). The constitutive lipid droplet protein PLIN2 regulates autophagy in liver. *Autophagy* 13, 1130–1144. doi: 10.1080/15548627.2017.1319544

Tsujimoto, Y., Shimizu, S., Eguchi, Y., Kamiike, W., and Matsuda, H. (1997). Bcl-2 and Bcl-xL block apoptosis as well as necrosis: possible involvement of common mediators in apoptotic and necrotic signal transduction pathways. *Leukemia* 11(Suppl. 3), 380–382.

Vinciguerra, M., Carrozzino, F., Peyrou, M., Carlone, S., Montesano, R., Benelli, R., et al. (2009). Unsaturated fatty acids promote hepatoma proliferation and progression through downregulation of the tumor suppressor PTEN. *J. Hepatol.* 50, 1132–1141. doi: 10.1016/j.jhep.2009.01.027

Wang, K. (2015). Autophagy and apoptosis in liver injury. *Cell Cycle* 14, 1631–1642. doi: 10.1080/15384101.2015.1038685

Wen, H., Glomm, W. R., and Halskau, O. (2013). Cytotoxicity of bovine alpha-lactalbumin: oleic acid complexes correlates with the disruption of lipid membranes. *Biochim. Biophys. Acta* 1828, 2691–2699. doi: 10.1016/j.bbamem.2013.07.026

Yamakami, Y., Miki, K., Yonekura, R., Kudo, I., Fujii, M., and Ayusawa, D. (2014). Molecular basis for premature senescence induced by surfactants in normal human cells. *Biosci. Biotechnol. Biochem.* 78, 2022–2029. doi: 10.1080/09168451.2014.946391

Yao, H. R., Liu, J., Plumeri, D., Cao, Y. B., He, T., Lin, L., et al. (2011). Lipotoxicity in HepG2 cells triggered by free fatty acids. *Am. J. Transl. Res.* 3, 284–291.

Zeng, X., Zhu, M., Liu, X., Chen, X., Yuan, Y., Li, L., et al. (2020). Oleic acid ameliorates palmitic acid induced hepatocellular lipotoxicity by inhibition of ER stress and pyroptosis. *Nutr. Metab.* 17:11. doi: 10.1186/s12986-020-0434-8

Zhong, J., Gong, W., Chen, J., Qing, Y., Wu, S., Li, H., et al. (2018). Micheliolide alleviates hepatic steatosis in db/db mice by inhibiting inflammation and promoting autophagy via PPAR-gamma-mediated NF-small ka, CyrillicB and AMPK/mTOR signaling. *Int. Immunopharmacol.* 59, 197–208. doi: 10.1016/j.intimp.2018.03.036

Conflict of Interest: The authors declare that the research was conducted in the absence of any commercial or financial relationships that could be construed as a potential conflict of interest.

frontiers in Cell and Developmental Biology

ORIGINAL RESEARCH
published: 18 March 2021
doi: 10.3389/fcell.2021.640094

Mitochondrial Dynamics and VMP1-Related Selective Mitophagy in Experimental Acute Pancreatitis

*Virginia Vanasco[1], Alejandro Ropolo[1], Daniel Grasso[1], Diego S. Ojeda[2], María Noé García[1], Tamara A. Vico[1], Tamara Orquera[1], Jorge Quarleri[2], Silvia Alvarez[1] and María I. Vaccaro[1]**

[1] Universidad de Buenos Aires, Consejo Nacional de Investigaciones Científicas y Técnicas (CONICET), Instituto de Bioquímica y Medicina Molecular (IBIMOL), Facultad de Farmacia y Bioquímica, Buenos Aires, Argentina, [2] Universidad de Buenos Aires, Consejo Nacional de Investigaciones Científicas y Técnicas (CONICET), Instituto de Investigaciones Biomédicas en Retrovirus y SIDA (INBIRS), Facultad de Medicina, Buenos Aires, Argentina

OPEN ACCESS

Edited by:
Konstantinos Zarbalis, University of California, Davis, United States

Reviewed by:
Yansheng Feng, The University of Texas Health Science Center at San Antonio, United States
Chunying Li, Georgia State University, United States

***Correspondence:**
María I. Vaccaro
maria.vaccaro@gmail.com

Specialty section:
This article was submitted to Cell Death and Survival, a section of the journal Frontiers in Cell and Developmental Biology

Received: *10 December 2020*
Accepted: *17 February 2021*
Published: *18 March 2021*

Citation:
Vanasco V, Ropolo A, Grasso D, Ojeda DS, García MN, Vico TA, Orquera T, Quarleri J, Alvarez S and Vaccaro MI (2021) Mitochondrial Dynamics and VMP1-Related Selective Mitophagy in Experimental Acute Pancreatitis. Front. Cell Dev. Biol. 9:640094. doi: 10.3389/fcell.2021.640094

Mitophagy and zymophagy are selective autophagy pathways early induced in acute pancreatitis that may explain the mild, auto limited, and more frequent clinical presentation of this disease. Adequate mitochondrial bioenergetics is necessary for cellular restoration mechanisms that are triggered during the mild disease. However, mitochondria and zymogen contents are direct targets of damage in acute pancreatitis. Cellular survival depends on the recovering possibility of mitochondrial function and efficient clearance of damaged mitochondria. This work aimed to analyze mitochondrial dynamics and function during selective autophagy in pancreatic acinar cells during mild experimental pancreatitis in rats. Also, using a cell model under the hyperstimulation of the G-coupled receptor for CCK (CCK-R), we aimed to investigate the mechanisms involved in these processes in the context of zymophagy. We found that during acute pancreatitis, mitochondrial O_2 consumption and ATP production significantly decreased early after induction of acute pancreatitis, with a consequent decrease in the ATP/O ratio. Mitochondrial dysfunction was accompanied by changes in mitochondrial dynamics evidenced by optic atrophy 1 (OPA-1) and dynamin-related protein 1 (DRP-1) differential expression and ultrastructural features of mitochondrial fission, mitochondrial elongation, and mitophagy during the acute phase of experimental mild pancreatitis in rats. Mitophagy was also evaluated by confocal assay after transfection with the pMITO-RFP-GFP plasmid that specifically labels autophagic degradation of mitochondria and the expression and redistribution of the ubiquitin ligase Parkin1. Moreover, we report for the first time that vacuole membrane protein-1 (VMP1) is involved and required in the mitophagy process during acute pancreatitis, observable not only by repositioning around specific mitochondrial populations, but also by detection of mitochondria in autophagosomes specifically isolated with anti-VMP1 antibodies as well. Also, VMP1 downregulation avoided mitochondrial degradation confirming that VMP1 expression is required for mitophagy during acute pancreatitis. In conclusion, we identified a novel DRP1-Parkin1-VMP1 selective autophagy pathway, which mediates

the selective degradation of damaged mitochondria by mitophagy in acute pancreatitis. The understanding of the molecular mechanisms involved to restore mitochondrial function, such as mitochondrial dynamics and mitophagy, could be relevant in the development of novel therapeutic strategies in acute pancreatitis.

Keywords: pancreatitis, autophagy, mitophagy, VMP1, mitochondrial dynamics, mitochondrial function, Parkin1, DRP1

HIGHLIGHTS

- The novel DRP1-Parkin1-VMP1 autophagy pathway, which mediates the selective degradation of damaged mitochondria by mitophagy, was unraveled in acute pancreatitis.
- Mitochondrial O_2 consumption and ATP production significantly decreased early after induction of acute pancreatitis, with a consequent decrease in the ATP/O ratio.
- Mitochondrial fission, mitochondrial elongation, and mitophagy are rapidly activated in pancreatic acinar cells during experimental mild pancreatitis in rats.

INTRODUCTION

Acute pancreatitis (AP) is a pancreatic inflammatory condition whose global estimates of incidence and mortality are between 33 and 74 cases per 100,000 person-years, with 1–60 deaths per 100,000 person-years for AP (Xiao et al., 2016). Most patients develop a mild and auto limited form of the disease, but about 20% of them suffer a severe disease presenting pancreatic necrosis, which can spread within the same pancreatic tissue and be accompanied by injury to other organs. Moreover, within deaths associated with AP, half of them occur during the first week due to multiple organ failure (Mukherjee et al., 2008). Despite recent advances, the pathogenesis of cellular damage occurring during inflammation in the severe form of the disease is unclear and no adequate specific treatments have been developed (Maléth et al., 2013).

Previous studies of our laboratory identified VMP1 (NM_138839) as a novel autophagy-related protein in which its expression is induced in the human pancreas with pancreatitis and in experimental pancreatitis under the G-coupled receptor CCK-R hyperstimulation (Ropolo et al., 2007; Vaccaro et al., 2008; Grasso et al., 2011). We also described the selective autophagic pathway, zymophagy, as an early protective mechanism in AP preventing acinar cell death (Grasso et al., 2011). Zymophagy is a selective type of autophagy that occurs during AP. It may be induced by CCK-R hyperstimulation, mediated by VMP1 expression, which recognizes and sequesters those zymogen granules that are initially activated by the disease. We propose that zymophagy is a protective mechanism set up by the acinar cell, and that may account for the self-limited form of AP (Vaccaro, 2012).

The relevance of autophagy as a protective mechanism in pancreatitis has been further confirmed in mice using pancreas-specific autophagy-related proteins (ATG) ATG5 or ATG7 knockout mice. These animals developed severe pancreatitis, with trypsinogen activation, fibrosis, inflammation, acinar-to-ductal metaplasia, and pancreas atrophy (Antonucci et al., 2015; Diakopoulos et al., 2015). In this context, mitochondria are essential players, not only as the main source of ATP and other biomolecules required during autophagy processes, but also in the regulation of intracellular Ca^{2+} homeostasis in the acinar cells. Therefore, a normal mitochondrial function could be necessary for zymophagy in response to AP. In this sense, it was described that mitochondria-deficient cells exhibit attenuated autophagic gene induction and autophagic flux in response to starvation (Graef and Nunnari, 2011). Even more, mitochondria are direct targets of damage during AP, since fatty acid ethyl esters (FAEEs) that have been reported increased in AP patients and in several models of AP tend to accumulate in the inner mitochondrial membrane affecting the mitochondrial polarization, producing uncoupling of oxidative phosphorylation, and inhibiting ATP production (Mukherjee et al., 2008). Therefore, cellular survival depends on the recovered mitochondrial function and efficient clearance of dysfunctional mitochondria.

The mitochondrial population is highly dynamic within cells, mitochondria form networks continually undergo fusion and fission events during cell life (Bereiter-Hahn and Voth, 1994). In mammals, mitochondrial fusion is mainly regulated by OPA1 proteins (optic atrophy 1, an internal mitochondrial membrane GTPase) (Cipolat et al., 2004), and by outer membrane GTPases or Mitofusin 1 and 2 (Mnf) (Santel and Fuller, 2001). Mitochondrial fission is mainly controlled by the cytosolic GTPase protein DRP1 (dynamin-related protein 1), whose translocation from cytoplasm to mitochondria is an essential step at the beginning of mitochondrial fragmentation (Smirnova et al., 2001). It is postulated that mitochondrial dynamics respond to cellular energy requirements (Liesa and Shirihai, 2013) triggered by other intracellular processes such as redox changes and autophagy (Willems et al., 2015; Cid-Castro et al., 2018; Ježek et al., 2018). Mitophagy, a selective form of autophagy, is a major route for the removal of damaged mitochondria. During mitophagy, mitochondria are sequestered in double-membrane vesicles and delivered to lysosomes for degradation. Narendra et al. (2008, 2010) found

Abbreviations: AP, acute pancreatitis; CAE, caerulein; CG, control group; DRP1, dynamin-related protein 1; FAEEs, fatty acid ethyl esters; LC3, microtubule associated protein 1 light chain 3; Mnf, Mitofusin; OPA1, optic atrophy 1; PEI, polyethylenimine; PINK1, PTEN-induced kinase 1; RCR, respiratory control ratio; ROS, reactive oxygen species; VMP1, vacuole membrane protein 1 (NM_138839).

that the decrease of mitochondrial membrane potential leads to PTEN-induced kinase 1 (PINK1) accumulation in the mitochondrial outer membrane, leading to the ubiquitination of damaged mitochondria by Parkin1, consequently carrying out autophagic degradation of dysfunctional mitochondria (Vincow et al., 2013). Therefore, it is important to unravel the mechanisms involved in the recovery of mitochondrial function that might be relevant in cellular and tissue recovery processes during mild AP.

Mitochondrial dysfunction has been reported in various models of severe AP in which loss of mitochondrial membrane potential and mitochondrial fragmentation seems to be involved (Shalbueva et al., 2013; Mukherjee et al., 2016; Biczo et al., 2018). Regardless of the underlying mechanisms, genetic or pharmacological prevention of mitochondrial depolarization resulted in the restoration of mitochondrial function, with a large decrease in local and systemic pathological responses in models of experimental severe pancreatitis (Shalbueva et al., 2013; Mukherjee et al., 2016; Biczo et al., 2018). However, the relevance of mitochondria function and dynamics in experimental models of mild pancreatitis are poorly elucidated.

In this work, we analyzed mitochondrial function, mitochondrial dynamics, and mitophagy in pancreatic acinar cells during experimental early pancreatitis in rats and in a cell model under the hyperstimulation of the G-coupled receptor for CCK (CCK-R). We have identified a VMP1 mediating pathway in mitophagy, which selectively sequesters and degrades damaged mitochondria during the initial steps of experimental pancreatitis.

MATERIALS AND METHODS

Drugs and Chemicals

Caerulein (CAE) was purchased from Sigma-Aldrich (St. Louis, MO, United States). Rabbit monoclonal antibodies against OPA1 (ab157457, Abcam Plc, Cambridge, United Kingdom), DRP1 (D6C7 rabbit mAb; Cell Signaling), LC3B [LC3B antibody (2775)]; Cell Signaling Technology, MA, United States), p62 [SQSTM1 (P-15): sc-10117; Santa Cruz Biotechnology, Santa Cruz, CA, United States)], VMP1 (D1y3E, Cell Signaling Technology, MA, United States); mouse monoclonal antibodies against Parkin (P6248, Sigma-Aldrich, St. Louis, MO, United States), V5 [13202 V5-Tag (D3H8Q) rabbit mAB-Cell Signaling)], β-actin [β-actin (C4): sc-47778; Santa Cruz Biotechnology, Santa Cruz, CA, United States)], beta tubulin (ab131205, Abcam Plc, Cambridge, United Kingdom); rabbit anti-goat antibody (Santa Cruz Biotechnology, Santa Cruz, CA, United States); goat policlonal antibodies against VDAC-1 (D-16 sc-32063; Santa Cruz Biotechnology, Santa Cruz, CA, United States); rabbit anti-mouse antibody [(315-035-048) Jackson InmunoResearch, Baltimore Pike, United States]; goat anti-rabbit antibody [(GAR):170-5046; Bio-Rad, CA, United States]. Other reagents, enzymes, and chemicals were of reagent grade and also from Sigma-Aldrich.

Animal Model (*in vivo* Model)

AP was induced through the use of supramaximal dose of CAE, which is a CCK homologue, leading to the activation of the intracellular proteolytic enzyme characteristic of this syndrome (Williams, 2008). Female Sprague-Dawley rats (between 40 to 50 days old) were treated with seven i.p. injections of 50 mg of CAE per kg body weight in 1 h intervals. Treated groups studied: CAE 1, animals sacrificed one hour after the first injection; CAE 3, animals sacrificed after 3 h of treatment; CAE 24 and CAE 48, animals injected and sacrificed at 24 and 48 h, respectively. Control groups (CG) were injected with vehicles following the same scheme as treated groups. Animal experiments were approved by the Animal Care and Research Committee of the School of Pharmacy and Biochemistry, University of Buenos Aires (CICUAL; Exp. 0039150/15), and strictly followed the International Guiding Principles for Biomedical Involving Animals (ICLAS).

Pancreatic Mitochondria Isolation

Rats were euthanized in CO_2 chamber and pancreas was excised and placed in ice-cold isolation buffer [58 mM sucrose, 192 mM mannitol, 2 mM Tris/HCl, 0.5 mM EDTA, 0.5% BSA, pH 7.4 (Hodârnâu et al., 1973)]. The tissue was homogenized in 15 ml of isolation buffer with 1 μg/ml pepstatin, 1 μg/ml aprotinin, 1 μg/ml leupeptin, and 0.4 mM PMSF (phenylmethanesulfonyl fluoride) using a glass/Teflon homogenizer. Homogenates were centrifuged at 650 *g* for 10 min, and the sediment which contains nuclei and cell debris was discarded. The supernatant was centrifuged at 8,000 *g* for 10 min to precipitate mitochondria. The mitochondrial pellet was then washed twice, and finally resuspended in the isolation buffer, according to Hordanau modified (Hodârnâu et al., 1973). To assay the purity of isolated mitochondria, the lactate dehydrogenase activity was measured and only mitochondria with less than 5% impurity were used (Cadenas and Boveris, 1980). Protein quantification was performed with the Folin reagent with bovine serum albumin as standard.

Mitochondrial Oxygen Uptake

Mitochondrial oxygen consumption was measured as described before (Vico et al., 2019), using a Clark-type oxygen electrode for high-resolution respirometry (Hansatech Oxygraph, Norfolk, United Kingdom). Briefly, 0.3–0.4 mg/ml of freshly pancreatic mitochondria were incubated in a respiration medium containing 120 mM KCl, 5 mM KH_2PO_4, 1 mM EGTA, 3 mM HEPES, 1 mg/ml BSA, 2 mM malate, and 5 mM glutamate, pH 7.2 at 25°C. Resting respiration rate (state 4) was measured in this condition. In order to measure an active respiration rate (state 3), 1 mM ADP was added (Vanasco et al., 2014). Respiratory control ratio (RCR) was calculated as the ratio between state 3/state 4 respiration rates. Results were expressed as ng-at O/min. mg protein.

Mitochondrial ATP Production Rate

ATP production rate was measured by the luciferin-luciferase chemiluminescent method in a liquid scintillation

counter LKB Wallac 1209 Rackbeta. Freshly pancreatic mitochondria (30–50 μg) were incubated at 28°C in a reaction medium containing 120 mM KCl, 20 mM Tris–HCl, 1.6 mM EDTA, 0.08% BSA, 8 mM K_2HPO_4/KH_2PO_4, 0.08 mM $MgCl_2$, pH 7.4, 40 μM luciferine, 1 μg/ml luciferase. As substrates, 6 mM malate, 6 mM glutamate, and 0.1 mM ADP were added (Vives-Bauza et al., 2007). As control, ATP production rate in the presence of 2 μg/ml oligomycin was determined, and a calibration curve was performed with ATP as standard (0–20 nmoles). Results were expressed as nmol ATP/min. mg protein. As a marker of mitochondrial efficiency, the ATP/O ratio was calculated as ATP production rate/state 3 oxygen consumption ratio (Vanasco et al., 2012).

Western Blot Analysis

Pancreas were removed and homogenized in 1 ml of ice-cold lysis buffer with 50 mM Hepes, 100 mM NaCl, 1 mM EDTA, 20 mM NaF, 20 mM $Na_4P_2O_7$, 1 mM $NaVO_3$, 1% Triton x-100, 1% SDS, pH 7.4; plus the addition of a mix of proteases inhibitors (1 μg/ml peptatin, 1 μg/ml aprotinin, 1 μg/ml leupeptin, and 0.4 mM phenylmethanesulfonyl fluoride). After an incubation for 10 min at 2°C, the sample was sonicated twice (30 s with 1 min interval) and centrifuged at 800 *g* for 20 min. The supernatant was then used for the western blot analysis (Towbin et al., 1979).

Equal amounts of proteins (80 μg) were separated by SDS-PAGE (7.5, 10, or 12%) and blotted into nitrocellulose films. Non-specific binding was blocked by incubation of the membranes with 5% nonfat dry milk in PBS for 1 h at room temperature. Membranes were incubated with the corresponding primary antibody at a dilution of 1:500 overnight at 4°C (Towbin et al., 1979). After incubation, nitrocellulose membrane was washed three times with PBS-Tween and then incubated with the respective secondary antibody conjugated with horseradish peroxidase (dilution between 1:10,000 and 1:5,000) for 60 min under continuous agitation. Membranes were revealed with ECL reagent. Band images were quantified by the ImageJ Software. Results were expressed as relative to β-actin/β-tubulin expression.

Processing of Samples for Analysis by Electron Microscopy and Micrograph Analysis

Animals were euthanized in a CO_2 chamber and pancreas was rapidly removed and washed with 0.1 M K_2HPO_4/KH_2PO_4, pH 7.4, and cut into cube of 1 mm^3. Tissue sample was fixed with 2.5% glutaraldehyde in 0.1 M K_2HPO_4/KH_2PO_4 (pH 7.4) for 2 h, and post-fixed in 1% osmium tetroxide in 0.1 M K_2HPO_4/KH_2PO_4 at 0°C for 90 min. Afterwards, samples were contrasted with 5% uranyl acetate at 0°C for 2 h, dehydrated, and embedded in Durcupan resin (Fluka AG, Switzerland) at 60°C for 72 h. Ultrathin sections were cut and observed with a Zeiss EM 109 transmission electron microscope (Oberkochen, Germany) and representative digital images were captured using a CCD GATAN ES1000W camera (CA, United States). Damaged mitochondria and mitochondria with swelling were analyzed.

Cells Culture, Differentiation, Treatment, and Transfection

AR42J pancreatic acinar cells were grown in a high glucose DMEM medium GlutaMAX™ supplement, supplemented with 10% fetal bovine serum and 100 μg/ml streptomycin. Cells were differentiated using 100 nM dexamethasone for 48 h.

In order to develop a model for studying the direct effect of hyperstimulation of CCK-R, differentiated AR42J cells were treated with 7.4 μM caerulein at different time intervals (from 0 to 60 min) (Grasso et al., 2011). Polyethylenimine (PEI) transfection Reagent (Sigma) was used to perform the transfection of AR42J cells with different plasmids: (a) RFP-LC3 plasmid which codes for the LC3 protein, involved in autophagy (Ropolo et al., 2007), (b) GFP-VMP1 plasmid (Dusetti et al., 2002), which codes to VMP1 protein involved in selective autophagy (Grasso et al., 2011), (c) pcDNA4/V5-His-rVMP1 expression plasmid (Ropolo et al., 2007), which encodes VMP1 protein and V5 as carboxyl-terminal tag, (d) pMITO, a tandem-tagged RFP-EGFP chimeric plasmid pAT016 encoding a mitochondrial targeting signal sequence fused in-frame with RFP and EGFP genes, as a mitophagy reporter plasmid (GFP-RFP-pMITO) (Kim et al., 2013; Ojeda et al., 2018). This plasmid loses the green color at acidic pH, which makes a sophisticated marker of mitochondrial input to the autolysosome, that is, a good marker of mitophagy (Kim et al., 2013). (e) GFP-sh-VMP1 plasmid for VMP1 down-regulation designed by Ropolo et al. (2020).

Confocal Microscopy

After GFP-RFP-pMITO transfection, treated AR42J cells were observed by the inverted confocal microscope Olympus FV1000 (PLAPON/1.42) to quantify mitophagy. The area of mitochondria per cell localized in autolysosomes (RFP-MITO) was quantified using the Fiji-win64 software.

To analyze mitochondria and lysosomes localization, treated AR42J cells were incubated with 200 nM of MitoTracker Red CMXRos and 50 nM of LysoTracker Blue DND-22 (Invitrogen) for 30 min at 37°C and subsequently washing them three times with PBS. Cells images were acquired through an Olympus Confocal Microscope FV1000 and images were acquired using the Zen Blue software (Zeiss) and processed on the AxioVision 4.2 software (Carl Zeiss). To analyze lysosomal area per cell, treated AR42J cells labeled with LysoTracker were analyzed in an Olympus Confocal Microscope FV1000 and quantified using the Fiji-win64 software in arbitrary units.

Immunofluorescence

AR42J cells were fixed for 15 min with 4% p-formaldehyde in PBS and immediately washed three times with PBS. Then, cells were treated with triton X-100 0.1% in PBS for 5 min, washed three times with PBS, and incubated in FBS 10% in PBS for 60 min. Later, cells were incubated with polyclonal antibodies against Parkin1 (P6248, Sigma-Aldrich; 1:100 diluted) overnight at 4°C. Rabbit anti-mouse Alexa Fluor 590 (Molecular Probe) antibody was used for immunofluorescence. Samples were mounted in DABCO (Sigma-Aldrich). The cell images were

acquired through an Olympus Confocal Microscope FV1000 with Spectral Detection System by Diffraction Network. Images were acquired using the Zen Blue software (Zeiss) and processed on the AxioVision 4.2 software (Carl Zeiss).

Immunoisolation of Autophagosomes

Autophagosomes were immuno-isolated using magnetic beads fused to anti-VMP1 or anti-V5 monoclonal antibodies, according to the previously described method (Ropolo et al., 2019). The presence of VDAC, as a mitochondrial marker, was evaluated by Western blot in autophagosome fractions isolated from caerulein-treated AR42J cells transfected with pcDNA4/V5-His-rVMP1.

Mitochondrial Membrane Potential Gradient and Mitochondrial Mass Assay in AR42J Cells

AR42J were incubated in the dark at 37°C and 5% of CO_2 for 15 min in 500 nM of tetramethylrhodamine methyl ester (TMRM, Invitrogen, California, United States), a potentiometric cationic probe red-orange-fluorescent dye that is permeable in active mitochondria with intact membrane potential, or with 100 nM MitoTraker^{TM} Deep Red (MTDR, Invitrogen, CA, United States) that reflexes mitochondrial mass. After the incubation, cells were acquired by a FACSCanto (BDBiosciences) equipped with a 488 and 640 nm argon laser. To exclude debris, samples were gated based on light-scattering properties, and 30,000 events per sample were collected. Emission of TMRM and MTDR were measured in the PE and APC channel and the mitochondrial depolarization and mass were calculated by measuring the decrease or increase in the fluorescence intensity ratio, respectively. Autofluorescence was evaluated in the samples without probe. Total depolarization induced by 2 μM m-CCCP was used as a positive control.

Statistics

Results were expressed as mean values ± SEM and represent the mean of, at least, five independent experiments. ANOVA followed by the Dunnett test was used to analyze differences among experimental groups. When two variables were analyzed, a Two-way ANOVA followed by the Tukey test was used. Statistical significance was considered at $p < 0.05$.

RESULTS

In vivo Model of AP

Mitochondrial Function Is Early Affected in the Rat Model of AP

With the aim of analyzing pancreatic mitochondrial function during mild pancreatitis, two different approaches were used in the animal model: O_2 consumption and ATP production rates which were measured in the isolated mitochondria. **Figure 1A** shows a representative trace of mitochondrial O_2 consumption in control conditions. The first slope represents the O_2 consumption corresponding to the mitochondrial resting respiration (state 4) in the presence of substrates, and the second slope represents the maximal physiological rate of O_2 uptake (state 3) in the presence of substrates plus ADP. **Figures 1B,C** show the results obtained in rats with AP. While no significant differences between experimental pancreatitis and controls were found in resting respiration (**Figure 1B**), a significant decrease of O_2 consumption in state 3 was found during the first 24 h of experimental pancreatitis (CG: 40 ± 5 ng-atO/min.mg protein, $p < 0.01$) (**Figure 1C**). Respiratory control ratio (RCR), calculated as the ratio between state 3/state 4 respiration rates, are shown in **Figure 1D**. RCR was found significantly decreased in experimental pancreatitis, without recovering after 24 h of the first CAE injection (**Figure 1D**), evidencing uncoupling of the mitochondrial respiratory chain from ATP production. Interestingly, RCR returned to control values after 48 h. **Figure 1E** shows a significant decrease (40–60%) of mitochondrial ATP production rates in the experimental model compared to controls (control value: 86.9 ± 0.9 nmol ATP/min mg protein, $p < 0.05$). These mitochondrial parameters spontaneously recovered by 48 h post the first CAE injection. To analyze mitochondrial efficiency, ATP/O ratio was measured, and data are shown in **Figure 1F**. ATP/O ratio was significantly reduced during the first 3 h after the CAE first injection, while it was completely recovered to control values at 24 h of treatment. These findings show that mitochondrial function is significantly affected during the acute phase of the experimental pancreatitis, but it is recovered after 48 h suggesting the induction of mitochondrial restoration mechanisms.

Mitochondrial Dynamics Changes Induced by Experimental AP

In order to evaluate mitochondrial dynamics, the expression of OPA1 (a marker of mitochondrial fusion) and DRP1 (a marker of mitochondrial fission) were analyzed using Western blot as shown in **Figure 2A**. **Figure 2Ai** shows a dramatic reduction of DRP1 being undetectable after 30 min of the first injection of CAE and remaining undetectable at 24 h. OPA1 expression was significantly decreased after 30 min of pancreatitis (**Figure 2Ai**). After 3 h of the first injection of CAE, OPA1 values returned to basal values. Although DRP1 suddenly increased, it remained lower than basal values (**Figure 2Ai**), probably due to the regulation of the sustained OPA1-dependent mitochondrial fusion effect. Western blots quantification is shown in **Figures 2Aii,iii**. Taking into account that we found significant changes in the expression of mitochondrial dynamics proteins after 30 min of CAE treatment, we analyzed ultrastructural changes in pancreas tissue during the early stage of AP. **Figure 2B** shows the electron microscopy ultrastructural analysis of pancreas tissue from the control (**Figure 2B**, panels a and b) and from animals subjected to experimental AP (**Figure 2B**, panels c to i). In control animals, pancreatic acinar cells cytosol appears normal, with zymogen granules and mitochondria embedded in a defined and compact endoplasmic reticulum area, and no lysosomes are observed. On the contrary, characteristics that resemble endoplasmic reticulum stress and mitochondrial dynamics were observed in animals with AP after CAE treatment, accompanied with an increase in the amount

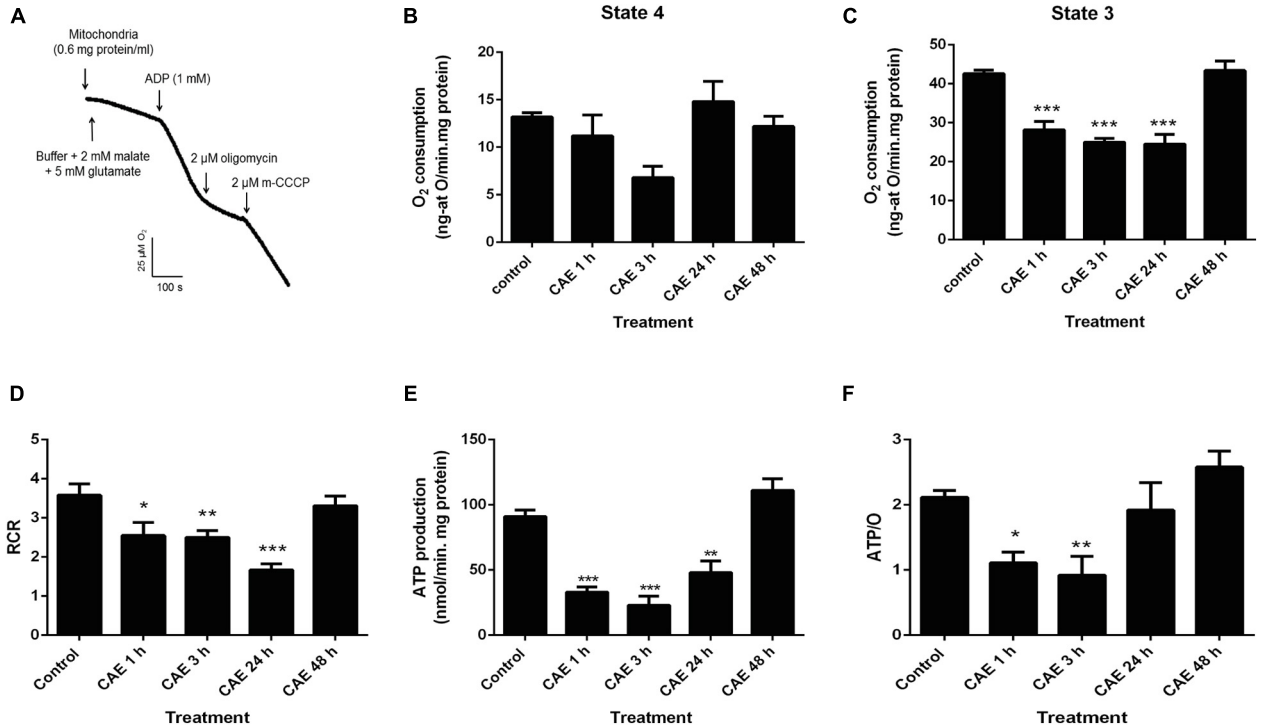

FIGURE 1 | Experimental pancreatitis produces mitochondrial dysfunction in rats. **(A)** Representative traces obtained during the assessment of pancreatic mitochondrial O_2 consumption in rest (state 4) and active (state 3) metabolic state, and after the addition of 2 μM oligomycin (state 4o) and 2 μM m-CCCP (state 3u) to the reaction chamber, in the control animal. Pancreatic mitochondria respiration in the control and CAE-treated animals in state 4 **(B)** and state 3 **(C),** $^{***}p < 0.001$ with respect to control group by ANOVA-Dunnett test, $n = 5$**. (D)** As a marker of mitochondrial coupling, respiratory control rate (RCR) was calculated as state 4/state 3. $^{*}p < 0.05$ with respect to the control group by ANOVA-Dunnett test, $n = 5$; $^{**}p < 0.01$ with respect to the control group by ANOVA-Dunnett test, $n = 5$; $^{***}p < 0.001$ with respect to the control group by ANOVA-Dunnett test, $n = 5$. **(E)** ATP production rate in pancreatic mitochondria from the control and CAE-treated rats. Malate plus glutamate were used as substrates. $^{**}p < 0.01$ with respect to the control group by ANOVA-Dunnett test, $n = 5$; $^{***}p < 0.001$ as compared with the control group, ANOVA-Dunnett test. **(F)**. As a marker of mitochondrial efficiency, ATP/O rate was calculated as ATP production rate/state3 oxygen consumption ratio, $^{*}p < 0.05$ with respect to the control group by ANOVA-Dunnett test, $n = 5$; $^{**}p < 0.01$ with respect to the control group by ANOVA-Dunnett test, $n = 5$.

and size of lysosomal structures (**Figure 2B**, panels c to i). These results demonstrate a dysregulation of mitochondrial dynamics during the development of AP, accompanied by endoplasmic reticulum stress and increased lysosomal activity.

Mitophagy Is Induced in the Rat Model of AP

We evaluated the autophagy process in the animal model in order to have the temporal relationship between mitochondrial function and dynamics. Autophagic flux was evaluated by analyzing protein expression of p62, LC3, and VMP1. **Figure 3A** shows a significant increase in LC3-II expression and a significant decrease in p62 expression in AP. These results were accompanied by an increase in VMP1 expression, which is compatible with the occurrence of VMP1-dependent autophagy (Ropolo et al., 2007). Western blots quantification is shown in **Figure 3A**, panels i to iii. Changes in the mitochondrial ultrastructure and its relationship with the lysosome during the occurrence of AP were evaluated. In **Figure 3B**, panels a and b, representative electron microscopy of control pancreatic tissue is shown. Characteristic lamellar shape of acinar cell mitochondria can be observed. The conserved mitochondrial ultrastructure can be clearly distinguished, given by the integrity of the outer and the internal membranes which form the mitochondrial crests. However, in animals treated with CAE for 60 min, mitochondrial swelling (evidenced by its roundness, clearance of the matrix, separation and disruption of mitochondrial crests) were observed (**Figure 3B**, panels c and e). In addition, structurally polarized mitochondria were observed; characteristically divided by intramitochondrial septa that separates the deeply damaged from normal mitochondrial portions (**Figure 3B**, panels c and e). Moreover, presence of autophagic vesicles with engulfed mitochondria (**Figure 3B**, panels d and f), and "isolation membrane" structures that partially surround mitochondria were found in the pancreas from the experimental model after 60 min of pancreatitis (**Figure 3B**, panels e and f). After 48 h of the first CAE injection, mitochondrial morphology has no differences with respect to the normal pancreas. These data are consistent with the occurrence of mitophagy of damaged mitochondria during the acute phase of experimental mild pancreatitis in rats.

In vitro Model of AP

Using an *in vitro* model previously described by the authors (Grasso et al., 2011), we defined the molecular mechanism involved in mitophagy of damaged mitochondria during

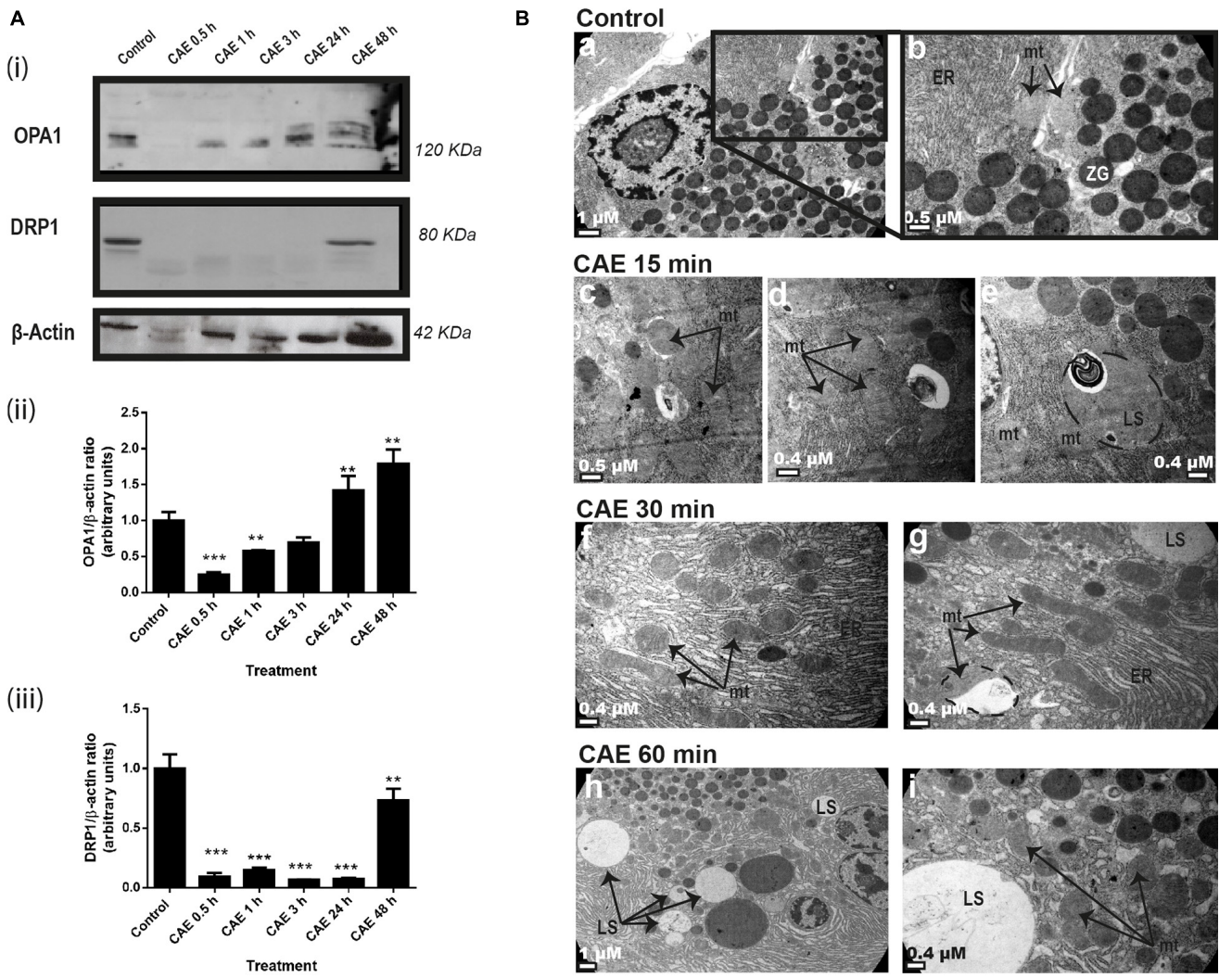

FIGURE 2 | Mitochondrial dynamics during experimental AP in rats. **(A)** Panel **(i)** shows typical examples of Western blots of pancreatic homogenates samples. ß-Actin was used as loading control. Bars in panel **(ii)** represent densitometric analysis of OPA1/ß-actin ratio. Bars in panel **(iii)** represent densitometric analysis of DRP1/ß-actin ratio blot measurements. $^{**}p < 0.01$ as compared with the control group by ANOVA-Dunnett test; $^{***}p < 0.001$ as compared with the control group by ANOVA-Dunnett test, $n = 4$. **(B)** Representative transmission electron micrographs shows the ultrastructure of acinar pancreatic tissue. A typical normal appearance of cytosolic acinar cell, with mitochondria (mt) and zymogens granules (ZG), included in a compact and defined area of endoplasmic reticulum (ER) is observed in control animals **(a)**. No lysosomal structures are observed in this tissue **(a,b)**. The ultrastructure corresponding to animals treated with CAE **(b–i)** showed a disorganization and swelling of endoplasmic reticulum (compatible with reticulum stress) and it is evident that an increase in lysosomal structures is a time dependent manner **(b–i)**. Scale bars: 1 μm in panels **(a,h)**; 0.5 μm in panels **(b,c)**, 0.4 μm in panels **(d,e,f,g,i)**.

pancreatitis next. For this goal, we have evaluated mitochondrial function, dynamics, and mitophagy at the cellular level in AR42J pancreatic acinar cells under hyperstimulation of the G-coupled receptor of CCK, a model for early cellular events in AP (Grasso et al., 2011).

Mitochondrial Dynamics Induced by CCK-R Hyperstimulation in AR42J Cells

Given that mitochondrial dysfunction can lead to changes in mitochondrial dynamics (Ferree and Shirihai, 2012), markers of mitochondrial dynamics such as the expression of DRP1 (mitochondrial fission) and OPA1 (mitochondrial fusion), as markers of mitochondrial dynamics, as well as the mitochondrial morphology, were evaluated. **Figure 4Ai** shows representative DRP1 and OPA1 Western blots. An earlier increase of DRP1 expression was found after 30 min, while OPA1 increased after 60 min of CAE treatment (**Figure 4A**, panels ii and iii). Consistent with these results, morphological images using the MitoTracker probe showed two mitochondrial populations: a small and rounded mitochondrial population after 30 min of treatment and a marked elongated mitochondrial population after 60 min of treatment (**Figure 4B**). As a whole, these results support the occurrence of mitochondrial fission after 30 min

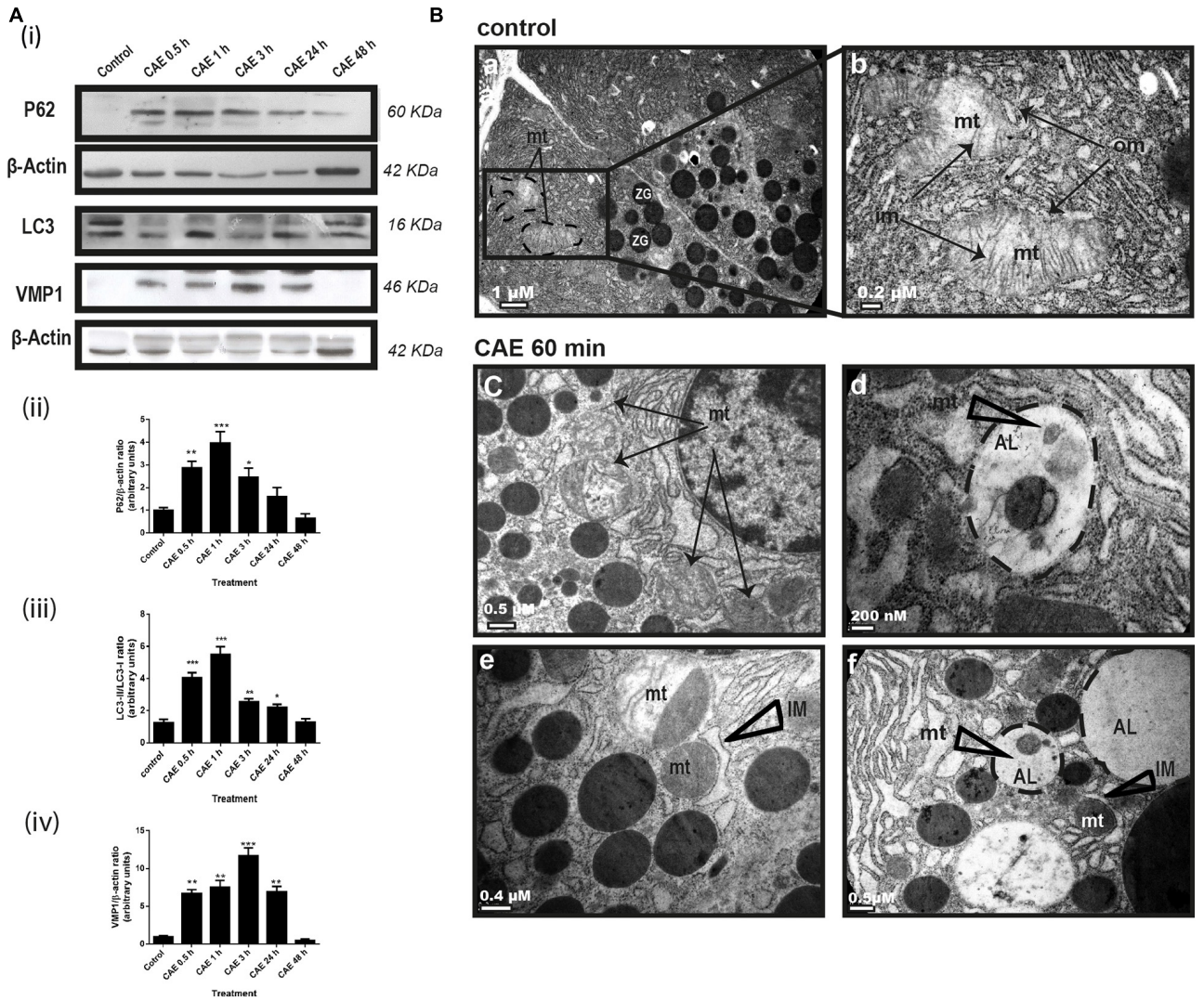

FIGURE 3 | Experimental pancreatitis induces autophagy and mitophagy in rats. **(A)** Changes in mitochondrial autophagy proteins expression during experimental AP. Panel **(i)** shows typical Western blots of pancreatic homogenates samples. ß-Actin was used as loading control. Bars in panel **(ii)** represent densitometric analysis of PG62/ß-actin ratio. Bars in panel **(iii)** represent densitometric analysis of LC3-II/LC3-I ratio blot measurements. Bars in panel **(iv)** represent densitometric analysis of VMP1/ß-actin ratio. *$p < 0.05$ as compared with the control group, ANOVA-Dunnett test; **$p < 0.01$ as compared with the control group, ANOVA-Dunnett test; ***$p < 0.001$ as compared with the control group, ANOVA-Dunnett test; $n = 4$. **(B)** Representative transmission electron micrographs of pancreas from control **(a,b)** and CAE 60 min treated animals **(c–f)**. **(a,b)**: control animals displayed normal mitochondria morphology. Typical organization of mitochondria (mt) clearly displayed the inner membrane (im) comprizing of cristae and well defined mitochondrial outer membrane (om). **(c–f)**: 1 h after CAE administration, mitochondria displayed several abnormalities, such as loss and/or disruption of cristae, clearer matrix, and swelling [black arrows, in panels **(c,e)**]. On the other hand, "isolation membranes" (IM) can be observed that partially surround mitochondria **(e,f)** and visible autolysosomes (AL) with remains of mitochondrial structures in their interior **(d,f)**, both structures compatible with mitophagy. Scale bars: 1 μm in panel **(a)**; 0.2 μm in panel **(b)**; 0.5 μm in panels **(c,f)**; 200 nm in panel **(d)**; and 0.4 μm in panel **(e)**.

accompanied by mitochondrial elongation after 60 min of CCK-R hyperstimulation.

Mitophagy Is Induced by CCK-R Hyperstimulation in AR42J Cells

We evaluated autophagy in cells transfected with RFP-LC3 as an autophagy marker. **Figure 5A** shows a time-dependent increase in autophagosome formation after CCK-R hyperstimulation evidenced by LC3 recruitment. In order to identify mitophagy, AR42J cells treated with CAE were transfected with the specific tandem probe pMITO-RFP-GFP. Using confocal analysis (**Figure 5B**), control cells exhibited a mitochondrial population mostly labeled in yellow indicating healthy organelles. On the contrary, two separate mitochondrial populations were observed after CCK-R hyperstimulation. One of them remained labeled in yellow, and the other one located in the apical area of the cytoplasm, labeled in red, indicating their autolysosome location. Therefore, confocal analysis using the specific tandem probe confirmed the occurrence of mitophagy in the cell model of AP.

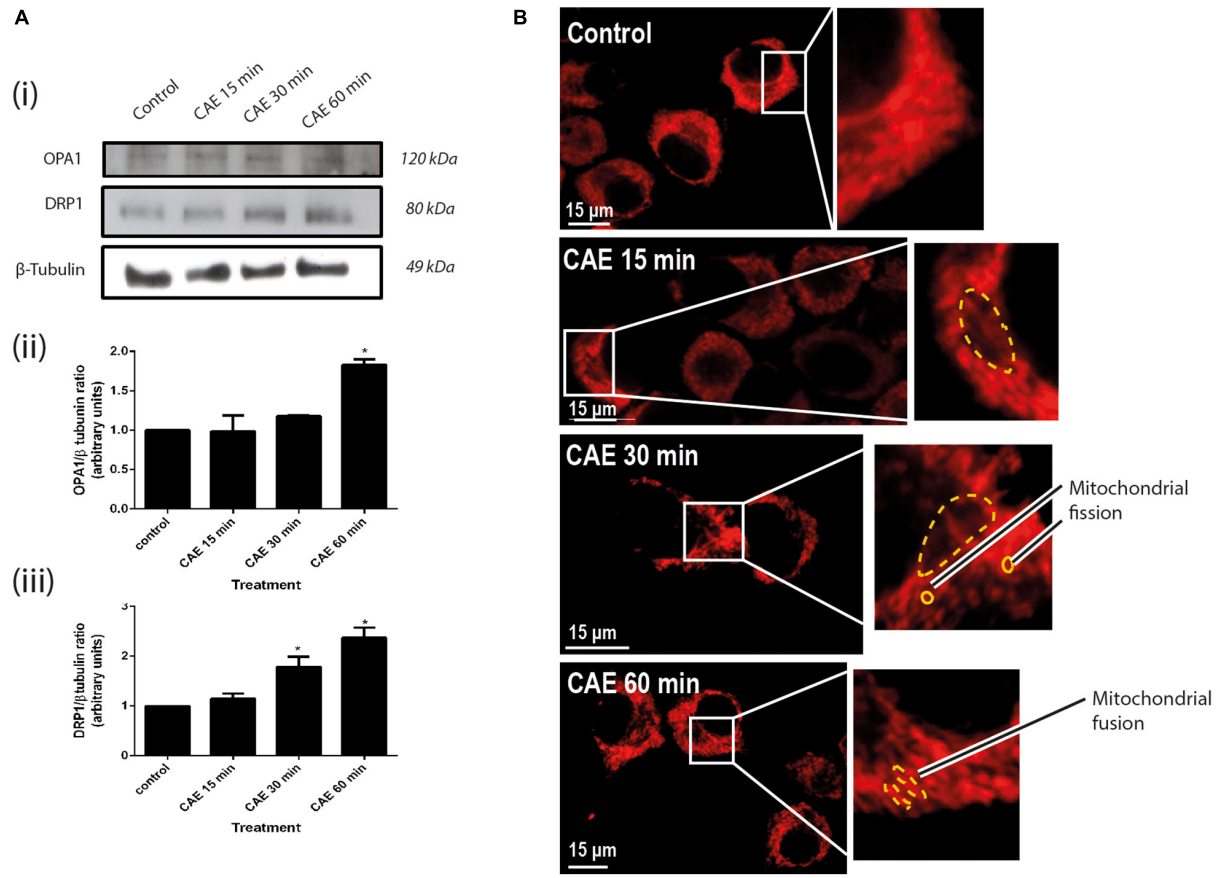

FIGURE 4 | Mitochondrial dynamics in AR42J cells under CCK-R hyperstimulation. **(A)** OPA1 and DRP 1 protein expression of AR42J pancreatic acinar cells treated with vehicle and CAE. Panel **(i)** shows typical examples of Western blots of pancreatic homogenates samples. ß-tubulin was used as loading control. Bars in panel **(ii)** represent densitometric analysis of OPA1/ß-tubulin ratio. Bars in panel **(iii)** represent densitometric analysis of DRP1/ß-tubulin ratio blot measurements. $^{*}p < 0.05$ as compared with control group, ANOVA-Dunnett test, $n = 4$. **(B)** Red-MitoTracker probe was used to mark the mitochondrial population. Control, CAE 15 min, CAE 30 min, and CAE 60 min representative images are shown. Populations of shortened mitochondria [panel **(B)**, CAE 30 min] and elongated mitochondria [panel **(B)**, CAE 60 min], morphologies compatible with changes in mitochondrial dynamics (mitochondrial fission and fusion), are observed in cells treated with CAE. Scale bar represents 15 μm.

Figure 5C shows that mitophagy is significantly increased under hyperstimulation of CCK-R.

Then, the subcellular distribution of healthy mitochondria (labeled with Red-MitoTracker) and lysosomes (labeled with blue-LysoTracker) was evaluated. **Figure 5D** shows healthy mitochondria labeled in red that did not localize with tenuous and small lysosomes appearing in the basal area of the control cells. While, under CCK-R hyperstimulation, the presence of large lysosomes was clearly evident (**Figure 5D**). Lysosomal area per cell was quantified and it is shown in **Figure 5E**. This "lysosomal pocket" coincided with the apical area where mitophagy was observed in **Figure 5B**, evidencing the presence of autolysosomes with damaged and degraded mitochondria inside that were not able to be labeled with the MitoTracker.

CCK-R-Hyperstimulation Induced Mitochondrial Dysfunction and Mitophagy in Pancreatic Acinar Cells

To determine mitochondrial function in AR42J cells that were submitted to CCK-R hyperstimulation, mitochondrial inner membrane potential was analyzed by flow cytometry using the TMRM potentiometric probe. **Figure 6Ai** shows representative time-dependent course histograms of hyperstimulation as a function of TMRM fluorescence intensity; panel Aii shows histograms quantification, represented as the percent of AR42J cells that preserve the inner membrane mitochondrial potential. In **Figure 6Aii**, a significant decrease in mitochondrial internal membrane potential was observed after 60 min of CCK-R hyperstimulation, indicating that mitochondrial damage in this cellular model of pancreatitis. Besides, to estimate the mitochondrial degradation in pancreatic cells submitted to CCK-R-hyperstimulation, an MTDR probe that remains inside intact mitochondria was used. **Figure 6B** is a representative histogram showing a time-dependent variation in the mitochondrial mass as a function of MTDR fluorescence intensity showing a significant decrease in MTDR fluorescence after 30 and 60 min of CAE hyperstimulation. These data suggest that pancreatitis not only affects mitochondrial function but also induces

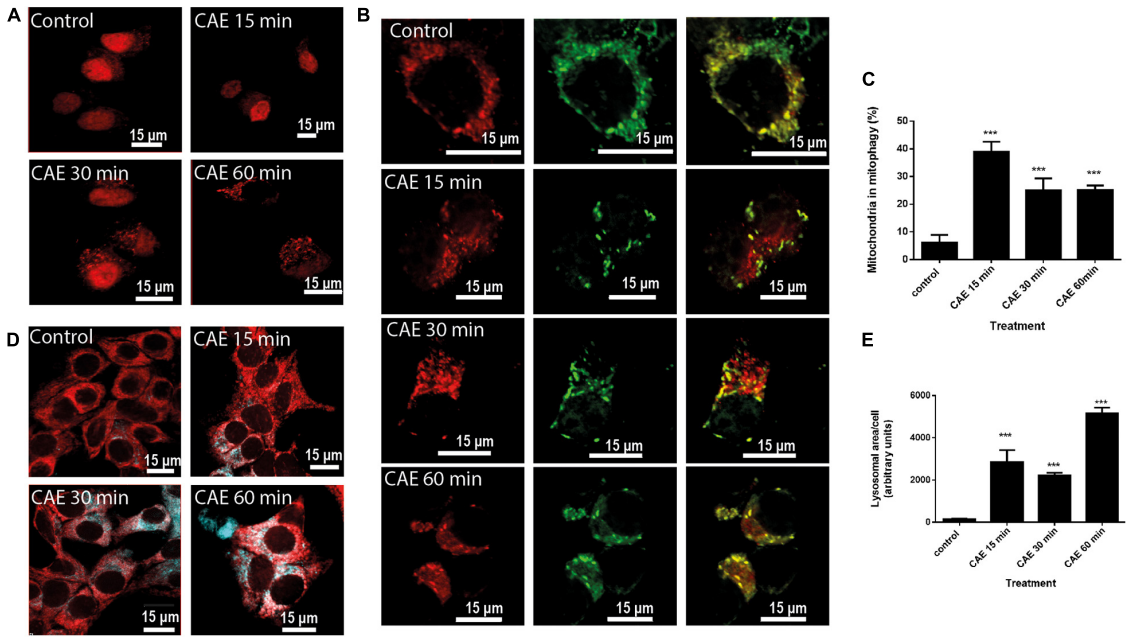

FIGURE 5 | Mitophagy is induced in AR42J cells under CCK-R hyperstimulation. **(A)** Representative confocal microscopy images of AR42J cells transfected with plasmid encoding for RFP-LC3 (control, CAE 15 min, CAE 30 min, and CAE 60 min). **(B)** AR42J cells treated with CAE and transfected with plasmids encoding for RFP-GFP-pMITO. The GFP signal is quenched at the lower pH of lysosomes, while RFP can be consistently visualized. Yellow fluorescence (RFP merged with GFP) indicates normal mitochondria population, whereas red fluorescence (RFP) indicates population of mitochondria undergoing mitophagy. **(C)** Quantification of the percentage of the mitochondrial population found in mitophagy. ***$p < 0.001$ compared with the control group, ANOVA-Dunnett test. **(D)** Representative confocal micrographs showing mitochondria detected with Red-MitoTracker and lysosome detected with Blue-LysoTracker in treated pancreatic AR42J cells (control, CAE 15 min, CAE 30 min, and CAE 60 min). Scale bar represents 15 µm. **(E)** Lysosomal area quantification per cell (in arbitrary units). ***$p < 0.001$ compared with the control group, ANOVA-Dunnett test.

early and significant degradation of damaged mitochondria as well.

Together with Mnf2, Parkin1 is one of the proteins that associates to the external mitochondrial membrane when mitochondrial membrane potential decreases. Parkin1 is a ubiquitin ligase that labels proteins of mitochondrial outer membrane to serve as substrates of autophagy-cargo recognition molecules such as p62, which interacts with LC3 to initiate selective autophagy. **Figure 6C** shows that under CCK-R hyperstimulation, Parkin1 expression assayed by western blot showed a rapid and significant increase under CCK-R hyperstimulation. Moreover, **Figure 6D** shows that while Parkin1 labeling is light and located in the cytosol in control cells, a marked translocation of Parkin1 from cytosol to mitochondria was observed after CCK-R hyperstimulation. These findings suggest that during AP, Parkin1 recognizes and recruits to damaged mitochondria in order to label them for autophagic degradation.

VMP1-Mediated Mitochondrial Degradation Is Induced in Pancreatic Acinar Cells Under CCK-R-Hyperstimulation

To investigate if VMP1 is involved in the selective autophagic degradation of damaged mitochondria during pancreatitis, the cells were transfected with EGFP-VMP1 and labeled mitochondria with red-MitoTracker. **Figure 7A** shows that in control cells, healthy mitochondria were labeled in red and did not localize with green VMP1. On the contrary, a dramatic redistribution of VMP1, now surrounding rounded mitochondria, can be observed after CCK-R hyperstimulation. Taking into account that VMP1 is a transmembrane protein of the autophagosomes, we isolated autophagosomes using magnetic beads fused to anti-VMP1 antibody, or anti-V5 antibody from AR42J cells expressing VMP1-V5. Both methods showed that after CCK-R hyperstimulation, autophagosome fractions contained mitochondrial VDAC markers. These data further confirm that VMP1 is involved in mitophagy during AP (**Figure 7B**). To investigate if VMP1 is required for mitochondrial degradation during pancreatitis, VMP1 expression was downregulated using a dual sh-VMP1 plasmid labeled with GFP allowing to distinguish two cellular outcomes after transfection and exclude by gating GFP negative cells. GFP positive cells were analyzed by flow cytometry to estimate mitochondrial degradation during experimental pancreatitis. As shown in **Figure 7C**, an increase in the $MTDR^{+}$ population was observed in all cells transfected with sh-VMP1 plasmid compared to non-transfected cells, for each treatment time. Furthermore, no significant changes were observed between the different treatment times in sh-VMP1 transfected cells. These results suggest that VMP1

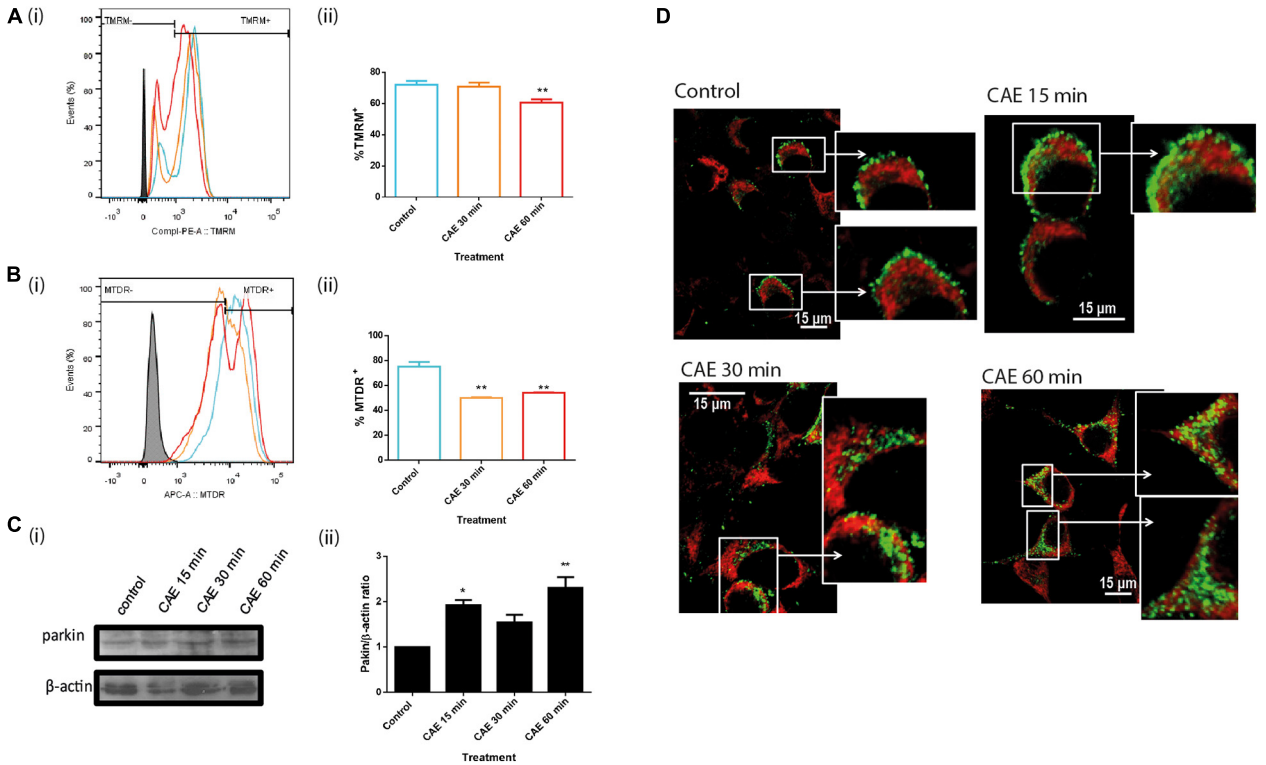

FIGURE 6 | Mitochondrial depolarization induces parkin-dependent mitophagy during CCK-R hyperstimulation. **(A)** Mitochondrial inner membrane potential evaluated by flow cytometry using TMRM probe **(i)** Overlaid histograms of mitochondrial event versus TMRM fluorescence intensity. Control (light blue), CAE 30 min (orange), CAE 60 min (red), and autofluorescence (full black). **(ii)** % $TMRM^+$ cells quantification. $^{**}p < 0.01$ compared with the control group, ANOVA-Dunnett test. **(B)** Mitochondrial mass evaluated by flow cytometry used MTDR. **(i)** Overlaid histograms of mitochondrial events versus MTDR fluorescence intensity. Control (light blue), CAE 30 min (orange), CAE 60 min (red), and autofluorescence (full black). **(ii)** % $MTDR^+$ cells quantification. $^{**}p < 0.01$ compared with the control group, ANOVA-Dunnett test. **(C)** Parkin expression by Western Blot assay in AR42J cells treated with CAE at different times. Panel **(i)** shows typical Western Blots of pancreatic homogenates samples. ß-actin was used as the loading control. Bars in panel **(ii)** represent densitometric analysis of parkin/ß-actin ratio. $^{*}p < 0.05$ as compared with the control group, ANOVA-Dunnett test, $n = 4$. **(D)** Representative confocal microscopy images of AR42J cells treated with CAE showing intracellular changes distribution of mitochondria (detected with Red-MitoTracker probe) and Parkin (detected by immunofluorescence in green).

inhibition preserves mitochondrial mass by inhibiting mitophagy. Together, these results show that VMP1 mediates the selective autophagy of damaged mitochondria during experimental pancreatitis. The fact that mitochondrial mass is preserved, even in control cells, suggests that VMP1-mediated mitophagy might also function as a homeostatic process regulating mitochondria function in pancreatic acinar cells.

DISCUSSION

AP is an inflammatory disease for which its pathogenesis is poorly understood and lacks a specific treatment. However, most of the cases are mild and self-limited forms and pancreas morphology and physiology is totally recovered. During the development of AP, pancreatic intracellular trypsinogen activation, mitochondrial damage with the consequent ATP depletion and inflammatory response are characteristic pathophysiological features (Maléth et al., 2013). This work is focused on the comprehensive study of mitophagy, its molecular mechanisms and its relationship with mitochondrial dynamics in two experimental models of AP. We have analyzed mitochondrial fusion and fission, as well as mitophagy, using two models: an *in vitro* cellular model, and *in vivo* model of mild and self-limited form of AP. These processes, which were historically described separately, lead to structural morphological changes necessary to maintain or restore mitochondrial function under physiological and pathological conditions.

While OPA1 is the protein related to mitochondrial fusion and elongation, DRP1 is a key molecule in the mitochondrial fission, a mechanism considered necessary to obtain mitochondrial fragments that are sequestered and degraded by autophagy (Gomes et al., 2011). Li et al. (2019) shows that DRP1 nitration (due to the increase of the powerful oxidant ONOO-) promotes its assembly and its recruitment to the mitochondrial outer membrane and induces the process of mitophagy mediated by the Pink1/Parkin1 pathway. This mechanism is relevant in the cell response to human pathologies. For instance, deficiency of OPA1 expression is accompanied by an excessive increase in fragmented mitochondria and a dysregulated mitophagy in mitochondrial optic neuropathies (Liao et al., 2017). Therefore, changes in DRP1

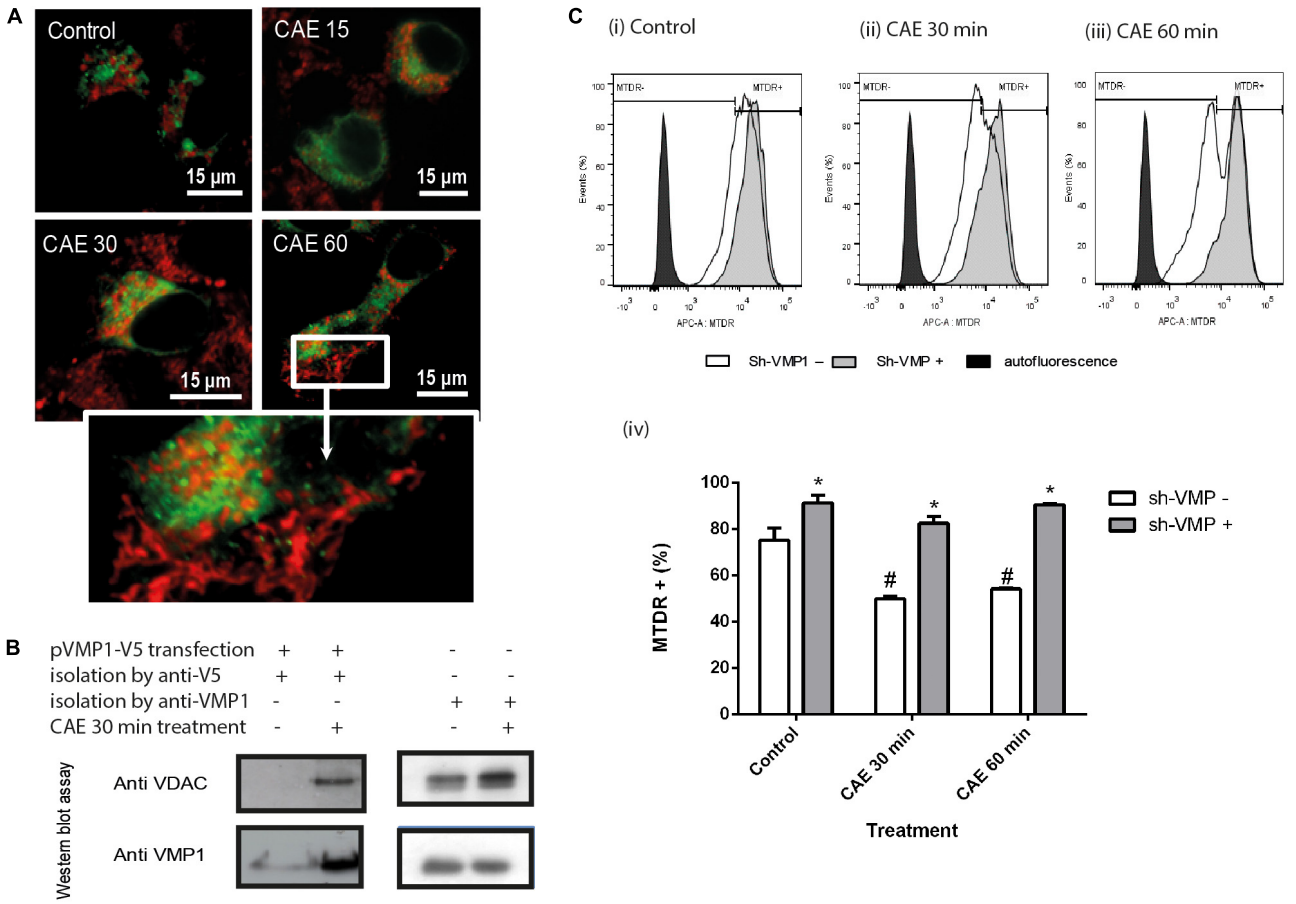

FIGURE 7 | Identification of the novel VMP1 pathway mediating selective mitophagy in experimental pancreatitis. **(A)** AR42J transfected cells with plasmid encoding for GFP-VMP1 and treated with CAE. Red-MitoTracker was used to show mitochondrial population. **(B)** Western Blot of isolated autophagosomes by magnetic beads linked to anti V5 or VMP1 antibodies from AR42J CAE-treated cells. The presence of the mitochondrial protein VDAC is observed only in the cells treated with CAE. **(C)** VMP1 inhibition attenuates mitophagy during pancreatitis, evaluated by flow cytometry using MTDR. AR42J cells were transfected with GFP-shVMP1 plasmid 48 h before CAE treatment. Overlaid histograms of AR42J events versus MTDR fluorescence intensity. shVMP1-transfected population and not transfected in panel **(i)** control, **(ii)** CAE 30 min, and **(iii)** CAE 60 min. **(iv)** MTDR fluorescence quantification, $^{*}p < 0.01$ as compared to the same treatment without transfection; $^{\#}p < 0.01$ as compared to the control group Two-way ANOVA-Tukey test.

and OPA1 expression are not only involved in mitochondrial dynamics but also in the clearance of damaged mitochondria by autophagy (Jin and Youle, 2012). In the present study, using the *in vivo* model of AP in rats, we found mitochondrial damage along with altered mitochondrial dynamics and autophagic degradation of mitochondria. These features were evidenced by the 24 h time course changes in DRP1 and OPA1 values and the simultaneous increase in autophagic markers such as LC3 and p62, as well as high expression of the selective autophagy marker VMP1 (Grasso et al., 2011). Mitochondrial dynamics changes were confirmed by electron microscopy, which showed ultrastructural damage such as polarized (fission) and elongated (fusion) mitochondria. Furthermore, significant increases in lysosomal structures were observed with internalized mitochondrial structures in degradation processes. Interestingly, the expression of proteins involved in fusion, fission, and autophagy returned to control values after 48 h, along with functional recovery of mitochondria.

In order to understand the molecular pathway of the selective degradation of damaged mitochondria in pancreatitis, we studied mitophagy in pancreatic cells under CCK-R hyperstimulation. Using this *in vitro* model, we observed an increase in Parkin1 expression, previously reported in AP by Biczo et al. (2018). Moreover, we observed the redistribution of Parkin1 from a cytosolic location to damaged mitochondria areas. Also, the increment of large lysosomes containing degraded mitochondria are in agreement with the described mitophagy. Using the GFP-RFP-pMITO tandem probe, we demonstrated that mitophagy is early induced in the pancreatic cell model under CCK-R hyperstimulation and remains activated during 60 min. Interestingly, two mitochondrial populations morphologically distinguishable were observed simultaneously. Those polarized after fission of damaged mitochondria, and the elongated ones after fusion of the healthy mitochondria, suggesting a selective mechanism of degradation of damaged mitochondria allowing the recovery of energetic

status. Pink1 is a protein located in the mitochondrial outer membrane, where it is continuously degraded by various processes (Bingol and Sheng, 2016). However, mitochondrial depolarization or malformed proteins accumulation in its matrix (both signs of mitochondrial damage) trigger mechanisms that stabilize Pink1 with its consequent accumulation in mitochondria (Geisler et al., 2010; Vives-Bauza et al., 2010). This Pink1 accumulation is Parkin's recruitment signal to the outer mitochondrial membrane, a signal recognized by the autophagic machinery for the degradation of these damaged mitochondria. Moreover, for the first time, here we are reporting the VMP1 involvement in the mitophagy process during AP, observable not only by repositioning around damaged mitochondrial populations, but also by the detection of mitochondria in autophagosomes specifically isolated with anti-VMP1 antibodies. Downregulation of VMP1 avoided mitochondrial degradation and confirmed that VMP1 expression is required for mitophagy during AP. We present evidence of a novel DRP1-Parkin1-VMP1 pathway, which mediates the selective degradation of damaged mitochondria by mitophagy in AP.

Furthermore, our results confirmed the early decrease of mitochondrial function in the mild model of pancreatitis through the determination of mitochondrial ATP production rate and the mitochondrial O_2 consumption and ATP/O ratio, as it was previously reported (Mukherjee et al., 2016). Mitochondrial dysfunction in pancreatitis has been described through decreased mitochondrial membrane potential, increased calcium uptake; decreased ATP levels, considering the latter as a marker of ATP synthase activity; or indirect determinations of ATP synthase activity in submitochondrial particles (Biczo et al., 2018). To our knowledge, direct assessment of the ATP production rate in intact mitochondria, as well as ATP/O ratio allows a better understanding of the degree of mitochondria dysfunction during AP.

In physiological conditions, more than 90–95% of the O_2 consumed by living beings is reduced to H_2O through the mitochondrial respiratory chain, by oxidative phosphorylation to produce ATP. Moreover, between 1 and 2% of the O_2 consumed is partially reduced to $O_2^{\cdot-}$ and H_2O_2 in the mitochondria, being the main source of active oxygen species as signaling molecules (Boveris and Cadenas, 1982). We found that both the mitochondrial O_2 consumption rate and the mitochondrial ATP production were significantly decreased (39 and 50%, respectively) up to 24 h of experimental AP. These results together with an abrupt decrease in ATP/O rate, as a marker of mitochondrial efficiency (Vanasco et al., 2012), suggest that part of the O_2 consumed is not used for ATP production, and

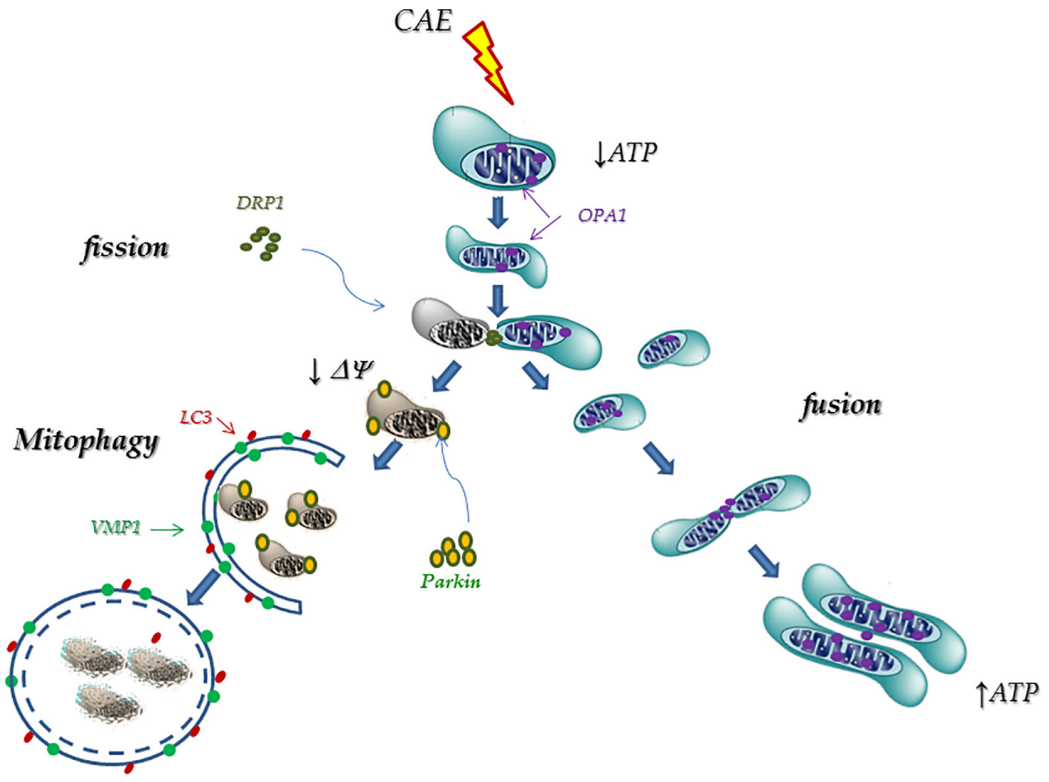

FIGURE 8 | Proposed mechanism: Mitophagy as a cellular rescue mechanism during pancreatitis. During AP, mitochondrial failure is able to induce phenotypic changes in acinar cells (OPA1, DRP1, Parkin1, and VMP1 expressions) that triggers mitochondrial remodeling processes. These changes include fusion events (through OPA1) which allow internal rearrangement of their structure; and fission events (through DRP1) that originate new functional mitochondria as well as damaged and depolarized mitochondria. The latter are labeled by Parkin1, and through the VMP1-dependent autophagic pathway, are selectively detected and degraded by mitophagy within the lysosomes.

it is used in other metabolic pathways such as in mitochondrial ROS generation instead. An increase in mitochondrial ROS has been observed by Booth et al. (2011b), during bile acid injury of pancreatic acinar cells. Moreover, MitoQ (an antioxidant targeted to mitochondria) reduces both inflammation and the presence of edema in acinar cells treated with caerulein (Huang et al., 2015). On the other hand, the decrease in ATP availability may lead to the inefficiency of the Ca^{2+} (ATP-dependent) pumps (Booth et al., 2011a), responsible for restoring basal Ca^{2+} cytosolic levels. In this way, apoptosis might also be compromised, since caspase activation is an ATP-dependent process, leading cells to necrosis.

The central role of mitochondrial dysfunction and impaired autophagy were reported in different animal models of severe AP such as in mice treated with L-arginine-induced pancreatitis (Biczo et al., 2018). In these models, mitochondrial dysfunction causes pancreatic ER stress, impaired autophagy, and deregulation of lipid metabolism. However, the administration of trehalose, an autophagy inductor, prevents intracellular trypsinogen activation, necrosis, and other parameters of pancreatic injury (Biczo et al., 2018). Also, we previously demonstrated that the induction of autophagy in the pancreas by the transgenic expression of VMP1 does not only induce pancreatitis but also prevents intracellular trypsinogen activation, necrosis, and other parameters of pancreatic injury in the mouse caerulein model of pancreatitis (Grasso et al., 2011). Interestingly, in the rat model of mild pancreatitis, we showed that the mitochondrial function is spontaneously and completely restored when pancreas tissue is also recovered, after 48 h of caerulein treatment. These findings suggest that the acinar cell can set up molecular mechanisms to restore cellular bioenergetics leading to the pancreas recovering.

Taking our results together, we hypothesize that during AP, mitochondrial failure can induce phenotypic changes in acinar cells (OPA1, DRP1, Parkin1, and VMP1 expressions) that triggers mitochondrial remodeling processes. These changes include fusion events (through OPA1) which allow internal rearrangement of their structure; and fission events (through DRP1) that originate new functional mitochondria as well as damaged and depolarized mitochondria. The latter, labeled by Parkin1 and through the VMP1-dependent autophagic pathway, is selectively detected and degraded by mitophagy within the lysosomes (**Figure 8**). A better understanding of the molecular mechanisms involved to restore mitochondrial function, such as changes in mitochondrial dynamics and mitophagy, could be relevant in the development of therapeutic strategies in AP.

DATA AVAILABILITY STATEMENT

The raw data supporting the conclusions of this article will be made available by the authors, without undue reservation.

ETHICS STATEMENT

The animal study was reviewed and approved by Comité Institucional para el Cuidado y Uso de Animales de Laboratorio (CICUAL-FFyB).

AUTHOR CONTRIBUTIONS

VV performed most of the experiments and wrote the manuscript. VV and AR designed the experiments and analyzed the results. DG, DO, MG, and TV contributed to the development of the experimental models, sample preparations, and assessments. TO performed expression plasmid designs and constructions. JQ discussed the results and revised the manuscript. SA designed and analyzed the data of mitochondrial function experiments on animal and cellular models and edited the manuscript. MV directed the work, designed the autophagy/mitophagy experiments in animal and cellular models of pancreatitis, discussed the results, and edited the manuscript. All the authors revised the final version of the manuscript.

FUNDING

This work was supported by grants from: Consejo Nacional de Investigaciones Científicas y Técnicas (CONICET) (PIPGI-11220150100160CO and PIP112201201006921); Agencia Nacional de Promoción Científica y Tecnológica (ANPCyT) (PICT2016-1032 PICT2013-2048; PICT-2016-1888; PICT-2013-3227; and PICT-2017-4069) and Universidad de Buenos UBACyT 2018-2021 (GC-20020170100082BA and UBACYT20162002015010018 6BA).

REFERENCES

Antonucci, L., Fagman, J. B., Kim, J. Y., Todoric, J., Gukovsky, I., Mackey, M., et al. (2015). Basal autophagy maintains pancreatic acinar cell homeostasis and protein synthesis and prevents ER stress. *Proc. Natl. Acad. Sci. U.S.A.* 112, E6166–E6174. doi: 10.1073/pnas.1519384112

Bereiter-Hahn, J., and Voth, M. (1994). Dynamics of mitochondria in living cells. *Microsc. Res. Tech.* 219, 198–219.

Biczo, G., Vegh, E. T., Shalbueva, N., Mareninova, O. A., Elperin, J., Lotshaw, E., et al. (2018). Mitochondrial dysfunction, through impaired autophagy, leads to endoplasmic reticulum stress, deregulated lipid metabolism, and pancreatitis in animal models. *Gastroenterology* 154, 689–703. doi: 10.1053/j.gastro.2017.10.012

Bingol, B., and Sheng, M. (2016). Mechanisms of mitophagy: PINK1, Parkin, USP30 and beyond. *Free Radic. Biol. Med.* 100, 210–222. doi: 10.1016/j.freeradbiomed.2016.04.015

Booth, D. M., Mukherjee, R., Sutton, R., and Criddle, D. N. (2011a). Calcium and reactive oxygen species in acute pancreatitis: friend or foe? *Antioxidants Redox Signal.* 15, 2683–2698. doi: 10.1089/ars.2011.3983

Booth, D. M., Murphy, J. A., Mukherjee, R., Awais, M., Neoptolemos, J. P., Gerasimenko, O. V., et al. (2011b). Reactive oxygen species induced by bile acid induce apoptosis and protect against necrosis in pancreatic acinar cells. *Gastroenterology* 140, 2116–2125. doi: 10.1053/j.gastro.2011.02.054

Boveris, A., and Cadenas, E. (1982). "Production of superoxide radicals and hydrogen peroxide in mitochondria," in *Superoxide Dismutase*, ed. L. W. Oberley (Boca Raton, FL: CRC press), 15–30.

Cadenas, E., and Boveris, A. (1980). Enhancement of hydrogen peroxide formation by protophores and ionophores in antimycin-supplemented mitochondria. *Biochem. J.* 188, 31–37. doi: 10.1042/bj1880031

Cid-Castro, C., Hernández-Espinosa, D. R., and Morán, J. (2018). ROS as regulators of mitochondrial dynamics in neurons. *Cell. Mol. Neurobiol.* 38, 995–1007. doi: 10.1007/s10571-018-0584-7

Cipolat, S., De Brito, O. M., Dal Zilio, B., and Scorrano, L. (2004). OPA1 requires mitofusin 1 to promote mitochondrial fusion. *Proc. Natl. Acad. Sci. U.S.A.* 101, 15927–15932. doi: 10.1073/pnas.0407043101

Diakopoulos, K. N., Lesina, M., Wörmann, S., Song, L., Aichler, M., Schild, L., et al. (2015). Impaired autophagy induces chronic atrophic pancreatitis in mice via sex- and nutrition-dependent processes. *Gastroenterology* 148, 626–638.e17. doi: 10.1053/j.gastro.2014.12.003

Dusetti, N. J., Jiang, Y., Tomasini, R., Azizi Samir, A., Calvo, E. L., Mallo, G. V., et al. (2002). Cloning and expression of the rat vacuole membrane protein 1 (VMP1), a new gene activated in pancreas with acute pancreatitis, which promotes vacuole formation. *Biochem. Biophys. Res. Commun.* 290, 641–649. doi: 10.1006/bbrc.2001.6244

Ferree, A., and Shirihai, O. (2012). Mitochondrial dynamics: the intersection of form and function. *Adv. Exp. Med. Biol.* 748, 13–40. doi: 10.1007/978-1-4614-3573-0_2

Geisler, S., Holmström, K. M., Skujat, D., Fiesel, F. C., Rothfuss, O. C., Kahle, P. J., et al. (2010). PINK1/Parkin-mediated mitophagy is dependent on VDAC1 and p62/SQSTM1. *Nat. Cell Biol.* 12, 119–131. doi: 10.1038/ncb2012

Gomes, L. C., Di Benedetto, G., and Scorrano, L. (2011). During autophagy mitochondria elongate, are spared from degradation and sustain cell viability. *Nat. Cell Biol.* 13, 589–598. doi: 10.1038/ncb2220

Graef, M., and Nunnari, J. (2011). Mitochondria regulate autophagy by conserved signalling pathways. *EMBO J.* 30, 2101–2114. doi: 10.1038/emboj.2011.104

Grasso, D., Ropolo, A., Lo Ré, A., Boggio, V., Molejón, M. I., Iovanna, J. L., et al. (2011). Zymophagy, a novel selective autophagy pathway mediated by VMP1-USP9x-p62, prevents pancreatic cell death. *J. Biol. Chem.* 286, 8308–8324. doi: 10.1074/jbc.M110.197301

Hodârnâu, A. A., Dancea, S., and Bârzu, O. (1973). Isolation of highly purified mitochondria from rat pancreas. *J. Cell Biol.* 59, 222–227. doi: 10.1083/jcb.59.1.222

Huang, W., Cash, N., Wen, L., Szatmary, P., Mukherjee, R., Armstrong, J., et al. (2015). Effects of the mitochondria-targeted antioxidant mitoquinone in murine acute pancreatitis. *Mediators Inflamm.* 2015:901780. doi: 10.1155/2015/901780

Ježek, J., Cooper, K. F., and Strich, R. (2018). Reactive oxygen species and mitochondrial dynamics: the yin and yang of mitochondrial dysfunction and cancer progression. *Antioxidants* 7:13. doi: 10.3390/antiox7010013

Jin, S. M., and Youle, R. J. (2012). PINK1-and Parkin-mediated mitophagy at a glance. *J. Cell Sci.* 125, 795–799. doi: 10.1242/jcs.093849

Kim, S. J., Khan, M., Quan, J., Till, A., Subramani, S., and Siddiqui, A. (2013). Hepatitis B virus disrupts mitochondrial dynamics: induces fission and mitophagy to attenuate *Apoptosis*. *PLoS Pathog.* 9:e1003722. doi: 10.1371/journal.ppat.1003722

Liao, C., Ashley, N., Diot, A., Morten, K., Phadwal, K., Williams, A., et al. (2017). Dysregulated mitophagy and mitochondrial organization in optic atrophy due to OPA1 mutations. *Neurology* 88, 131–142. doi: 10.1212/WNL.0000000000003491

Liesa, M., and Shirihai, O. S. (2013). Mitochondrial dynamics in the regulation of nutrient utilization and energy expenditure. *Cell Metab.* 17, 491–506. doi: 10.1016/j.cmet.2013.03.002

Li, W., Feng, J., Gao, C., Wu, M., Du, Q., Tsoi, B., et al. (2019). Nitration of Drp1 provokes mitophagy activation mediating neuronal injury in experimental autoimmune encephalomyelitis. *Free Radic. Biol. Med.* 143, 70–83. doi: 10.1016/j.freeradbiomed.2019.07.037

Maléth, J., Rakonczay, Z., Venglovecz, V., Dolman, N. J., and Hegyi, P. (2013). Central role of mitochondrial injury in the pathogenesis of acute pancreatitis. *Acta Physiol.* 207, 226–235. doi: 10.1111/apha.12037

Mukherjee, R., Criddle, D. N., Gukvoskaya, A., Pandol, S., Petersen, O. H., and Sutton, R. (2008). Mitochondrial injury in pancreatitis. *Cell Calcium* 44, 14–23. doi: 10.1016/j.ceca.2007.11.013

Mukherjee, R., Mareninova, O. A., Odinokova, I. V., Huang, W., Murphy, J., Chvanov, M., et al. (2016). Mechanism of mitochondrial permeability transition pore induction and damage in the pancreas: inhibition prevents acute pancreatitis by protecting production of ATP. *Gut* 65, 1333–1346. doi: 10.1136/gutjnl-2014-308553

Narendra, D., Tanaka, A., Suen, D. F., and Youle, R. J. (2008). Parkin is recruited selectively to impaired mitochondria and promotes their autophagy. *J. Cell Biol.* 183, 795–803. doi: 10.1083/jcb.200809125

Narendra, D. P., Jin, S. M., Tanaka, A., Suen, D. F., Gautier, C. A., Shen, J., et al. (2010). PINK1 is selectively stabilized on impaired mitochondria to activate Parkin. *PLoS Biol.* 8:e1000298. doi: 10.1371/journal.pbio.1000298

Ojeda, D. S., Grasso, D., Urquiza, J., Till, A., Vaccaro, M. I., and Quarleri, J. (2018). Cell death is counteracted by mitophagy in HIV-productively infected astrocytes but is promoted by inflammasome activation among non-productively infected cells. *Front. Immunol.* 9:2633. doi: 10.3389/fimmu.2018.02633

Ropolo, A., Catrinacio, C., Renna, F. J., Boggio, V., Orquera, T., Gonzalez, C. D., et al. (2020). A Novel E2F1-EP300-VMP1 pathway mediates gemcitabine-induced autophagy in pancreatic cancer cells carrying oncogenic KRAS. *Front. Endocrinol. (Lausanne)* 11:411. doi: 10.3389/fendo.2020.00411

Ropolo, A., Grasso, D., Pardo, R., Sacchetti, M. L., Archange, C., Lo Re, A., et al. (2007). The pancreatitis-induced vacuole membrane protein 1 triggers autophagy in mammalian cells. *J. Biol. Chem.* 282, 37124–37133. doi: 10.1074/jbc.M706956200

Ropolo, A., Grasso, D., and Vaccaro, M. I. (2019). "Measuring autophagy in pancreatitis," in *Methods in Molecular Biology*, ed. J. M. Walker (Totowa, NJ: Humana Press Inc), 541–554. doi: 10.1007/978-1-4939-8873-0_35

Santel, A., and Fuller, M. T. (2001). Control of mitochondrial morphology by a human mitofusin. *J. Cell Sci.* 114, 867–874.

Shalbueva, N., Mareninova, O. A., Gerloff, A., Yuan, J., Waldron, R. T., Pandol, S. J., et al. (2013). Effects of oxidative alcohol metabolism on the mitochondrial permeability transition pore and necrosis in a mouse model of alcoholic pancreatitis. *Gastroenterology* 144, 437–446. doi: 10.1053/j.gastro.2012.10.037

Smirnova, E., Griparic, L., Shurland, D. L., and Van der Bliek, A. M. (2001). Dynamin-related protein Drp1 is required for mitochondrial division in mammalian cells. *Mol. Biol. Cell* 12, 2245–2256. doi: 10.1091/mbc.12.8.2245

Towbin, H., Staehelin, T., and Gordon, J. (1979). Electrophoretic transfer of proteins from polyacrylamide gels to nitrocellulose sheets: procedure and some applications. *Proc. Natl. Acad. Sci. U.S.A.* 76, 4350–4354. doi: 10.1073/pnas.76.9.4350

Vaccaro, M. I. (2012). Zymophagy: selective autophagy of secretory granules. *Int. J. Cell Biol.* 2012:396705. doi: 10.1155/2012/396705

Vaccaro, M. I., Ropolo, A., Grasso, D., and Iovanna, J. L. (2008). A novel mammalian trans-membrane protein reveals an alternative initiation pathway for autophagy. *Autophagy* 4, 388–390. doi: 10.4161/auto.5656

Vanasco, V., Magnani, N. D., Cimolai, M. C., Valdez, L. B., Evelson, P., Boveris, A., et al. (2012). Endotoxemia impairs heart mitochondrial function by decreasing electron transfer, ATP synthesis and ATP content without affecting membrane potential. *J. Bioenerg. Biomembr.* 44, 243–252. doi: 10.1007/s10863-012-9426-3

Vanasco, V., Saez, T., Magnani, N. D., Pereyra, L., Marchini, T., Corach, A., et al. (2014). Cardiac mitochondrial biogenesis in endotoxemia is not accompanied by mitochondrial function recovery. *Free Radic. Biol. Med.* 77, 1–9. doi: 10.1016/j.freeradbiomed.2014.08.009

Vico, T. A., Marchini, T., Ginart, S., Lorenzetti, M. A., Adán Areán, J. S., Calabró, V., et al. (2019). Mitochondrial bioenergetics links inflammation and cardiac contractility in endotoxemia. *Basic Res. Cardiol.* 114:38. doi: 10.1007/s00395-019-0745-y

Vincow, E. S., Merrihew, G., Thomas, R. E., Shulman, N. J., Beyer, R. P., MacCoss, M. J., et al. (2013). The PINK1-Parkin pathway promotes both mitophagy and selective respiratory chain turnover *in vivo*. *Proc. Natl. Acad. Sci. U.S.A.* 110, 6400–6405. doi: 10.1073/pnas.1221132110

Vives-Bauza, C., Yang, L., and Manfredi, G. (2007). Assay of mitochondrial ATP synthesis in animal cells and tissues. *Methods Cell Biol.* 80, 155–171. doi: 10.1016/S0091-679X(06)80007-5

Vives-Bauza, C., Zhou, C., Huang, Y., Cui, M., De Vries, R. L. A., Kim, J., et al. (2010). PINK1-dependent recruitment of Parkin to mitochondria in mitophagy. *Proc. Natl. Acad. Sci. U.S.A.* 107, 378–383. doi: 10.1073/pnas.0911187107

Willems, P. H. G. M., Rossignol, R., Dieteren, C. E. J., Murphy, M. P., and Koopman, W. J. H. (2015). Redox homeostasis and mitochondrial dynamics. *Cell Metab.* 22, 207–218. doi: 10.1016/j.cmet.2015.06.006

Williams, J. A. (2008). Receptor-mediated signal transduction pathways and the regulation of pancreatic acinar cell function. *Curr. Opin. Gastroenterol.* 24, 573–579. doi: 10.1097/MOG.0b013e32830b110c

Xiao, A. Y., Tan, M. L. Y., Wu, L. M., Asrani, V. M., Windsor, J. A., Yadav, D., et al. (2016). Global incidence and mortality of pancreatic diseases: a systematic review, meta-analysis, and meta-regression of population-based cohort studies. *Lancet Gastroenterol. Hepatol.* 1, 45–55. doi: 10.1016/S2468-1253(16)30004-8

Conflict of Interest: The authors declare that the research was conducted in the absence of any commercial or financial relationships that could be construed as a potential conflict of interest.

frontiers in Cell and Developmental Biology

ORIGINAL RESEARCH
published: 25 May 2021
doi: 10.3389/fcell.2021.621906

Sp1 Targeted PARP1 Inhibition Protects Cardiomyocytes From Myocardial Ischemia–Reperfusion Injury via Downregulation of Autophagy

Yifeng Xu[1†], Boqian Wang[2†], Xiaoxiao Liu[1], Yunfei Deng[1], Yanqi Zhu[1], Feng Zhu[1], Yanyan Liang[1] and Hongli Li[1*]*

[1] Department of Cardiology, Shanghai General Hospital, School of Medicine, Shanghai Jiao Tong University, Shanghai, China, [2] State Key Laboratory of Oncogenes and Related Genes, Institute for Personalized Medicine, School of Biomedical Engineering, Shanghai Jiao Tong University, Shanghai, China

Myocardial ischemia–reperfusion injury (MIRI), characterized by post-ischemic cardiomyocytes death and reperfusion myocardial damage, is a lethal yet unresolved complication in the treatment of acute myocardial infarction (AMI). Previous studies have demonstrated that poly(ADP-ribose) polymerase-1 (PARP1) participates in the progression of various cardiovascular diseases, and various reports have proved that PARP1 can be a therapeutic target in these diseases, but whether it plays a role in MIRI is still unknown. Therefore, in this study, we aimed to explore the role and mechanism of PARP1 in the development of MIRI. Firstly, we demonstrated that PARP1 was activated during MIRI-induced myocardial autophagy *in vitro*. Moreover, PARP1 inhibition protected cardiomyocytes from MIRI through the inhibition of autophagy. Next, we discovered that specificity protein1 (Sp1), as a transcription factor of PARP1, regulates its target gene PARP1 through binding to its target gene promoter during transcription. Furthermore, silencing Sp1 protected cardiomyocytes from MIRI via the inhibition of PARP1. Finally, the functions and mechanisms of PARP1 in the development of MIRI were also verified *in vivo* with SD rats model. Based on these findings, we concluded that PARP1 inhibition protects cardiomyocytes from MIRI through the inhibition of autophagy, which is targeted by Sp1 suppression. Therefore, the utilization of PARP1 exhibits great therapeutic potential for MIRI treatment in future.

Keywords: myocardial ischemia-reperfusion injury, oxygen-glucose deprivation/reperfusion, PARP1, Sp1, autophagy

OPEN ACCESS

Edited by:
Konstantinos Zarbalis, University of California, Davis, United States

Reviewed by:
Rasheedunnisa Begum, Maharaja Sayajirao University of Baroda, India
Peifeng Li, Qingdao University, China
Hui-Hua Li, Beijing Chaoyang Hospital, Capital Medical University, China

***Correspondence:**
Yanyan Liang
yanyan.liang@shgh.cn
Hongli Li
lihongli@sjtu.edu.cn

† These authors have contributed equally to this work

Specialty section:
This article was submitted to Cell Death and Survival, a section of the journal Frontiers in Cell and Developmental Biology

Received: *27 October 2020*
Accepted: *24 March 2021*
Published: *25 May 2021*

Citation:
Xu Y, Wang B, Liu X, Deng Y, Zhu Y, Zhu F, Liang Y and Li H (2021) Sp1 Targeted PARP1 Inhibition Protects Cardiomyocytes From Myocardial Ischemia–Reperfusion Injury via Downregulation of Autophagy. Front. Cell Dev. Biol. 9:621906. doi: 10.3389/fcell.2021.621906

Abbreviations: AD, adenovirus; AMI, acute myocardial infarction; BEZ235, NVP-BEZ235; ChIP, chromatin immunoprecipitation; DAPI-4,6, diamidino-2-phenylindole; ECG, electrocardiogram; FS, fractional shortening; H&E staining, hematoxylin and eosin staining; LAD, left anterior descending coronary artery; LC3, micro-tubule-associated protein1 light chain 3; LVEF, left ventricular ejection fraction; MIRI, myocardial ischemic-reperfusion injury; NC, negative control; OGD/R, oxygen-glucose deprivation/reperfusion; PARP1, poly(ADP-ribose) polymerase-1; PCI, percutaneous coronary intervention; Real-time PCR, real-time polymerase chain reaction; ROS, reactive oxygen species; Sp1, specificity protein 1; TF, transcription factor; TUNEL, terminal dexynucleotidyl transferase (TdT)-mediated dUTP nick end labeling; 3′UTR, 3′untranslated regions.

INTRODUCTION

Acute myocardial infarction (AMI), associated with high mortality and morbidity, is one of the major causes of death in the world (Penna et al., 2013; Pu et al., 2014). With the application of reperfusion therapies, such as percutaneous coronary intervention (PCI) and thrombolysis, that restore the blood flow to the ischemic area, the impaired myocardium can be salvaged (Xuan and Jian, 2016; González-Montero et al., 2018). However, myocardial reperfusion is likely to cause an excessive production of reactive oxygen species (ROS), contributing to the activation of autophagy, the induction of post-ischemic cardiomyocyte death, and the generation of cardiac dysfunction, which was termed as myocardial ischemia-reperfusion injury (MIRI) (Movassagh and Foo, 2008; Gustafsson and Gottlieb, 2009; Morales et al., 2014). Accompanied by clinical complications like reperfusion arrhythmias, lethal reperfusion, myocardial stunning and no-reflow (González-Montero et al., 2018), MIRI is a common yet fatal clinical disease which remains to be solved. Therefore, it is of urgent demand to explore the molecular mechanisms of MIRI and to develop novel molecular interventions that may reduce the occurrence of MIRI and improve the prognosis of AMI patients (He et al., 2014).

Poly(ADP-ribose) polymerase-1 (PARP1), characterized by attaching ADP-ribose polymer chains to the target proteins and promoting DNA repair, is a post-translational modification enzyme (Kim et al., 2004, 2005; Pirrotta, 2004). Previous studies have shown that PARP1 is associated with many cardiovascular diseases, including hypertension, atherosclerosis, myocardial hypertrophy and circulatory shockn (Molnár et al., 2006; Pacher and Szabó, 2007; Esposito and Cuzzocrea, 2009; Xu et al., 2014). It has been demonstrated that PARP1 can be activated by starvation (Wang H. et al., 2018), angiotensin II (Wang et al., 2013) and high glucose (Jagtap and Szabo, 2005). Additionally, evidence showed that PARP1 overexpression can bring about damage to cardiac structure and cardiac function during the progression of heart failure (Pillai et al., 2005), whereas PARP1 inhibition can prevent cardiac remodeling (Pillai et al., 2006), apoptosis, fibrosis and inflammation (Gilad et al., 1997; Wayman et al., 2001; Jagtap and Szabo, 2005; Wang et al., 2013; Wang H. et al., 2018). Therefore, PARP1 inhibition was proved to be cardiac-protective in heart failure and post-infarction myocardial remodeling (Halmosi et al., 2016), but whether it is involved in MIRI is unknown.

Specificity protein 1(Sp1) transcription factor (TF) is a member of the Sp/Kruppel-like factor family, which is involved in embryonic development and cell cycle regulation (Safe et al., 2014). Generally, the biological function of Sp1 is activated when it is binding to its target DNA binding sites (Chintharlapalli et al., 2007). Furthermore, it was reported that down-regulation of Sp1 and Sp1-related genes are considered as drug-dependent (Abdelrahim et al., 2007). It has been reported that Sp1 is closely related to cancers, and high level of Sp1 in human blood is perceived as a negative prognostic factor to cancers (Mertens-Talcott et al., 2007; Chadalapaka et al., 2008, 2013; Chintharlapalli et al., 2009, 2011; Papineni et al., 2009; Colon et al., 2011). However, the role of Sp1 in the progression of MIRI remains unclear.

Autophagy, also nominated as type II programmed cell death, plays an essential role in the pathophysiological progression of MIRI (Thapalia et al., 2014). It is a process of transporting damaged, denatured or aged organelles to lysosomes for degradation, and the formation of double-membraned autophagosomes are the symbol of autophagy, during which the activation of Beclin1, LC3 (Micro-tubule-associated protein1 light chain 3) and ATG12 are characteristic biomarkers to trigger this process (Ma et al., 2012; Zou et al., 2019). Under physiological conditions, autophagy maintains intracellular homeostasis, and thus it assists in preserving normal function and survival of cells; while under pathological circumstances, autophagy leads to a variety of diseases, such as inflammation (Virgin and Levine, 2009), aging (Rubinsztein et al., 2011), cancer (Yang et al., 2011), metabolic syndrome (Codogno and Meijer, 2010), liver disease (Hidvegi et al., 2010) and heart disease (Nakai et al., 2007). When it comes to ischemic heart diseases, autophagy is beneficial and adaptive during ischemia, but harmful and fatal during reperfusion. As expected, MIRI is the result of this autophagy, which is out of control. In the previous ischemic area, the existence of coronary microvascular occlusion sustains for 48 h, while the autophagy effect lasts for 72 h. Due to the intracellular autophagy, the final clinical manifestation of MIRI is presented as expanded infarct myocardium size, deteriorated left ventricular ejection fraction, aggravated left ventricular remodeling and worse clinical prognosis (Thapalia et al., 2014). Therefore, the regulation of autophagy is an potential target for the intervention of MIRI.

In this study, we have discovered the role and mechanism of PARP1 in the progression of MIRI. Function experiments indicated that PARP1 was activated by MIRI-induced myocardial autophagy. By *in vivo* and *in vitro* experiments, we demonstrated that inhibiting PARP1 could alleviate myocardial injury triggered by MIRI whereas promoting autophagy could reverse the myocardial protection effect of PARP1 inhibition. Further exploration of the mechanism identified that PARP1 inhibition protects cardiomyocytes from MIRI through inhibition of autophagy, which is targeted by Sp1 suppression.

MATERIALS AND METHODS

Cell Culture and Establishment of Oxygen-Glucose Deprivation/Reperfusion (OGD/R) Model

A cellular model of Oxygen-Glucose Deprivation/Reperfusion (OGD/R) was adopted to simulate *in vivo* myocardial ischemia reperfusion. Briefly, embryonic rat heart-derived H9c2 cells were cultured in 6-well plates in a humidified and 5% CO_2 atmosphere at 37°C, with DMEM supplemented with 10% FBS. When the cells grew to about 80% density, the medium of the OGD/R group was replaced with sugar-free medium that had been prefilled with 95% N_2 and 5% CO_2 for 30 min to replace the oxygen in the solution, and then the cells were placed in an anoxic

incubator, filled with 95% N_2 and 5% CO_2 mixed gas. After 6 h of OGD, the cells were transferred into the regular incubator for reperfusion, placed for 2 h, and then collected for subsequent assays (**Supplementary Figure 1**).

Cell Transfection

H9c2 cells were seeded in 60 mm cell culture dishes and cultured in medium without antibiotics overnight. To knockdown the expression of Sp1, cells at 40% confluence were transfected with Sp1 shRNA, using Lipofectamine 2000 reagent according to the manufacturer's instructions. At 36 h after transfection, H9c2 cells were incubated in ischemic conditions for 12 h, as previously described.

Real-Time PCR

Total RNA was isolated from H9c2 cells with TRIzol Reagent (Ambion, 15596026, Texas, United States). PrimeScriptTM RT reagent Kit (TAKARA, RR037A, Takara Bio, Otsu, Japan) was adopted to determine the mRNA expression level. According to the manufacturer's instructions, real-time PCR was performed with related forward and reverse primers with SYBR® Premix Ex Taq^{TM} II (Takara, RR420A, Takara Bio, Otsu, Japan) in real-time system (Roche, LightCycler® 96, Switzerland). The relative mRNA expression levels were calculated using $2^{-\Delta\Delta Ct}$ method and were presented as fold changes relatively to the expression levels of the control group. The following primers were used in the real-time PCR: GAPDH forward, 5′-CCTGCACCACCAACTGCTTA-3′ and reverse, 5′-CATCACGCCACAGCTTTCCA-3′; PARP1 forward, 5′-ACCACGCACAATGCCTATGA-3′ and reverse, 5′-AGTCTCCGGTTGTGAAGCTG-3′; Beclin-1 forward, 5′-AGCCTCTGAAACTGGACACG-3′ and reverse, 5′-CCTCTTCCTCCTGGCTCTCT-3′; LC3 forward, 5′-CCGTAGTTCGCTGTACGAGG-3′ and reverse, 5′-CCGTAGTTCGCTGTACGAGG-3′; ATG-12 forward, 5′-GCTGAAGGCTGTAGGAGACAC-3′ and reverse, 5′-GGAAGGGGCAAAGGACTGATT-3′; Gabarapl-1 forward, 5′-AGAGGACCACCCCTTCGAATA-3′ and reverse, 5′-GAGCCTTCTCCACGATGACC-3′.

Western Blot Analysis

Total protein was extracted from H9c2 cells with RIPA lysis buffer (dilution:1:1000, Beyotime, P0013B, Nan Tong, China) supplemented with PMSF (Amresco, 329-98-6, United States). The protein lysates were resolved with SDS-PAGE gels and electro-transferred onto a nitrocellulose membrane (Millipore, HATF00010, Germany). At room temperature, TBST buffer with 5% non-fat milk powder (Sangon Biotech, NB0669-250g, Shanghai, China) was used to block the membranes for 1.5 h. At 4°C, related primary antibodies were incubated with the membrane overnight. At room temperature, the membrane was washed with PBS (Genom, GNM20012, Hangzhou, China) and incubated with a horseradish peroxidase labeled secondary antibody (Beyotime, A0208, A0216, Nantong China) for 1 h. The membrane was analyzed with the Chemiluminescence imaging system (Clinx, ChemiQ4600, Shanghai, China). The relative protein expression levels were presented as fold changes relative to the expression levels of the control group. Antibodies against Cleaved PARP1 (Abcam, ab32064, 1:1000, Cambridge, United Kingdom), Beclin1 (Abcam, ab207612, 1:2000, Cambridge, United Kingdom), Gabarapl1 (Abcam, ab86497, 1:1000, Cambridge, United Kingdom), ATG12 (Abcam, ab155589, 1:1000, Cambridge, United Kingdom), LC3A/B (Cell Signaling Technology CST, 12741, 1:1000, MA, United States), GATA1 (Abbexa, abx121608, 1:10, United Kingdom), Sp1(Abcam, ab13370, 1:10, Cambridge, United Kingdom), YYI (Abcam, ab109237, 1:10, Cambridge, United Kingdom), CTCF (Abcam, ab70303, 1:10, Cambridge, United Kingdom), β-actin (Abcam, ab8227, 1:5000, Cambridge, United Kingdom), GAPDH (Abcam, ab181602, 1:10000, Cambridge, United Kingdom) were used as primary antibodies. Cleaved PARP1 is an active form of PARP1 and was used in this study to represent the expression of PARP1.

Immunofluorescence Microscopy

The H9c2 cells were seeded onto sterilized coverslips, and cultured in the 5% CO_2 incubator (Corning, Wuxi, China) at 37 °C for about 6 h. The cells were then rinsed with PBS, fixed with 4% paraformaldehyde (Sinopharm, Shanghai, China) for 60 min, treated with 0.5% TritonX-100 for 20 min, and blocked with 3% H_2O_2 for 15 min, all at room temperature. Afterward, related primary antibodies were incubated with the cells overnight at 4°C. At room temperature, the cells were washed with PBS and incubated with fluorescent secondary antibodies for 2 h, followed by staining with DAPI (10 μg/ml, Beyotime, Nantong, China) for 5 min. Cells were observed and imaged with a fluorescence microscope (Leica, Germany).

Flow Cytometry

The H9c2 cell culture medium was sucked out into a suitable centrifuge tube. Then the adherent H9c2 cells were washed by PBS once and digested by trypsin cell digestion solution, which contained EDTA (Solarbio, T1300-100, Beijing, China). After incubation at room temperature, we added the cell culture medium which was collected before, and transfered it to the centrifugal tube, then centrifuged 1000 *g* for 5 min (Bioridge, TDZ4-WS, Shanghai, China). The H9c2 cells were centrifuged and resuspended with 195 μl Annexin V-FITC binding solution and 5 μl Annexin V-FITC (Beyotime, C1062, Nantong, China), incubated at 4°C for 15 min. Then, the cells were centrifuged again and resuspended with 190 μl Annexin V-FITC binding solution and 10 μl propidium iodide staining solution (Beyotime, Nantong, China), incubated at 4°C for 5 min. The fluorescence was detected by flow cytometer (BD, Accuri C6, United States).

MTT Assay

The H9c2 cells were cultured with 96-well plates. After the treatments of each experimental group, the culture medium was replaced with 20 μl MTT solution (Beyotime, Nantong, China). After incubation at 37°C for 4 h, the supernatant in each well was removed, replaced with 150 μl DMSO (Sigma, Germany). The plate was shaken for 10 min at a low speed to fully dissolve the crystals. The absorbance was measured at 490 nm by plate reader (Thermo, Carlsbad, CA, United States).

Chromatin Immunoprecipitation (ChIP)

Proteins and DNA of proliferating H9c2 cells were crosslinked at room temperature for 10 min with 10 ml Fix Buffer (10 mM HEPES pH = 7.6, 1 M sucrose, 5 mM KCl, 5 mM $MgCl_2$, 1% formaldehyde, 14 mM mercaptoethanol, 0.6% TritonX-100, and 0.4 mM PMSF, all from Sangon Biotech and Sinopharm). To terminate the crosslinking, 0.8 ml 2 M Glycine (Sigma, Germany) was added. The cells were placed on ice for 30 min before being scraped down and transferred to a pre-cooled centrifugal tube, centrifuged for 20 min at 4 000 rpm, 4°C. The supernatant was removed and cells were resuspended with 1 mL pre-cooled Extraction Buffer (0.4 M sucrose, 10 mM $MgCl_2$, 5 mM mercaptoethanol, 10 nM Tris-HCl pH = 8.0, and 1% proteinase inhibitor; Tris-HCl and proteinase inhibitor were from Sigma, Germany). The sample was crushed by ultrasonic (Sonics, United States). The pyrolysis solution was diluted by 10 times with pre-cooled Chip Buffer (1.1%TritonX-100, 1.2 mM EDTA, 16.7 mM Tris-HCl pH = 8.0, and 167 mM NaCl from Sinopharm, Shanghai, China). Protein A agarose beads (Cell Signaling Technology, MA, United States) were prepared with salmon sperm DNA (Sigma, Germany), and rinsed for three times with Chip Buffer. Then the pyrolysis solution was mixed with Chip Buffer, centrifuged at 4°C, 13000 rpm for 30 s. The pyrolysis solution was preserved at −20°C for Input. TE Buffer (10 mM Tris-HCl, 1 mM EDTA pH = 8.0), NaCl, SDS (Sinopharm, Shanghai, China) were added to Input. Protein K (TIANGEN, Beijing, China) was added to immune complex. The supernatant was extracted by adding chloroform (Sangon Biotech, Shanghai, China) of equal volume at room temperature and centrifuging at 13000 rpm for 15 min. DNA samples were added to the centrifugal tube overnight at −20°C with NaAc (Aladdin, Shanghai, China), ethanol (Sangon Biotech, Shanghai, China) and glycogen (Sinopharm, Shanghai, China). The DNA sample was washed with 70% ethanol, dried in incubator at 37 °C and precipitated with 50 μl 10 mM Tris-HCl (pH = 7.5), before its concentration was determined and adjusted for the subsequent qRT-PCR experiment.

Dual-Luciferase Reporter Assay

Due to the high transfection efficiency of 293T cells, 293T cells were used and incubated on 24-well plates at 37°C. When the cells grew to about 70–80% density, the medium was replaced with serum-free MEM (Gibco, Carlsbad, CA, United States) without antibiotics, incubated overnight. The plasmid and Lipofectamine^{TM} 2000 (Invitrogen, Carlsbad, CA, United States) were, respectively, diluted with MEM, and incubated at room temperature for 5 min. Then they were fully mixed and placed at room temperature for 20 min. The medium in the 24-well plate was replaced with the mixture. After 4–6 h of incubation, the transfection solution was replaced with MEM containing 10% FBS. After 48 h of transfection, the cells were fully lysed. Bright-Lumi^{TM} II Firefly Luciferase Reporter Gene Assay Kit and Renilla-Lumi^{TM} Luciferase Reporter Gene Assay Kit (Beyotime, Nantong, China) and the fluorescein enzyme detection buffer of sea kidney (Beyotime, Nantong, China) were used to detect the luciferase activity with a plate reader (Promega, United States). The RLU (relative light unit) was determined by mixing 100 μl samples with 100 μl reagent solution. Cell lysate without regent was used as blank control.

Establishment of the Rat MIRI Model

The study was conducted on 42 male SD rats (2 ± 1 months of age, weighing 220 ± 20g) bought from Shanghai SLAC Laboratory Animal Co., Ltd (project number SCXK 2017-0005). The rats were anesthetized with isoflurane. A four-limb electrocardiogram (ECG) was recorded to monitor ST segment amplitude changes. After removing the hair on the chest of rats, the thorax was opened, and the heart was exposed via left thoracotomy in the fourth intercostal space. A 6–0 silk ligature (Solarbio, Beijing, China) was used to ligate the left anterior descending coronary artery (LAD). Ischemia was monitored and confirmed visually via the ST segment elevation on ECG and prompt and sustained pallor of the anterior wall distal to the ligation site. After 45 min of ischemia, the ligature was loosened for 24 h, and reperfusion was confirmed by prompt return of color to the myocardium. Sham control group rats were treated with the same surgical procedures except the ligation of the left coronary artery. The AD vector packed with PARP1. The Control group and the I/R group were administered with the intragastrical injection of Sp1 shRNA NC. In contrast, the I/R + Sp1 shRNA and I/R+ AD-PARP1 group were given a 30 μl injection of recombinant Sp1 shRNA and AD-PARP1 around the infarction region, respectively.

The rats were randomly divided into seven groups (n = 5 for each groups). The groups were assigned as follows: (1) sham (0.9% normal saline, Sham group), (2) I/R (0.9% normal saline, I/R group), (3) I/R + AG-14361 at a dose of 5 mg/kg (Intraperitoneal injection once a day for 5 days), (4) I/R +AG-14361+BEZ235 at a dose of 50 mg/kg (Intraperitoneal injection), (5) I/R +SP1 shRNA NC (10^8 CFU/100 g weight), (6) I/R +SP1 shRNA (10^8 CFU/100 g weight), (7) I/R + AD-PARP1 (10^8 CFU/100 g weight).

Masson's Trichrome Staining

Masson's trichrome staining was done with Masson's Trichrome Stain Kit (Shanghai Xinfan Biotechnology Co., Ltd, Shanghai, China), according to the manufacturer's instructions. The Sections were fixed in 4% formaldehyde and embedded in paraffin. The stains of sections were observed and imaged with optical microscopy (Olympus, Japan).

Hematoxylin and Eosin (H&E) Staining

The myocardial tissues were fixed, dehydrated, transparent, soaked in wax, embedded in paraffin and sectioned. Then they were stained with hematoxylin and eosin (Sinopharm, Shanghai, China), clarified with xylene (Beijing Leagene Co., Ltd, Beijing, China) and sealed with neutral balsam (Sinopharm, Shanghai, China). The sections were observed and imaged with optical microscopy (Olympus, Japan).

TUNEL Assay

According to the manufacturer's instructions (KeyGEN BioTECH, Nanjing, China), cells were fixed in 4%

paraformaldehyde solution for 30 min at room temperature, and counterstained with DAPI (10 μg/ml, Beyotime, Nantong, China). The slides were sealed and visualized by fluorescence microscopy (Leica, Germany).

Statistical Analysis

All data were presented as means ± standard deviation, and all the experiments were performed at least three times. Statistics were done with SPSS version 22.0. The one way-ANOVA test was used for comparison between multiple groups, while multiple intra-groups comparisons were achieved through SNK test. When *P*-value is below 0.05, the change is considered statistically significant.

RESULTS

PARP1 Was Activated by OGD/R Induced Myocardial Autophagy

A cell model of oxygen-glucose deprivation/reperfusion (OGD/R) was adopted to simulate MIRI *in vitro* and induce autophagy. H9c2 cells were cultured in an oxygen-glucose-deprived incubator for 6 h, and then reperfused by oxygen and glucose for 2 h to cultivate the OGD/R model. Real-time PCR analysis showed that the mRNA expression of *PARP1* increased in the OGD/R model, compared to control group (**Figure 1A**). Meanwhile, the result of western blot also showed the expression of PARP1 was increased, compared to that in control group (**Figure 1B**).

PARP1 Inhibition Protected Cardiomyocytes From OGD/R Through Inhibition of Autophagy

To examine whether PARP1 inhibition could protect cardiomyocytes from MIRI, we used PARP1 inhibitor AG-14361 (S2178, Selleck Chemicals) to suppress the expression of PARP1 (Smith et al., 2016). After treating H9c2 cells with OGD/R model, western blot showed that compared to control group, the expression of PARP1 and autophagy related proteins such as LC3 and Beclin1 increased, indicating that the autophagy related cardiac injury was induced by OGD/R. However, treating cardiomyocytes with 10 μM AG-14361 for 1 h (Vazquez-Ortiz et al., 2015; Deng and Mi, 2016), we observed that the expression of PARP1 and autophagy related proteins were downregulated (**Figure 2A**). Simultaneously, we observed that in the GFP-LC3 assay, compared to control group, the number of GFP puncta increased in H9c2 cells when exposed to OGD/R, but reduced when treating cardiomyocytes with AG-14361 (**Figure 2B**). It was also detected by flow cytometry that the number of necrotic and apoptotic H9c2 cells increased when exposed to OGD/R. Treating cardiomyocytes with AG-14361, we discovered that the percentage of apoptotic cells decreased (**Figure 2C**). Therefore, PARP1 inhibition protected cardiomyocytes from OGD/R.

To further study the way that PARP1 inhibition protect cardiomyocytes from MIRI, we use NVP-BEZ235 (Selleck Chemicals), a novel autophagy promoter, to increase the effect of autophagy related cardiac injury (Liu et al., 2018). After treating H9c2 cells with 0.25 μM BEZ235 for 24 h, western blot analysis indicated that the expression of PARP1 and autophagy-related proteins (LC3 and Beclin1) increased again, compared to the group in which cardiomyocytes were treated with AG-14361 (**Figure 2D**). Identically, GFP-LC3 assay, which assessed autophagic flux, confirmed the same result. Compared to control group, the number of GFP puncta increased in H9c2 cells when exposed to OGD/R, indicating that autophagic flux was upregulated under OGD/R treatment. Treating cardiomyocytes with AG-14361, we observed that GFP puncta reduced, whereas treating cardiomyocytes with BEZ235, GFP puncta increased again (**Figure 2E**). At the same time, flow cytometry analysis revealed that the number of necrotic and apoptotic H9c2 cells increased when exposed to OGD/R, compared to control group. Treating cardiomyocytes with AG-14361, we detected that the percentage of necrotic and apoptotic cells reduced, whereas treating cardiomyocytes with BEZ235, the percentage of necrotic and apoptotic cells was increased again (**Figure 2F**). Accordingly, as showed in MTT assay, the cell viability of H9c2 cells decreased when exposed to OGD/R, compared to control group. Treating cardiomyocytes with AG-14361, we identified that the cell viability of H9c2 cells increased, whereas treated with BEZ235, the cell viability of H9c2 cells decreased again (**Figure 2G**). As is mentioned above, treating cardiomyocytes with BEZ235 could reverse the myocardial protection effect of PARP1 inhibition.

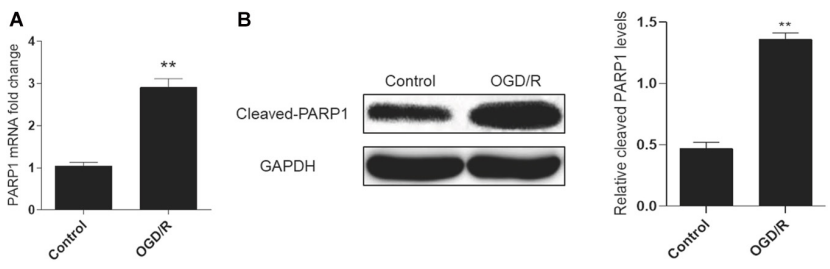

FIGURE 1 | PARP1 was activated by OGD/R-induced myocardial autophagy. H9c2 cells were cultured in an oxygen/glucose-deprived incubator for 6 h, and then reperfused by oxygen and glucose for 2 h to cultivate an OGD/R model. **(A)** Real-time PCR showed the mRNA level of PARP1 increased when H9c2 cells were exposed to OGD/R. **(B)** Western blot showed the protein level of PARP1 also rose when H9c2 cells were exposed to OGD/R. Compared with control group, $^{**}P < 0.01$. $N = 4$ for each group.

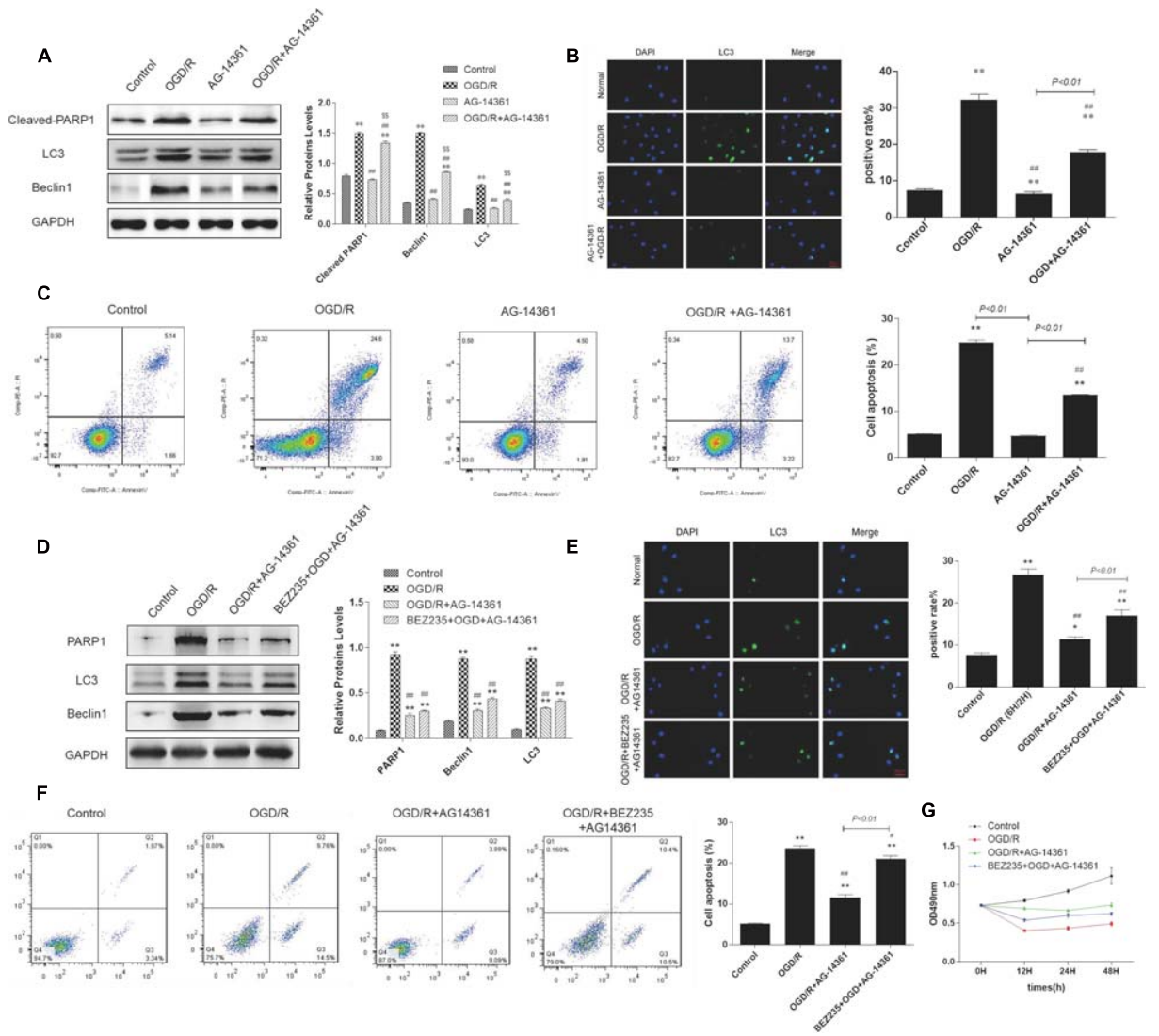

FIGURE 2 | PARP1 inhibition protected cardiomyocytes from OGD/R through inhibition of autophagy. The OGD/R-modeled H9c2 cells were treated with PARP1 inhibitor AG-14361 (10 μM) for 1 h and a novel autophagy promoter NVP-BEZ235 (0.25 μM) for 24 h. **(A)** Western blot showed the expression of PARP1 and autophagy related proteins rose when H9c2 cells were treated with AG-1436. **(B)** GFP-LC3 assay showed the different level of GFP puncta between control group and other groups. Magnification: 630×. **(C)** Flow cytometry analysis assessed the apoptotic rate of control group and other groups. **(D)** Western blot assessed the expression of PARP1 and autophagy related proteins when H9c2 cells was treated with PARP1 inhibitor and BEZ235. **(E)** GFP-LC3 assay showed the different level of GFP puncta between control group and other groups. Magnification: 630×. **(F)** Flow cytometry analysis showed the apoptotic rate of control group and other groups. **(G)** MTT assay showed the OD value of cells in control group and other groups. Compared with control group, $^{*}P < 0.05$, $^{**}P < 0.01$; compared with OGD/R group, $^{\#}P < 0.05$, $^{\#\#}P < 0.01$; Compared with AG-14361 group, $^{\$}P < 0.05$, $^{\$\$}P < 0.01$. $N = 4$ for each group.

Taken together, these results demonstrated that PARP1 inhibition can protect cardiomyocytes from OGD/R through inhibition of autophagy.

Sp1 Is a Transcription Factor of PARP1 That Regulates Its Expression During Transcription

According to bioinformatics analysis[1], *Sp1, YY1, CTCF, GATA-1* were selected as transcription factors of PARP1. To determine whether there exists a targeted regulation between Sp1 and PARP1, ChIP assay was conducted. We used IgG as negative control and input as positive control. After ChIP verification, IgG did not show any band. The DNA fragment size of target protein antibody PARP1 and input group IP were 100–200 bp, which matched with the requirements of ChIP experiment (**Figure 3A**). Furthermore, Western blot analysis indicated that when exposed to OGD/R model, the expression of Sp1 was the highest among these transcription factors (**Figure 3B**). We also performed real-time PCR to show that compared with control group, the mRNA expression of PARP1 recruited by all these transcription factors

[1]https://bigd.big.ac.cn/databasecommons/

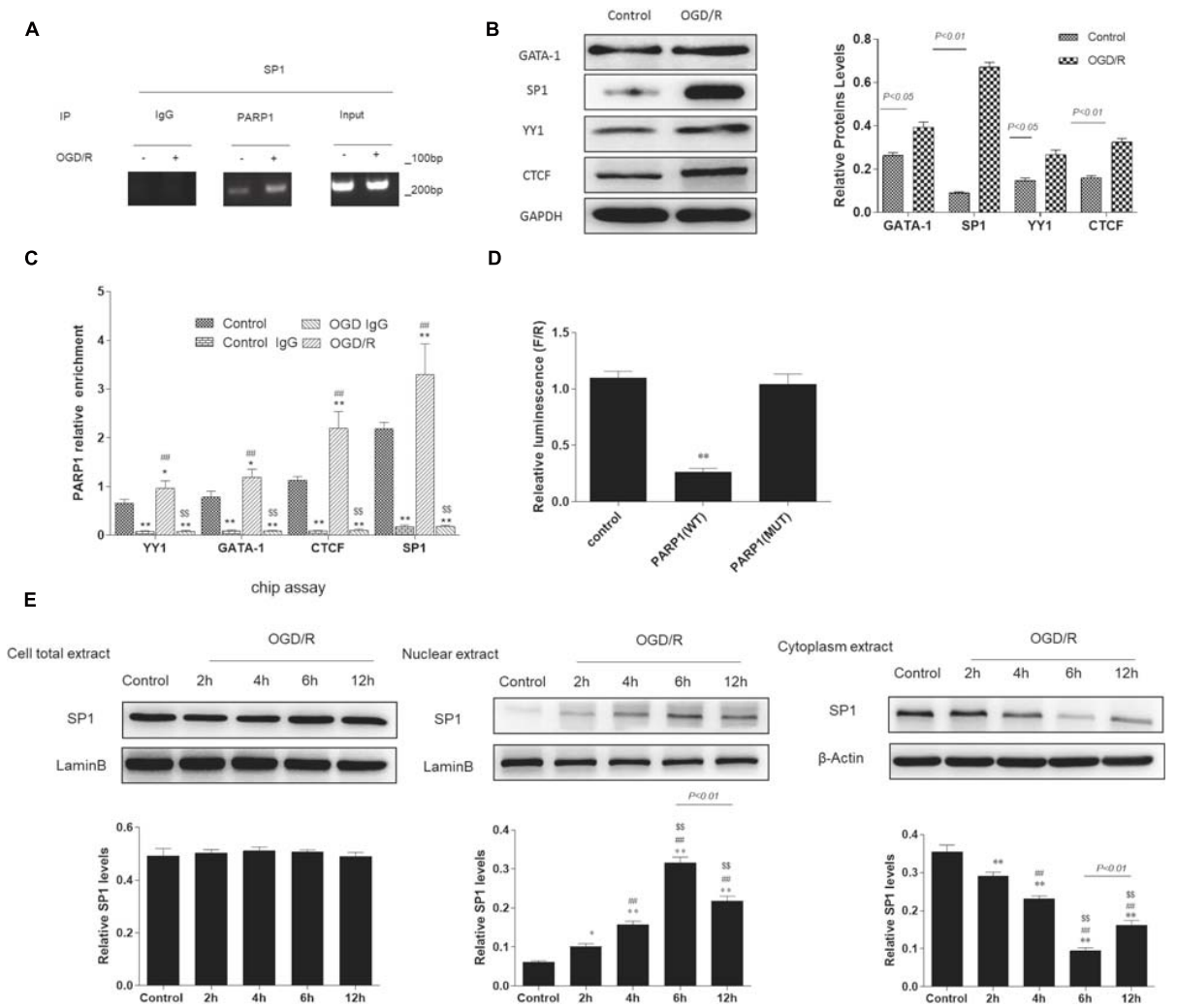

FIGURE 3 | Sp1 is a transcription factor of PARP1 that regulates the target gene of PARP1 during transcription. **(A)** In ChIP assays, the DNA fragment size of target protein antibody PARP1 and input group IP were 100-200 bp. IgG was served as a negative control and input was a positive control. **(B)** Western blot analysis showed the expression of different transcription factors. Compared with control group, $^{*}P < 0.05$, $^{**}P < 0.01$. **(C)** Real-time PCR showed the mRNA expressions of PARP1 which were recruited by different transcription factors. Compared with control group, $^{*}P < 0.05$, $^{**}P < 0.01$; compared with control IgG group, $^{\#\#}P < 0.01$; compared with OGD/R group, $^{\$\$}P < 0.01$. **(D)** The fluorescein value in the dual-luciferase reporter assay decreased significantly after mutation of PARP1, indicating that there was a targeted regulation between Sp1 and PARP1. Compared with control group, $^{**}P < 0.01$. **(E)** Western blot was performed in nuclear extract level, cytoplasm extract level and cell total extract level to show different protein expression levels of Sp1. Compared with control group, $^{*}P < 0.05$, $^{**}P < 0.01$; compared with OGD/R-2 h group, $^{\#}P < 0.05$, $^{\#\#}P < 0.01$; compared with OGD/R-4 h group, $^{\$}P < 0.05$, $^{\$\$}P < 0.01$. $N = 4$ for each group.

was the highest when exposed to OGD/R model (**Figure 3C**). To confirm the relationship between PARP1 and Sp1, dual-luciferase reporter assay was performed. The results showed that the fluorescence decreased significantly after mutation of PARP1, indicating that there was a targeted regulation between Sp1 and PARP1 (**Figure 3D**). To further confirm that it was during transcription that Sp1 regulate the biological effect of PARP1, western blot was performed in nuclear extract level, cytoplasm extract level and cell total extract level. The results showed that in nuclear extracts from OGD/R-exposed H9c2 cells, the expression of Sp1 significantly increased with time and reached the peak at 6 h, whereas it simultaneously decreased with time and hit the bottom at 6 h in cytoplasm extracts. At the same time, in cell total extract level, the expression of Sp1 was almost constant over time (**Figure 3E**). Therefore, Sp1 regulates the biological effect of PARP1 during transcription, as the transcription occurs in nuclear level (Mollion et al., 2018).

Altogether, these results supported that Sp1 is a transcription factor of PARP1, and it regulates the target gene of PARP1 during transcription.

Silencing Sp1 Prevented Cardiomyocytes From OGD/R

Though we have confirmed that *Sp1* is a transcription factor of PARP1, whether Sp1 has similar biological effect as PARP1 in the

pathophysiological progression of OGD/R-induced H9c2 cells is still unknown. Therefore, we transfected H9c2 cells with Sp1 shRNA and negative control of Sp1 shRNA-NC for 72 h to explore the role of Sp1 in OGD/R.

Western blot analysis showed that the expression level of Sp1 was evidently increased when exposed to OGD/R, whereas transfecting H9c2 cells with Sp1 shRNA could decrease the expression level of Sp1, compared to the Sp1 shRNA-NC-transfected cells (**Figure 4A**).

Furthermore, we performed western blot to demonstrated that compared to control group, the expression of PARP1 and autophagy related proteins increased when H9c2 cells were exposed to OGD/R, while treating H9c2 cells with Sp1 shRNA, we observed that the expression of PARP1 and autophagy related proteins decreased, compared to Sp1 shRNA-NC group (**Figure 4B**). Consistently, in GFP-LC3 assay, compared to control group, the number of GFP puncta rose in H9c2 cells when exposed to OGD/R, and declined when treating H9c2 cells with Sp1 shRNA, compared to Sp1 shRNA-NC group (**Figure 4C**). We also observed by flow cytometry that compared to control group, the number of necrotic and apoptotic H9c2 cells increased when exposed to OGD/R, while treating H9c2 cells with Sp1 shRNA, the number dropped compared to Sp1 shRNA-NC group (**Figure 4D**). Therefore, silencing Sp1 prevented cardiomyocytes from OGD/R.

Sp1 Suppression Prevented Cardiomyocytes From OGD/R Through PARP1 Inhibition

We have demonstrated that silencing Sp1 can prevent cardiomyocytes from OGD/R, but the potential mechanism under this phenomenon remains unclear. Since we have proved that there was a targeted regulation between Sp1 and PARP1, we still transfected H9c2 cells with Sp1 shRNA as well as Sp1 shRNA-NC for 72 h and treating cardiomyocytes with 10 uM AG-14361 for 1 h to explore the association between Sp1 and PARP1 in the development of OGD/R in H9c2 cells.

Flow cytometry analysis showed that the percentages of necrotic and apoptotic cells was decreased in Sp1 shRNA or AG-14361 transfected cells, whereas treating cardiomyocytes with Sp1 shRNA-NC, the percentages of necrotic and apoptotic cells was increased again (**Figure 5A**). In support of this, MTT assay was performed to analyze the cell viability of H9c2 cells. Results showed that the cell viability of Sp1 shRNA or AG-14361 transfected cells increased, whereas treated with Sp1 shRNA-NC, the cell viability of H9c2 cells were decreased again (**Figure 5B**). Accordingly, immunofluorescence showed that the positive rate of Sp1 in control group was lower than that in other groups, while the positive rate of Sp1 in OGD/R group and OGD/R+Sp1 shRNA-NC group was significantly higher. Furthermore, the positive rate of Sp1 in OGD/R+Sp1 shRNA group and OGD/R+AG-14361 group was significantly lower than that in OGD/R group and OGD/R+Sp1 shRNA-NC group (**Figure 5C**). These three results all demonstrated that both Sp1 suppression and PARP1 inhibition can prevent cardiomyocytes from OGD/R. Additionally, the regulation between Sp1 and PARP1 was positive.

To further confirm the regulation between Sp1 and PARP1, we infected H9c2 cells with Sp1 shRNA to downregulate Sp1 and AD-PARP1 adenovirus (MOI = 25) for 72 h to upregulate PARP1. Western blot analysis showed that under OGD/R exposition, the expression of PARP1 and autophagy-related proteins increased. However, when transfected H9c2 cells with Sp1 shRNA, the expression of PARP1 and autophagy-related proteins decreased, whereas infecting H9c2 cells with AD-PARP1 adenovirus upregulated the expression of PARP1 and autophagy-related proteins again (**Figure 5D**). In line with this, we performed real-time PCR. Results showed that compared to the OGD/R group, the expression of PARP1 mRNA and autophagy-related protein mRNAs decreased when H9c2 cells were transfected with Sp1 shRNA, while infecting H9c2 cells with AD-PARP1 adenovirus increased the expression of PARP1 mRNA and autophagy-related protein mRNAs (**Figure 5E**). As is mentioned above, treating cardiomyocytes with AD-PARP1 adenovirus could reverse the myocardial protection effect of Sp1 suppression. Taken together, Sp1 suppression prevented cardiomyocytes from OGD/R through PARP1 inhibition.

PARP1 Inhibition Protected Cardiomyocytes From MIRI Through Inhibition of Autophagy, Which Was Targeted by Sp1 Suppression

To confirm the role and mechanism of PARP1 in the development of MIRI, we established a MIRI animal model by 45 min of ischemia via ligating left anterior descending branch (LAD) of the SD rats, and then reperfused for 24 h. The model was considered successfully established when electrocardiogram showed that the ST-segment elevated during myocardial ischemia period and dropped at least 50% during reperfusion period. Furthermore, the expressions of PARP1 and Sp1 in MIRI tissues are both significantly higher than those in control group, which were examined by immunofluorescence (**Supplementary Figure 2**). Then, we transfected Sp1 shRNA, negative control Sp1 shRNA-NC and AD-PARP1 adenovirus (MOI = 25) all for 72 h in SD rats, and used 10 μM AG-14361 for 1 h and 0.25 μM BEZ235 for 24 h to confirm the results from *in vitro* experiments.

Electrocardiogram showed that the ST-segment elevated when exposed to MIRI, compared to control group. The elevated ST-segment dropped after treating rats with AG-14361, whereas using BEZ235 elevated the ST-segment again. Moreover, compared to Sp1 shRNA-NC group, electrocardiogram showed that the ST-segment dropped in rats transfected with Sp1 shRNA, whereas infecting rats with AD-PARP1 adenovirus elevated the ST-segment again (**Figure 6A**). Consistently, echocardiography result showed that compared to control group, left ventricular ejection fraction (LVEF%) and fractional shortening (FS%) significantly decreased when exposed to MIRI. After treating rats with AG-14361, LVEF% and FS% increased, whereas using BEZ235 deteriorated LVEF% and FS% again. Furthermore, echocardiography revealed that LVEF% and FS% was increased in rats transfected with Sp1 shRNA, whereas infecting rats

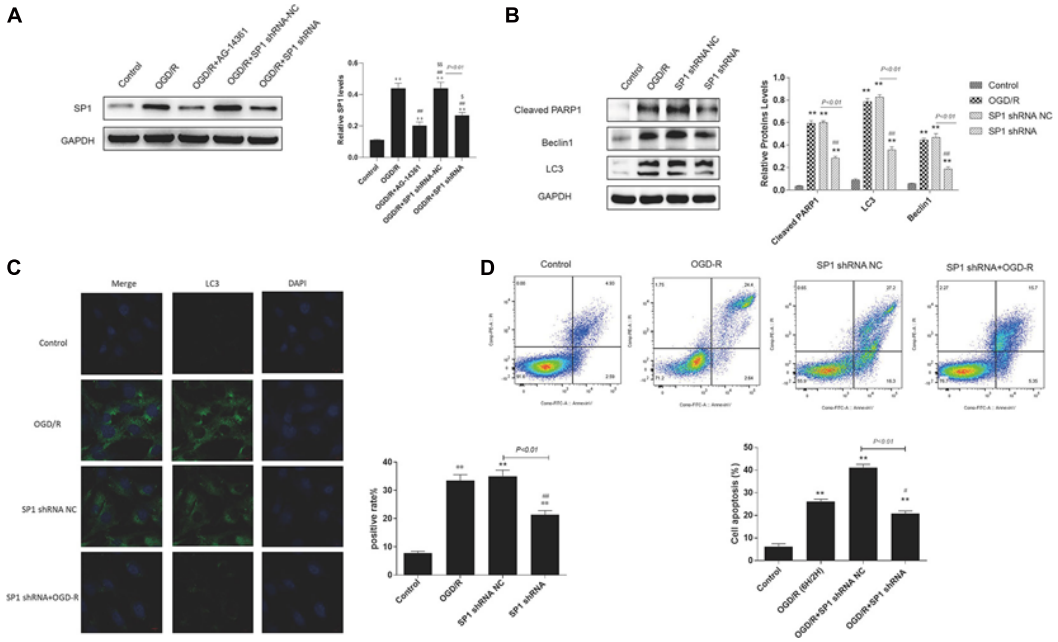

FIGURE 4 | Silencing Sp1 prevented cardiomyocytes from OGD/R. The OGD/R-modeled H9c2 cells were treated with Sp1 shRNA-NC and Sp1 shRNA. **(A)** Western blot assay showed the expression level of Sp1 when transfecting H9c2 cells with Sp1 shRNA and Sp1 shRNA-NC. **(B)** Western blot showed the expression of PARP1 and autophagy related proteins when treating H9c2 cells with Sp1 shRNA and Sp1 shRNA-NC. **(C)** GFP-LC3 assay showed the number of GFP puncta in H9c2 cells when treating H9c2 cells with Sp1 shRNA and Sp1 shRNA-NC. Magnification: 630×. **(D)** Flow cytometry analysis showed the number of necrotic and apoptotic H9c2 cells when treating H9c2 cells with Sp1 shRNA and Sp1 shRNA-NC. Compared with control group, $^{*}P < 0.05$, $^{**}P < 0.01$; compared with OGD/R group, $^{\#}P < 0.05$, $^{\#\#}P < 0.01$. $N = 4$ for each group.

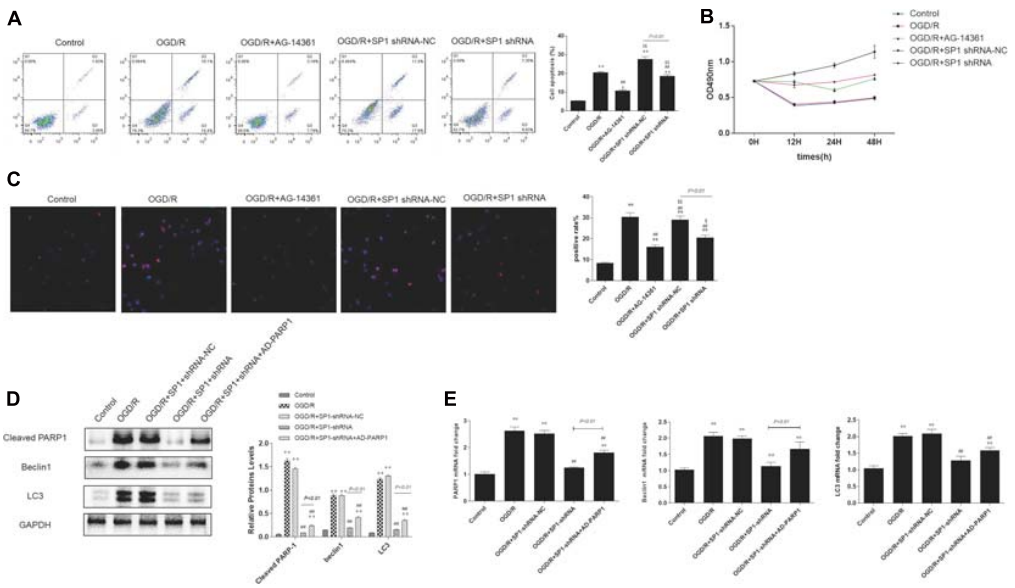

FIGURE 5 | Sp1 suppression prevented cardiomyocytes from OGD/R through PARP1 inhibition. The OGD/R-modeled H9c2 cells were treated with Sp1 shRNA-NC, Sp1 shRNA, PARP1 inhibitor AG-14361 and AD-PARP1 adenovirus. **(A)** Flow cytometry analysis showed that the percentages of necrotic and apoptotic cells when treating H9c2 cells with Sp1 shRNA, Sp1 shRNA-NC and AG-14361. **(B)** MTT assay was performed to analyze the cell viability of H9c2 cells when treating H9c2 cells with Sp1 shRNA, Sp1 shRNA-NC and AG-14361. **(C)** Immunofluorescence showed the positive rate of Sp1 when treating H9c2 cells with Sp1 shRNA, Sp1 shRNA-NC and AG-14361. Magnification: 200×. **(D)** Western blot showed the expression of PARP1 and autophagy related proteins when treating H9c2 cells with Sp1 shRNA, Sp1 shRNA-NC and AD-PARP1 adenovirus. **(E)** Real-time PCR showed the mRNA level of PARP1 and autophagy related proteins when treating H9c2 cells with Sp1 shRNA, Sp1 shRNA-NC and AD-PARP1 adenovirus. Compared with control group, $^{*}P < 0.05$, $^{**}P < 0.01$; compared with OGD/R group, $^{\#}P < 0.05$, $^{\#\#}P < 0.01$; compared with OGD/R+AG-14361 group, $^{\$}P < 0.05$, $^{\$\$}P < 0.01$. $N = 4$ for each group.

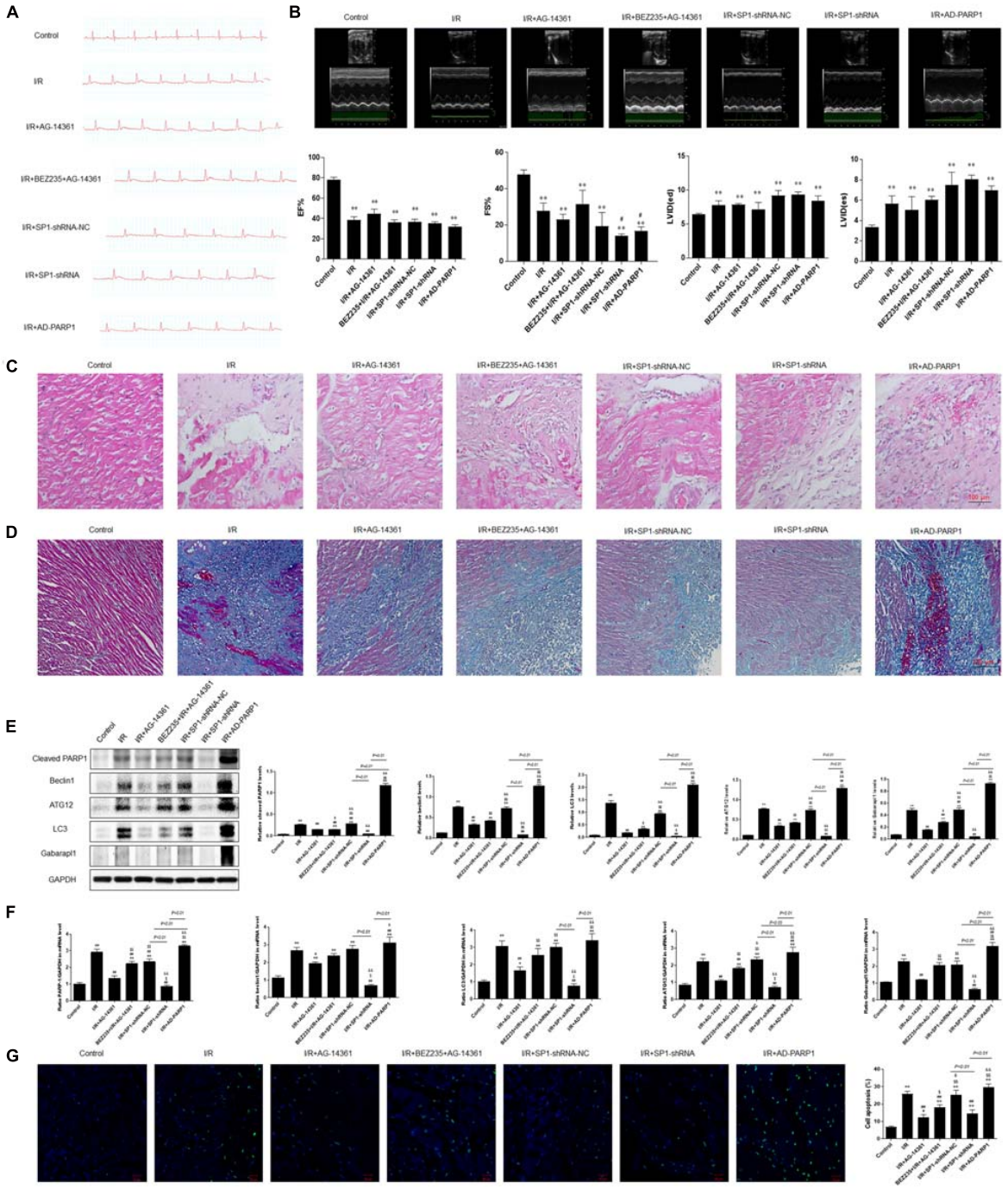

FIGURE 6 | PARP1 inhibition protected cardiomyocytes from MIRI *in vivo* via inhibition of autophagy, which is targeted by Sp1 suppression. An MIRI rat model was established by 45 min of ischemia via ligating left anterior descending branch (LAD), and then refused for 24 h. MIRI-modeled SD rats were treated with Sp1 shRNA-NC, Sp1 shRNA, PARP1 inhibitor AG-14361 and AD-PARP1 adenovirus. **(A)** Electrocardiogram showed the ST-segment variation of SD rats when treated with Sp1 shRNA-NC, Sp1 shRNA, PARP1 inhibitor AG-14361 and AD-PARP1 adenovirus under MRI model. **(B)** Echocardiography showed the different left ventricular ejection fraction (LVEF%) and fractional shortening (FS%) of SD rats when treated with Sp1 shRNA-NC, Sp1 shRNA, PARP1 inhibitor AG-14361 and AD-PARP1 adenovirus under MIRI model. **(C,D)** Hematoxylin and eosin (H&E) and Masson trichrome staining were performed to assess myocardial fibrosis of SD rats when treated with Sp1 shRNA-NC, Sp1 shRNA, PARP1 inhibitor AG-14361 and AD-PARP1 adenovirus under MIRI model. Magnification: 100×. **(E)** Western blot analysis showed the expression of PARP1 and autophagy-related proteins of SD rats when treated with Sp1 shRNA-NC, Sp1 shRNA, PARP1 inhibitor AG-14361 and AD-PARP1 adenovirus under MIRI model. **(F)** Real-time PCR analysis showed the mRNA expression of PARP1 and autophagy-related proteins of SD rats when treated with Sp1 shRNA-NC, Sp1 shRNA, PARP1 inhibitor AG-14361 and AD-PARP1 adenovirus under MIRI model. **(G)** TUNEL assay showed the different apoptotic rate of SD rats when treated with Sp1 shRNA-NC, Sp1 shRNA, PARP1 inhibitor AG-14361 and AD-PARP1 adenovirus under MIRI model. Magnification: 100×. Compared with control group, $^{*}P < 0.05$, $^{**}P < 0.01$; compared with OGD/R group, $^{\#}P < 0.05$, $^{\#\#}P < 0.01$; compared with OGD/R+AG-14361 group, $^{\$}P < 0.05$, $^{\$\$}P < 0.01$; compared with BEZ235+OGD/R+AG-14361 group, $^{\&}P < 0.05$, $^{\&\&}P < 0.01$. $N = 4$ for each group.

with Sp1 shRNA and AD-PARP1 adenovirus deteriorated FS%, compared to Sp1 shRNA-NC group (**Figure 6B**). Sp1 shRNA and AD-PARP1 showed less effect on LVEF% compared to Sp1 shRNA-NC group. Then, H&E and Masson trichrome staining were performed to assess myocardial fibrosis after MIRI. Compared with control group, the expression of fibrosis increased when exposed to MIRI. When rats were treated with AG-14361 or infecting rats with Sp1 shRNA, myocardial fibrosis was attenuated. However, using BEZ235 or infecting rats with Sp1 shRNA and AD-PARP1 adenovirus aggravated myocardial fibrosis (**Figures 6C,D**). According to western blot results, the expression of PARP1 and autophagy-related proteins decreased when rats were treated with AG-14361 or transfected with Sp1 shRNA, whereas rats were treated with BEZ235 or infected with Sp1 shRNA and AD-PARP1 adenovirus increased the expression of PARP1 and autophagy-related proteins again (**Figure 6E**). Consistently, real-time PCR showed that the expression of PARP1 and autophagy-related mRNAs decreased when rats were treated with AG-14361 or Sp1 shRNA, whereas BEZ235 or Sp1 shRNA and AD-PARP1 adenovirus increased the expression of PARP1 and autophagy-related mRNAs again (**Figure 6F**). Furthermore, TUNEL assay showed that the apoptotic rate decreased when rats were treated with AG-14361 or Sp1 shRNA, whereas BEZ235 or Sp1 shRNA and AD-PARP1 adenovirus increased the apoptotic rate (**Figure 6G**).

Taken together, these results demonstrated that PARP1 inhibition protects cardiomyocytes from myocardial ischemia-reperfusion injury through inhibition of autophagy by Sp1 suppression.

DISCUSSION

Myocardial ischemia-reperfusion injury (MIRI) has been reported to be associated with autophagy, and this disease can increase the level of autophagy in cardiomyocytes (Kloner and Jennings, 2001; Rochitte et al., 1998; Baines, 2011; Thapalia et al., 2014). It has been reported that autophagy, mitochondrial damage and endoplasmic reticulum stress (ERs) are important mechanisms of ischemia-reperfusion injury. Previous studies suggest that moderate autophagy can protect myocardium, while excessive autophagy can promote apoptosis and damage myocardial function (Thapalia et al., 2014). However, how to alleviate MIRI through targeting the pathway of autophagy remains elusive. In this work, we provide original findings on the mechanism underlying MIRI and autophagy. In our experiments, a cell model of oxygen-glucose deprivation/reperfusion (OGD/R) was adopted to simulate MIRI *in vitro*. We confirmed that PARP1 was activated by MIRI-induced myocardial autophagy. Treating cardiomyocytes with PARP1 inhibitor AG-14361, we observed that cardiac injury triggered by OGD/R was alleviated, whereas treating cardiomyocytes with NVP-BEZ235, a novel autophagy promoter, could reverse the myocardial protection effect that was mediated by PARP1 inhibition. Thus, PARP1 inhibition protected cardiomyocytes from OGD/R through inhibition of autophagy. Further exploration of the mechanism revealed Sp1 as a transcription factor of PARP1, which regulated the target gene of PARP1 through binding to its promoter during transcription. Additionally, silencing Sp1 prevented cardiomyocytes from OGD/R. Furthermore, we demonstrated that it was via PARP1 inhibition that Sp1 suppression prevented cardiomyocytes from OGD/R. *In vivo*, we established an MIRI animal model, and the same role and mechanism of PARP1 in the progression of MIRI have been verified. These results justified that Sp1 targeted PARP1 inhibition protected cardiomyocytes from MIRI via downregulation of autophagy. Therefore, PARP1 may be a therapeutic target for MIRI in the future.

Recent studies have proved that PARP1 inhibition can protect diabetic heart via activating SIRT1-PGC1 alpha axis (Waldman et al., 2018); Through activating SIRT1-induced inhibition of PARP1, post myocardial infarction infammation and cardiac remodeling can be prevented (Eid et al., 2020). Apart from cardiovascular diseases, deficiency of PARP1 can also alleviate pulmonary fibrosis (Zhang et al., 2018), while PARP1 overactivation can lead to hepatic fibrosis (Mukhopadhyay et al., 2014). Their results indicated that PARP1 inhibition can be a therapeutic target for the treatment of cardiovascular diseases. In our study, we are dedicated to exploring the effect of PARP1 inhibition in MIRI, which has rarely been studied before. OGD/R model was adopted to simulate MIRI *in vitro*. Our results showed that PARP1 was activated in OGD/R model (**Figure 1**). Moreover, it was demonstrated that PARP1 was inhibited by AG-14361, and PARP1 inhibition could protect cardiomyocytes from OGD/R (**Figures 2A–C**).

Autophagy begins in the early stage of myocardial ischemia and persists or even exacerbates in the late stage of reperfusion (Thapalia et al., 2014). Furthermore, autophagy is not only a pathophysiological process during MIRI, but also a potential regulated target to affect the progression of MIRI. Wang et al. reported that via regulating autophagy, PARP1 inhibition can attenuate cardiac fibrosis which is induced by myocardial infarction (Wang C. et al., 2018). Huang et al. indicated that DNA damage response 1 overexpression protected against the development of post-MI heart failure by enhancing autophagy and reducing apoptosis via the mTOR signaling pathway (Huang et al., 2019). In our study, autophagy was successfully induced by OGD/R model (**Figures 2A–C**). Then, a series of rescue experiments were conducted to prove that through downregulation of autophagy, PARP1 inhibition can protect cardiomyocytes from OGD/R. AG-14361 was used to suppress the expression of PARP1, while BEZ235 was used to increase the effect of autophagy related cardiac injury. We discovered that PARP1 inhibition could alleviate the cardiac damage of OGD/R, while increasing the extent of autophagy could reverse the myocardial protection effect of PARP1 inhibition (**Figures 2D–G**). Therefore, PARP1 inhibition can protect cardiomyocytes from OGD/R through inhibition of autophagy.

It has been reported that Sp1 is a transcription factor of the Sp/Kruppel-like factor family, and it plays an important role in apoptosis, differentiation and cell growth (Vizcaíno et al., 2015). Furthermore, Sp1 can regulate the gene expression via activating the transcription of many cellular genes which contain Sp1 binding sites in their promoters (Safe et al., 2014). Our research showed that Sp1 was selected as a transcription factor

of PARP1, and there was a targeted regulation between Sp1 and PARP1. Here, we also verified that Sp1 could regulate the target gene of PARP1 through binding to its target gene promoter during transcription (**Figures 3D,E**). Wei et al. argued that downregulate Sp1 could decrease the progression of carcinogenesis in pancreatic cancer (Wei et al., 2004). Additionally, previous researches have demonstrated that Sp1 is a drug target. A number of antineoplastic agents inhibit the expression of Sp1 (Safe et al., 2014), which are effective on tumors. Therefore, we speculate that Sp1 suppression might have myocardial protective effect in MIRI. We transfected H9c2 cells with Sp1 shRNA to inhibit Sp1 and infected H9c2 cells with AD-PARP1 adenovirus to upregulate PARP1. Sp1 suppression attenuated cell autophagy and alleviated cell apoptosis, showing a myocardial protective effect (**Figures 4B,D**). Suppressing Sp1 can lead to PARP1 inhibition, which induces autophagy inhibition, and finally results in cardioprotection from MIRI (**Figure 5**).

Consistently, we also observed the same myocardial protective effect *in vivo* by inhibiting Sp1. Furthermore, Sp1 suppression could also protect the cardiac function of MIRI rats and palliate their cardiac remodeling.

There are also limits in our research such as LC3 immunofluorescence only represented the autophagosome formation, not the autophagy flux, and mRFP-GFP-LC3 label should be used in the experiment. Furthermore, H9c2 cells were used in all experiments *in vitro*, and the cultured neonatal rat cardiomyocytes were not involved in the present study. *In vivo*, the experiments of detecting quantification of heart infarct size and fibrosis were not performed. Further investigations should aim at those unsettled obstacles, and these will be a part of our future research.

In conclusion, we have discovered the role and mechanism of PARP1 in the progression of MIRI. For the first time, we demonstrated that PARP1 inhibition protected cardiomyocytes from MIRI through inhibition of autophagy, which was targeted by Sp1 suppression. This exposits a promising therapeutic target in treating myocardial reperfusion injury in the future.

DATA AVAILABILITY STATEMENT

The original contributions presented in the study are included in the article/**Supplementary Material**, further inquiries can be directed to the corresponding author/s.

ETHICS STATEMENT

The animal study was reviewed and approved by Shanghai General Hospital Affiliated to Shanghai Jiao Tong University [Permission Number: SYXK (Su) 2017-0007].

AUTHOR CONTRIBUTIONS

YX and HL designed the experiments. YX and BW conducted the experiments and wrote the manuscript. XL, YD, YL, YZ, and FZ amended the protocol of the experiments. All authors revised and approved the manuscript.

FUNDING

This research was supported by Shanghai Natural Science Foundation (17ZR1422200).

ACKNOWLEDGMENTS

The authors gratefully thank to every membership in the lab who had helped to finish this research.

SUPPLEMENTARY MATERIAL

The Supplementary Material for this article can be found online at: https://www.frontiersin.org/articles/10.3389/fcell.2021.621906/full#supplementary-material

According to OGD real-time PCR analysis, the mRNA expression of autophagy related genes increased to the peak at 6 h and then decreased, compared to control group (**Supplementary Figure 1A**). Therefore, 6 h was chosen as the model OGD time. Identically, OGD/R real-time PCR analysis confirmed that the mRNA expression of autophagy-related genes increased to the peak at 2 h and then decreased, compared to control group (**Supplementary Figure 1B**). Therefore, 2 h of reoxygenation was chosen as the model time.

The expression of Sp1 and PARP1 were both confirmed in sham control and MIRI tissues by immunofluorescence. Our results showed that the expressions of PARP1 and Sp1 in MIRI tissues are both significantly higher than those in control group (**Supplementary Figure 2**).

A model depicting the mechanism of Sp1 targeted PARP1 inhibition protects cardiomyocytes from myocardial ischemia–reperfusion injury via downregulation of autophagy was added as a Graphical Abstract.

Supplementary Figure 1 | H9c2 cells were cultured in an oxygen/glucose-deprived incubator for 6 h, and then reperfused by oxygen and glucose for 2 h to cultivate an OGD/R model. **(A)** Real-time PCR showed that when OGD was 6 h, the mRNA expression of each autophagy related genes was the highest. **(B)** Real-time PCR showed that when OGD/R was 2 h, the mRNA expression of each autophagy related genes was the highest. Compared with control group, $^{*}P < 0.05$, $^{**}P < 0.01$. $N = 4$ for each group.

Supplementary Figure 2 | Immunofluorescence examined the expression of Sp1 and PARP1 in sham control and MIRI tissues. **(A)** The expression of PARP1 was significantly higher in MIRI tissues than that in sham control group. **(B)** Compared to sham control group, the expression of Sp1 expression was conspicuously increased in MIRI tissues. Magnification: 200×. $N = 4$ for each group.

Supplementary Graphical Abstract | A model depicting the mechanism of Sp1 targeted PARP1 inhibition protects cardiomyocytes from myocardial ischemia–reperfusion injury via downregulation of autophagy.

REFERENCES

Abdelrahim, M., Baker, C. H., Abbruzzese, J. L., Sheikh-Hamad, D., Liu, S., Cho, S. D., et al. (2007). Regulation of vascular endothelial growth factor receptor-1 expression by specificity proteins 1, 3, and 4 in pancreatic cancer cells. *Cancer Res.* 67, 3286–3294. doi: 10.1158/0008-5472.CAN-06-3831

Baines, C. P. (2011). How and when do myocytes die during ischemia and reperfusion: the late phase. *J. Cardiovasc. Pharmacol. Ther.* 16, 239–243.

Chadalapaka, G., Jutooru, I., Chintharlapalli, S., Papineni, S., Smith, R., Li, X., et al. (2008). Curcumin decreases specificity protein expression in bladder cancer cells. *Cancer Res*. 68, 5345–5354. doi: 10.1158/0008-5472.CAN-07-6805

Chadalapaka, G., Jutooru, I., Sreevalsan, S., Pathi, S., Kim, K., Chen, C., et al. (2013). Inhibition of rhabdomyosarcoma cell and tumor growth by targeting specificity protein (Sp) transcription factors. *Int. J. Cancer* 132, 795–806. doi: 10.1002/ijc.27730

Chintharlapalli, S., Papineni, S., Abdelrahim, M., Abudayyeh, A., Jutooru, I., Chadalapaka, G., et al. (2009). Oncogenic microRNA-27a is a target for anticancer agent methyl 2-cyano-3,11-dioxo-18beta-olean-1,12-dien-30-oate in colon cancer cells. *Int. J. Cancer* 125, 1965–1974. doi: 10.1002/ijc.24530

Chintharlapalli, S., Papineni, S., Lee, S. O., Lei, P., Jin, U. H., Sherman, S. I., et al. (2011). Inhibition of pituitary tumor-transforming gene-1 in thyroid cancer cells by drugs that decrease specificity proteins. *Mol. Carcinog*. 50, 655–667. doi: 10.1002/mc.20738

Chintharlapalli, S., Papineni, S., Ramaiah, S. K., and Safe, S. (2007). Betulinic acid inhibits prostate cancer growth through inhibition of specificity protein transcription factors. *Cancer Res*. 67, 2816–2823. doi: 10.1158/0008-5472.CAN-06-3735

Codogno, P., and Meijer, A. J. (2010). Autophagy: a potential link between obesity and insulin resistance. *Cell Metab*. 11, 449–451. doi: 10.1016/j.cmet.2010.05.006

Colon, J., Basha, M. R., Madero-Visbal, R., Konduri, S., Baker, C. H., Herrera, L. J., et al. (2011). Tolfenamic acid decreases c-Met expression through Sp proteins degradation and inhibits lung cancer cells growth and tumor formation in orthotopic mice. *Invest. New Drugs* 29, 41–51. doi: 10.1007/s10637-009-9331-8

Deng, H., and Mi, M. T. (2016). Resveratrol attenuates Aβ25-35 caused neurotoxicity by inducing autophagy through the TyrRS-PARP1-SIRT1 signaling pathway. *Neurochem. Res*. 41, 2367–2379. doi: 10.1007/s11064-016-1950-9

Eid, R. A., Alharbi, S. A., El-Kott, A. F., Eleawa, S. M., Zaki, M. S. A., El-Sayed, F., et al. (2020). Exendin-4 ameliorates cardiac remodeling in experimentally induced myocardial infarction in rats by inhibiting PARP1/NF-κB Axis in a SIRT1-dependent mechanism. *Cardiovasc. Toxicol*. 20, 401–418. doi: 10.1007/s12012-020-09567-5

Esposito, E., and Cuzzocrea, S. (2009). Superoxide, no, peroxynitrite and PARP in circulatory shock and inflammation. *Front. Biosci*. 14:263–296. doi: 10.2741/3244

Gilad, E., Zingarelli, B., Salzman, A. L., and Szabó, C. (1997). Protection by inhibition of poly(ADP-ribose) synthetase against oxidant injury in cardiac myoblasts in vitro. *J. Mol. Cell. Cardiol*. 29, 2585–2597. doi: 10.1006/jmcc.1997.0496

González-Montero, J., Brito, R., Gajardo, A. I., and Rodrigo, R. (2018). Myocardial reperfusion injury and oxidative stress:therapeutic opportunities. *World J. Cardiol*. 10, 74–86. doi: 10.4330/wjc.v10.i9.74

Gustafsson, A. B., and Gottlieb, R. A. (2009). Autophagy in ischemic heart disease. *Circ. Res*. 104, 150–158. doi: 10.1161/CIRCRESAHA.108.187427

Halmosi, R., Deres, L., Gal, R., Eros, K., Sumegi, B., and Toth, K. (2016). PARP inhibition and postinfarction myocardial remodeling. *Int. J. Cardiol*. 217(Suppl.), S52–S59. doi: 10.1016/j.ijcard.2016.06.223

He, Q., Pu, J., Yuan, A., Lau, W. B., Gao, E., and He, B. (2014). Activation of LXRa but not LXRb protects against myocardial ischemia/reperfusion injury. *Circ. Heart Fail*. 7, 1032–1041. doi: 10.1161/CIRCHEARTFAILURE.114.001260

Hidvegi, T., Ewing, M., Hale, P., Dippold, C., Beckett, C., Kemp, C., et al. (2010). An autophagy-enhancing drug promotes degradation of mutant alpha1-antitrypsin Z and reduces hepatic fibrosis. *Science* 329, 229–232. doi: 10.1126/science.1190354

Huang, P., Fu, J., Chen, L., Ju, C., Wu, K., Liu, H., et al. (2019). Redd1 protects against post-infarction cardiac dysfunction by targeting apoptosis and autophagy. *Int. J. Mol. Med*. 44, 2065–2076. doi: 10.3892/ijmm.2019.4366

Jagtap, P., and Szabo, C. (2005). Poly(adp-ribose) polymerase and the therapeutic effects of its inhibitors. *Nat. Rev. Drug Discov*. 4, 421–440. doi: 10.1038/nrd1718

Kim, M. Y., Mauro, S., Gévry, N., Lis, J. T., and Kraus, W. L. (2004). NAD+-dependent modulation of chromatin structure and transcription by nucleosome binding properties of PARP-1. *Cell* 119, 803–814. doi: 10.1016/j.cell.2004.11.002

Kim, M. Y., Zhang, T., and Kraus, W. L. (2005). Poly(ADP-ribosyl)ation by PARP-1: 'PAR-laying' NAD+ into a nuclear signal. *Genes Dev*. 19, 1951–1967. doi: 10.1101/gad.1331805

Kloner, R. A., and Jennings, R. B. (2001). Consequences of brief ischemia: stunning, preconditioning, and their clinical implications. *Circulation* 104, 3158–3167. doi: 10.1161/hc5001.100039

Liu, X., Deng, Y., Xu, Y., Jin, W., and Li, H. (2018). MicroRNA-223 protects neonatal rat cardiomyocytes and H9c2 cells from hypoxia-induced apoptosis and excessive autophagy via the Akt/mTOR pathway by targeting PARP-1. *J. Mol. Cell. Cardiol*. 118, 133–146. doi: 10.1016/j.yjmcc.2018.03.018

Ma, X., Liu, H., Foyil, S. R., Godar, R. J., Weinheimer, C. J., Hill, J. A., et al. (2012). Impaired autophagosome clearance contributes to cardiomyocyte death in ischemia/reperfusion injury. *Circulation* 125, 3170–3181. doi: 10.1161/CIRCULATIONAHA.111.041814

Mertens-Talcott, S. U., Chintharlapalli, S., Li, X., and Safe, S. (2007). The oncogenic microRNA-27a targets genes that regulate specificity protein transcription factors and the G2-M checkpoint in MDA-MB-231 breast cancer cells. *Cancer Res*. 67, 11001–11011. doi: 10.1158/0008-5472.CAN-07-2416

Mollion, M., Ehlers, B. K., Figuet, E., Santoni, S., Lenormand, T., Maurice, T., et al. (2018). Patterns of genome-wide nucleotide diversity in the gynodioecious plant *Thymus vulgaris* are compatible with recent sweeps of cytoplasmic genes. *Genome Biol. Evol*. 10, 239–248. doi: 10.1093/gbe/evx272

Molnár, A., Tóth, A., Bagi, Z., Papp, Z., Edes, I., Vaszily, M., et al. (2006). Activation of the poly(ADP-ribose) polymerase pathway in human heart failure. *Mol. Med*. 12, 143–152. doi: 10.2119/2006-00043.Molnar

Morales, C. R., Pedrozo, Z., Lavandero, S., and Hill, J. A. (2014). Oxidative stress and autophagy in cardiovascular homeostasis. *Antioxid. Redox. Signal*. 20, 507–518. doi: 10.1089/ars.2013.5359

Movassagh, M., and Foo, R. S. (2008). Simplifified apoptotic cascades. *Heart Fail. Rev*. 13, 111–119. doi: 10.1007/s10741-007-9070-x

Mukhopadhyay, P., Rajesh, M., Cao, Z., Horváth, B., Park, O., Wang, H., et al. (2014). Poly (ADP-ribose) polymerase-1 is a key mediator of liver inflammation and fibrosis. *Hepatology* 59, 1998–2009. doi: 10.1002/hep.26763

Nakai, A., Yamaguchi, O., Takeda, T., Higuchi, Y., Hikoso, S., Taniike, M., et al. (2007). The role of autophagy in cardiomyocytes in the basal state and in response to hemodynamic stress. *Nat. Med*. 13, 619–624. doi: 10.1038/nm1574

Pacher, P., and Szabó, C. (2007). Role of poly(ADP-ribose) polymerase 1 (PARP-1) in cardiovascular diseases: the therapeutic potential of PARP inhibitors. *Cardiovasc. Drug Rev*. 25, 235–260. doi: 10.1111/j.1527-3466.2007.00018.x

Papineni, S., Chintharlapalli, S., Abdelrahim, M., Lee, S. O., Burghardt, R., Abudayyeh, A., et al. (2009). Tolfenamic acid inhibits esophageal cancer through repression of specificity proteins and c-Met. *Carcinogenesis* 30, 1193–1201. doi: 10.1093/carcin/bgp092

Penna, C., Perrelli, M. G., and Pagliaro, P. (2013). Mitochondrial pathways, permeability transition pore, and redox signaling in cardioprotection: therapeutic implications. *Antioxid. Redox. Signal*. 18, 556–599. doi: 10.1089/ars.2011.4459

Pillai, J. B., Gupta, M., Rajamohan, S. B., Lang, R., Raman, J., and Gupta, M. P. (2006). Poly(ADP-ribose) polymerase-1-deficient mice are protected from angiotensin II-induced cardiac hypertrophy. *Am. J. Physiol. Heart Circ. Physiol*. 291, H1545–H1553. doi: 10.1152/ajpheart.01124.2005

Pillai, J. B., Russell, H. M., Raman, J., Jeevanandam, V., and Gupta, M. P. (2005). Increased expression of poly(ADP-ribose) polymerase-1 contributes to caspase-independent myocyte cell death during heart failure. *Am. J. Physiol. Heart Circ. Physiol*. 288, H486–H496. doi: 10.1152/ajpheart.00437.2004

Pirrotta, V. (2004). The ways of PARP. *Cell* 119, 735–736. doi: 10.1016/j.cell.2004.12.002

Pu, J., Mintz, G. S., Biro, S., Lee, J. B., and Maehara, A. (2014). Insights into echo-attenuated plaques, echolucent plaques, and plaques with spotty calcification: novel fifindings from comparisons among intravascular ultrasound, near-infrared spectroscopy, and pathological histology in 2294 human coronary artery segments. *J. Am. Coll. Cardiol*. 63, 2220–2233. doi: 10.1016/j.jacc.2014.02.576

Rochitte, C. E., Lima, J. A., Bluemke, D. A., Reeder, S. B., McVeigh, E. R., Furuta, T., et al. (1998). Magnitude and time course of microvascular obstruction and tissue injury after acute myocardial infarction. *Circulation* 98, 1006–1014.

Rubinsztein, D. C., Mariño, G., and Kroemer, G. (2011). Autophagy and aging. *Cell* 146, 682–695. doi: 10.1016/j.cell.2011.07.030

Safe, S., Imanirad, P., Sreevalsan, S., Nair, V., and Jutooru, I. (2014). Transcription factor Sp1,also known as specificity protein 1 as a therapeutic target. *Expert Opin. Ther. Targets* 18, 759–769. doi: 10.1517/14728222.2014.914173

Smith, A. J., Ball, S. S., Bowater, R. P., and Wormstone, I. M. (2016). PARP-1 inhibition influences the oxidative stress response of the human lens. *Redox. Biol.* 8, 354–362. doi: 10.1016/j.redox.2016.03.003

Thapalia, B. A., Zhou, Z., and Lin, X. (2014). Autophagy, a process within reperfusion injury: an update. *Int. J. Clin. Exp. Pathol.* 7, 8322–8341.

Vazquez-Ortiz, G., Chisholm, C., Xu, X., Lahusen, T. J., Li, C., Sakamuru, S., et al. (2015). Drug repurposing screen identifies lestaurtinib amplifies the ability of the poly (ADP-ribose) polymerase 1 inhibitor AG14361 to kill breast cancer associated gene-1 mutant and wild type breast cancer cells. *Breast Cancer Res.* 16:R67. doi: 10.1186/bcr3682

Virgin, H. W., and Levine, B. (2009). Autophagy genes in immunity. *Nat. Immunol.* 10, 461–470. doi: 10.1038/ni.1726

Vizcaíno, C., Mansilla, S., and Portugal, J. (2015). Sp1 transcription factor: a long-standing target in cancer chemotherapy. *Pharmacol. Ther.* 152, 111–124. doi: 10.1016/j.pharmthera.2015.05.008

Waldman, M., Nudelman, V., Shainberg, A., Abraham, N. G., Kornwoski, R., Aravot, D., et al. (2018). PARP-1 inhibition protects the diabetic heart through activation of SIRT1-PGC-1α axis. *Exp. Cell Res.* 373, 112–118. doi: 10.1016/j.yexcr.2018.10.003

Wang, C., Xu, W., Zhang, Y., Zhang, F., and Huang, K. (2018). PARP1 promote autophagy in cardiomyocytes via modulating FoxO3a transcription. *Cell Death Dis.* 9:1047. doi: 10.1038/s41419-018-1108-6

Wang, H., Yang, X., Yang, Q., Gong, L., Xu, H., and Wu, Z. (2018). PARP-1 inhibition attenuates cardiac fibrosis induced by myocardial infarction through regulating autophagy. *Biochem. Biophys. Res. Commun.* 503, 1625–1632. doi: 10.1016/j.bbrc.2018.07.091

Wang, Y., Wang, L., Zhang, F., Zhang, C., Deng, S., Wang, R., et al. (2013). Inhibition of PARP prevents angiotensin II-induced aortic fibrosis in rats. *Int. J. Cardiol.* 167, 2285–2293. doi: 10.1016/j.ijcard.2012.06.050

Wayman, N., McDonald, M. C., Thompson, A. S., Threadgill, M. D., and Thiemermann, C. (2001). 5-aminoisoquinolinone, a potent inhibitor of poly(adenosine 5'-diphosphate ribose) polymerase, reduces myocardial infarct size. *Eur. J. Pharmacol.* 430, 93–100. doi: 10.1016/s0014-2999(01)01359-0

Wei, D., Wang, L., He, Y., Xiong, H. Q., Abbruzzese, J. L., and Xie, K. (2004). Celecoxib inhibits vascular endothelial growth factor expression in and reduces angiogenesis and metastasis of human pancreatic cancer via suppression of Sp1 transcription factor activity. *Cancer Res.* 64, 2030–2038. doi: 10.1158/0008-5472.can-03-1945

Xu, S., Bai, P., Little, P. J., and Liu, P. (2014). Poly(ADP-ribose) polymerase 1 (PARP1) in atherosclerosis: from molecular mechanisms to therapeutic implications. *Med. Res. Rev.* 34, 644–675. doi: 10.1002/med.21300

Xuan, F., and Jian, J. (2016). Epigallocatechin gallate exerts protective effects against myocardial ischemia/reperfusion injury through the PI3K/Akt pathway-mediated inhibition of apoptosis and the restoration of the autophagic flux. *Int. J. Mol. Med.* 38, 328–336. doi: 10.3892/ijmm.2016.2615

Yang, S., Wang, X., Contino, G., Liesa, M., Sahin, E., Ying, H., et al. (2011). Pancreatic cancers require autophagy for tumor growth. *Genes Dev.* 25, 717–729. doi: 10.1101/gad.2016111

Zhang, Y., Pötter, S., Chen, C. W., Liang, R., Gelse, K., Ludolph, I., et al. (2018). Poly(ADP-ribose) polymerase-1 regulates fibroblast activation in systemic sclerosis. *Ann. Rheum. Dis.* 77, 744–751. doi: 10.1136/annrheumdis-2017-212265

Zou, D., Li, R., Huang, X., Chen, G., Liu, Y., Meng, Y., et al. (2019). Identification of molecular correlations of RBM8A with autophagy in Alzheimer's disease. *Aging* 11, 11673–11685. doi: 10.18632/aging.102571

Conflict of Interest: The authors declare that the research was conducted in the absence of any commercial or financial relationships that could be construed as a potential conflict of interest.

Advantages of publishing in Frontiers

OPEN ACCESS
Articles are free to read for greatest visibility and readership

FAST PUBLICATION
Around 90 days from submission to decision

HIGH QUALITY PEER-REVIEW
Rigorous, collaborative, and constructive peer-review

TRANSPARENT PEER-REVIEW
Editors and reviewers acknowledged by name on published articles

Frontiers
Avenue du Tribunal-Fédéral 34
1005 Lausanne | Switzerland

Visit us: www.frontiersin.org
Contact us: frontiersin.org/about/contact

REPRODUCIBILITY OF RESEARCH
Support open data and methods to enhance research reproducibility

DIGITAL PUBLISHING
Articles designed for optimal readership across devices

FOLLOW US
@frontiersin

IMPACT METRICS
Advanced article metrics track visibility across digital media

EXTENSIVE PROMOTION
Marketing and promotion of impactful research

LOOP RESEARCH NETWORK
Our network increases your article's readership